

Airway Smooth Muscle Dynamics

Gijs IJpma

A thesis submitted to Auckland University of Technology

in fulfilment of the degree of

Doctor of Philosophy



Auckland, New Zealand

© Gijs IJpma

Declarations

I hereby declare that I am the sole author of this thesis.

I authorise the Auckland University of Technology to lend this thesis to other institutions for individuals for the sole purpose of scholarly research

Gijs IJpma

I further authorise the Auckland University of Technology to reproduce this thesis by photocopying or by other means, in total or in part, at the request of other institutions or individuals for the sole purpose of scholarly research.

Gijs IJpma

Borrowers Page

The Auckland University of Technology requires the signatures of all people using or photocopying this thesis. Accordingly all borrowers are required to fill out this page.

Date

Name

Address

Signature

To my wife,

Lee-Yan Marquez

Acknowledgements

There are many people without whom this work would not have been possible. First and foremost is my wife Lee-Yan, who supported me throughout this thesis and for whom I came to New Zealand,. Thank you for the sacrifices of the past 4 years, I promise I'll make it up to you. I'd also like to thank my family, especially my parents and my sister for supporting my decision even if it meant that I had to move halfway across the world. Bedankt!

My sincere gratitude to Prof. Ahmed Al-jumaily for his supervision and for looking out for me over the years, and to Dr. Simeon Cairns for his assiduous critique of my work. Thanks to IBTec for financially supporting me these 4 years. Thanks as well to everyone at IBTec - to David, Joe, Robert, Ingrid, Prasika, Max and Fred, and also to recent arrivals Pablo, Meha and Mohammed - who have (tried) to keep me sane over the years. To AUT's support staff, in particular Chris Whyburd and Ross Reichardt; and to Prof. Steve Henry, Debby Blake and Sandy Ferguson for enabling me to conduct experiments at KODE Biotech labs.

Special thanks go to Professor Gary Sieck of the Mayo Clinic in Rochester, MN, USA for making it possible for me to complete my experimental work at their facilities, and for providing invaluable feedback on my research. Last but not the least, I would like to thank Lucas Meuchel, Elizabeth Townsend, Wen Zhi, Yun Hua, Rebecca Macken, Dr. Prakash and the rest of the team at Mayo for their patience, kindness and assistance throughout my stay.

Abstract

The current study aims to investigate the relative contributions of each of the processes that govern airway smooth muscle mechanical behaviour. Studies have shown that breathing dynamics have a substantial effect on airway constriction in healthy and diseased subjects, yet little is known about the dynamic response of the main instigator of airway constriction, Airway Smooth Muscle (ASM). In this work several models are developed to further the understanding of ASM dynamics, particularly the roles and interactions of the three dominant processes in the muscle: contractile dynamics, length adaptation and passive dynamics.

Three individual models have been developed, each describing a distinct process or structure within the muscle. The first is a contractile model which describes the contractile process and the influence of external excitation on contractile behaviour. The second model incorporates the contractile model to describe length adaptation, which includes the reorganisation and polymerisation of contractile elements in response to length changes. The third model describes the passive behaviour of the muscle, which entails the mechanical behaviour of all non-contractile components and processes. As little data on the passive dynamics of the muscle was available in the literature, a number of experiments were conducted to investigate relaxed ASM dynamics.

The experimental data and mathematical modelling showed that passive dynamics plays not only a dominant role in relaxed ASM, but contributes considerably to the dynamics of contracted muscle as well. A novel theory of sequential multiplication in passive ASM is proposed and implemented in a mathematical model. Experiments and literature validated the model simulations. Further integration of the models and improved force control modelling of length adaptation is proposed for future study. It is likely that the coupling of the models presented here with models describing other airway wall components will provide a more complete picture of airway dynamics, which will be invaluable for understanding respiratory disease.

Table of Contents

Declarations	ii
Borrowers Page	iii
Acknowledgements	v
Abstract	vi
Table of Contents	vii
List of Figures	xi
List of Tables	xiv
List of Terms and Abbreviations	xv
CHAPTER 1: Introduction	1
1.1 Background	1
1.2 Respiratory Physiology	2
1.3 Asthma	4
1.3.1 Medicinal Treatments	4
1.3.2 Alternative Treatments	5
1.3.3 The Role of Airway Wall Components	6
1.3.4 The Role of Lung Parenchyma	7
1.3.5 Heterogenic Behaviour of Airways	7
1.3.6 The Role of Airway Smooth Muscle	8
1.4 Airway Dynamics in Respiratory Function	8
1.5 Molecular Basis of Airway Smooth Muscle Contraction	9
1.5.1 The Thick Filament	12
1.5.2 The Thin Filament	12
1.5.3 Thick and Thin Filament Polymerisation and Depolymerisation	13
1.5.4 The Contractile Process	13
1.6 The Cytoskeleton	14
1.7 Closure	14
CHAPTER 2: Literature Survey: Airway Smooth Muscle Dynamics and Modelling	16
2.1 Introduction	16
2.2 Quasi steady-state ASM response	16
2.3 ASM dynamics	19
2.3.1 Mechanisms of Smooth Muscle Response to Oscillations	20

2.4	Mathematical Modelling of Smooth Muscle Dynamics	21
2.4.1	Tissue Level Empirical Contraction Models	22
2.4.2	Cross-bridge Models	23
2.4.3	Length Adaptation Models	29
2.4.4	Passive ASM models	33
2.4.5	Fabry's Soft Glasses Theory	33
2.5	Additional findings	35
2.6	Research Plan and Objectives	36
CHAPTER 3: Preliminary Investigation		39
3.1	Introduction	39
3.2	Equipment, procedures and programs	39
3.2.1	Tissue acquisition	40
3.2.2	Dissection	40
3.2.3	Experimental Set-up	41
3.2.4	Programs	43
3.2.5	Reference length procedure	43
3.2.6	Tissue Rejection criterion	46
3.2.7	Equilibration	46
3.3	Experiments	46
3.3.1	Experimental, protocols	46
3.4	Results	50
3.5	Analysis and Discussion	57
3.6	Closure	63
CHAPTER 4: Contraction and Length Adaptation Model		64
4.1	Introduction	64
4.2	Contraction model criteria	65
4.3	4-state Latch bridge model	67
4.3.1	Methodology	67
4.3.2	Results	76
4.3.3	Discussion	81
4.4	Strain Dependent Release Model	82
4.4.1	Methodology	82
4.4.2	Results	84
4.4.3	Discussion	87
4.5	Hill-Type model	88
4.5.1	Methodology	88
4.5.2	Results	89
4.6	Contractile model discussion	91
4.7	Length adaptation	92
4.7.1	Stochastic network model	93
4.7.2	Methodology	94
4.7.3	Results	97

4.7.4	Discussion	100
4.8	Closure	101
CHAPTER 5:	Passive Dynamics Models	102
5.1	Introduction	102
5.2	Modelling criteria	102
5.3	Soft glasses Rheology (SGR) Model	103
5.3.1	Methodology	103
5.3.2	Results	104
5.4	Spring damper model	105
5.4.1	Methodology	106
5.4.2	Results	106
5.5	Fractional differentials	107
5.5.1	Methodology	108
5.5.2	Results	111
5.6	Sequential multiplication: logarithmic superposition	112
5.6.1	Methodology	113
5.6.2	Results	115
5.7	Model comparison	117
5.8	Closure	117
CHAPTER 6:	Validation and Parameter Generation	119
6.1	Introduction	119
6.2	Protocols, Equipment and Programs	120
6.2.1	Tissue acquisition	120
6.2.2	Equilibration and reference length protocol	120
6.2.3	Equipment	121
6.2.4	Labview interface	122
6.3	Experimental protocols and rationale	123
6.3.1	Comparison of Contracted and Relaxed ASM.	123
6.3.2	Step protocols	125
6.4	Results	127
6.4.1	Dynamic response of contracted versus relaxed ASM	127
6.4.2	Power law confirmation and characterisation	131
6.4.3	Sequential multiplication	132
6.4.4	Temperature effects	133
6.5	Discussion and Analysis	134
6.5.1	Comparing Contracted and Relaxed ASM	134
6.5.2	Confirmation of Power law relaxation of force	136
6.5.3	Quantification of power law parameters	137
6.5.4	Sequential multiplication	137
6.5.5	Mechanical explanation	138
6.6	Closure	138

CHAPTER 7:	Model Validation and Adjustment	139
7.1	Introduction	139
7.2	Length adaptation	139
7.3	Passive ASM	140
7.3.1	Methodology	142
7.3.2	Results and discussion	143
CHAPTER 8:	Conclusions and Future Work	147
8.1	Introduction	147
8.2	Conclusions	147
8.3	Future work	150
	Bibliography	152
	Appendix A : Matlab Modelling Code	163
	Appendix B : Matlab Experiment Analysis Code	185
	Appendix C : Labview Programs	195

List of Figures

Figure 1.1: Diagram of lungs and alveoli (inset) (adapted from Wikipedia).....	3
Figure 1.2: Healthy versus asthmatic airway.....	6
Figure 1.3: Ultrastructure of smooth muscle versus skeletal muscle.....	10
Figure 1.4: Proposed cross-bridge cycle in smooth muscle.....	11
Figure 1.5: Side-polar configuration versus Bi-polar configuration of contractile elements.....	12
Figure 2.1: Length–Force relationship in ASM [110].	17
Figure 2.2: Length adaptation in relaxed (C and D) and contracted (A and B) ASM.	18
Figure 2.3: 4 state Huxley, Hai and Murphy model with rate constants.....	25
Figure 2.4: Attachment (f) and detachment (g) rates as a function of myosin head position relative to actin binding position (x) in Huxley, Hai and Murphy model	26
Figure 2.5: Sinusoidal length oscillations with constant mean length:.....	28
Figure 2.6: Parallel to series transition.	30
Figure 2.7: Comparison of Lambert's model and Silveira's model to experimental data.....	33
Figure 2.8: Flow chart of research plan	38
Figure 3.1: Schematic representation of dissection process.	41
Figure 3.2: System diagram of tissue testing set-up.	41
Figure 3.3: Drawing of Aurora Scientific 805A set-up.	42
Figure 3.4: Data from optimal length procedure.	45
Figure 3.5: Length step protocol types applied to the muscle.	49
Figure 3.6: Comparison of experimental results (B) with Fredberg et al. [123] data (A).....	50
Figure 3.7: Force response to step length changes.	51
Figure 3.8: Double logarithmic force response to step length changes.	51
Figure 3.9: Power law exponents (left) and power law multipliers (right) versus amplitude of stretch.	52
Figure 3.10: Power law exponents (top) and power law multipliers (bottom) of force response to staircase functions applied to the muscle.	53
Figure 3.11: Representative sample (n=3) of double logarithmic force response curves of step increase (top) and decrease (bottom)	54
Figure 3.12: Double logarithmic force curves of step length changes after oscillations at various frequencies	54
Figure 3.13: Double logarithmic force curves of response to length steps at 0.5% of Lref after oscillation duration variation	55
Figure 3.14: Double logarithmic force curves of step length changes after oscillations with amplitude variation.	55
Figure 3.15: Double logarithmic force-curves of pulse length steps with varying pulse durations.....	56
Figure 3.16: Double logarithmic force curves of compound step response with duration and direction variation. Blue curves are same direction 2%, 0.5% Lref, red curves are opposite direction 2.5%, 0.5% Lref. Panel A shows positive total length change, panel B shows negative total length change	56
Figure 3.17: Illustration of the close resemblance of curve fits of a different nature.	57
Figure 3.18: Curve fits to pulse response data, using paradigm one and two.....	59
Figure 3.19: Integrated error difference for pulses (B) and two-phase length changes (A).....	62
Figure 3.20: Staircase relative power law multipliers.	63
Figure 4.1: Acetylcholine contractions in dog trachealis smooth muscle [86]. Line labels show ACh concentrations.	65
Figure 4.2: Force - shortening velocity relationship at different times during contraction with neural stimulation (EFS) in bovine trachealis smooth muscle.	66
Figure 4.3: Method of characteristics.	68
Figure 4.4: Visual representation of grid shifting.....	71
Figure 4.5: Effect of series and parallel elastic elements on force and length of contractile element ...	73
Figure 4.6: Attachment and detachment parameters in HHM model as a function of myosin head position relative to actin (x).	75
Figure 4.7: Comparison of model simulations.....	77
Figure 4.8: Contraction in HHM model, with varying serial elastic stiffness.	78
Figure 4.9: Length history during shortening velocity manoeuvre.....	80
Figure 4.10: Shortening velocity versus clamp force.	80

Figure 4.11: Force-length curves of constant velocity oscillations at 4 amplitudes.	81
Figure 4.12: Schematic of SDR model.	83
Figure 4.13: Attachment and detachment rates for SDR mode as a function of x_l	83
Figure 4.14: Force development during contractions in SDR model. Force is normalised to maximum force during a contraction without series elastic element.	85
Figure 4.15: Force, phosphorylation and ATPase activity during a contraction in the SDR model.	85
Figure 4.16: Shortening velocity in the SDR model. different colour lines represent changes in time after initiation of contraction at which shortening velocity manoeuvre was applied.	86
Figure 4.17: Sinusoidal oscillations of varying amplitude in the SDR model.	87
Figure 4.18: Constant velocity oscillations of varying amplitude in SDR model.	87
Figure 4.19: Force and contractile element length development at three series elastic element stiffness levels for Hill type model.	90
Figure 4.20: Shortening velocity at 3 time points for the Hill type model.	90
Figure 4.21: Sinusoidal oscillations simulated by the Hill-type model.	91
Figure 4.22: Evolution of an active element.	95
Figure 4.23: Gradual development peak contractile force in stochastic network model.	98
Figure 4.24: Shortening velocity in the length adaptation model.	99
Figure 4.25: Force-length curve length oscillations.	100
Figure 4.26: Length and Force traces during length oscillations.	100
Figure 5.1: Step response SGR model.	105
Figure 5.2: Representation of spring damper model.	106
Figure 5.3: Force relaxation in response to length change in the spring damper model.	107
Figure 5.4: Double logarithmic plot of force response to step length change in fractional derivative model.	111
Figure 5.5: Relative force response to step length changes.	112
Figure 5.6: Force multiplier versus power law exponent for step length changes.	114
Figure 5.7: Step response power law parameters in the sequential multiplication model. Panel A shows the multipliers and panel B the power law exponents.	115
Figure 5.8: Force-length loops of sinusoidal oscillations in sequential multiplication model.	116
Figure 5.9: Force-length loops of oscillations in relaxed muscle.	117
Figure 6.1: System Diagram of muscle test system hardware.	121
Figure 6.2: Tissue bath.	122
Figure 6.3: Representation of the various length step protocols used.	126
Figure 6.4: Hysteresivity dependence on amplitude (A) and frequency (B), and dependence of asymmetry on amplitude and frequency (C and D).	128
Figure 6.5: Hysteresivity and asymmetry versus frequency for triangular wave oscillations.	129
Figure 6.6: Sample of force-length loops of triangular wave oscillations at different frequencies.	129
Figure 6.7: Normalised shortening velocity after oscillations or early release.	130
Figure 6.8: Exponent change after oscillations in contracted and relaxed muscle.	131
Figure 6.9: Sample of force ratio versus power law exponent correlation.	132
Figure 6.10: Sample of curve fits of negative length steps followed by positive length steps.	133
Figure 6.11: Quality of fit analysis using integrated error.	133
Figure 6.12: Temperature sensitivity of stiffness, force and power law exponent ($n=6$).	134
Figure 7.1: Sample of power law exponent versus length change amplitude.	141
Figure 7.2: Force-length loops of sinusoidal oscillation.	144
Figure 7.3: Force-length loops of sinusoidal oscillations in contracted ASM.	144
Figure 7.4: Simulation of triangular wave data.	145
Figure 7.5: Force and length traces from model and experimental data.	146
Figure A.1: Mode diagram of length adaptation model.	173
Figure C.2: Front panel Data_generation.vi.	195
Figure C.3: Block diagram Data_generation.vi.	196
Figure C.4: Block diagram Ramp_single.vi.	197
Figure C.5: Block diagram fixedlevelramp.vi.	197
Figure C.6: Block diagram Ramp_osc.vi.	198
Figure C.7: Block diagram Sheneq.vi.	198
Figure C.8: Block diagram fixed_front.vi.	199
Figure C.9: Fixedlevel.vi.	199
Figure C.10: Block diagram Two_step.vi.	199
Figure C.11: Block diagram staircase.vi.	200
Figure C.12: Block diagram Step_function.vi.	200

Figure C.13: Block diagram Breathing_oscil .vi	201
Figure C.14: Block diagram perturb sine.vi	202
Figure C.15: Block diagram Group_all.vi	202
Figure C.16: Front panel Data_Acquisition.vi.....	203
Figure C.17: Data_Acquisition.vi.....	204
Figure C.18: read-rates_n_sizes.vi	205
Figure C.19: Filename_generation.vi	206
Figure C.20: Downsample.vi.....	206
Figure C.21: FilterVI.vi	207
Figure C.22: Resample.vi	207

List of Tables

Table 3-1: Data on summation of power laws.....	60
Table 3-2: Data on power law multiplication.....	61
Table 4-1: Parameter values used for HHM model.....	76
Table 4-2: Parameter values SDR model.....	83
Table 4-3: Parameter values of Hill type model.....	89

List of Terms and Abbreviations

ASM	Airway Smooth Muscle
ACh	Acetylcholine
Active	When referring to muscle: contracted. When referring to force it is the difference between the force in relaxed muscle and in contracted muscle. When referring to elements: contractile.
Asymmetry	The degree of deviation from a symmetrical ellipsoid of a force vs. length loop. Defined as the difference in area above and below the line connecting the maxima and minima, divided by the total area of the loop
Bronchodilation	A dilation of airways, usually from a state of excessive airway constriction.
Bronchoprotection	A reduction in airway responsiveness to stimulants.
Contracture	Sustained contraction, in this work always elicited by ACh 10-6
Cross-bridge cycling	This cycle refers to the cycle of attachment and detachment of the myosin heads to the actin filament.

Dynamics	In this work dynamics refers to the continuous response to length changes, in contrast to steady state responses.
EFS	Electrical Field Stimulation
HBSS	Hank's Balanced Salt Solution
Hysteresivity	The hysteresis of a force vs. length loop during an oscillation and corrected for the loop shape.
Integrated error	The area between the fitting curve and the fitted data on logarithmic axes
Oscillations	Any length changes of a periodic nature. In this work either sinusoidal or triangular.
Passive	Not actively contracting. The term passive does not exclude non contractile elements subject to reorganisation, polymerisation and depolymerisation.
PSS	Physiological Salt Solution
Reference length	The length at which the muscle is set after the reference length procedure. This length is anticipated to be close to the current optimal length for force generation of the tissue

CHAPTER 1

Introduction

1.1 Background

The fundamental causes of asthma have eluded researchers for many years. Some treatments have been developed with varying degrees of success, however asthma cannot yet be cured. Even with the best medication and care, patients still experience a significant level of discomfort. Moreover, a large portion of patients do not respond well to existing medication [1]*, and side-effects do occur, sometimes with fatal consequences [2-4]. This can be largely attributed to limited understanding of the disease, and respiratory physiology. The lungs are highly complex structures, which can malfunction in many different ways. However, regardless of the various biochemical or mechanical pathways which lead to an asthma attack, it always results in airway constriction. Consequently, airway mechanics is of vital importance in asthma research.

Because we breathe continuously, the airways are part of an inherently dynamic environment, changing in circumference with every breath. Breathing dynamics have been demonstrated to be important in asthma pathology [5-9]. This can be attributed to the altered behaviour of asthmatic airways in this dynamic environment.

The current research focuses on airway smooth muscle (ASM) dynamics. ASM is a tissue comprised of smooth muscle cells embedded in the airway walls and constitutes the only actively contracting component of the airways. The contraction of ASM is assumed to be the final step in the chain of events that lead to an asthma attack [10, 11]. The main aim of this research is to investigate the relative contributions of the processes that govern ASM mechanical behaviour. This involves a detailed investigation of the dynamic response of ASM, both when contracted (active) and when relaxed (passive). A deeper understanding of ASM dynamics may lead to the advancement of non-medicinal alternative treatments based on altering the airway's

* Numbers between square brackets refer to references, which are listed in the Bibliography prior to the Appendices.

dynamic environment, e.g., breathing therapy and/or external excitation. Moreover, understanding of ASM dynamics may provide a crucial context for the understanding of biochemical events in ASM.

This chapter provides a general description of respiratory physiology (section 1.2), followed by a description of asthma, its symptoms and available treatments (section 1.3). The importance of airway dynamics in respiratory function is discussed in section 1.4. ASM contraction and individual components that play an important role in the contraction process are discussed in section 1.5. The specific objectives relating to the presented aim are discussed at the end of the literature review in Chapter 2.

1.2 Respiratory Physiology

The respiratory system is involved with the exchange of gases, primarily oxygen and carbon dioxide. To allow for optimal oxygen uptake and carbon dioxide removal, a large surface area for diffusion in and out of the bloodstream has to exist. The respiratory system has to fulfil this task of optimal exposure to the outside air while minimising exposure of the bloodstream to airborne diseases and toxic particles. This renders the respiratory system especially prone to an hypersensitive immune response as is the case in many and possibly all cases of asthma[12].

The respiratory system's first line of defence is the nose where particles are filtered from the air which is then moisturised and heated to near core body temperature. Any remaining particles are caught by mucus lining the airway walls, which is then propelled towards the throat by cilia extending from the epithelium cells lining the airways. After passing the larynx (voice box) the filtered air enters the trachea which consists of a series of c shaped cartilage discs with a layer of smooth muscle and epithelium. The smooth muscle and epithelium span from the ends of the cartilage disks where the trachea borders the oesophagus (Figure 1.1). This smooth muscle serves as a regulator of trachea compliance in the force balance between oesophageal expansion during swallowing and trachea rigidity during deep expiration [13, 14]. Smooth muscle tissues used in most studies of ASM are derived from the trachea of a variety of animal species because of the relative ease of dissection and uniform orientation.

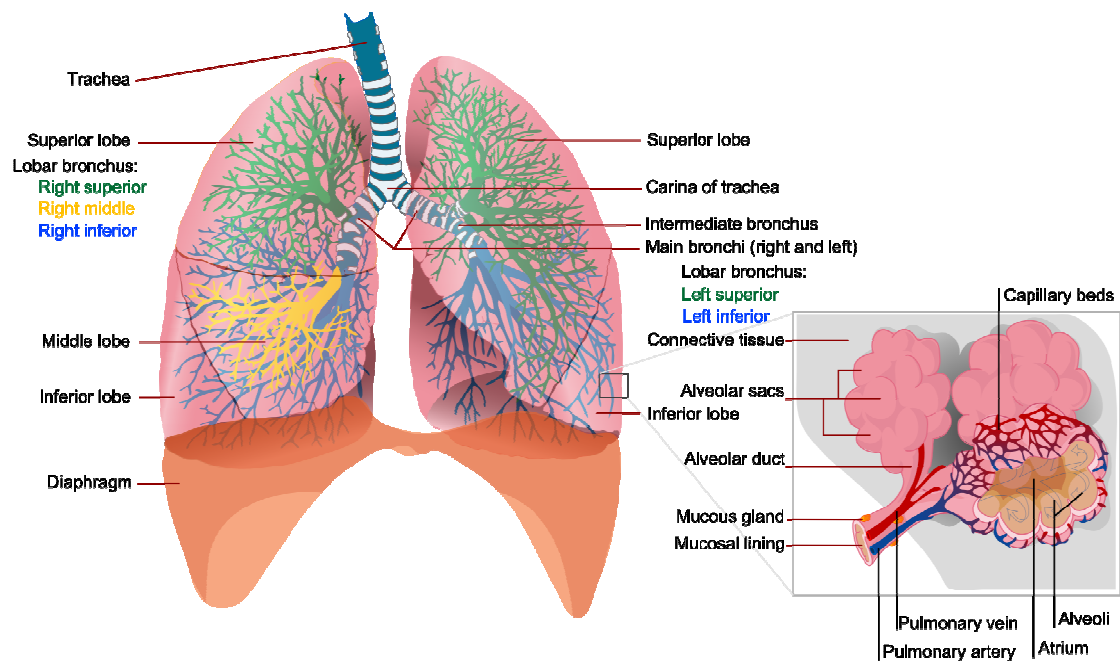


Figure 1.1: Diagram of lungs and alveoli (inset) (adapted from Wikipedia).

At the end of the trachea the airway splits into two primary bronchi, each leading to a single lung, followed by a second branching into the five lung lobes, three on the right and two on the left. The upper bronchi have stiff walls made of circular cartilage discs, smooth muscle embedded in collagen and elastin, and an epithelium layer [15]. Where the bronchi enter the lung lobes the subsequent airways are tethered to the parenchyma, a sponge-like material which consists of the smallest airways, alveoli and other lung structures. The airways keep on bifurcating, becoming smaller and less stiff with each split. Around the sixth to ninth bifurcation the bronchi become bronchiole as the cartilage disappears from its walls. From this point on, the lumen of the bronchiole is determined by smooth muscle, epithelium, transmural pressure differences and the attachment to the parenchyma [15]. The bronchioles eventually become terminal bronchioles, which form the last part of the conducting zone of the respiratory system.

The terminal bronchioles split into the respiratory bronchioles which are lined with the first of the alveoli which provide the surface area for gas exchange (Figure 1.1 inset). Further bifurcation leads to the alveolar ducts and finally the alveolar sacs. The alveolar walls consist mainly of a fine mesh of capillaries, providing a total surface area for diffusion into and out of the blood of around 75 m² for a healthy adult male

[15]. The alveoli make up the majority of the lung volume and the parenchyma and can change in volume in response to pressure changes.

1.3 Asthma

Asthma is a respiratory disease which is characterised by chronic inflammation, hypersensitivity, and obstruction of the airways [15]. During an asthma attack, excessive contraction of ASM occurs simultaneously with mucous accumulation and reduction of the bronchial diameter. This increases resistance to airflow particularly during exhalation [15]. As a consequence, the patient experiences wheezing, shortness of breath, chest tightness and coughing [15]. During an asthma attack, ASM contraction is limited to some extent by the rigidity of other airway wall components and the surrounding parenchyma. In asthmatic patients the biophysical properties of ASM and other airway wall components permit total airway collapse upon allergen challenge. In contrast, ASM contractile forces are insufficient to collapse airways completely in healthy subjects.

The real culprit of asthmatic symptoms has not yet been identified, mainly because of the complex cause and effect relationship between airway wall components. As a result, a distinct marker of asthma has yet to be determined. This sometimes leads to misdiagnosis and mistreatment of the symptoms [16].

1.3.1 Medicinal Treatments

Currently there is no known cure for asthma although medications can relieve the symptoms. Generally there are two types of medication: 1) bronchodilators that induce relaxation of ASM (e.g. β_2 -adrenergic agonists) [15]; 2) agents that prevent attacks by reducing inflammation of the airways (e.g. corticosteroids). Often a large fraction of the medicine deposits outside the appropriate lung region or is exhaled [17], and some show notable side effects. The most severe reactions involve long lasting β_2 -agonists. Indeed a recent study attributed many asthmatic fatalities in the USA to the chronic use of β_2 -agonists [18]. Other serious side-effects of β_2 -agonists include cardiac arrhythmias, sleep disturbances, low blood potassium levels, muscle cramps and allergic reactions [15]. Other side effects of β_2 -agonists include fine tremors, especially of the hands, restlessness, nervousness, headaches, flushing and palpitations [15]. Long term use of corticosteroids also leads to severe problems such

as a predisposition to infection, osteoporosis, cataracts, glaucoma, indigestion and thinning of the skin/excessive bruising [3]. Short term use of corticosteroids has other side effects which include sleep loss, increased appetite, increased blood sugar and blood pressure levels [2]. Many patients dislike taking steroids which can result in irregular intake, thereby limiting its effectiveness [4].

1.3.2 Alternative Treatments

At best, drug-free approaches in asthma treatment have shown reduced dependency on medication in clinical trials. Such drug-free approaches include breathing techniques (Yoga, Buteyko), bronchial thermoplasty and continuous positive airway pressure.

Some techniques to alter breathing patterns have helped reduce medicinal dependency. In clinical trials the Buteyko method has been shown to curtail drug intake but it did not improve lung function, which may explain its limited use by physicians [19, 20]. Clinical trials for Yoga breathing exercises show limited reductions in the use of β_2 -agonists [8, 21].

Bronchial thermoplasty involves thermal damage to ASM via a bronchoscope to inhibit ASM contraction. Initial studies show improved lung function and reduced medicinal use, confirming the importance of ASM in asthma [22]. The cost and invasiveness of this procedure will probably limit the application of this technique to severe asthmatics.

Continuous positive airway pressure can increase average lung volume and is being developed as a treatment method. It may be effective in helping restore natural lung volume in overweight asthmatics. Positive results such as increased end expiratory volume have been achieved, and the technique has been expanded to obstructive sleep apnoea patients, with mixed results [23, 24].

The efficacy of various breathing techniques and continuous positive airway pressure could indicate that changes in breathing volume, respiratory rate and mean lung volume can reduce ASM contractility. Improved understanding of ASM and airway dynamics could greatly improve these techniques.

1.3.3 The Role of Airway Wall Components

In asthma the structural composition of airway wall components differs from healthy airways. These changes are referred to as airway remodelling, which includes any form of chronic change to airway wall morphology. This is likely caused by a process linked to injury and repair of the airway wall [22-24]. Chronic changes in airway diameter can result in airway remodelling. Such changes can originate from chronic low lung volumes or changes in parenchyma or airway wall components [24]. Continuous positive airway pressure methodologies for asthma relief are in part based on the assumption that an increased mean airway diameter reverses airway remodelling [23].

**This image has been removed
by the author of this thesis
for copyright reasons.**

Figure 1.2: Healthy versus asthmatic airway. (1) Mucous (2) Epithelium layer (3) Basement membrane (4) Deposition of extracellular matrix components (5) Neovascularisation (6) Smooth muscle (7) Airway adventitia (8) Parenchyma (adapted from [25])

A comparison of the morphology of asthmatic and non-asthmatic airways shows considerable increases in epithelium, submucosa and smooth muscle content in asthmatic patients (Figure 1.2). Even without changes in the force generating capacity of ASM these structural changes are sufficient to bring about full airway closure [26]. Any structural weakening of airway wall components facilitates airway constriction upon ASM activation [27]. Conversely increased airway wall thickness and/or stiffness reduces oscillation of the airway diameter during breathing which increases

ASM contractility (Chapter 2). Changes in the structural composition of cartilage without changes in the cartilage quantity have been demonstrated in asthmatic patients [28]. Although such changes have yet to be tested for their effect on stiffness, a reduction in cartilage stiffness can result in hyper-responsiveness [29].

1.3.4 The Role of Lung Parenchyma

The parenchyma is composed of the bulk of alveoli, small airway walls and pulmonary blood vessels (Figure 1.2). During breathing, the distending forces arising from the movements of the diaphragm and chest are transferred to the airway wall through parenchymal connections. The elasticity of the parenchyma determines the magnitude of these distending forces. Consequently airway narrowing during allergen challenge is considerably more pronounced at low lung volumes [30]. This implies that elasticity of the parenchyma may play an important role in airway constriction.

In post-mortem studies, where asthma was diagnosed as the cause of death, airway parenchyma uncoupling in the smaller airways has been found [31]. Analysis of breathing mechanics in severe asthma has shown that the compliance of the lungs is reduced, which implies a structural change of the parenchyma [32]. Besides directly affecting airway diameter through reduced distending forces, changes in parenchyma and parenchymal connections also cause decoupling of lung volume from airway diameter which could contribute to hyper-responsiveness [30].

1.3.5 Heterogenic Behaviour of Airways

A complicating factor in the analysis of respiratory function is the heterogenic behaviour of airways. Heterogeneity is defined as an inhomogeneous response of the airways to their mechanical or biochemical environment. High resolution computed tomography studies of allergen challenged lungs have shown that similar sized airways can be fully collapsed or fully dilated simultaneously [33]. Mathematical modelling has shown that the airways may exist in a bistable configuration, in which airways are either fully dilated or fully collapsed [33]. Moreover, heterogeneity might be attributed to airway interdependence from flow alterations [34].

Studies of airway behaviour are complicated by the apparent mismatch in the response to allergen challenge when this is applied locally versus globally. Global allergen challenge (using a nebulizer) does not collapse larger airways at any

concentration. In contrast, locally allergen challenged airways collapse at relatively low allergen concentrations [35]. This may be attributed either to a limitation of the administration of global allergen challenge using a nebulizer [35], or to airway and parenchyma interdependence.

1.3.6 The Role of Airway Smooth Muscle

ASM is the only active component in the airway walls, to be activated either neurologically or biochemically. Consequently acute airway collapse in asthma has to be caused by ASM contraction. Moreover, while airway walls in asthma are often inflamed, airway hyper responsiveness has been shown to persist in the absence of inflammation, which is further evidence of the importance of ASM in the disease[27]. Isolated ASM can contract to 80-90% of its initial length [36], which is sufficient to collapse even cartilaginous airways. However, in healthy subjects, a supramaximal allergen challenge does not fully collapse the airways [36-38]. Conversely, allergen challenge results in airway closure at relatively low concentrations in asthma. The difference in response to allergens is used as a marker to diagnose asthma, regardless of the underlying cause.

Although its direct link to asthma is uncertain, it is well established that the ASM in asthmatics differs to that in healthy individuals. In fatal asthma lung autopsies ASM cell mass and number are increased. Moreover, studies have found evidence of altered signalling pathways [37], increased unloaded shortening velocity, greater force generation [38-41] and a decrease in passive tension [38].

1.4 Airway Dynamics in Respiratory Function

In asthma research the importance of deep inspiration in lung function tests is well established [27, 42-53]. In healthy subjects respiratory movements involving deep inspiration have been shown to induce bronchodilation for 1-2 min [51]. However, such manoeuvres are less effective in asthmatics and can even lead to additional bronchoconstriction. Furthermore, inhibition of deep inspiration in healthy subjects leads to increased bronchoconstriction at low allergen concentrations and subsequent deep inspirations fail to reverse this [6, 45]. Although asthmatic symptoms can not be explained solely by a difference in response to deep inspirations [27, 46], the potential importance of this response has been the focus of ongoing investigation.

Tidal breathing also affects bronchoconstriction. Increasing tidal volume has been shown to result in a reduced recovery time from bronchoconstriction in rabbits [5] and dogs [9, 54, 55], and bronchoprotection (reduced severity of subsequent bronchoconstriction) in dogs [56]. Tidal volume changes also results in improved ventilation of lungs without allergen challenge [57]. Moreover, a reduction in average lung volume in sheep showed a significant increase in force generation in the ASM [58]. The sensitivity to breathing and deep inspiration of airway calibre indicates the importance of ASM function in asthma [26].

1.5 Molecular Basis of Airway Smooth Muscle Contraction

The complexity of ASM dynamic behaviour cannot be captured by current mechanical or empirical models (Chapter 2). Hence, an understanding of the processes themselves rather than their cumulative effects is necessary to understand the ASM response to oscillations. This section describes the ASM components and their interactions.

The cellular components of ASM have a less regular structural organisation compared to skeletal muscle, see Figure 1.3. This complicates the understanding of its contractile mechanism. The primary constituents of the contractile apparatus in ASM are the thin (actin) and thick (myosin) filaments. Thin and thick filaments are generally organised parallel to the cell axis. Each thick filament is surrounded by fifteen to thirty thin filaments, but it interacts only with up to six thin filaments [59]. Thin filaments are anchored to cytosolic dense bodies or to membrane associated dense plaques and form hexagonal arrays around the thick filaments [60]. A thick filament and its associated thin filaments make up a contractile element. These contractile elements are believed to be suspended in the cytoskeleton (see Section 1.6).

**This image has been removed
by the author of this thesis
for copyright reasons.**

Figure 1.3: Ultrastructure of smooth muscle versus skeletal muscle. Small arrows show thick filaments, large arrows show dense bodies. While an organised filament arrangement is clearly visible in skeletal muscle, no such organisation is found in smooth muscle [61].

The foundation for the knowledge on muscle contraction was laid by Andrew Huxley in 1957 in his article on filament sliding in skeletal muscle [62]. He proposed that muscle contraction is caused by the cyclical attachment and detachment of flexible heads on the thick filaments to thin filaments, which results in the relative sliding of these filaments. Despite major advances in technology and knowledge the basis of this model still has ongoing support [63]. A similar but modified contraction process is thought to drive contraction in ASM [64, 65].

The cycle of attachment and detachment of myosin heads to actin is ATP dependent (Figure 1.4, 1-2-3-4-5). The relative displacement of the filaments originates in the mechanical configuration change (power stroke) of the myosin heads, which extend from the thick filament. First ATP hydrolysis tilts a detached myosin head around its neck region. Second, upon attachment or shortly thereafter, ADP and inorganic phosphate are released, which tilts the head back. Consequently the myosin head exerts a force on the actin filament. ATP binding subsequently reduces the affinity of myosin for actin, leading to detachment.

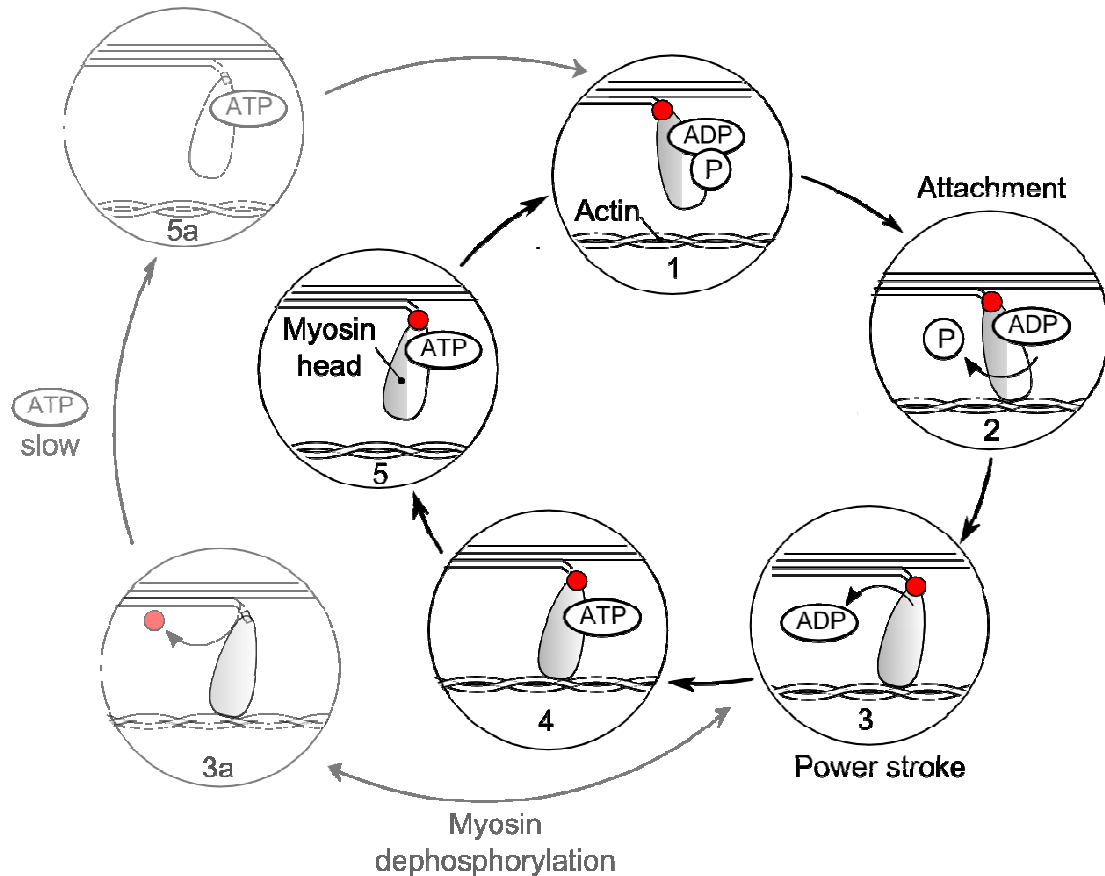


Figure 1.4: Proposed cross-bridge cycle in smooth muscle. Black rimmed circles show standard cross-bridge cycling process, gray rimmed circles show latch bridge process.

ASM thin filaments bind in a side-polar fashion to thick filaments [66, 67]. Figure 1.5 shows this side-polar configuration compared to the bi-polar configuration found in skeletal muscle. As the myosin heads extend in opposite directions from the myosin filaments, a single actin filament can associate with the full length of myosin rather than less than half the length in bi-polar configurations. Experiments have shown that at optimal length (that at which maximum force generation can be achieved), the myo-filaments fully overlap. This determines the number of potential active attachment sites and consequently the potential maximum force. The side polar binding of myosin to actin likely influences the force-length relationship of the muscle. In ASM a parabolic relationship between steady-state force and tissue length has been observed [67-69].

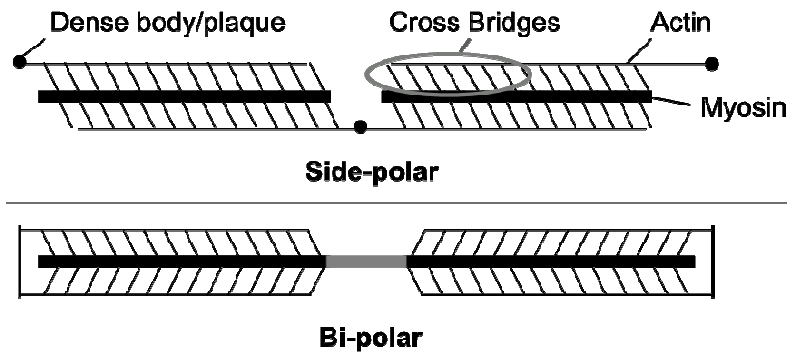


Figure 1.5: Side-polar configuration versus Bi-polar configuration of contractile elements.

1.5.1 The Thick Filament

Monomeric myosin molecules polymerise to form the thick filament. Each myosin molecule consists of six polypeptide chains: two heavy chains, a pair of essential light chains, and a pair of regulatory light chains [60]. The heavy chain dimer consists of a long α -helical coiled body which ends in two elongated globular heads. The body of the myosin heavy chain forms the thick filament backbone, from which the myosin heads extend radially. One regulatory and one essential light chain are located in the neck region of each myosin head. Phosphorylation of the regulatory chain activates the cross-bridge cycle. *In vitro* experiments have shown a 25 to 1000 fold increase of actin activated myosin ATPase activity when the regulatory light chain is phosphorylated [68].

1.5.2 The Thin Filament

The thin filament is composed primarily of filamentous actin (F-actin), which is the polymerised form of globular actin (G-actin) [60]. In addition there are several proteins bound along the length of F-actin, i.e. tropomyosin and caldesmon among others. The F-actin molecules are arranged in a double-stranded helix with a continuous strand of tropomyosin along its length. Troponin, a regulatory protein associated with the actin filament in skeletal muscle, is absent in ASM. Caldesmon is thought to replace troponin in ASM, although its importance in regulating contractile activation is not fully understood [60, 69, 70]. Electron microscopy studies of single thin filaments have shown that when caldesmon is phosphorylated, it displaces tropomyosin to reveal the myosin binding sites on actin [70]. While the primary regulator of cross-bridge activity in ASM is the phosphorylation the myosin regulatory light chain, some regulation might take place on the actin filament as well

[71-74]. Moreover, tropomyosin displacement might be responsible for cooperative attachment of myosin by simultaneously revealing several actin binding sites [75]. The location of the myosin binding sites on actin filaments is uncertain in ASM, but the distance between the binding sites is assumed to be equal to the overlapping distance of the double stranded helix, which is around 15 nm [60, 71].

1.5.3 Thick and Thin Filament Polymerisation and Depolymerisation

Both thick and thin filaments are seen as dynamic structures in ASM, which change length through polymerisation and depolymerisation [76-82]. G-actin constitutes about 40% of the total actin content of ASM cells in the relaxed state. Upon activation, the G-actin content decreases by up to 30%, likely because of polymerisation into F-actin [76, 78]. Several research groups have attributed length adaptive effects of ASM to actin mobility and polymerisation [42, 44, 48, 60, 61, 76, 82-95]. This is supported by the finding that inhibition of actin polymerisation results in a notable reduction in ASM force generation [76]. Actin has also been found to be mobile, which means that actin can detach from one dense body, and attach to another within the cell [60, 96]. This process might explain greater length adaptation than can be attributed to polymerisation and depolymerisation alone.

Myosin polymerisation may be more important than actin polymerisation with respect to length adaptation in ASM [59, 81, 95, 97]. The myosin to actin filament ratio increases when the muscle is contracted [59]. A dramatic increase in myosin filament content by up to 80% (dependent on the initial ASM length) has been found within seconds of activation [97]. Furthermore, after large length oscillations in relaxed ASM strips, thick filament density was reduced by around 30%, which confirms the lability of dephosphorylated myosin filaments [82]. Moreover it has been shown that the presence of thin filaments facilitates myosin filament assembly [95]. This process could explain the development of optimal overlap of thin and thick filaments upon activation by restricting the development of thick filaments to locations along thin filaments.

1.5.4 The Contractile Process

The contractile apparatus in smooth muscle enables constant force generation and maintenance over a large length range at a low energy (ATP) cost. The most

commonly accepted sequence of events in smooth muscle contraction is displayed in Figure 1.4. The low ATP cycling rates [98] imply a cross-bridge cycling process which is much slower than would be expected based on the initial speed of contraction and the magnitude of the contractile force. Hence, it has been proposed that smooth muscle can exist in two attached states, a myosin phosphorylated and dephosphorylated state [64, 65, 99-102]. Attached myosin in the phosphorylated state can detach rapidly (Figure 1.4, sequence 1-2-3-4-5) while dephosphorylated attached myosin has a reduced affinity for ATP, resulting in a much slower detachment rate (Figure 1.4, sequence 1-2-3-3a-5a). The cross-bridges are believed to move constantly between these states, influenced by the length and contraction history of the muscle. Activation of the muscle initially drives the majority of cross-bridges to the fast cycling configuration, but when the length is stabilised, the slower cycling latch configuration will become more prevalent. The balance between fast cycling and slow cycling bridges may be disturbed by changes in length or activation levels. Another explanation for force maintenance at low ATPase turnover rates may be found in the strain dependent release of ADP [103-105]. If ADP release is delayed until the myosin head is sufficiently strained by relative movement of the myo-filaments, then in isometric contractions ADP will remain bound to the myosin head, preventing ATP attachment and subsequent detachment of the myosin head from actin. This greatly reduces ATPase turnover during force maintenance.

1.6 The Cytoskeleton

The cytoskeleton is defined here as the collection of all structural elements responsible for maintaining the cell shape and integrity but excluding the contractile elements [106]. The main structure consists of a network of cytoskeletal β -actin and intermediate filaments connected by dense bodies and attached to the cell membrane by dense plaques [59, 60]. Dense bodies and dense plaques are considered to be the main anchoring points for all structural components in the cell. Like the contractile apparatus, the cytoskeleton also adapts to length changes [107-109].

1.7 Closure

This chapter has presented the context in which ASM operates as well as some of the muscle's components and their function. To understand airway constriction and the dynamics of airway behaviour it is necessary to understand how contractile processes

influence the mechanical behaviour of the muscle, and what role non-contractile components play. Therefore the next chapter will discuss the current available models and their ability to describe the dynamics of ASM.

CHAPTER 2

Literature Survey: Airway Smooth Muscle Dynamics and Modelling

2.1 Introduction

The effects of breathing patterns on bronchoconstriction are most likely mediated by their effects on ASM. Historically the study of ASM dynamics focussed on the steady-state response of the muscle, in particular force-length relationships. Later research showed that these force-length curves change considerably depending on length and activation history. This chapter discusses these investigations and the attempts to model this behaviour.

The quasi steady-state response and the variability of force-length relationships in ASM are discussed in Section 2.2. Next the dynamics of the muscle are described (Section 2.3). Mathematical models on the three dominant processes responsible for ASM dynamics are reviewed in Section 2.4. The chapter concludes with a section on the objectives and planning of the current research.

2.2 Quasi steady-state ASM response

ASM dynamics can be separated into passive and active (contractile) components. The passive component is believed to be dominant in relaxed, unstimulated muscle, while the active component dominates in contracted muscle. Both components have been analysed using force-length relations. The result of one such force-length study is shown in Figure 2.1. These force-length curves are created by repeatedly contracting the muscle at increasing muscle length. The force prior to each contraction is the passive force and the peak force during a contraction is the total force. The active force is defined as the difference between the total force and the passive force. The force-length record shows a negligible passive force for all lengths below $L_{10\%}$, which was defined as the length at which the passive force was 10% of the total force. Beyond this length the passive force shows a steep force increase. The total force reaches a plateau which is maintained over a wide range of lengths until

the force suddenly increases. Consequently the active force-length relation has a large plateau as well.

**This image has been removed
by the author of this thesis
for copyright reasons.**

Figure 2.1: Length–Force relationship in ASM [110]. Porcine ASM was contracted using electrical field stimulation (EFS) at a range of lengths. ●=Total force; ○=active force; ■=passive force. Data are means ± SD.

When applying the same sequence of stretch and activation to different ASM samples, these force-length relations are quite reproducible. However, changing the sequence or magnitude of the applied length changes can drastically alter these relations. Wang et al. (2000) [94] compared the active and passive force-length relations of ASM under three conditions: one set was allowed to passively shorten for 24 h; the second set was fixed at the slack length after dissection; the third set was maintained at the *in situ* length (stretched) for the same period of time. The resulting force-length curves are shown in Figure 2.2. Apparently the force-length curves can adapt to any length, at least within the examined range, to develop the same maximum contractile force. The passive force–length curve shifts correspondingly. The authors subsequently found that when tissues from the first (shortened) and third (lengthened) set were fixed at the length of the second set, a series of isometric contractions caused the muscle to adapt rapidly to that new length. Furthermore Pratusевич et al. (1995) showed that while the contractile force can adapt to achieve the same force at a range of lengths, the shortening velocity and compliance increase with length [85].

**This image has been removed
by the author of this thesis
for copyright reasons.**

Figure 2.2: Length adaptation in relaxed (C and D) and contracted (A and B) ASM. ●=equilibrated at lengths shorter (A and C) or larger (B and D) than reference length, ○=equilibrated at reference length [94].

Length adaptation seems to occur mainly when length changes are applied in relaxed muscle [85, 94]. However, in contracted ASM some adaptive effects have also been observed. Several studies have shown that length increases in contracted muscle result in an overall reduction in the force in contractile force-length relations, while the force after length decreases fully recovered [87, 111]. Another study found that a more constant relation exists between ASM force and stiffness [86]. Different contractile stimuli (Electrical Field Stimulation (EFS) and AcetylCholine (ACh)) and intensity resulted in the same force-stiffness relations, and only small changes in the force stiffness-relations were found after length changes in contracted muscle. In cells a similar relation exists between stiffness and prestress [112-114].

In the analysis of contractile force the contribution of the passive force is often ignored [64, 65, 69, 115, 116], in part because the contractile force is up to fifty times greater than the force in relaxed ASM [110]. However, studies have suggested that passive components do contribute to the mechanical behaviour of contracted muscle. First, upon ACh contractile stimulation, actin polymerisation results in stiffening of the muscle, even when myosin phosphorylation, and thus contractile force generation, is inhibited [74, 78, 79]. Second, an increase in ASM stiffness occurs long after force

has plateaued, which indicates ongoing cytoskeletal stiffening after cross-bridge recruitment has ceased [86]. Third, both relaxed and contracted ASM display the same featureless frequency response and power law relaxation, which was also found in other non-contractile cell types [117]. Neither this power law relaxation response nor the associated passive mechanisms are well understood. These mechanisms include the interactions between inter- and intra-cellular components of a non-contractile nature which include cell membranes, their intercellular connections, along with the cytoskeleton and unattached intracellular proteins.

Differences in ASM behaviour between species have been found in several studies [69, 118]. Passive force in human ASM tissues (with epithelium) can be up to 60% of the active force, while in rats, pigs and dogs it is less than 10%. The small active to passive force ratio may be caused by the high average age of the human subjects (mean above 60 years), which is associated with muscle stiffening ([119, 120]). The epithelium might also have affected these observations.

2.3 ASM dynamics

As the lungs expand and contract, the airway walls change diameter accordingly, resulting in ASM length changes. If airway compliance values are similar to total lung compliance, then ASM could consequently stretch during normal breathing by about 4% and during deep inspiration by up to 30%. Although the cartilage reinforced airways are likely to be much stiffer, the assumption of equal compliance seems valid for the peripheral airways [121]. These oscillations might disrupt cross-bridge cycling [115, 122-124] or alternatively cytoskeletal structures, resulting in force reductions and shortening velocity changes.

In vitro pressure oscillations in airways have been compared with oscillation of ASM length, leading to mixed results in response [125]. Length oscillation applied before allergen challenge resulted in force dampening in ASM tissue, but equivalent diameter oscillations of airways resulted in force potentiation [43]. Other experiments have shown that oscillations applied after allergen challenge reduce forces similarly in both airways and ASM tissue [54]. Other *in vitro* experiments further indicate that the bronchoprotective and bronchodilating effects of breathing originate from ASM dynamics [122, 123, 126-129]. ASM constrictive forces were dampened up to 50% when ASM was exposed to length oscillations of up to 1 Hz [115, 122, 129]. Higher

frequency stimulation (5-100Hz) caused a reduction of smooth muscle stiffness [130]. Force reduction has a strong dependence on oscillation amplitude and a weak dependence on oscillation frequency, with a plateau in frequency dependency for oscillations above 30-50Hz.

2.3.1 Mechanisms of Smooth Muscle Response to Oscillations

Empirical and mathematical investigation of ASM dynamics both suggest that mechanical oscillation affects ASM force in two ways: through disturbance of the cross-bridge cycle [122, 123, 128, 129, 131, 132] and through adaptive length changes [128, 129]. The response of ASM to oscillations most likely involves the disruption of the contractile system in various ways. ATP turnover is increased during ASM oscillation [133] as is hysteresis of the force-length relationship [123]. Both of these features are believed to be indicators of the cross-bridge cycling speed [133]. An increase in cross-bridge cycling speed may indicate that oscillations cause a reduction in the number of latch bridges. This is contradicted by experiments showing decreased shortening velocity after oscillations [128]. Furthermore, force dampening did not change with allergen concentration, which indicates that deactivation of cross-bridges did not occur [127]. If force dampening was caused by deactivation of cross-bridges, low allergen concentrations should show less force dampening because there are less cross-bridges to deactivate. In contrast, changes in the stimulation pathway using different allergens revealed changes in force dampening, indicating some role for mechanosensitive pathways [127].

Large length oscillations (up to 30% of length) caused long term (>30 min) reductions in isometric force when ASM is allergen challenged after the cessation of oscillations [48, 129]. Hence length oscillations in relaxed muscle modulate the length adaptive processes. Increasing the amplitude and frequency of oscillation both caused exacerbated force reductions. Length oscillations could also incur length adaptation in contracted ASM. Small amplitude oscillation resulted in larger force dampening when applied directly after greater length oscillations when compared to small amplitude oscillations applied in isolation [122]. Furthermore, during oscillations in allergen challenged ASM, the maximum force level reached in stable force-length loops trends towards the steady-state force level that existed before oscillations started. This trend is most pronounced in large amplitude oscillations, regardless of the actual maximum

length during oscillations [123, 134-136]. The lack of response to deep inspiration in asthma might be attributed to an increased shortening velocity in asthmatic ASM [38-41]. The increase in shortening velocity of ASM in asthmatics could explain the reduced bronchodilating effect of breathing in asthma [40, 137]. A higher shortening velocity requires greater breathing frequencies for a similar level of ASM force dampening, which is possibly beyond the patient's abilities. This increased shortening velocity can be attributed to either a different arrangement of contractile elements (a higher series to parallel ratio in asthmatic ASM), or an increased speed of cross-bridge cycling. If chronically shortened ASM in asthma is caused by higher shortening velocities, force reduction and ASM lengthening may be attained with higher frequency oscillations.

2.4 Mathematical Modelling of Smooth Muscle Dynamics

Data on ASM behaviour indicate that several processes are responsible for its mechanical response. In general the literature focuses on two main processes thought to be the main driving mechanism behind ASM behaviour: cross-bridge cycling and length adaptation. These two have individually been modelled in various ways. A third component in ASM dynamics, which is often overlooked, is the passive ASM dynamics, which is attributed to the collective behaviour of the cytoskeleton and its interaction with the internal smooth muscle cell environment. Having separate mathematical models for each of the mechanisms may be useful to explain them individually and predict some of the behaviour of the muscle. However, a complete model that incorporates all these mechanisms would be more useful to understand the quantitative contribution of each mechanism. It is thought that such a model would help to identify the amount of force generated by each mechanism when external loading is applied.

These three processes are intertwined, yet sufficiently complex to require individual modelling. For convenience, the major modelling assumptions in the literature are that length adaptive processes cease when ASM is subjected to contractile stimulation and that passive ASM behaviour does not change upon activation. However, the validity of these assumptions has been challenged by data on partial ASM activation [96], passive smooth muscle behaviour [92, 138] and evidence of length adaptation in active ASM [87, 122, 123].

2.4.1 Tissue Level Empirical Contraction Models

Because of the incomplete understanding of ASM physiology some researchers have attempted to model active ASM dynamics empirically. The two models that are most cited and most applicable to the current research are discussed here. The first is that of Anafi and Wilson (2001) [135], which describes the dynamic force-length relationship of ASM for use in an airway dynamics model. The experimental data of Shen et al. (1997) on constant velocity oscillations [134] was used to develop the mathematical curve fits, after which the model was validated using the sinusoidal oscillation data of Fredberg et al. (1997) [123]. Two sets of ordinary differential equations were used to describe the shortening and lengthening domains as well as a third equation to address the mechanical history effect. The model's ten curve fitting parameters were determined by an extensive trial and error approach, which created a decent fit of curve shapes for the data by Shen et al., and a less accurate approximation of the data by Fredberg et al., with considerable differences in peak force values. As the shortening and lengthening phases of oscillations are separately modelled, this approach only applies to a limited domain.

The second model by Bates et al. (2005) [136] was developed to establish the role of passive elastic components. A mixed empirical mechanical model was proposed and fitted to the same experimental data as the model by Anafi and Wilson. A non-linear spring, modelled arbitrarily as a fourth-order polynomial, was coupled with a curve fit of ASM steady-state behaviour. The near constant peak oscillation force in the experimental data was attributed to length adaptive effects. Consequently the force response to length oscillations was transposed to result in constant peak oscillation force. This approach limits the domain to periodic oscillations. Both these models have focused on the experiments by Fredberg et al. [134] and Shen et al. [123]. Both experiments showed clear force-length loops, though only the stable force-length loops achieved after several oscillations were published. These models have not been tested for their ability to predict the onset of oscillations or any other type of length changes.

A dynamic empirical model has been developed to determine the effect of higher frequency oscillations (5-100 Hz) on stiffness reduction in ASM [130]. The core of the model is a finite element representation of an ASM strip consisting of two rows of

triangular plane stress elements. The stiffness is expressed as a function of (sinusoidal) oscillation duration and frequency, which limits its use to sinusoidal waves only. The model showed a reasonable fit of the data, but its domain is too small for extensive analysis.

2.4.2 Cross-bridge Models

Andrew Huxley's original cross-bridge model for skeletal muscle contraction [62, 139] forms the basis of most smooth muscle contraction models. This section first discusses Huxley's model, after which the leading smooth muscle contraction model is discussed.

2.4.2.1 *Huxley's Model of Skeletal Muscle Contraction*

Huxley et al. (1957) developed the theory that muscle contraction is caused by filaments (actin and myosin) sliding past each other. In Huxley's interpretation of cross-bridge events, actin and myosin exist in two states, attached and detached. Attachment (f) and detachment (g) rates are dependent on the distance between the equilibrium position of each myosin head and its binding site on actin (x). Detachment rates are high for negative values of x , and increase from zero for positive values of x in a linear manner (Figure 2.4). Attachment is only possible in a range defined by the thermal oscillatory range of the myosin head, with a bias to one side to force shortening. Inside the attachment range, the attachment rate increases in proportion to x . With these conditions, binding of the myosin head is biased towards a pre-strained configuration in one direction, supporting contraction of the muscle. This results in the following governing formulas in which $n(x,t)$ represents the fraction of attached cross-bridges and (v) is the relative speed of thin versus thick filaments:

$$\begin{aligned}\frac{\partial n}{\partial t} &= (1-n)f - ng \\ -v \frac{\partial n}{\partial x} &= f - (f+g)n\end{aligned}\tag{2.1}$$

The total muscle shortening rate (V) is then calculated from the sarcomere length (s):

$$-\frac{sV}{2} \frac{\partial n}{\partial x} = f - (f+g)n\tag{2.2}$$

The total force F is dependent on the myosin head stiffness k and is derived as:

$$F = \int_{-\infty}^{\infty} nkx dx \quad (2.3)$$

Other characteristics such as energy liberation (based on the ATP turnover), cycling speed and muscle force were formulated as well. The system of equations is solved either numerically as a set of partial differential equations or by using various mathematical simplifications such as eliminating space dependency assuming a Gaussian distribution of attached myosin [140]. The complexity of solving the partial differential equations has led to several attempts to reformulate the model.

Several changes to the original model follow the evolution of the understanding of cross-bridge processes. The original model did not include a power stroke, instead it contained a myosin head perturbed by thermal oscillation with location dependent attachment and detachment rates. The net effect of this assumption is equal to a single phase power stroke if it occurs instantaneously on attachment. Some experiments indicate that the relative movement of actin versus myosin filaments occurs in discrete steps, which may be attributed to a multiphase power stroke [141].

2.4.2.2 *Hai and Murphy's model for smooth muscle contraction*

Some changes to Huxley's model have been made to model smooth muscle contraction. Firstly, the regulation of smooth muscle contraction is dominated by myosin phosphorylation instead of actin activation [60]. Secondly, in smooth muscle the level of phosphorylation influences the shortening velocity [101, 142]. As shortening velocity is directly related to the cross-bridge cycling rate, a relation between cross-bridge cycling rate and phosphorylation is likely. Thirdly, the ability of smooth muscle to maintain force with very low ATP consumption indicates that during the force maintenance phase a lower cross-bridge cycling rate occurs.

Hai and Murphy [64] were the first to incorporate these findings into a model for smooth muscle contraction. Their goal was to develop a minimum kinetic model that explains the latch state in smooth muscle. Instead of modelling the myosin heads as either attached or detached, they hypothesised that in smooth muscle a second, slower cross-bridge cycle exists, represented by a second attached state in a 4-state model

(Figure 2.3). This second attached state appears when myosin heads attach to actin and subsequently dephosphorylate, resulting in a more stable attachment. This representation of events accounts for two distinct cycling speeds and the dependence of cycling speed on phosphorylation level. It also explains the relatively low energy efficiency of smooth muscle compared to skeletal muscle contraction since ATP hydrolysis is required for the phosphorylation-dephosphorylation cycle as well as the power stroke.

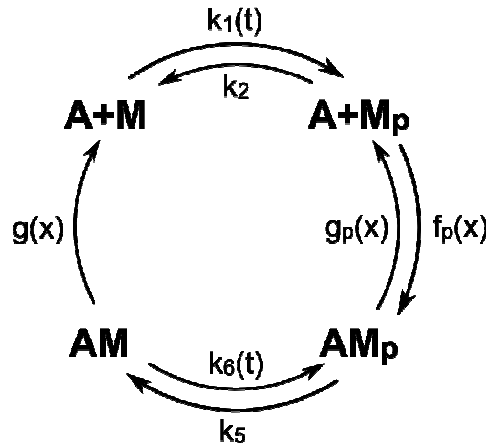


Figure 2.3: 4 state Huxley, Hai and Murphy model with rate constants. $k1(t)=k6(t)$ and $k2=k5$. A =actin, M =myosin, Mp =phosphorylated myosin, AM =attached species, $A+M$ = detached species.

Hai and Murphy subsequently released an expanded version of their model [65] (later dubbed the Huxley Hai and Murphy model (HHM) [122]) which merged their original model with the location dependent attachment and detachment constants from Huxley's model.

This results in the following governing equations, where n represents the fraction of myosin heads at position x at time t , D is the differential operator $\frac{d}{dt}$ and T the state transition matrix:

$$\frac{Dn(x,t)}{Dt} = T(x,t)n(x,t) \quad (2.4)$$

Where the state transition matrix is given by:

$$T(x,t) = \begin{bmatrix} -k_1(t) & k_2 & 0 & g(x) \\ k_1(t) & -k_2 - f_p(x) & g_p(x) & 0 \\ 0 & f_p(x) & -k_5 - g_p(x) & k_6(t) \\ 0 & 0 & k_5 & -k_6(t) - g(x) \end{bmatrix} \quad (2.5)$$

The rate constants k_i equal the phosphorylation and dephosphorylation rates, while the attachment ($f(x)$ and $f_p(x)$) and detachment ($g(x)$ and $g_p(x)$) are given in Figure 2.4.

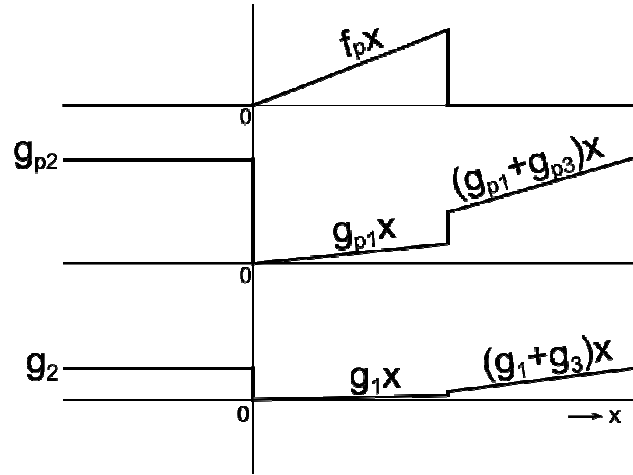


Figure 2.4: Attachment (f) and detachment (g) rates as a function of myosin head position relative to actin binding position (x) in Huxley, Hai and Murphy model

All attached cross-bridges collectively determine the stiffness of the tissue, and their individual displacement relative to the actin binding site determines the total force generated by the contractile element. Total cell behaviour is calculated through extrapolation using sarcomere length, filament density and individual cross-bridge stiffness, which in ASM are more difficult to obtain than in skeletal muscle [115]. In the model, filament sliding occurs because of asymmetric attachment and detachment rates, as in Huxley's original model.

Challenges to this hypothesis come from the measured basal myosin phosphorylation levels when there is minimal or no muscle resting tension [75, 143]. Cooperative attachment of cross-bridges has been proposed, which requires a threshold value of

phosphorylation before any cross-bridge cycling can occur [75, 144]. The number of cooperative cross-bridges that provided the best fit of available data was seven, which was linked to the length of tropomyosin which spans seven G-actin strands. Equivalent cooperative regulation has also been found in skeletal muscle [145].

A further update of the model was published to accommodate actin regulation, which effectively creates an 8 state model [146]. The eight states are created following the assumption that all 4 states represented in the HHM model exist in two actin activation varieties. Transition between the two sets of four states occurs only between the unbound dephosphorylated myosin states. It is assumed that the two actin configurations result in two sets of rate constants, with one set being a factor of 100 smaller than the other. The adjusted model is able to represent phorbol ester induced contractions, which show increased force generation without changes in phosphorylation levels or intracellular calcium concentrations $[Ca^{2+}]_i$ [146].

Although the HHM model was originally developed and tested using data from carotid smooth muscle, the model has been used extensively for ASM [115, 122, 123]. A slightly adapted version of the original HHM model has been applied to dynamic loading by Mijailovic et al. to look at the effects of tidal breathing on phosphorylation levels and force development in ASM tissue [115, 122, 123, 131, 133]. Length and force oscillations both showed a dynamic or perturbed equilibrium, in which a constant force-length loop is achieved after several oscillations. Length changes equivalent to tidal breathing reduced the force generating capacity of ASM by 50% for the isometric case (Figure 2.5).

**This image has been removed
by the author of this thesis
for copyright reasons.**

Figure 2.5: Sinusoidal length oscillations with constant mean length: Experimental data [123] versus Huxley, Hai and Murphy model simulation [115]. Panel A shows experimental results, B the simulation results.

Mijailovic et al. hypothesised that in a dynamic equilibrium, cross-bridge cycling rates in activated smooth muscle are influenced by the amplitude and frequency of force oscillations, such as those caused by tidal breathing. As the mechanical oscillation continually modulates the cross-bridge cycling rates, a stable force-length cycle is established. They concluded that the observed dynamic effects of ASM can be attributed to a disturbed cross-bridge cycling process [122, 123]. The results of their models compare quite favourably to experimental results when looking at average stiffness and force development during oscillations, and in some degree to hysteresivity as well.

However, some trends shown in the experimental data are not seen in the simulations. Firstly, as the length oscillation amplitude is increased, the experimental results show an increasingly non-symmetrical force-length loop. The asymmetry can be attributed to non-linear stiffness of cross-bridges, the influence of passive forces or the timing of power strokes. The timing of a power stroke will have the strongest effect in high frequency oscillations. When the duration of attachment approaches the development time of a power stroke, some cross-bridges will generate less force and/or displacement than predicted by the model. For large strains and high velocities, force generation might be reduced considerably, especially during shortening.

A second discrepancy is the trend in maximum force levels when the amplitude is increased. Some processes in smooth muscle seem to regulate the maximum force during these oscillations towards the optimal isometric force. This could be a length adaptive effect. Fredberg et al. [123] found unexpected length adaptive process in allergen challenged smooth muscle when large amplitude oscillations were immediately followed by low amplitude oscillations. The resulting force-length loop was distinctly different from the force-length loop when the low amplitude oscillations were performed separately. If indeed a length adaptive process caused this effect, the shape and especially the maximum forces would be affected. In a later article from the same group, a series of experiments is described in which ASM is loaded against a variable load determined by the loading expected to occur *in vivo* [131]. Length changes equivalent to tidal breathing resulted in a gradual increase in length and decrease in force for equilibrated activated ASM. Although the experimental results were reported to confirm the perturbed equilibrium theory, ASM length did not return to its previous steady-state value when tidal oscillation stopped. This could indicate that at least part of the effects of oscillations on ASM is caused by length adaptive processes. Wang et al. provided further evidence that cross-bridge dynamics alone might not be sufficient to explain ASM dynamics [128]. Their experiments show that a decrease in shortening velocity occurs directly after oscillation, which contradicts the predicted increase in shortening velocity in the HHM model.

2.4.3 Length Adaptation Models

The long term changes in ASM behaviour brought about by its mechanical history indicate large reorganisation of structural components in ASM [42, 44, 48, 61, 76, 82-95, 147, 148]. ASM can generate approximately the same maximum force over a three fold length range [110], although some studies find less stable force values [149]. The most likely explanations for this length adaptability involve polymerisation and/or depolymerisation of actin and myosin filaments, changes in the cytoskeleton and motility of contractile elements. Polymerisation seems to occur at the onset of activation, and depolymerisation in the relaxed state, with a considerable increase in myosin depolymerisation during oscillations [82]. Consequently, the fluidity of the contractile system in the smooth muscle cell is shown to be far greater in relaxed muscle compared to activated muscle [148, 150].

When smooth muscle adapts to length changes, the maximum force generation is inversely related to unloaded shortening velocity [151]. Unloaded shortening velocity of a single contractile element (one myosin filament with its associated actin filaments) is probably determined only by the cross-bridge cycling speed independent of the number of cycling cross-bridges on the element. Consequently, the shortening velocity of a single ASM cell is related to the number of contractile elements in series, while the stiffness of the cell is related to the number of contractile elements in parallel assuming the number of cross-bridges per element does not change (Figure 2.6). In effect many of the length adaptive changes in ASM result in a change in the relative organisation of the contractile elements, and consequently a change of the parallel to series ratio of these elements [42, 76, 82, 85-87, 89, 91, 93, 95]. This is the basis of the theory of parallel to series transition of contractile elements on which length adaptation models are based [85, 86, 91, 151, 152].

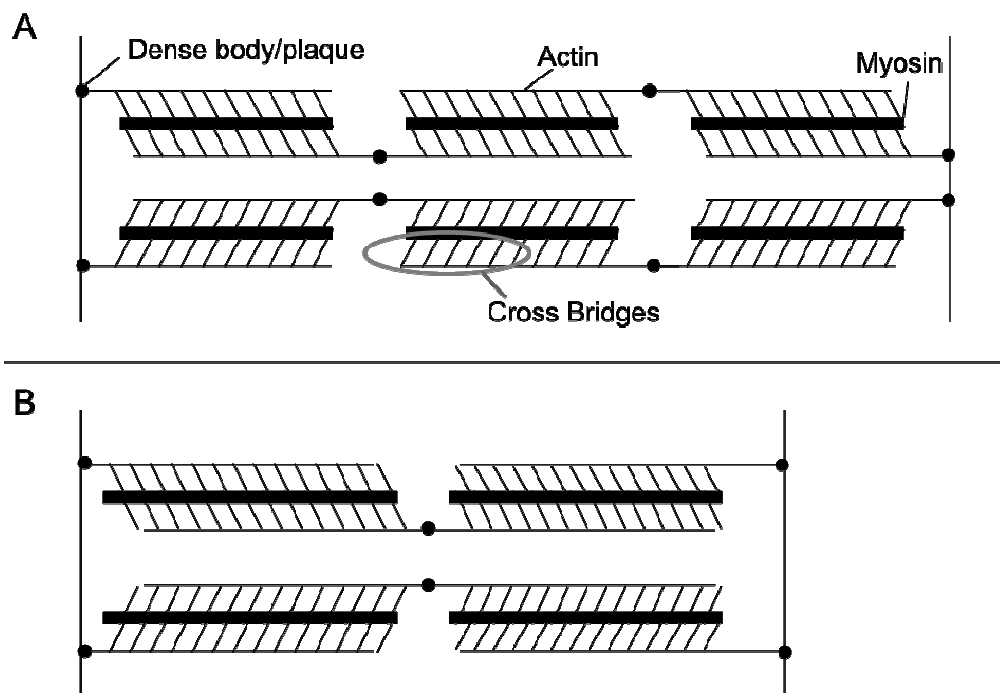


Figure 2.6: Parallel to series transition. While the total number of cross-bridges is the same in B as in A, the ratio of cross-bridges acting in parallel compared to series is changed, which reduces the shortening velocity but increases the force.

2.4.3.1 Lambert's Plasticity Model

Lambert et al. (2004) developed a mathematical model for steady-state length adaptation calculations [89]. In their model the mechanisms responsible for the restructuring of the myosin filaments and cytoskeleton are not addressed. The ASM

cell is represented as a cylinder containing multiple trains of contractile elements interconnected by dense bodies. Consequently the total number of contractile elements is the product of the elements in series (N_s) and the elements in parallel (N_p). All contractile elements in the model act in unison, with identical parameters and behaviour. It is assumed that when fully adapted, actin myosin overlap (overlap length defined as l) is optimal. Consequently, the force (F) and the velocity (V) can be described as:

$$F = \alpha N_p l \quad (2.6)$$

$$V = N_s v \quad (2.7)$$

With α = proportionality constant between N_p and l , and v = shortening velocity of one contractile element. With power defined as $F \cdot v$, the power is proportional to the total number of cycling cross-bridges in the cell.

The density of myosin filaments is calculated from the cross-sectional area of the cell and the number and length of contractile elements in series and parallel. These data was compared with morphometric analysis of cross sectional slices of ASM cells. The model agrees with the findings of constant maximum force at a range of adapted lengths from literature data [85, 153]. Moreover, the simulations showed the same linear relationship between adapted length and myosin filament density, power, ATP consumption and shortening velocity. In the model this was achieved with a constant number of elements in parallel, and a changing number of elements in series (Figure 2.6), with proportionality constants α and β (for scaling power) constant. Experiments on the effects of oscillations in relaxed state on subsequent force generation produced values for increased shortening velocity, decreased isometric force and decreased muscle power [128]. Using shortening velocity and force to find values for N_s and $N_p l$, the power decrease calculated from the model quite accurately matched the power measured (11% versus 13.6 %).

2.4.4 Stochastic Network Model

Silveira and Fredberg (2005) [93, 154] developed a two-dimensional stochastic network model of the ASM cell in a move towards a length adaptation-cross-bridge all inclusive model. Inspired by the soft glasses theory (see Section 2.4.5), this model

does not require any specific knowledge on polymerisation, depolymerisation or relocation of actin or myosin filaments. Instead, non-descript links form and dissolve at any length in a stochastic setting. Contraction-relaxation processes and contractile force development are not modelled directly, but rather as the potential force generation of all elements combined. Similarly shortening velocity is assumed to be only a function of the average number of elements in series. The cell is regarded as a two dimensional grid of nodes representing dense bodies that can be connected by deformable links in all directions (contractile elements, intermediate filaments etc.). Links are formed based on the availability and length of unbound contractile units as well as the distance between nodes and the degree of network activation. Link dissolution is proportional to the noise temperature as defined in the soft glasses theory, which is calculated using the measurable quantity hysteresivity. Axial contraction of the cell is dominant because of the length/width ratio of the cell, even though the links can be formed and broken in all directions. Each contractile element is assumed to be at its optimal length upon link formation, with maximum overlap of actin and myosin filaments. Each link consists of a chain of contractile elements, resulting in an unloaded shortening velocity proportional to the link length. The nodes in this model are fixed to an immobile substrate, allowing only length controlled simulations. Shortening velocity is calculated as the shortening velocity the model would have if it were allowed to shorten without load. Constants were determined by curve fitting noise temperature and force development over time during a contraction, see [92]. When tested against the same data used for validation of Lambert's model, there is a slightly improved fit especially for force generation (Figure 2.7). Further validation was achieved by comparing the experimental results on the reversibility of length adaptation [94] and on the timing of rapid length change and allergen challenge [86, 92].

It is not clear if the two dimensional approach with random formation of links in all directions is necessary to produce the stated results. As the difference between perpendicular cross-sectional slices of smooth muscle cells show, contractile elements are formed mainly in axial orientation [81]. The effect would be a higher efficiency of contraction, which has not been calculated for this model. The model is not capable of simulating continuous force/length data, but rather it predicts the potential maximum contractile force at any point in time.

This image has been removed
by the author of this thesis
for copyright reasons.

Figure 2.7: Comparison of Lambert's model and Silveira's model to experimental data. \circ show data from [85] and [153]. Solid black line represents simulation data from Silveira et al, dashed line show's the simulation data from Lambert et al.[89]. Adapted from [85].

2.4.5 Passive ASM models

As the passive structural components in ASM are generally ignored, a limited number of models on passive ASM mechanisms exist. In the above described models passive structural elements are either not taken into account, or represented as (non-) linear elastic elements, which ignores the established hysteresivity of passive ASM as well as its strong mechanical history dependence.

2.4.6 Fabry's Soft Glasses Theory

The soft glasses theory is not aimed at passive ASM *per se* but at cellular mechanics in general. Experiments on ASM cells have shown that the soft glasses theory applies

equally to several non-contractile cell types and contractile smooth muscle cells. The basis of this theory lies in the observation that despite the myriad of reported biochemical and micromechanical events in cells the net mechanical behaviour seems to collapse onto a single framework. Quite unexpectedly, this framework also appears in the group of inorganic materials called soft glasses.

Sollich et al. (1997) [155] developed a framework for the mechanics of the material group of soft glasses, which includes foams, pastes, emulsions and others. Soft glassy materials mechanically behave in a fashion similar to glass, however they have very low elastic moduli. The particles in soft glasses are never in thermodynamic equilibrium, but in a metastable configuration in which thermal motion alone is not enough to create thermodynamic equilibrium. Particles in these materials are trapped in their locations by surrounding particles, which are not easily disturbed by thermal motion. An elevation of temperature increases the likelihood of disturbance of these traps, increasing the fluidity of the material. At relatively high temperatures the material behaves like a fluid while at relatively low temperatures (below the glass transition temperature) it behaves as a solid. In cells it is not the thermodynamic temperature that determines its fluidity but the noise temperature, representing the non-thermal jostling of its particles.

To belong to the group of soft glassy materials, a material has to meet the following conditions [61, 156]. Firstly, the Young's modulus has to be several orders of magnitude lower than the weakest man made polymers or rubbers. Secondly, the dynamics must be scale free: when measuring matrix stiffness in the frequency domain, no particular frequency stands out. The stiffness follows the weak power law f^{x-1} in response to a length change, in which x represents the noise temperature, being close to but larger than unity. Thirdly, the dominant frictional stress is proportional to the elastic stress, with the constant of proportionality being the hysteresitivity (η), of the order of magnitude of 10^{-1} .

The mechanical properties of ASM match these three criteria, as do several other cell types [61, 80, 92, 138, 156, 157]. The central component that causes the behaviour of soft glasses and glasses alike is the crowded state of the material that prevents establishment of a least energy configuration. Particles in the material are trapped by surrounding particles. Jostling caused by thermal agitation or external factors can

cause individual particles to hop out of their trap. The large variety of processes and components in the smooth muscle cell interact in such a way that individual processes collapse into one net effect, being a change in noise temperature. This holds true even for some degree of cellular organisation as seen in ASM cells (Figure 1.3).

The noise temperature is an easily measured parameter and is related to hysteresivity (η) through:

$$x = \arctan\left(\frac{2\eta}{\pi}\right) \quad (2.8)$$

Fabry et al. (2001) found that when exposed to a variety of chemicals known for altering the contractile system, the mechanical behaviour of ASM cells is still determined by the noise temperature only [61, 80, 156]. The noise temperature in ASM is elevated in the relaxed state and increases initially upon activation. Soon after the onset of activation the noise temperature drops to below that in the relaxed state, representing a rigid internal structure. At the onset of relaxation a small peak of noise temperature appears again [61].

The soft glasses theory for living cells is relatively new and not fully developed and its implications have only recently been studied. Extensive modelling using this theory has not yet been published, although initial results from experimental studies are promising [80, 92, 138, 156].

2.5 Additional findings

ASM faces constant dynamic loading *in vivo* and variable cycles of activation and relaxation. This dynamic loading likely prevents full length adaptation to any length. Therefore, Ali et al. (2007) [96] looked at length adaptation as it progresses in time after a length change. Their experiments point towards two processes of length adaptation, with different adaptation speeds. While force adaptation took 30 min with repeating contraction-relaxation cycles, the shortening velocity adjusted almost instantaneously. As shortening velocity is dependent on the number of contractile elements in series, this suggests that contractile element rearrangement either happens upon activation or instantaneously during length changes in relaxed muscle. The delay in force adaptation might be caused by a slower myosin filament polymerisation to maximum filament overlap, though this is contradicted by experiments on myosin

filament lability [82]. Force generation is reduced when ASM is stimulated immediately after a length change, although a length decrease showed exacerbated force decrease (50%) compared to a length increase (20%). This may be attributed to changes in the cytoskeleton, resulting in reduced transmission of the contractile element forces. This may be caused by slack in cytoskeletal structural filaments.

2.6 Research Plan and Objectives

The current research forms part of a larger effort by the Institute of Biomedical Technologies at the Auckland University of Technology to investigate the potential of altering the dynamic environment of airways in the treatment of asthma. A detailed understanding of the role of ASM and in particular the dynamic response is a key feature of this research. To understand how disease affects ASM and how treatments might alleviate symptoms, it is essential to identify and understand the individual processes contributing to ASM behaviour. Hence, the main aim of the current research is:

To investigate the relative contributions of each of the processes that govern ASM mechanical behaviour.

Three components of ASM dynamics are identified: cross-bridge cycling, length adaptation and a passive component. Comprehensive models of each of these processes and their interactions can reveal the role each process plays in the dynamic response of the muscle. Such a model also allows for a more targeted investigation of the differences between healthy and diseased muscles, which could lead to the development of new methodologies for the treatment of diseases.

The literature review indicates that there is no model yet that can fully explain the dynamic behaviour of ASM. Specifically, none of the models are able to quantitatively predict the dynamics response of each of the processes. To address these issues, the main objectives are:

1. Quantify ASM passive dynamics (Chapter 3 & 6)

Part of this investigation, the literature survey of available data, has been covered in this chapter. The lack of quantitative data on passive ASM dynamics necessitates a preliminary investigation on relaxed ASM prior to

mathematical modelling of the passive muscle. This preliminary investigation will focus on the force response to single event length changes. Similar to conventional mechanical analyses where step, ramp and sinusoidal responses are assessed, the muscle will be subjected to step length changes to investigate the instantaneous force change and the subsequent relaxation response. Superposition of these length changes will be analysed to provide a bridge between single event responses and continuous dynamics.

2. Develop an ASM dynamics model with the following components

a. Contractile dynamics (Chapter 4)

The predominant model of smooth muscle contraction, the Huxley Hai and Murphy model will be analysed on a novel set of conditions to assess its applicability to dynamic situations. This study will investigate if the large number of undetermined parameters in this model are necessary and whether reducing the complexity and the number of parameters of the model is feasible. Lastly an empirical model will be attempted in an effort to further reduce the number of indirectly determined parameters.

b. Length adaptation (Chapters 4 and 7)

The aim is to develop a model of length adaptation that incorporates a multitude of contractile elements in a network setting. This model should incorporate contractile dynamics and be suitable for force response dynamic analysis.

c. Passive dynamics (Chapter 5 and 7)

As the current knowledge of passive dynamics in the muscle is insufficient to develop a quantitative model, a number of theories (available as well as newly developed in this work) will be explored based on the experimental preliminary investigation and literature data through mathematical modelling.

3. Validation of the developed models (Chapters 6, 7)

Where the literature data is insufficient, an extensive experimental study will be conducted for parameter generation and to confirm findings from the preliminary investigation. Where needed the models will be improved to better reflect new findings.

A schematic of the planned approach is given in Figure 2.8.

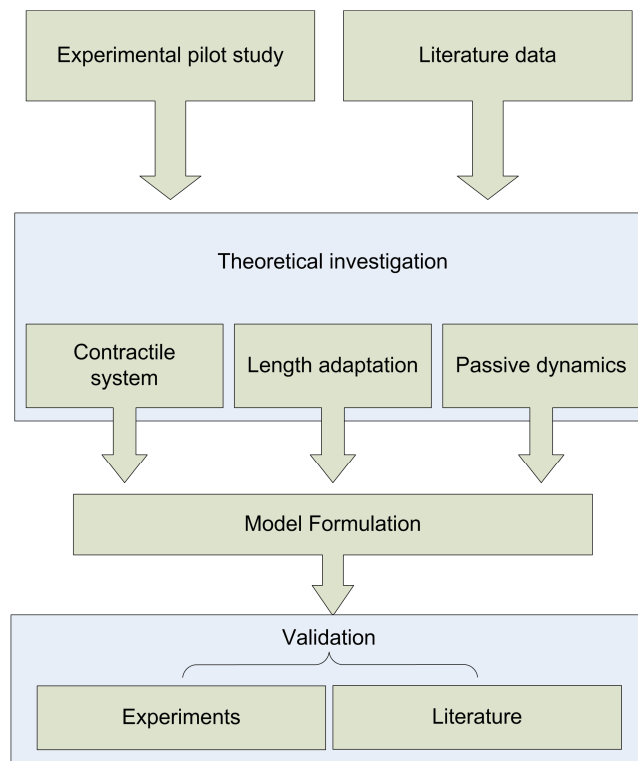


Figure 2.8: Flow chart of research plan

CHAPTER 3

Preliminary Investigation

3.1 Introduction

This chapter describes a series of experiments which were designed to increase the understanding of the dynamic behaviour of relaxed ASM. While a large body of data exists on contracted ASM (Chapters 1 and 2), little has been reported on relaxed ASM, particularly with regards to tissue dynamics. The experiments discussed in this chapter were designed to explore the behaviour of relaxed ASM leading to the development of mathematical models described in Chapter 5. Parameter generation and validation experiments are discussed in Chapter 6.

This experimental study is based on a novel approach to the research into passive ASM dynamics. Where most of the published experiments focus on the frequency response, the current research looks at individual mechanical events to analyse the relaxation response in isolation. The isolated mechanical events take the form of step length changes, which are hypothesised to show power law relaxation of force. It is thought that a thorough understanding of this power law relaxation combined with understanding of the superposition of length changes can lead to a mathematical model capable of describing continuous dynamics.

The experiments were conducted at Auckland University of Technology. The majority of the set-up had to be acquired, and protocols for tissue handling, reference procedures and solutions had to be developed.

The set-up, control programs and protocols are discussed in Section 3.2. Verification of the set-up and protocol performance is discussed in Section 3.3. The 4th section of this chapter deals with the applied experimental protocols followed by the results in Section 3.5. Section 3.6 contains the analysis of the results.

3.2 Equipment, procedures and programs

A brief description of the equipment, procedures and programs is given here, with more specific details in referenced appendices.

3.2.1 Tissue acquisition

Prior to tissue acquisition a physiological salt solution (PSS, composition in mM: 110 NaCl, 0.82 MgSO₄, 1.2 KH₂PO₄, 3.39 KCl, 2.4 CaCl₂, 25.7 NaHCO₃ and 5.6 Dextrose) was made with Millipore MilliQ 18 MΩ water. The solution is bubbled for at least 10 min with 95% O₂/5% CO₂ and subsequently stored in an airtight container on ice. Another batch of PSS was left at room temperature and bubbled continuously.

Tissues were acquired from porcine tracheas from Auckland Meat Processors. The experiments were not subject to ethics approval requirements at AUT. Each trachea was extracted from the animals less than 30 min after slaughter. Connective tissue was removed and the trachea was flushed with the chilled PSS before it was placed in an airtight container containing chilled PSS and placed on ice for transport. On arrival at the laboratory the PSS was refreshed and bubbled for at least 5 min. Preliminary investigations showed little change in viability of tissue in the first 48 h after tissue acquisition. All experiments were performed within these 48 h.

3.2.2 Dissection

A section of approximately 3 cartilage rings was dissected from the trachea. The connective tissue on the outside of the section was removed until the trachea showed no loose appendages or bloody tissue. An axial section was dissected opposite the site of smooth muscle connection. This allowed the section to be laid flat without straining the muscle connection between the open ends of the c-shaped cartilage rings (Figure 3.1a). The four corners of the section were pinned onto a silicon dissection tray filled with chilled PSS, with the epithelium facing upwards. Two incisions were made through the epithelium on both sides of the ASM connection sites to allow removal of the epithelium, which was subsequently stripped from the airway (Figure 3.1b). Next, the connective tissue on the opposite side of the smooth muscle layer was removed after turning the airway section (Figure 3.1c). The airway was again turned and two incisions were made along the muscle length axis 3 mm apart. Silk thread (3/0 USP) was used to bind both ends of the muscle with square knots (Figure 3.1d). The silk threads were then suspended from the motor lever and the base connector of the set-up.

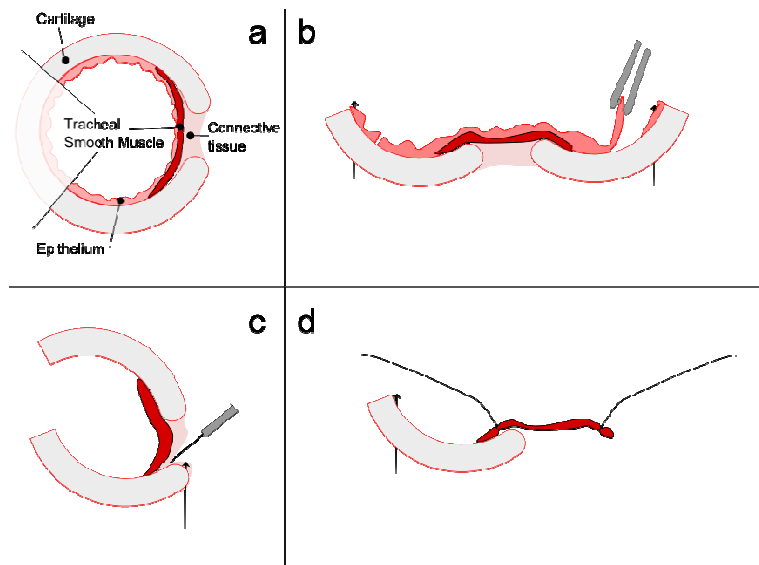


Figure 3.1: Schematic representation of dissection process. In (a) a cross-section of the tracheal ring is shown. (b) Shows the removal of epithelium. In (c) the connective tissue is removed and in (d) the smooth muscle bundle is tied with silk strings.

3.2.3 Experimental Set-up

A tissue testing set-up was acquired and assembled. A system diagram of the tissue set-up is given in Figure 3.2. Each of the components shown in the diagram is briefly discussed below.

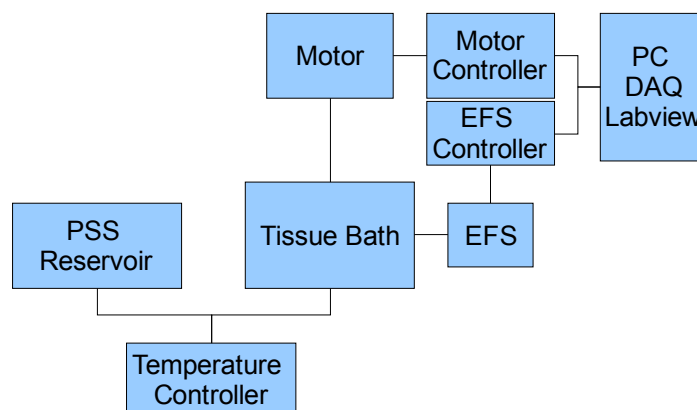


Figure 3.2: System diagram of tissue testing set-up. EFS=Electrical Field Stimulations, DAQ=Data Acquisition.

- Tissue Bath (Figure 3.3): This consists of a 50 ml water jacketed reservoir with in and outlets for flow-through of temperature regulated fluid. A gas bubbler for bubbling with 95% O₂/ 5% CO₂ is inserted in the bottom

connector and an entry valve and exit valve are mounted at the top and bottom of the bath, respectively. The bath can be moved vertically relative to the dual mode motor, tissue bottom clamp and Electrical Field Stimulation (EFS) electrodes. The tissue was suspended vertically using silk threads, one connected to the motor, another to a screw operated clamp.

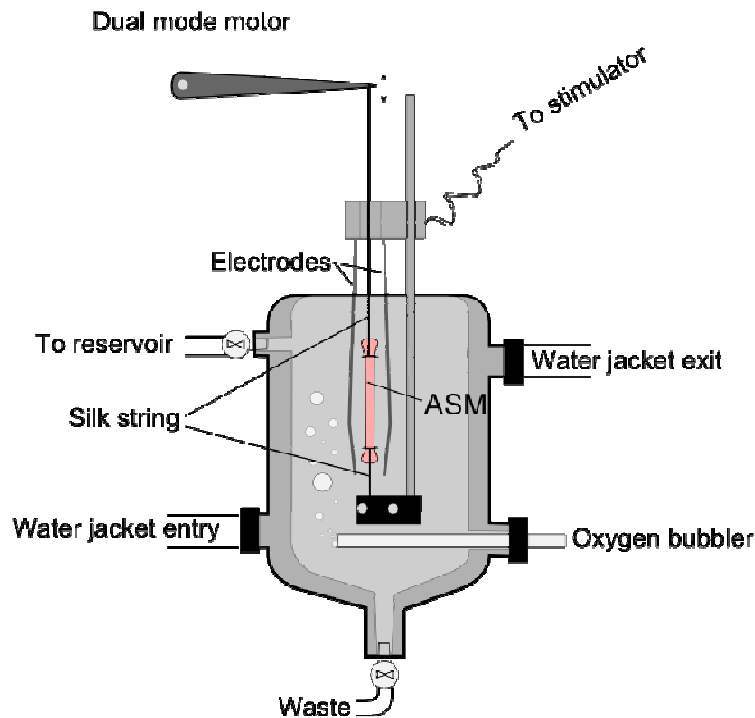


Figure 3.3: Drawing of Aurora Scientific 805A set-up.

- Reservoir: A 1 L water jacketed reservoir is filled with PSS and connected to the tissue bath. The fluid flow to the tissue bath is regulated by a 2 way valve.
- Temperature control: A circulating temperature controller (B.Braun Thermomix 1419) is attached to both the PSS reservoir and the tissue bath. While the described experiments were performed at room temperature (21 °C), the temperature controller was primarily used as a fluid pump to warm up the reservoir fluid, which was stored at 4 °C.
- EFS and EFS controller: rectangular EFS platinum electrodes (2x50 mm, 30 AWG (American Wire Gauge)) were positioned in the tissue bath around the tissue. The electrodes were controlled by an Aurora Scientific Stimulator 800A, allowing for both unidirectional and bidirectional 0-80 V DC pulsed (0.1, 0.5 or 1 ms) 0-1 A current limited EFS.
- Dual mode motor and controller: A Cambridge 300C dual mode motor and controller provide switchable length (0-3 mm range) and force (0-500 mN)

control of the tissue by analogue input signal or through dial operation on the controller. The controller also provides an analogue output force and length signal with variable amplification (1-10 x) with a maximum output range of -10 to 10 V on both channels with total ranges equal to the input ranges.

- The system was controlled through a Data Acquisition Card (NI 6024E) using National Instruments Labview (version 6.0).

3.2.4 Programs

For data acquisition of the force and length signal and the generation of the force and length signal three programs were developed. Similar but improved programs were used for the experiments discussed in Chapter 6, which are described in Appendix C.

- Equilibration.vi: A small program that reads the force data (10 Hz) while the tissue is equilibrating after it is mounted in the set-up. The force data is stored in a Tab-separated spreadsheet file in an automatically generated folder (based on date) and file (based on time).
- Data_generation.vi: This program generates input files for the length and EFS signals in a Labview native file format. The input screen allows for a number of functions to be generated, such as step, staircase, sinusoidal and triangular functions.
- Data_acquisition.vi: This program reads the files generated by Data_generation.vi and generates the length and EFS signals accordingly. Simultaneously the length and force data is recorded and written to two automatically generated files in Tab-separated text files, one at 3000 Hz for high resolution analysis and one at 100 Hz for high speed analysis.

3.2.5 Reference length procedure

To minimise variability of tissue behaviour between samples, a reference length procedure was developed. Several approaches for defining the reference length have been suggested in the literature, none of which are unanimously agreed upon [106]. Unlike skeletal muscle, ASM does not possess a constant optimal length for force generation (Chapter 2). However, it is assumed that ASM does possess a length range at which it can adapt to a stable optimal force generating capacity. This length range is most likely set by the length of the muscle prior to slaughter and storage, and the

dissection and mounting procedures applied subsequently. The purpose of a reference length procedure is to find the present optimal length for maximum force generation. This minimises the subsequent force changes caused by continuing length adaptation. The methodology used for finding the present optimal length has a strong influence on the actual optimal length found. Several studies have shown that differences in stretch amplitudes, contractile stimuli and timing can result in large differences in optimal length [109, 158-160].

Several procedures are commonly used:

Single stretch from slack length. The muscle is stretched by a certain percentage of slack length (for instance, 200 % in bladder smooth muscle [161]) under the assumption that this brings the tissue close to optimal length. However, some preliminary experiments have shown that a clearly defined slack length does not exist or is difficult to establish.

Manually adjust to predetermined starting force. The length of the tissue is adjusted until a certain predetermined force is reached, as a percentage of anticipated contractile force [128, 162]. To correct for the different force generating capacities of tissues, the width or estimated cross-sectional area of the tissue is used to scale the setting force. However, large variations in starting length to optimal length ratios means cross-sectional area ratios between the two lengths will vary equally.

Passive to active force ratio. The optimal length has been found to correlate with the length at which the force in relaxed ASM is about 10 % of the force in contracted porcine ASM [110]. This force-ratio is species specific [69, 118]. To find this length, a series of contraction relaxation cycles has to be applied.

Direct search for optimal length. The most common approach to establishing a reference length is by conducting a search for the current optimal length [41, 77, 133]. A series of stretch, equilibration, contraction and relaxation cycles is applied and the reference length is defined as the length at which the difference between the total contractile force and the prior relaxed force (i.e. the active force) stabilises or decreases from one contraction to the next.

While each of the above procedures does not guarantee establishing the same reference length repeatedly, the direct search procedure is the most repeatable. The greatest benefit of this procedure is that it does not rely on either the hard to determine slack length or the variable force generating potential. Although the procedure is more time consuming than others, if the time between contractions and the magnitude of length changes is kept constant, the optimal length range will be clearly defined. The main pitfalls of this procedure lie in applying excessive length changes which may damage/alter the tissue, or insufficient length changes, which may result in too much length adaptation during the procedure.

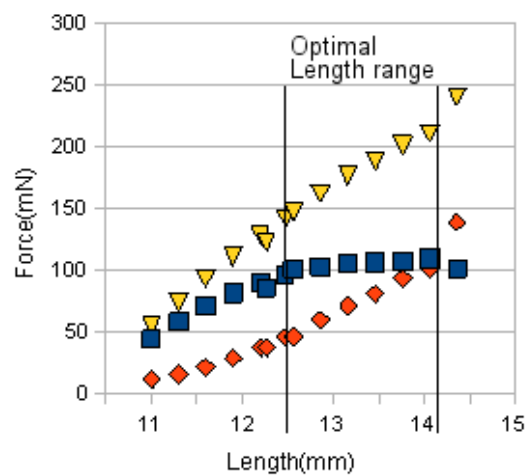


Figure 3.4: Data from optimal length procedure. ▼ = Total Force; ■ = Active Force; ◆ = Passive Force. Optimal length range represents the range at which active force reaches a plateau.

In this research a series of optimal length procedures showed that rather than an optimal length, a large optimal length range is found (Figure 3.4). The following procedure was developed to find the onset of this optimal length range:

1. After suspending the tissue in the tissue bath it is allowed to rest for 1 h close to slack length at the first sign of tension (about 1 mN of force).
2. Subsequently the tissue was subjected to cycles of the following sequence:
 - a. Stretch (approximately 5% of tissue length)
 - b. Rest (2 minutes) to allow the force to stabilise.
 - c. EFS (1 minute) to establish the current contractile force.

- d. Rest (3 minutes) to allow the force to stabilise after contractile stimulation.
3. When the active force was found to level off for 3 subsequent cycles, the tissue was stimulated 3 more times with EFS to further accommodate the tissue to the current length before the experiments commenced.

3.2.6 Tissue Rejection criterion

The tissue was rejected when the active force development was less than 80% of the peak active force at the end of the reference length procedure as this rundown reflects deterioration of the tissue. Often however the peak active force increased with time, especially if the tissue was allowed to rest for a prolonged stretch of time.

3.2.7 Equilibration

Tissues were equilibrated between experiments to minimise the effect of prior experiments on future length changes. Equilibration consisted of a contracture with ACh 10^{-5} M for 300 s followed by a recovery in PSS for 500 s until force had completely stabilised.

3.3 Experiments

Three sets of experiments were conducted at this stage of the research. The first set consists of a series of experiments to check the accuracy of the setup by replicating data from the literature. The second set was to assess the power law relaxation, in particular to investigate if it extends to power law relaxation of force and power law force adaptation after length reductions. The last set was designed to further investigate the fundamentals of power law relaxation.

3.3.1 Experimental protocols

3.3.1.1 *Validation.*

The only established systematic analyses of dynamic ASM tissue behaviour to date are from Gunst (1983) [129], Shen et al. (1997) [134] and Fredberg et al. (1997) [122, 123]. The experiments by Gunst involved large amplitude oscillations (30% of the starting length), which lead to permanent changes in the behaviour of the tissue. This is not desirable for verification purposes. The constant velocity oscillations of

varying magnitude and frequency by Shen et al. were applied in direct succession whilst ignoring any mechanical history effects of prior oscillations. However, the sinusoidal oscillations by Fredberg et al. were applied at each frequency and amplitude during individual contractures, which minimises any mechanical history effects. For validation purposes this was deemed most repeatable.

The following procedure was applied. The tissue was activated with 10^{-5} M ACh. After equilibration for 10 min the tissue was exposed to sinusoidal length changes of 0.2 Hz for 120 s, followed by a 5 min equilibration. Subsequently the tissue was relaxed in PSS for 10 min and the process was repeated for different amplitudes of oscillation.

3.3.1.2 Power law relaxation investigation

Two key features of ASM dynamic behaviour have been revealed in isolated cell experiments: (1) power law relaxation of the stiffness after a sudden application and release of torque in a cell and (2) a featureless frequency response. The second feature indicates a lack of resonance frequencies over a wide range of the investigated frequencies. Conventional springs and damper configurations cannot explain such a frequency response or power law relaxation. As these features may be related, finding a mathematical description of one of the features might explain the other feature as well.

To understand the dynamic behaviour of a material or mechanism, usually its response to external excitation such as step length changes, pulses and ramped length changes is assessed. In ASM tissues, step length changes can reveal both the instantaneous stiffness and the relaxation response. Ramped length changes can provide information on the viscous nature of the tissue and the dependence of the relaxation parameters on the speed of length changes. Rapid consecutive length changes show what principle of superposition applies to the muscle, to provide a bridge to continuous length change response.

Besides these three types of length changes the effect of oscillations on subsequent length changes was assessed to determine if strain induced softening or ‘fluidization’ central to the soft glasses theory applies by changing subsequent step length responses. Each of the applied protocols is described below in detail.

Protocol 1: Power law relaxation (Figure 3.5A). To test for the existence of power law relaxation of force and the stability of this power law relaxation, a series of length steps were applied with amplitude $a_s=0.5$ and 1% of L_{ref} and $\Delta t_{s1} = \Delta t_{s2}=200s$. At the same time the effect of different length change velocities was assessed by applying 0.5% L_{ref} length steps with varying ramp time $\Delta t_r=1;2$ and 4s. Other length steps in this protocol were performed with $\Delta t_r=1s$. All subsequent experiments used $\Delta t_r=0.2s$.

Protocol 2: Step amplitude (Figure 3.5A). A more detailed analysis of the sensitivity and nature of power law relaxation was performed by applying length steps, with amplitudes $a_s=0.15; 0.25; 0.5; 1$ and 2% of L_{ref} in that order. Subsequently a series with the same amplitudes but randomised in order was applied to assess whether mechanical history affects the response. $\Delta t_s=200s$.

Protocol 3: Length correlation (Figure 3.5B). To assess the correlation of power law parameters with length, several staircase functions were applied to the tissue. A staircase function from L_{ref} with 10 steps of $a_s=0.5\% L_{ref}$ to a total $a_{tot}=5\% L_{ref}$ and $\Delta t_s=5s$ was applied, followed by a 50s rest period and an equal staircase function in opposite direction. After another 50s rest period the same sequence of two staircase functions was applied in opposite direction, first decreasing in length, then increasing back to L_{ref} .

Protocol 4: Length oscillations and length steps (Figure 3.5C). The effect of length oscillations on the step response was tested to confirm if length oscillations would result in strain induced softening. The tissue was subjected to length events of the type depicted in Figure 3.5C. A total of three series of experiments was performed, with as a reference length event $a_o=1\% L_{ref}$ $a_s=0.5\% L_{ref}$; $f_o=0.2$ Hz , $\Delta t_o=10$ s , $\Delta t_{o_s}=1$ s and $\Delta t_s=200$ s:

1. Variation of Δt_{o_s} (in order: 1; 10; 150s; 10; 150; and 1 s, for $a_o=1;2$ and 4 % of L_{ref} in separate series)
2. Variation of f_o (0.2; 1 and 10 Hz)

3. Variation in amplitude ratio a_0/a_s ($a_0 = 0.5; 1$ and $2 \% L_{ref}$, with $a_s = 0.5 \% L_{ref}$, $a_0 = 0.5; 1$ and $2 \% L_{ref}$, with $a_s = 1 \% L_{ref}$, $a_0 = 0.5; 1$ and $2 \% L_{ref}$, with $a_s = 2 \% L_{ref}$)

Protocol 5: Two-phase steps and pulses (Figure 3.5D). Two series of experiments were performed to investigate the effect of proximity of one step length change to a prior step length change. First a series of length steps was applied according to Figure 3.5A, with $\Delta t_{s1} = 1; 2; 4; 8$ and 16 s for an amplitude of 0.5% and -0.5% L_{ref} and $\Delta t_{s2} = 200$ s. Second a series of experiments according to Figure 3.5B was applied, with $L_2 - L_1 = 1\%$, $L_3 - L_2 = 0.25\%$ and $L_4 = L_1$ while varying Δt_{s1} as $1, 5$ and 20 s. This was followed by $L_2 - L_1 = 1.25\%$, $L_3 - L_2 = -0.25\%$ and $L_4 = L_1$ while varying Δt_{s1} as $1, 5$ and 20 s. The same sequence was applied in opposite direction.

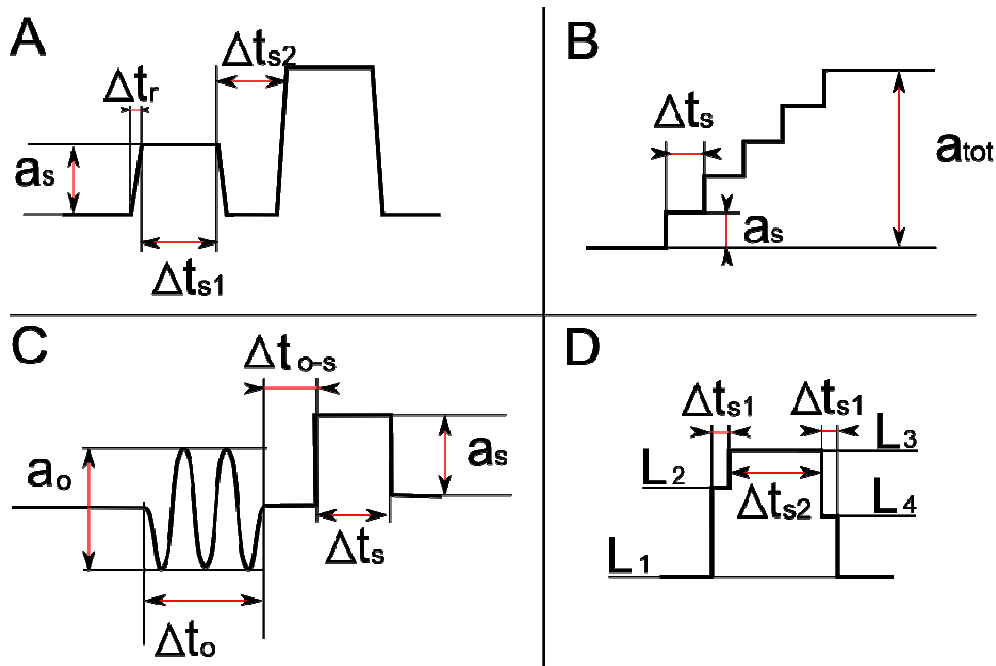


Figure 3.5: Length step protocol types applied to the muscle. A: step amplitude variation; B staircase functions; C oscillation-step protocols; D two-phase length steps. Where Δt_r is not shown its value equals 0.2 s.

All curve fits were conducted in Matlab using the EZfit package. This package uses the least squares method to generate an optimal fit. The Package fitted the power functions by minimising R^2 on logarithmic scale.

3.4 Results

Validation. The experimental force-length curves compare to Fredberg's data in shape and relative force (Figure 3.6) when relative length changes were set to approximately 75% of the length changes applied by Fredberg et al. This difference might be attributed to a species difference, as [122, 123] used bovine tracheal smooth muscle.

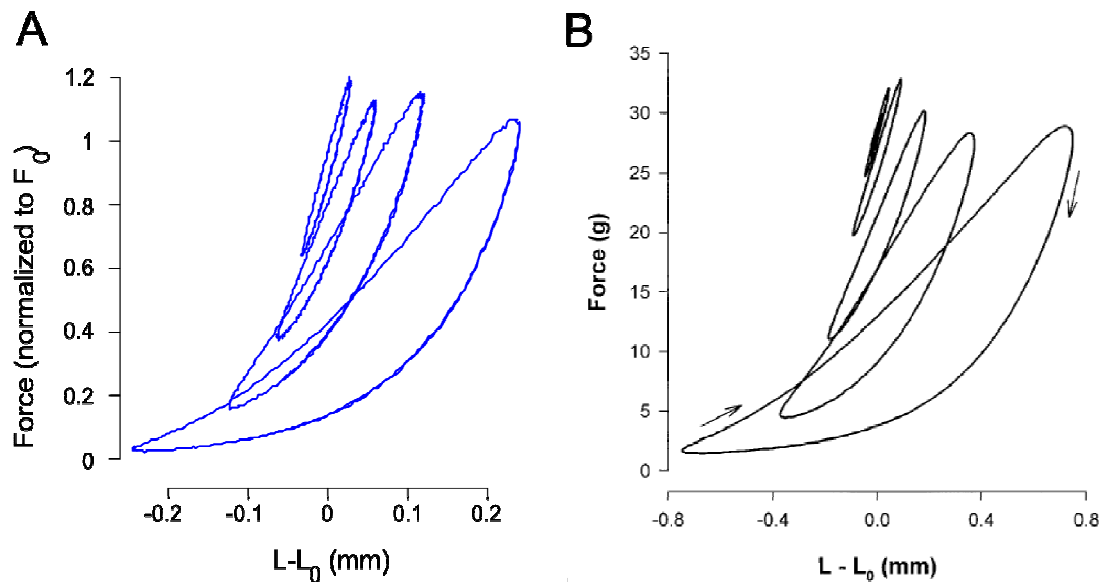


Figure 3.6: Comparison of experimental results (B) with Fredberg et al. [123] data (A)

Protocol 1. Power law relaxation. In Figure 3.7 the force response to step changes is plotted on logarithmic axes. A power law relaxation is evidenced by the near straight line on a logarithmic plot. The slight deviation in the first few samples was caused by the slow speed of length change. Length reduction showed force adaptation according to a power law, similar to power law relaxation. The power law exponent was found to nearly double with a doubling of the amplitude of stretch. Force response was very stable for each tissue independent of variations in ramp time Δt_r . However, power law relaxation and force adaptation showed large variations between tissues ($n=3$).

Subsequent experiments were conducted with a reduced ramp time $\Delta t_r=0.2$ s to enable a more detailed assessment of the power law response directly after a length change.

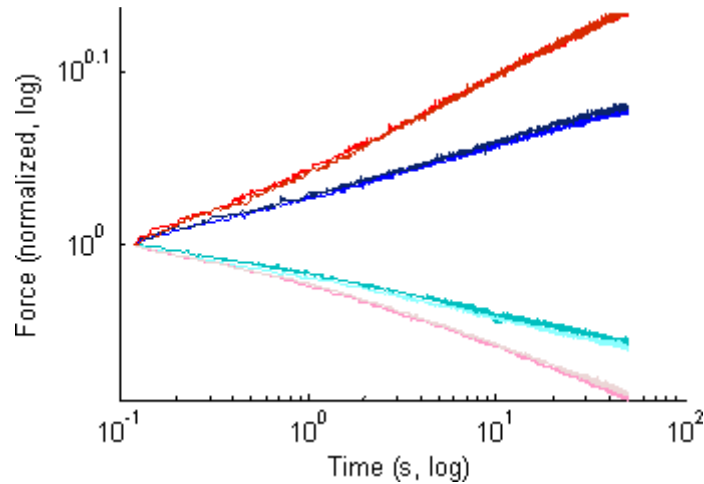


Figure 3.7: Force response to step length changes. Red lines show 2% L_{ref} length changes, blue lines 1%. Dark lines are for negative length changes, light for positive ones.

Protocol 2. Step amplitude. The force responses are plotted in Figure 3.8 on logarithmic axes. Each of the curves was normalised to the force directly after application of the length change. The dependence of step amplitude and power law exponent found in the first protocol was confirmed and extended, showing a reasonably stable force response in the first 10 s, independent of prior length changes. After the first application of the 2 % length step the subsequent length changes, particularly the smallest amplitude length steps, showed a clear deviation from power law relaxation beyond $t=10$ s. The 2 % length change also resulted in a reduction in the force level at L_{ref} which was not recovered until the next contraction.

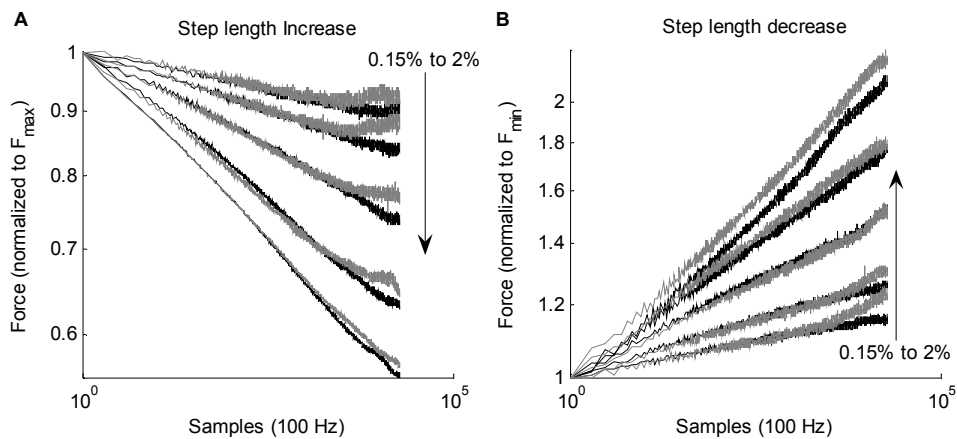


Figure 3.8: Double logarithmic force response to step length changes. Length changes applied in order of increasing amplitude are shown with black lines, random order length changes are shown with grey lines. Step amplitudes relative to L_{ref} are: 0.15%; 0.25%; 0.5%; 1% and 2%.

The step length decrease data show similar results as step length increases, but a better adherence to power functions. Deviations from power law behaviour here and in subsequent experiments were found to be caused by previous length changes. In this work this is referred to as the mechanical history effect. The absolute power law exponents were about 30% greater for length decreases and showed a non-linear correlation with step amplitude (Figure 3.9). Power law multipliers showed a strong and variable non-linear correlation with step amplitude, particularly for length increases.

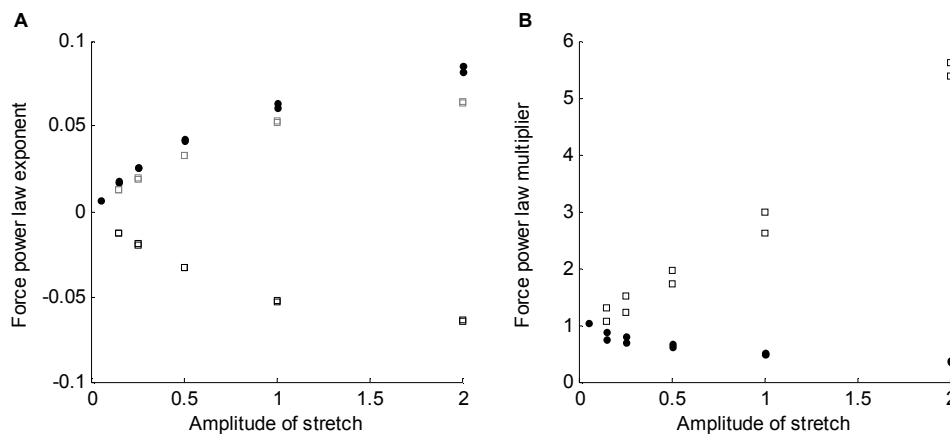


Figure 3.9: Power law exponents (left) and power law multipliers (right) versus amplitude of stretch. Circles represent length decreases, squares represent length increases. On left grey squares represent absolute values of exponents.

Protocol 3. Length dependence. A staircase function was applied to the tissue to see if the power law exponents and multipliers are dependent on the length of the tissue. For length increases the power law exponent did not vary significantly (Figure 3.10 A) while for length decreases a negative correlation with length seemed to exist, although the partial resetting of the exponent after the 50 s prolonged step (jump from red to green in Figure 3.10 B) indicates this can be accounted for at least partially by mechanical history of previous length steps. The multipliers in either case show a strong dependence on length, with a jump in the value of the multiplier after the 50 s prolonged step.

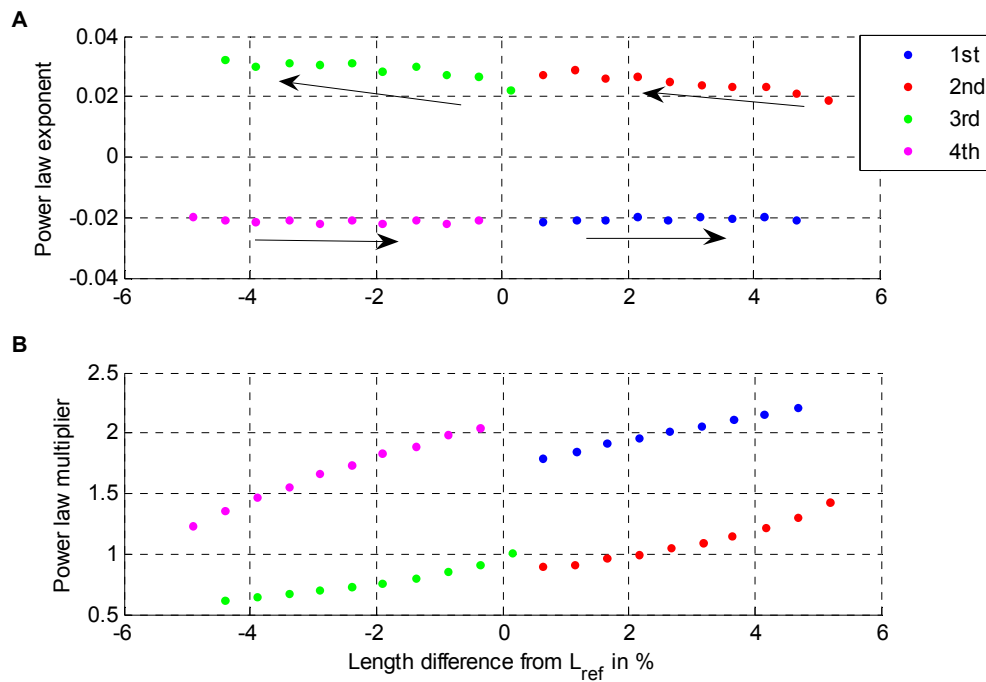


Figure 3.10: Power law exponents (top) and power law multipliers (bottom) of force response to staircase functions applied to the muscle. Arrows indicate the order in which steps were applied. Legend refers to the order in which the datasets were applied.

Protocol 4. Oscillations and step length changes. The application of oscillations prior to a length step of equal amplitude showed a small reduction in power law relaxation exponents, but only for large amplitude oscillations (Figure 3.11). Variation in the time between oscillations and subsequent length change, Δt_{o-s} , resulted in only a small difference in power law exponents, but a larger deviation from a power function for larger oscillation amplitudes. As in some of the other experiments the first length step after an EFS-relaxation cycle showed a much larger mechanical history effect from the prior oscillation and a slightly larger power law exponent (black line in Figure 3.11). Any oscillation effects were either dissipated by the time the length decrease was applied, or length decreases are less sensitive to prior mechanical events.

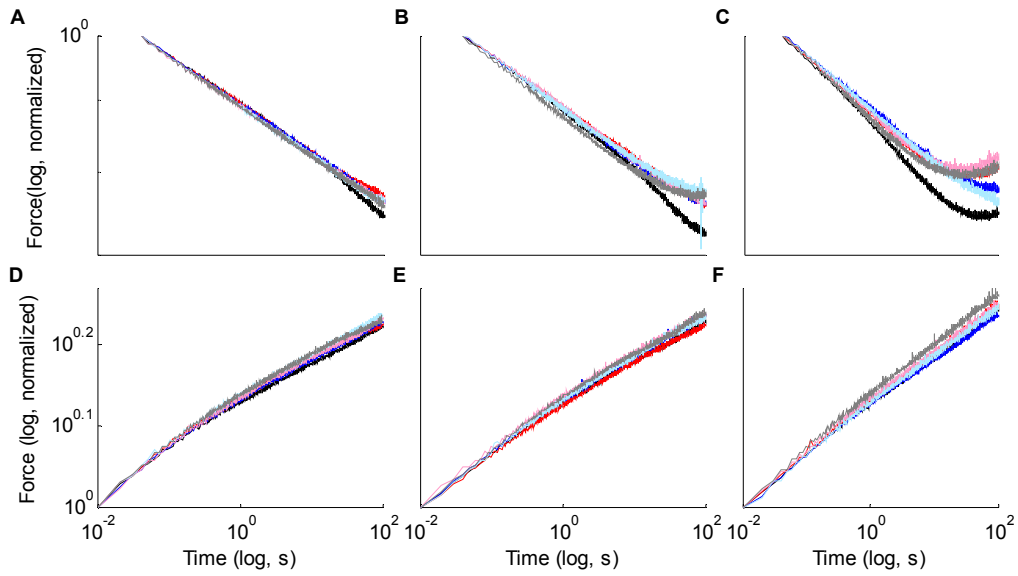


Figure 3.11: Representative sample ($n=3$) of double logarithmic force response curves of step increase (top) and decrease (bottom) in length of $0.5\% L_{ref}$ preceded by 0.5% (left), 1% (middle) or 2% (right) of L_{ref} oscillation. Colours show different values of Δt_{o-s} : $\text{—} = 1s$ $\text{—} = 10s$ $\text{—} = 150s$ $\text{—} = 10s$ $\text{—} = 150s$ $\text{—} = 1s$ (in order of application)

Increasing the frequency of the oscillations showed a clear reduction in power law exponent, which was most visible for larger oscillation amplitudes (Figure 3.12). Deviation from the power law behaviour was also more pronounced at higher frequencies. The frequency variations had no effect on subsequent step length decreases.

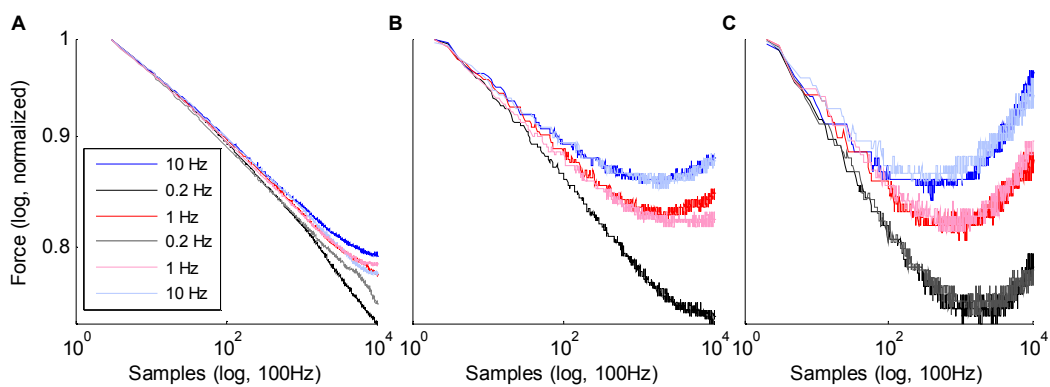


Figure 3.12: Double logarithmic force curves of step length changes after oscillations at various frequencies (see legend) and 0.5% (A), 1% (B) and 2% (C) of L_{ref} amplitudes.

Increasing the duration of oscillations showed no further change of power law exponents, but a considerable increase of the deviation from power law behaviour

(Figure 3.13). The longer duration also showed a small effect on the subsequent length decreases, but with little consistency.

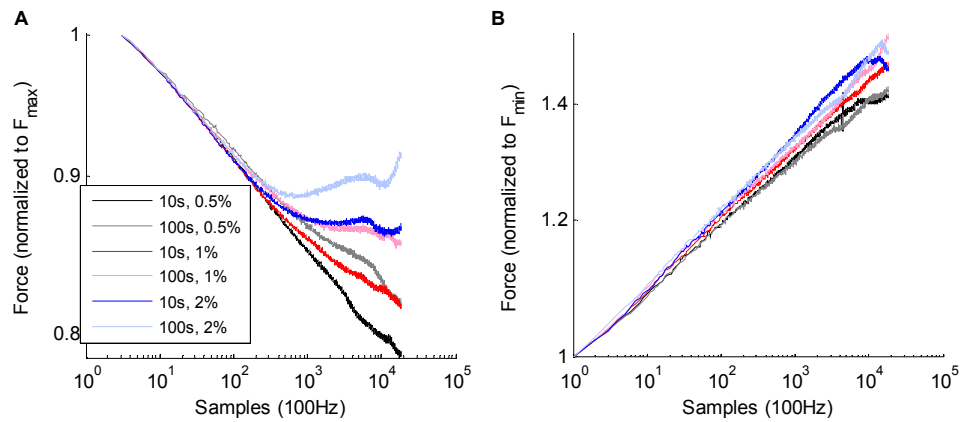


Figure 3.13: Double logarithmic force curves of response to length steps at 0.5% of L_{ref} after oscillation duration variation

Lastly, the effect of the ratio of oscillation amplitude and step amplitude was investigated. A larger ratio of a_o/a_s resulted in a larger deviation from power law behaviour (Figure 3.14). Additionally for larger step amplitudes a slight decrease in initial power law exponent was found for larger ratios of a_o/a_s . Little effect on the length step decrease was found.

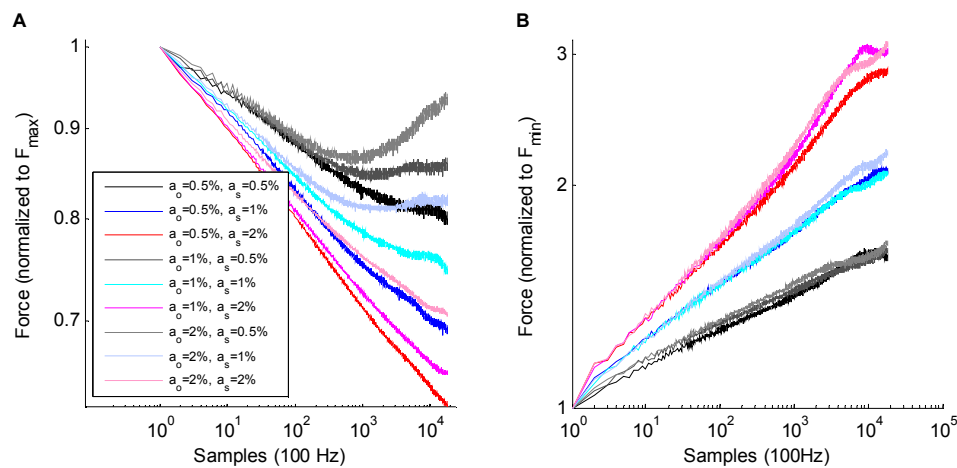


Figure 3.14: Double logarithmic force curves of step length changes after oscillations with amplitude variation. Length increase in A, length decrease in B.

Protocol 5. Two phase steps and pulses. The double logarithmic plots of the force response after a pulse length change showed a clear effect of the previous length change (Figure 3.15). The mechanical history effect in downward pulses seems to be

more pronounced. A larger time delay between steps resulted in a delayed and less pronounced history effect of the first step.

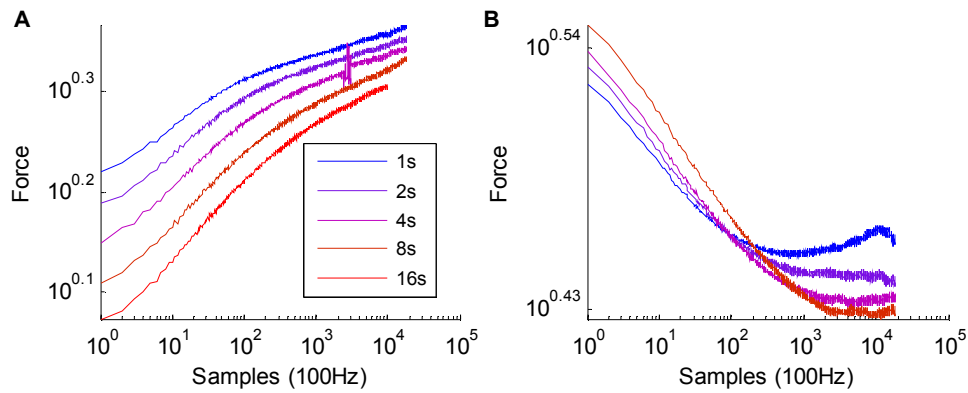


Figure 3.15: Double logarithmic force-curves of pulse length steps with varying pulse durations. Panel A shows length increase pulses, panel B shows length decrease pulses.

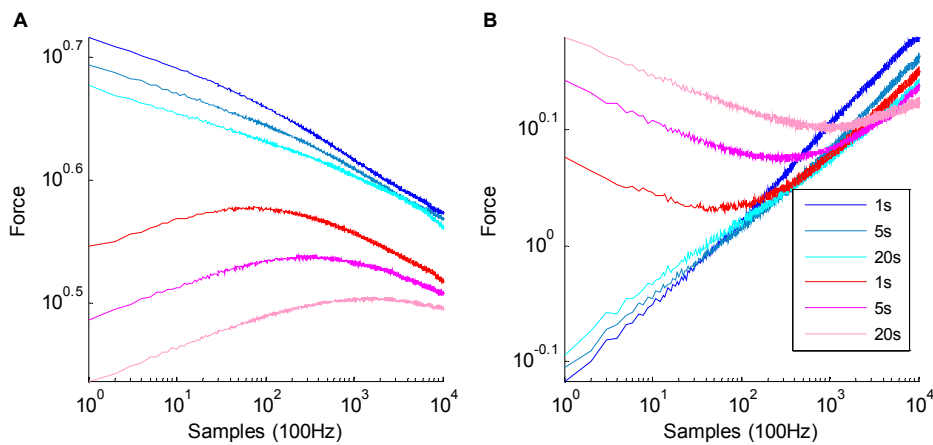


Figure 3.16: Double logarithmic force curves of compound step response with duration and direction variation. Blue curves are same direction 2%, 0.5% L_{ref} , red curves are opposite direction 2.5%, 0.5% L_{ref} . Panel A shows positive total length change, panel B shows negative total length change.

Two-phase length steps showed again that the first length step has a pronounced effect on the force response to the second length step, and the time Δt_{s1} between these length changes determined the location and curvature of the bending point of the force response curves (Figure 3.16). The effect of a prior length step in the same direction was comparatively small.

3.5 Analysis and Discussion

The force response to a step length change can be fitted accurately with a power law function of the form $F(t)=at^b$. However, a high quality of fit does not exclude other fitting functions. Even with high signal to noise ratios it is often difficult to distinguish between a low exponent power law and a logarithmic function of the form $F(t)=alog(t) + b$ (Figure 3.17). Additionally, where a good fit can be found with a power law, many good fits using a vertically shifted power law ($F(t)=at^b + c$) can be found as well.

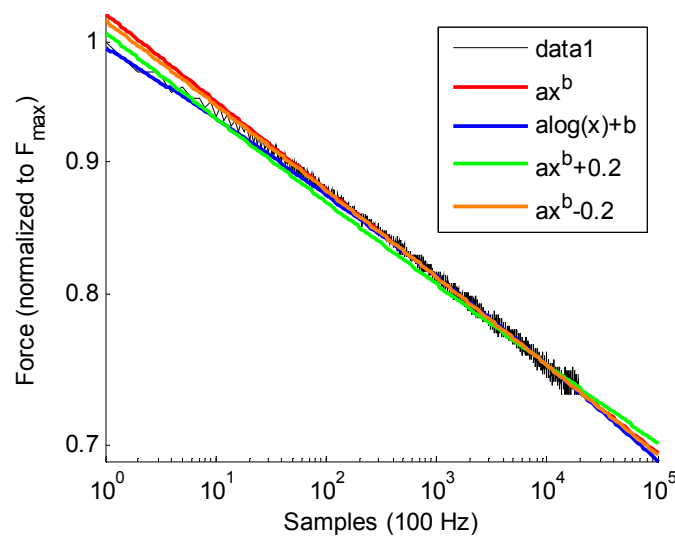


Figure 3.17: Illustration of the close resemblance of curve fits of a different nature.

Those length steps which resulted in the largest power law exponents for the assumed $F(t)=at^b$ fitting function provide the best information on which of the described functions fit ASM behaviour best. For fitting functions at^b , $alog(t)+b$ or at^b+F_{prior} , the average R^2 ($n=4$, 10 length changes per tissue) were 0.997; 0.986 and 0.987 respectively. The difference in fitting quality was more pronounced in the first 100 samples.

The effect of oscillations on power law behaviour did not seem to follow strain induced softening/fluidization. The soft glasses theory suggests that the larger power law exponent for large amplitude length changes has to be the result of greater fluidisation. Accordingly, oscillations would be expected to fluidise the tissue, resulting in higher power law exponents. What seems to be the case is that oscillations

do not affect the power law exponents much except when their amplitude is much larger than the subsequent step length change. Instead of raising the power law exponent, the power law exponent is decreased. Possibly an increased fluidisation from oscillations could reduce the internal distortion from a length change and accordingly result in a lower power law exponent. Nonetheless oscillations seem to have a lasting effect on subsequent step responses as large deviations from power law response were found after large oscillations relative to step length changes.

To get a better understanding of the principle of mechanical history superposition a curve fitting analysis of the pulse and two-phase response experiments was performed. Two different possible mechanical history paradigms are analysed:

1. Power law cumulative history

Power law cumulative history describes the superposition of mechanical events as a linear superposition of force. For two consecutive length steps the expected force response of the 2nd length step is then:

$$F_c(t) = F_{prior} + a_1(t)^{b_1} + a_2(t - \Delta t)^{b_2} \quad (3.1)$$

With Δt the time between the two steps and a_i and b_i constants. F_{prior} is the force prior to the first length step, t is zero directly after the first length change

2. Power law multiplicative history

Multiplicative history describes the superposition of mechanical events as a multiplication of their individual effects. This theory is proposed because multiplication of two power law functions leads to summation of their exponents. Consequently a linear correlation between step amplitude and power law exponent results, which seems close to the observed data. While multiplication of responses seems counterintuitive, it is equivalent to linear superposition on logarithmic scale. As a power function is linear in a double logarithmic domain, superposition of length changes is likely to obey linear superposition in this domain. For two consecutive length steps this would lead to a force response after the 2nd length step of:

$$F_m(t) = a_1(t + \Delta t)^{b_1} a_2 t^{b_2} \quad (3.2)$$

The principles proposed here are certainly not exhaustive, and none of the principles have to occur in their proposed form.

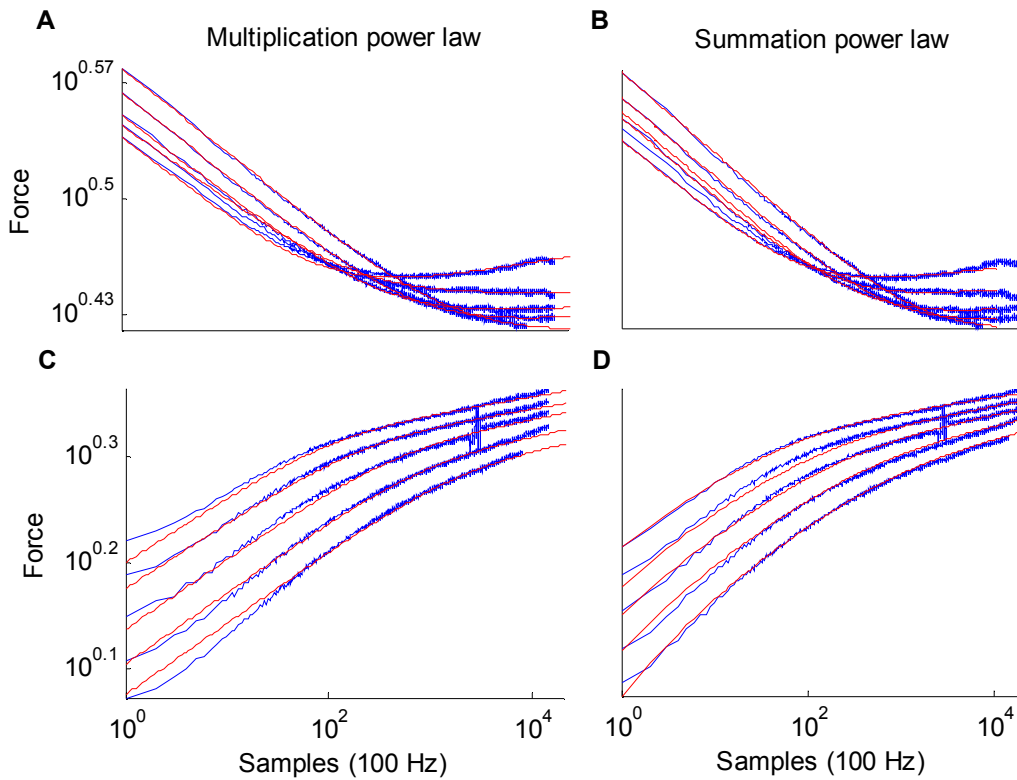


Figure 3.18: Curve fits to pulse response data, using paradigm one and two.

Using $F_c(t)$ with a_1 and b_1 according to the first length change did not result in a high quality of fit in any of the pulse functions. For negative length change pulse functions no good fit could be found for the first length change at all. If a_1 and b_1 were kept as variables, resulting in a 4 parameter curve-fit, a decent fit of the data could be found (Figure 3.18, Table 1). These fits are not unique, as with four free parameters the least squares fitting procedure can result in many local minima.

Table 3-1: Data on summation of power laws. Constants refer to the constants in Eq. 3.1. The data represent the assisted curve fit values determined by forcing a_2 and either d_2 or b_2 to be constant. These conditions provided the most accurate curve fits as determined by the regression coefficient R^2 .

Δt , for $L_p > L_e$	a_2	b_2	c_2	d_2	F_{prior}
1	4.0342	-0.0181	-4.5404	-0.028	2.369
2	4.0342	-0.016	-4.6495	-0.028	2.3331
4	4.0342	-0.015	-4.6589	-0.028	2.2585
8	4.0342	-0.014	-4.7005	-0.028	2.1972
16	4.0342	-0.0133	-4.7802	-0.028	2.1663
Δt , for $L_p < L_e$	a_2	b_2	c_2	d_2	F_{prior}
1	-2.5372	-0.1	2.1911	-0.0888	2.9193
2	-2.5372	-0.1	2.2725	-0.096	2.8638
4	-2.5372	-0.1	2.3043	-0.0956	2.77
8	-2.5372	-0.1	2.3517	-0.0963	2.7153
16	-2.5372	-0.1	2.4545	-0.1018	2.6911

Curve fitting using fitting function $F_m(t)$ led to a much improved result (Figure 3.18, Table 2). For positive length change pulse functions, full conservation of the power law exponent of the first length change was found (Table 2). Negative length changes showed a much better quality of fit for the first length change from L_1 to L_2 than the fits found for cumulative paradigm, but full conservation of the power law exponent was not found. As only three free parameters for curve-fitting were required for $F_m(t)$ ($a_1 \cdot a_2$ is taken as one variable), good quality of fit curve fits could be found without trial and error parameter searches. While the power law exponent of the first length change was not maintained for negative length pulses, the power law exponent seemed to be consistently reduced by a factor 3, independent of the time between the first and second length change. Additionally for both positive and negative pulses the second length step resulted in an approximately constant power law exponent.

Solidification-fluidisation theory would suggest one power law exponent for both length steps when their effects are combined. This was not found in either of the tested mechanical history principles. As the multiplicative mechanical history theory seems to represent the data most accurately, the remainder of the data was further analysed under the assumption of the existence of a (partial) multiplicative power law mechanical history.

Table 3-2: Data on power law multiplication. Constants a and b are defined in Eq. 3.1. Curve-fits were determined by setting a_1 equal to the multiplier of the force response curve of the first length change.

Δt , for $L_p > L_e$	a_1	b_1	a_2	b_2	c_2
1	6.3578	-0.0457	1.956	-0.0457	0.06183
2	6.3892	-0.0466	1.9179	-0.0466	0.06204
4	6.3695	-0.0474	1.8227	-0.0474	0.06601
8	6.3676	-0.049	1.7648	-0.049	0.06715
16	6.3374	-0.0488	1.707	-0.0488	0.06751
Δt , for $L_p < L_e$	a_1	b_1	a_2	b_2	c_2
1	0.4575	0.16138	2.6885	0.05457	-0.0472
2	0.44466	0.1562	2.7105	0.04648	-0.0435
4	0.42191	0.15418	2.6421	0.04806	-0.0453
8	0.40609	0.15143	2.6251	0.04905	-0.0476
16	0.39538	0.14712	2.6577	0.04788	-0.0493

To further investigate the sequential multiplication in ASM, the variable amplitude pulse experiments and the variable amplitude ratio two phase step experiments were fitted with fitting function $F_m(t)$. For every pulse or two phase step first the assumption of power law exponent conservation was applied. Secondly both power law exponents were assumed variable and the integrated error on double logarithmic scale for each fit was compared to assess whether conservation of power law exponent applied (Figure 3.19). The integrated error is defined as the area between the data and the fitting curve on logarithmic axes. Both positive amplitude pulses and two phase length steps with a positive first length change showed an integrated error difference close to zero, indicating that the quality of fit of the two parameter curve fit was similar to the three parameter curve fit. As previously found for the pulse data in Table 3-2, negative amplitude pulses and two phase length steps with a negative first length step showed a larger integrated error difference. For pulses this error was larger for larger pulse amplitudes, but this might have been caused by the larger parameter sensitivity of these pulses and does not necessary imply a worse fit. For two phase length steps the smallest $\Delta L_1 / \Delta L_2$ ratios for negative ΔL_1 showed a much larger

integrated error, even though the parameter sensitivity of the power law exponents is smallest for these small $\Delta L_1 / \Delta L_2$ ratios.

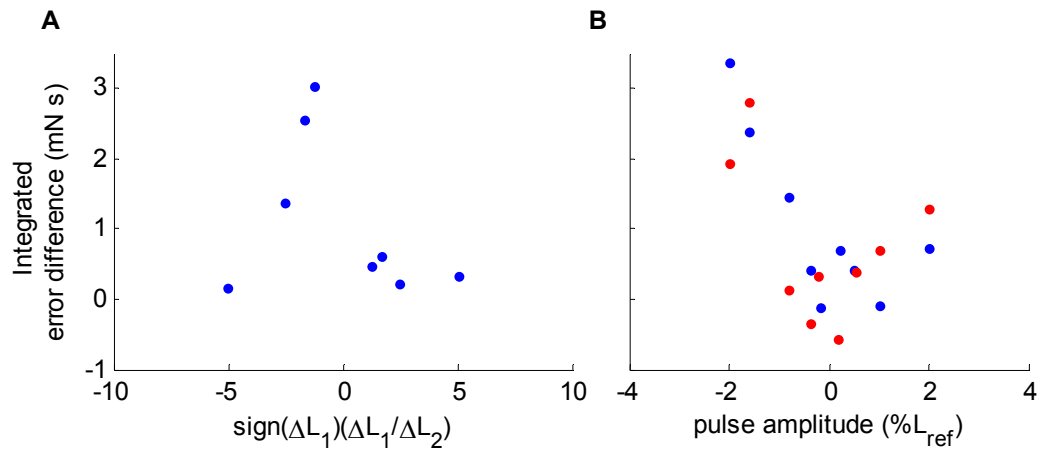


Figure 3.19: Integrated error difference for pulses (B) and two-phase length changes (A).

The main outcome of this analysis is that sequential multiplication with full conservation of power law exponent applies quite accurately to any sequence of two length steps where the first length step is positive. When the first length step is negative the power law exponent of the first length step is reduced if the second length step is comparatively large. This could mean that sequential multiplication exists, but large positive length steps can partially erase the effect of prior length steps, while negative length steps of any size do not affect the prior length step relaxation at all.

With the assumption of sequential multiplication, the stiffness might be expressed as $F_{\text{post}}/F_{\text{prior}}$ rather than absolute force change (Figure 3.20). Like the relatively constant power law exponent found in Figure 3.10 the relative force change also showed nearly constant values, except for a small increase for positive length changes at very small lengths.

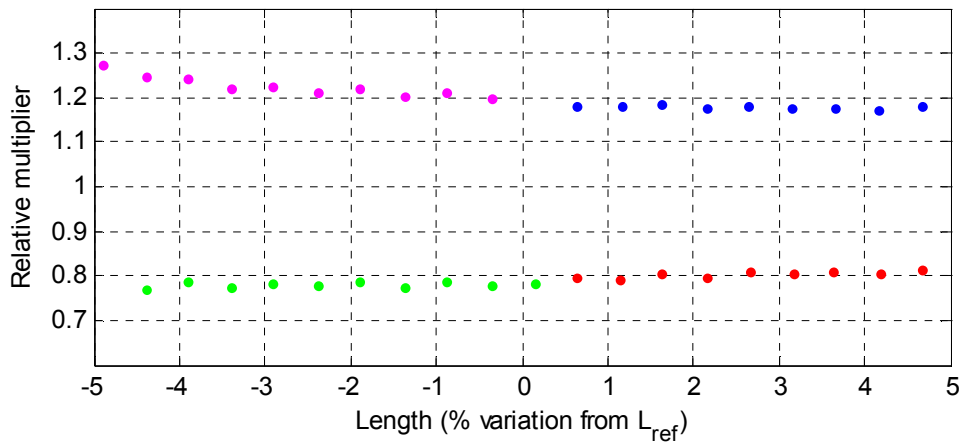


Figure 3.20: Staircase relative power law multipliers. Staircase functions were applied in the following order: ●=positive length changes, ●=negative length changes, ●=positive length changes.

3.6 Closure

While the number of repeat experiments discussed in this chapter do not suffice for statements of statistical significance, some important trends have been identified that warrant further investigation. Firstly the existence of power law behaviour was confirmed for a wide range of length change amplitudes and length change ramp times. Secondly sequential multiplication seems to apply to relaxed ASM tissues. The detailed experimental investigation described in Chapter 6 was designed to confirm these two major findings and to characterise the sequential multiplication.

CHAPTER 4

Contraction and Length Adaptation Model

4.1 Introduction

The development of a contraction and length adaptation model is discussed in this chapter. As discussed in Chapter 2, there are a number of mathematical models available to describe ASM cell mechanical behaviour with respect to contractile mechanics. The most commonly used model of smooth muscle contraction is the 4 state latch bridge model proposed by Hai and Murphy [64, 65]. This model and the later proposed improvements aimed to describe the biochemical processes within the cell and the force development in isometric contractions. Validation of the model is based on a combination of experiments on some of these biochemical processes and isometric contractions. However, no direct evidence exists as yet of the dephosphorylated slow cycling latch bridge, which is a key feature of the model. Also little data exist on the robustness of the model under conditions of varying load or length. Therefore to find a suitable model of contractile dynamics, the HHM model needs to be further analysed under dynamic conditions and compared with simplified models to reveal whether the complexity of the HHM model is warranted, particularly for use in a length adaptation model.

Here contraction and length adaptation in ASM dynamics is investigated using a modelling approach. The criteria for the performance of a contraction model are formulated in Section 2 of this chapter. The contraction model investigation starts with the implementation and a novel analysis of the HHM model in Section 3. Next, in Section 4, a simplified model is proposed and analysed based on the HHM model. In Section 5 an empirical contraction model is proposed and analysed under the same conditions. Section 6 discusses the performance of each of the three models based on the criteria in Section 2. In the 7th section a novel length adaptation model is described, which is discussed in Section 8.

4.2 Contraction model criteria

ASM contraction differs from skeletal muscle contraction in its ability to allow force maintenance at low energy cost, slower contraction speeds and a decrease in shortening velocity from the onset of contraction. A major limitation in determining the minimum requirements to be satisfied by a contractile model is that the effects of passive elements and the potential evanescent and recurring non-contractile cross links between structural proteins are unknown. A reduction in shortening velocity may be attributed to a change in the resistance to shortening. Similarly, any reported dynamic behaviour of contracted ASM could be caused by a mixture of matrix material, contractile element behaviour and length adaptive behaviour. Consequently, the strength of a contraction model is strongly dependent on the strength of the length adaptation and passive element models. As a result, some of the criteria were deemed weaker than others. In this work the following criteria are considered.

Activation increases force on reported timescales, see

1. Figure 4.1.

A contractile model must show contraction, i.e. a gradual increase in force upon activation, followed by a force plateau. Some studies ignore the activation process and only analyse contracted muscles. To work in parallel with a length adaptive model, which is expected to show most changes at the onset of a contracture, this early phase of contraction is essential to be simulated in the model. However, the timescales of contraction might be influenced by the passive material context and the potential length adaptive events at the onset of contraction.

**This image has been removed
by the author of this thesis
for copyright reasons.**

Figure 4.1: Acetylcholine contractions in dog trachealis smooth muscle [86]. Line labels show ACh concentrations.

2. Optimal length characteristics.

While optimal length is not a fixed property in ASM, many studies have shown the existence of optimal length behaviour (Chapter 2). Optimal length is defined as the length at which maximum force can be generated during contraction, which is believed to coincide with optimum actin-myosin filament overlap [106]. This feature could be implemented as a correction factor following from a length adaptation model.

Shortening velocity decreases from onset of contraction.

While shortening velocity in smooth muscle is the result of a balance of forces between passive and contractile processes, the pronounced reduction in shortening velocity after the initial spike at the onset of a contraction is usually attributed to contractile action [142, 163]; see Figure 4.2. It is possible that increased cross linking of the cytoskeletal matrix and contractile elements results in a decrease in shortening velocity potential.

**This image has been removed
by the author of this thesis
for copyright reasons.**

Figure 4.2: Force - shortening velocity relationship at different times during contraction with neural stimulation (EFS) in bovine trachealis smooth muscle. From top to bottom curves were measured at 5, 15, 60 s and 30 minutes after onset of EFS [142].

- ## 3. Oscillations with peak length above L_{ref} reduce contractile force while oscillations with peak length equal to L_{ref} do not.

The only known systematic investigations on oscillations in contracted ASM tissue which describe oscillations are the sinusoidal oscillations by Fredberg et al. (1997) [122, 123] and the constant velocity oscillations by Shen et al. (1997) [134]. The effect of oscillations above L_{ref} could also be attributed to length adaptive processes [87] or passive element behaviour.

4. The Central Processing Unit (CPU) intensity of the model must be sufficiently small to enable the calculation of force in multiple contractile elements in the length adaptation model.
5. Parameters should be uniquely defined for given circumstances, and easily obtained using experimental data.

This criterion minimises the ambiguity of the contractile model component in the analysis of the total ASM dynamic behaviour.

For any model to be developed the performance is assessed based on these criteria.

4.3 4-state Latch bridge model

The 4-state model developed by Hai and Murphy [64, 65, 99] is the most widely used model for smooth muscle contraction. Mijailovich et al. (2000) [115] used this model to simulate sinusoidal oscillations. Here a similar implementation of the model is combined with novel implementations of grid shifting, series and parallel elastic elements and filament overlap correction. The full implementation of the model is described below.

4.3.1 Methodology

The governing equations for the 4-state model were given in 2.4 and 2.5. When written out fully these lead to (see Chapter 2 for nomenclature):

$$\begin{aligned}
\frac{\partial n_1(x,t)}{\partial t} + \frac{dx}{dt} \frac{\partial n_1(x,t)}{\partial x} &= -k_1 n_1(x,t) + k_2 n_2(x,t) + g(x) n_4(x,t) \\
\frac{\partial n_2(x,t)}{\partial t} + \frac{dx}{dt} \frac{\partial n_2(x,t)}{\partial x} &= k_1 n_1(x,t) - (k_2 + f_p(x)) n_2(x,t) + g_p(x) n_3(x,t) \\
\frac{\partial n_4(x,t)}{\partial t} + \frac{dx}{dt} \frac{\partial n_4(x,t)}{\partial x} &= -(g(x) + k_6) n_4(x,t) + k_5 n_3(x,t) \\
\frac{\partial n_3(x,t)}{\partial t} + \frac{dx}{dt} \frac{\partial n_3(x,t)}{\partial x} &= -(g_p(x) + k_5) n_3(x,t) + f_p(x) n_2(x,t) + k_6 n_4(x,t)
\end{aligned} \tag{4.1}$$

In these equations x represents the position of the myosin head fulcrum to the actin filament. As the filaments are assumed inelastic, dx/dt is uniform for all myosin heads. This allows for solving the set of equations using the method of characteristics [115, 164], which calculates the solution to the partial differential equations by defining them as a family of ordinary differential equations on the characteristic curves representing the myosin head positions x as a function of t as expressed in Figure 4.3.

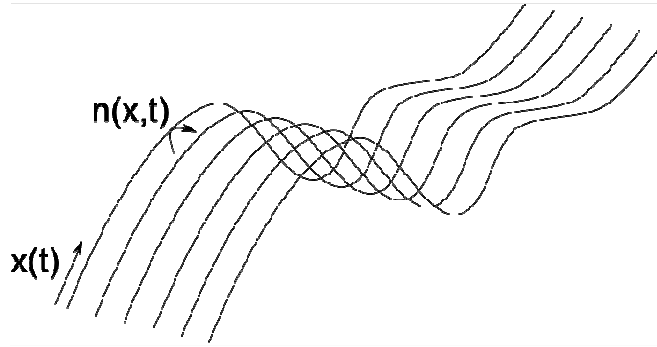


Figure 4.3: Method of characteristics. The parallel set of curved lines $x(t)$ shows the global movement of myosin heads relative to the actin filament. As the myosin filament moves as a whole, each of the myosin heads has the same dx/dt , but different starting values of x . the variation of $n(x,t)$ occurs on these common curves, and can be expressed through ODEs for given $x(t)$.

On the characteristic curve n_i is only dependent on the variable t , which reduces the equations to:

$$\begin{aligned}
\frac{dn_1(x,t)}{dt} &= -k_1 n_1(x,t) + k_2 n_2(x,t) + g(x) n_4(x,t) \\
\frac{dn_2(x,t)}{dt} &= k_1 n_1(x,t) - (k_2 + f_p(x_0)) n_2(x,t) + g_p(x) n_3(x,t) \\
\frac{dn_4(x,t)}{dt} &= -(g(x) + k_6) n_4(x,t) + k_5 n_3(x,t) \\
\frac{dn_3(x,t)}{dt} &= -(g_p(x) + k_5) n_3(x,t) + f_p(x) n_2(x,t) + k_6 n_4(x,t) \\
x(t, x_0) &= x_0 + \int_0^t v(\tau) d\tau
\end{aligned} \tag{4.2}$$

In which x_0 represents the starting positions of the myosin heads and $x(t, x_0)$ are the characteristic curves.

In the isometric and length controlled case, $x(t, x_0)$ is known and the model can be solved directly using numerical methods. The numerical solution is found using the Runge-Kutta 4/5 method as follows:

Rewriting Eq. 4.3 as a set of functions f with N a vector containing $n_1..n_4$ gives:

$$\frac{dN}{dt} = f(t, x(t, x_0), N(t)) \tag{4.3}$$

Applying the Runge-Kutta 4/5 method results in the following set of weighting functions P_i :

$$\begin{aligned}
P_1 &= f(t_n, x(t_n, x_0), N(t_n)) \\
P_2 &= f(t_n + \frac{1}{2} dt, x(t_n + \frac{1}{2} dt, x_0), N(t_n) + \frac{1}{2} dt P_1) \\
P_3 &= f(t_n + \frac{1}{2} dt, x(t_n + \frac{1}{2} dt, x_0), N(t_n) + \frac{1}{2} dt P_2) \\
P_4 &= f(t_n + dt, x(t_n + dt, x_0), N(t_n) + dt P_3)
\end{aligned} \tag{4.4}$$

In which dt is the time step interval. The fractional state populations at time t_{n+1} then become:

$$N(t_{n+1}) = N(t_n) + \frac{1}{6} dt (P_1 + P_2 + P_3 + P_4) \tag{4.5}$$

The above equations are calculated for each myosin head position, which are implemented as an equal spaced grid stretching from 0 to 1 with a set number of grid points (N_g). The total stiffness can now be calculated as the sum of the population fraction of attached cross-bridges:

$$K(t) = \sum_{x_n} n_3(t, x_i) + n_4(t, x_i) \quad (4.6)$$

The force on one myosin head can be calculated as the displacement of the head relative to its unstrained position (x) multiplied by the stiffness of a single myosin head, k_{cb} . The total force then becomes the sum of these forces from all attached heads:

$$F(t) = \sum_{x_n} k_{cb} x_i n_3(t, x_i) + k_{cb} x_i n_4(t, x_i) \quad (4.7)$$

The used rate constants are from Mijailovich et al. [115] and given in Table 4-1.

4.3.1.1 Grid shifting

This definition of the total force will only be valid for isometric (constant length) contractions as the model assumes a single actin binding location for all myosin heads ($dx/dt=0$). During length changes some detached myosin heads move away from the area within which the myosin head can bind to the actin binding location. On the actin filament the distance between myosin head binding locations is assumed to be h , which equals the distance between myosin heads. As the model is centred around the myosin head rather than actin, a myosin head which attaches to the next actin binding location results in the same force according to Eq. 4.7. In this work this is avoided by relocating the detached myosin head populations that move from one actin binding region to another to $1/h$ (the distance between myosin binding locations on actin) back into the initial actin binding region.

A visual explanation of this restructured grid is given in Figure 4.4. In A, an unattached myosin head fulcrum (red) moves within attaching distance of an actin binding site, and a fraction of the myosin heads at this location attach (green). Moving further, a fraction of heads remains attached, but now causing a drag on the movement (B). At this point the detached myosin heads have moved from the region around the

first actin binding site to within the next actin binding region. By moving all the detached heads a distance h (the distance between two actin binding locations) to the left (B-C), the actin binding landscape for these heads remains the same. As detached heads do not contribute to the total stiffness or the total force, the mechanical properties of the system are not changed. Now the detached myosin heads can again attach to the actin binding site (D) while the drag from the previous attachment remains until these heads detach. A consequence of this grid shifting is that the size of the grid has to be equal to the largest imposed relative movement between actin and myosin.

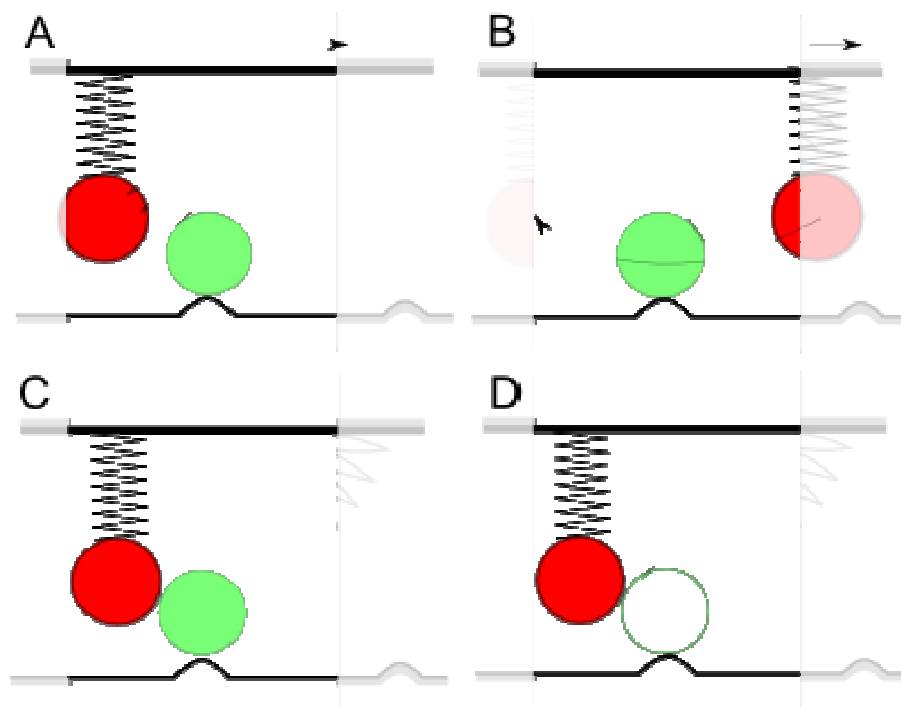


Figure 4.4: Visual representation of grid shifting. From A to D: a myosin head (green ball) attaches to actin in A, which is strained as the myosin filament moves to the right (B). As the model's myosin reference frame only looks at one actin binding location, the unattached myosin (red ball) in B can not attach to actin, despite it being in the binding region of the rightmost actin binding site. To correct this, the myosin head is moved one binding distance (h) to the left (C), which, as it is unattached, does not affect force or stiffness values. Subsequently the myosin head can bind to the unique actin binding location (D).

4.3.1.2 Optimal length

In this work, to account for an optimal length (L_{opt}) of the contractile element, a correction factor (α) for both stiffness and force is introduced. For an individual contractile element this correction factor is directly dependent on the actin and myosin

filament overlap and thus on the length of the actin and myosin filaments (L_{range}). This leads to the following formulation of the correction factor:

$$\alpha = -\left| \frac{L - L_{opt}}{L_{range}} \right| + 1 \quad L_{opt} - L_{range} \leq L \leq L_{opt} + L_{range} \quad (4.8)$$

$$\alpha = 0 \quad L < L_{opt} - L_{range} \quad or \quad L > L_{opt} + L_{range}$$

An alternative approach is to reduce the number of active myosin heads according to Eq. 4.8 and assuming a return to the unattached state when the contractile element moves towards optimal length. This requires a more complicated implementation while the difference in response is expected not to be significant.

4.3.1.3 Force control

Force control has been implemented for the analysis of shortening velocity. A novel iterative sequence is proposed to calculate the element length for a given force:

1. The element force is calculated without length change.

$$\Delta L_1 = 0 \quad (4.9)$$

2. The second iteration estimates the length change from the previously calculated force, the given force and the stiffness of the contractile element.

$$\Delta L_2 = \frac{F_{in} - F_1}{K_1} \quad (4.10)$$

3. Subsequent iterations estimate the length change from the previous length change plus an estimated change in length based on the ratio of the change in length and force between the previous two iterations, which is multiplied by the remaining error in force of the previous iteration. This is equivalent to a linear extrapolation of reduction in force error and the applied change in length of the previous two iterations.

$$\Delta L_i = \frac{(F_{i-1} - F_{in})(\Delta L_{i-1} - \Delta L_{i-2})}{(F_{i-2} - F_{i-1})} + \Delta L_{i-1} \quad i > 2 \quad (4.11)$$

During force oscillations a relative accuracy within 10^{-7} % of the actual force could be achieved within three to six iterations.

4.3.1.4 Parallel and series elastic elements

In this work the HHM model was extended to include either a series or a parallel linear elastic element. A parallel elastic element represents the elasticity of the cell membrane and extracellular tissues. The series elastic element makes up 7-20% of the muscle length compared to less than 1% in skeletal muscle [165, 166]. This elasticity is attributed to a combination of the sections of the contractile elements which are not currently overlapping and the part of the cytoskeleton responsible for the transmission of contractile force. A parallel elastic element, in a length controlled simulation, acts as an additional force and stiffness, without any effect on the contractile element's behaviour. However, a series elastic element affects the contractile element as the length of the contractile element is not constant anymore. The influence of series and parallel elements in force controlled simulations is reversed as a series element transmits the applied force directly the contractile element, while a parallel elastic element absorbs part of the applied force, dependent on the length. These relations are summarised in Figure 4.5.

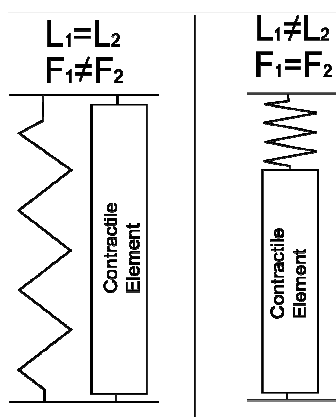


Figure 4.5: Effect of series and parallel elastic elements on force and length of contractile element. In parallel an elastic element has the same length as the contractile element, but not necessarily the same force, while in series the lengths differ, but the forces in both elements are the same.

To implement the parallel elastic element for force controlled simulations, the iteration scheme of 4.3.1.3 is changed only in the second iteration to account for the

stiffness of the parallel elastic element (K_{pe}) in the first estimation of the required length change:

$$\Delta L_2 = \frac{F_{in} - (F_1)}{K_1 + K_{pe}} \quad (4.12)$$

In the case of length control the total force is calculated simply as the sum of the forces in the contractile element and the parallel elastic element.

A series elastic element is implemented in length controlled simulations using a different iteration scheme. Rather than minimizing the error in force as in the iterations of 4.3.1.3, this scheme minimises the error between the set length and the actual total length which is determined by the sum of the length of the contractile element and the series elastic element:

1. As in 4.3.1.3 the length change of the contractile element is set to zero in the first iteration. The resulting force in the contractile element is used to calculate the length of the series elastic element.

$$\Delta L_1 = 0 \quad (4.13)$$

2. The total length of contractile element and series elastic element (L_i) is compared to the set length (L_{in}) and the required change in length of the contractile element is estimated from the combined stiffness of the series stiffness K_{se} and contractile element momentary stiffness K_{ce} . This combined stiffness is given by:

$$\begin{aligned} \frac{1}{K_{tot}} &= \frac{1}{K_{se}} + \frac{1}{K_{ce}} \\ K_{tot} &= \frac{K_{ce}K_{se}}{K_{ce} + K_{se}} \end{aligned} \quad (4.14)$$

Which leads to the following formulation for the second iteration:

$$\Delta L_2 = \frac{(L_{in} - L_i)(K_1 + K_{se})}{K_1 K_{se}} \quad (4.15)$$

3. Subsequent iterations estimate the required change in length of the contractile element from a linear extrapolation in the error of the total length and the difference in length changes of the prior two iterations:

$$\Delta L_i = \frac{(L_{i-1} - L_{in})(\Delta L_{i-1} - \Delta L_{i-2})}{(L_{i-2} - L_{i-1})} + \Delta L_{i-1} \quad i > 2 \quad (4.16)$$

For the contractile element only the length change expressed in units of h is of importance, which has to be matched by the length change of the series elastic element in isometric contractions. The initial absolute and relative lengths of neither the contractile nor the series elastic element need to be known to run the model. Therefore the starting lengths of the contractile and series elastic elements are taken as 0.

4.3.1.5 Parameter values

The determination of parameter values is complicated not only by the number of parameters, but the apparent different behaviour of smooth muscles under different contractile conditions. The original implementation of this model did not result in a single set of parameters but rather specific sets for specific data sets [64, 65]. The parameters used here are based on the parameters used by Mijailovic et al. (see Table 4-1). Figure 4.6 shows the attachment and detachment parameter dependence on the location x .

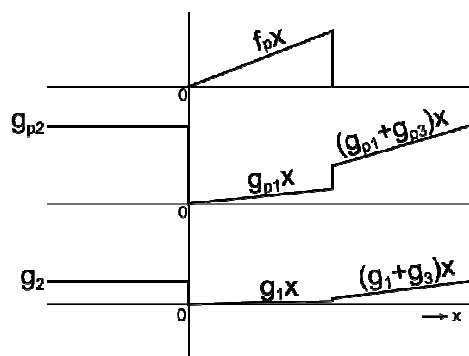


Figure 4.6: Attachment and detachment parameters in HHM model as a function of myosin head position relative to actin (x). Values for f_p, g_{pi} and g_i are given in Table 4-1.

Table 4-1: Parameter values used for HHM model

Parameter	Value	Parameter	Value
$k_1 (0 < t < 5 \text{ s})$	0.35 s^{-1}	g_3	0.03 s^{-1}
$k_1 (t > 5 \text{ s})$	0.05 s^{-1}	k_5	0.1 s^{-1}
k_2	0.1 s^{-1}	$k_6 (0 < t < 5 \text{ s})$	0.35 s^{-1}
f_{p1}	0.88 s^{-1}	$k_6 (t > 5 \text{ s})$	0.05 s^{-1}
g_{p1}	0.22 s^{-1}	k_7	0.005 s^{-1}
g_{p2}	4.4 s^{-1}	h	15.6 nm
g_{p3}	0.66 s^{-1}	s	$2 \text{ } \mu\text{m}$
g_1	0.01 s^{-1}	L	1
g_2	0.2 s^{-1}	K_{ce}	1

For Matlab implementation see Appendix A.1.

4.3.2 Results

The model was analysed on the simulation results of the following conditions:

- Isometric contraction

Primarily the effect of a series elastic element was investigated to assess how this affects the model performance and parameter settings.

- Shortening velocity

In the literature the shortening velocity is calculated directly from the relative state populations of phosphorylated and dephosphorylated attached cross-bridges. The shortening velocity in smooth muscle is measured by suddenly releasing the muscle during an isometric contraction to a certain force. The slope of the length curve after the initial sudden length decrease is the measured shortening velocity. In this work the experimental method of determining the shortening velocity was simulated and compared with experimental results from the literature

- Oscillations

Sinusoidal oscillations and constant velocity oscillations were simulated and compared with literature data.

Prior to these evaluations a simulation of sinusoidal oscillations was compared with the simulation results by Mijailovich et al. [115] to confirm if the model developed here was implemented correctly. Figure 4.7 shows that no visible difference between the two implementations exists.

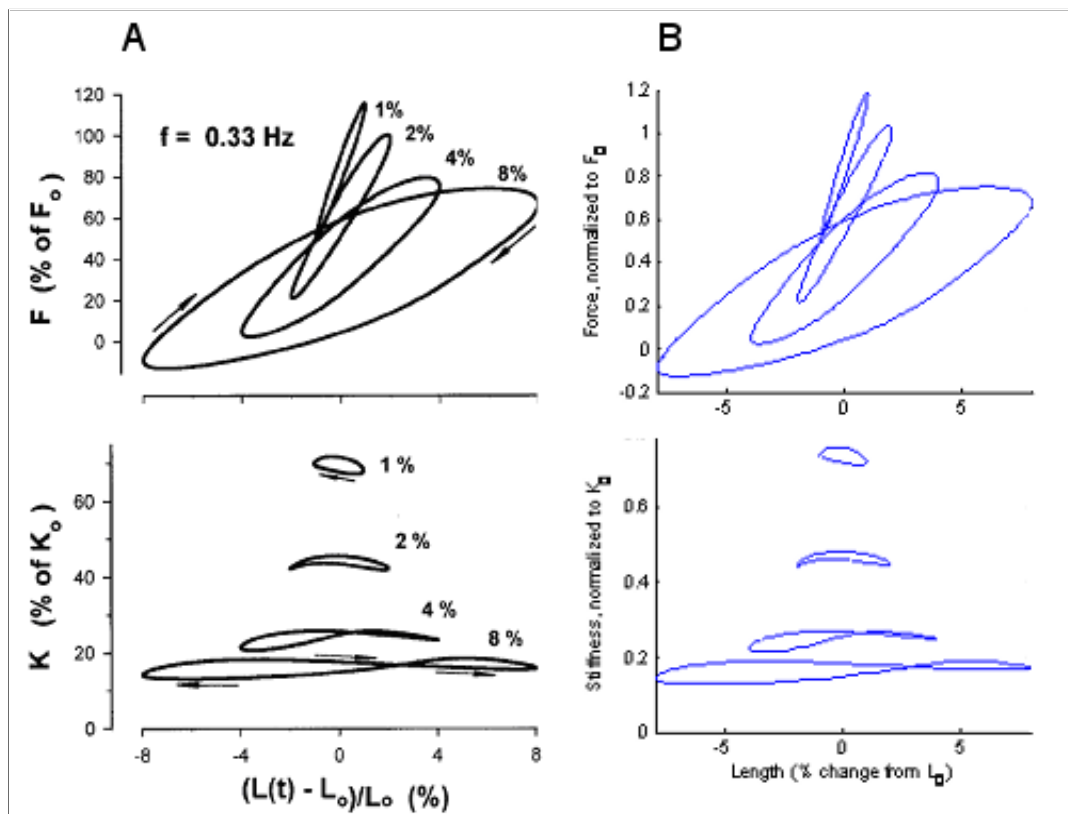


Figure 4.7: Comparison of model simulations. A: results Mijailovich [115]; B: current 4-state model implementation.

4.3.2.1 Isometric contraction

Contractions were simulated either without any series elastic elements (equivalent to an element of infinite stiffness) or with a series elastic element of 1, 2/3 and 1/3 of F_{\max}/h , the ratio of the maximum contractile force and the distance between myosin heads. This unit of stiffness was chosen to assure a known displacement of the grid and consequently no unexpected contractile element length changes beyond the allowable grid change, see 4.3.1.1. The optimal length correction factor was set to one

for all lengths as it is assumed that the shortened contractile element in case of the existence of series elasticity achieves its optimal length upon full contraction.

In Figure 4.8 the force development in time of each of these simulations is shown. The series elastic elements resulted in a decrease in the speed of force development, which is attributed to the gradual shortening of the contractile element as the series elastic element is stretched. This shortening results in additional detachment of cross-bridges because of myosin head displacement on top of the background cross-bridge attachment-detachment cycling already occurring without length changes. To match the experimental data the model parameters for attachment and detachment would have to be increased to speed up the cross-bridge cycling.

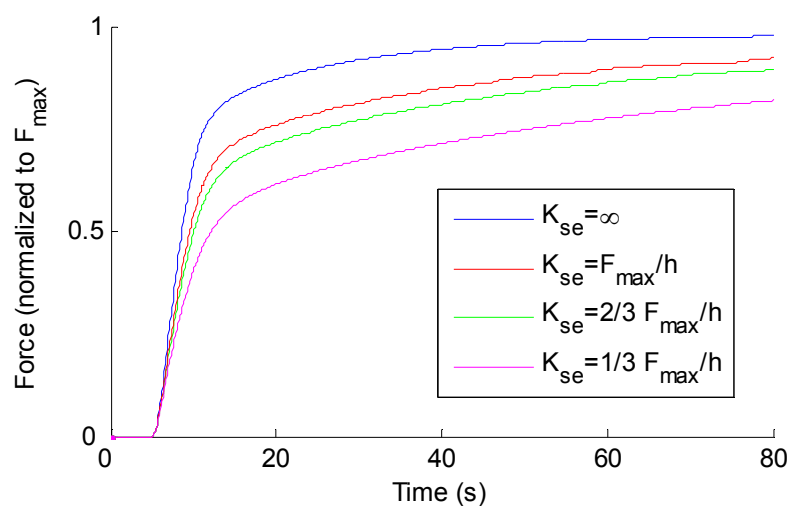


Figure 4.8: Contraction in HHM model, with varying serial elastic stiffness. Force is normalised to the maximum force during a contraction without series elastic element.

4.3.2.2 Shortening velocity

In the literature shortening velocity in the HHM model is calculated directly from the state configurations of the muscle [65, 115]. Shortening velocity is experimentally determined by releasing the contracted muscle to a certain clamp force. This results in an instantaneous shortening of the muscle, followed by a more gradual shortening process presumably governed by cross-bridge turnover rates. The instantaneous large

reduction in length upon applying the load clamp affects the cross-bridge state configurations in the muscle and filament overlap.

To investigate this effect these experimental shortening velocity manoeuvres were simulated in the HHM model. The model was contracted isometrically and at either 5, 10 or 60 seconds after initiation of the contraction a switch to force control at loads of 0; 0.2; 0.4; 0.6 and 0.8 x the maximum contractile force was simulated. This force control state was maintained for 2 s after which the model was returned to the isometric state at starting length. Figure 4.9 shows the resulting length curves. The shortening velocity was measured as the average shortening velocity in the last second of force clamp.

As shown in Figure 4.10 shortening velocity displayed similar trends to the experimental results in Figure 4.2. The shortening velocity is reduced as the contraction progresses and larger force clamp values result in smaller shortening velocities. To convert the velocities given in $h\ s^{-1}$ to $L_0\ s^{-1}$, the myosin head distance and average sarcomere length needs to be known. The myosin head distance in most studies is assumed to be around 15nm [65], and the average sarcomere length is about 2 μm [152]. Assuming sidepolar myosin filaments the shortening velocity of the contractile element is twice the shortening velocity of one actin filament relative to the myosin filament. Consequently a contractile element length change of 1 h corresponds with 1.5% total length change. Mijailovic et al. further assumed that contractile element length changes are 36% of the total muscle length changes because of series elasticity [167], which would result in a 4.2% length change per h. In shortening velocity manoeuvres however the constant load would not result in any shortening velocity contribution of the series elastic element. As a result a shortening velocity of 0.6 $h\ s^{-1}$ corresponds with a total shortening velocity of 0.009 $L_0\ s^{-1}$. This is more than twenty times smaller than in experimental data on ASM, see Figure 4.2, [85, 142, 168].

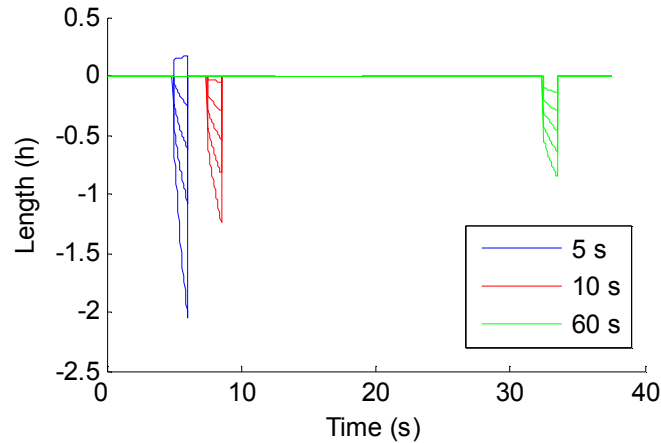


Figure 4.9: Length history during shortening velocity manoeuvre. Contraction is initiated at $t=5s$. Blue, red and green lines show shortening velocity measured at 5 10 and 60 s after onset of contraction. For each time point 5 force clamps were applied (5, 10, 15, 20 and 25% of maximum potential force) . Shortening is represented as negative length changes.

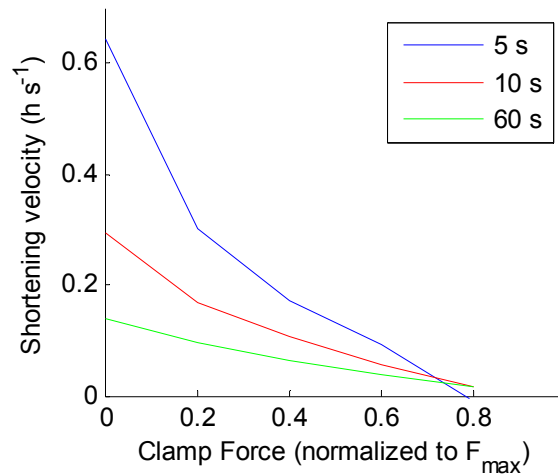


Figure 4.10: Shortening velocity versus clamp force. Unit h equals the distance between myosin heads. Different colour lines represent different times in contraction at which shortening velocity procedure is simulated.

4.3.2.3 Oscillations

Sinusoidal oscillation simulations are shown in Figure 4.7, and show a clear reduction in peak force and a reduction in force after oscillation. Full recovery of this force occurred in 20-50 s depending on the amplitude of the oscillations. Constant velocity oscillations as in Shen et al [134] showed much less of a reduction in force (Figure 4.11), in agreement with the data. The shape of the force-length curves and the

overlap of shortening legs of the force-length loops of equal shortening velocity are not accurately represented here.

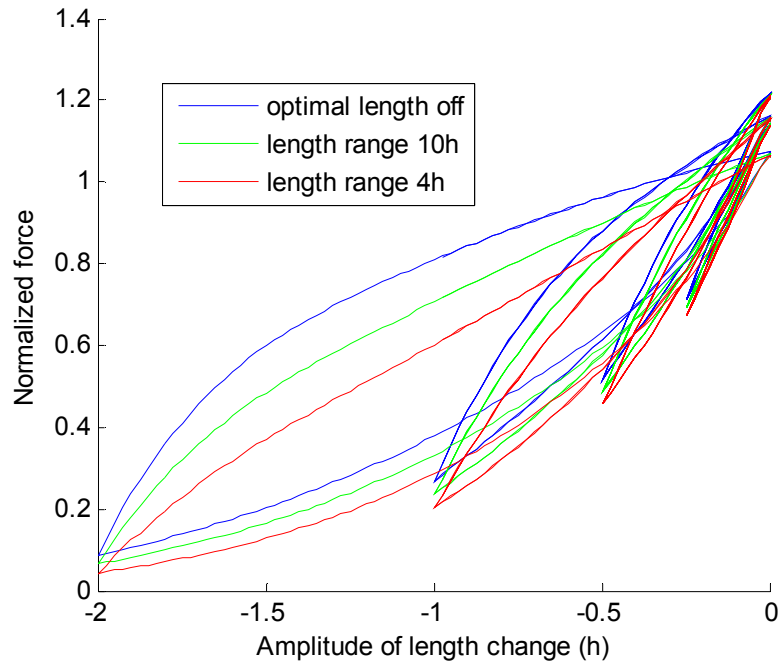


Figure 4.11: Force-length curves of constant velocity oscillations at 4 amplitudes. Force was normalised to force prior to the first oscillation, 100s after the start of the contraction. 3 different contractile element length ranges were assumed, from infinite to 4 h.

4.3.3 Discussion

The HHM model analysis showed that the model is capable of at least qualitatively reproducing a number of data sets. However, the number of parameters to be determined and the large variability in the required parameter values for different sets of experiments make it difficult to use the model for quantitative predictions. If model parameters were adjusted to reflect the shortening velocities in ASM, the >10 h relative displacements of the contractile filaments would require a very large grid size and very small time step for accurate simulation results. An initial investigation showed that this would require many months of simulation time with current PCs. Also, it seems unlikely that the required rapid cross-bridge cycling speeds would result in realistic ATP turnover rates. Moreover, the phosphorylation rates would have to be severely reduced to compensate for the much faster force development of the active cross-bridges.

4.4 Strain Dependent Release Model

To reduce the complexity of the 4 state model, particularly with regards to the number of parameters, a model much closer to the original Huxley model was developed. To ensure the low energy force maintenance characteristics of smooth muscles a reduced detachment rate in the attachment zone is applied. The result can be interpreted as a strain dependent release (SDR) model, where low energy force maintenance is not explained by a chemically different state of a lower cross-bridge cycling speed, but rather by a mechanical limit on detachment. In the SDR model, myosin heads are still assumed to generate force by rotating around a fulcrum in the neck region, but now a strain dependent mechanism prevents detachment of the myosin head until a certain portion of the rotation has been completed. Biochemically such a phenomenon has been observed in smooth muscle myosin heads [103]. In these experiments, myosin heads did not release ADP until a certain part of the power stroke was completed. The inability to release ADP implies an inability to bind with ATP. Consequently, detachment of the myosin head cannot occur until ADP is released, as ATP attachment is assumed to be necessary for detachment of the myosin head from actin.

With no direct evidence for the connection between dephosphorylation of the myosin head and the latch state, a two state model might be equally or more applicable to smooth muscle contraction if the low energy force maintenance condition can be satisfied. Additionally dephosphorylation might be an integrated part of the attachment detachment cycle, which may explain a low phosphorylation level during force maintenance in an SDR model.

4.4.1 Methodology

The SDR model is modelled here as a three state version of the HHM 4 state model, see Figure 4.12. The fourth dephosphorylated latch state is removed, but the detached dephosphorylated state is preserved to simulate the initial phosphorylation of myosin heads at the onset of a contraction. Detachment rates are quite similar to the 4 state model, with a reduced detachment rate within the attachment zone (Figure 4.13). Attachment rates in the SDR model are set to form a parabolic shape around 0.5h, which seems more likely to represent the probability of myosin head attachment rather than the ramped approach of Huxley and the HHM model. $K_1(t)$ is zero in

relaxed and high in contracted muscle while $k_2(t)$ is zero in contracted and high in relaxed muscle. The numerical solution is equivalent to the HHM model.

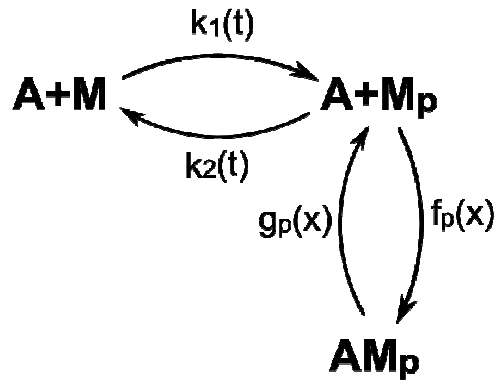


Figure 4.12: Schematic of SDR model.

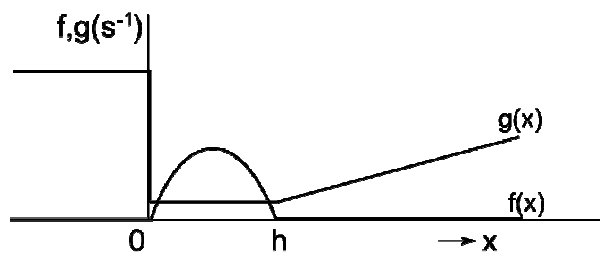


Figure 4.13: Attachment and detachment rates for SDR mode as a function of x .

The parameter values are given in Table 4-2.

Table 4-2: Parameter values SDR model

Parameter	Value
$k_{1(\text{active})}$	1 s^{-1}
f_p	0.88 s^{-1}
g_{p1}	0.05 s^{-1}
g_{p2}	4.4 s^{-1}
g_{p3}	0.66 s^{-1}
h	15.6 nm
s	$2 \text{ }\mu\text{m}$
L	1
K_{ce}	1

And $f(x)$ is given by

$$f(x) = f_p (x - 0.5 * h)^2 + 0.25 * f_p \quad (4.17)$$

For Matlab implementation see Appendix A.2.

4.4.2 Results

To allow direct comparison with the HHM model performance the same set of simulations was conducted for the SDR model.

4.4.2.1 *Contraction*

The SDR model was contracted similar to the HHM model, with the same series elastic elements values. Figure 4.14 shows great similarity to the results of the HHM model. To investigate whether the SDR model might provide an alternative means of explaining the myosin phosphorylation development in smooth muscle, force development, fractional phosphorylation and ATPase activity are shown in Figure 4.15. For this simulation it is assumed that dephosphorylation of attached myosin heads forms an integral part of the crossbridge cycle and occurs instantaneously upon attachment. The figure shows that as a consequence the myosin phosphorylation levels peak after contraction followed by a gradual reduction to a lower plateau level. This closely resembles experimental data [64, 111]. ATPase activity peaks at the instant of contractile activation, which is a result of the instantaneous activation in the simulation. A realistic contractile activation shows a more gradual phosphorylation rate development, and consequently a less pronounced peak in ATPase activity.

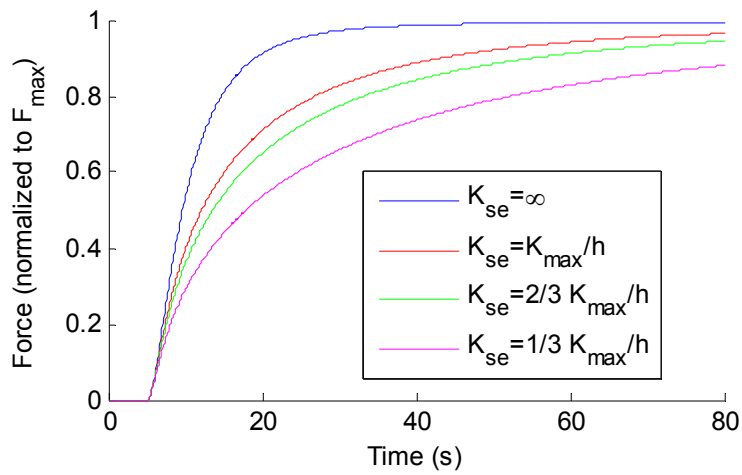


Figure 4.14: Force development during contractions in SDR model. Force is normalised to maximum force during a contraction without series elastic element.

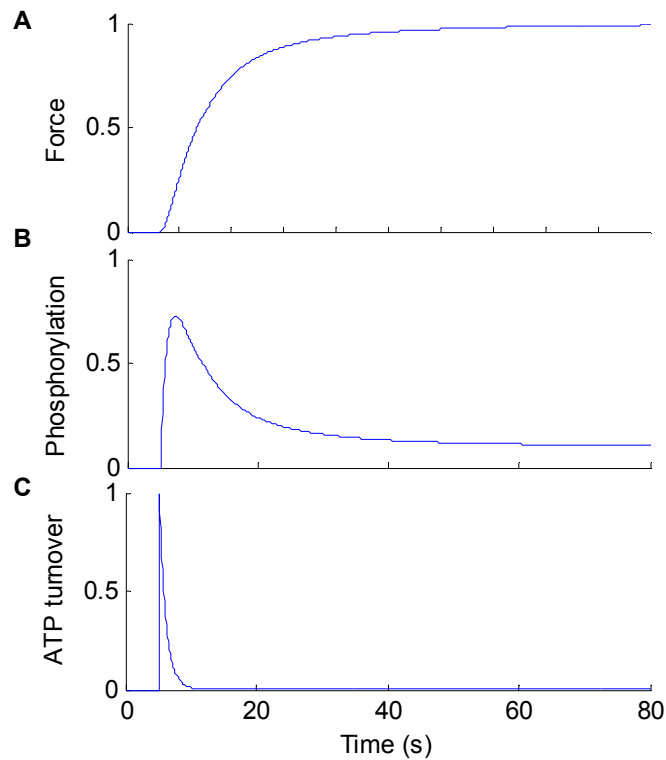


Figure 4.15: Force, phosphorylation and ATPase activity during a contraction in the SDR model. Force is normalised by dividing the total force by the number of myosin heads. Phosphorylation is expressed as a fraction of the number of myosin heads and ATPase activity is expressed as a fraction of the theoretical maximum ATPase activity.

4.4.2.2 Shortening velocity

When the same shortening velocity manoeuvres as presented in 4.3.2.2 are applied to the SDR model, the force-shortening velocity shows no change over time. In the HHM model the two crossbridge cycles, with or without dephosphorylation of the myosin heads, enable a change in shortening velocity in time as the slow cycling bridges become more dominant. Figure 4.16 shows that with a single cross-bridge cycle the shortening velocity instead becomes constant over time. The variation in shortening velocity over time could instead be caused by a change in crossbridge cycling speed because of the gradual reduction in $[Ca^{2+}]_i$. This can be modelled by making the attachment and detachment rates a function of time.

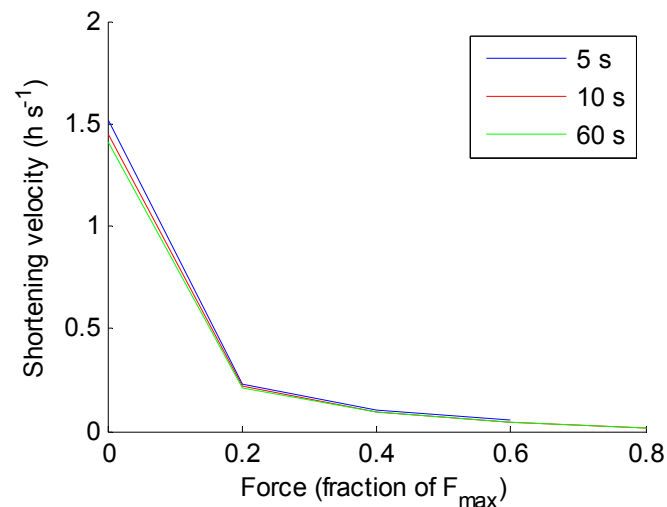


Figure 4.16: Shortening velocity in the SDR model. different colour lines represent changes in time after initiation of contraction at which shortening velocity manoeuvre was applied.

4.4.2.3 Oscillations

The force-length loops of sinusoidal oscillations are shown in Figure 4.17. For large length oscillations a much larger peak force than both the HHM model and experimental data is found. The increase in force seems to be caused by a ratchet mechanism: the relatively low detachment rate assures that cross-bridges get progressively stuck at larger lengths as the oscillation averaged attachment rate is

higher than the detachment rate. As a result the force after oscillation is slightly above the force prior to oscillation. The distinct bend in the curve at a length change of zero can be attributed to the linear optimal length correction factor which increases the slope of the curve for negative length changes, but decreases the slope for positive length changes.

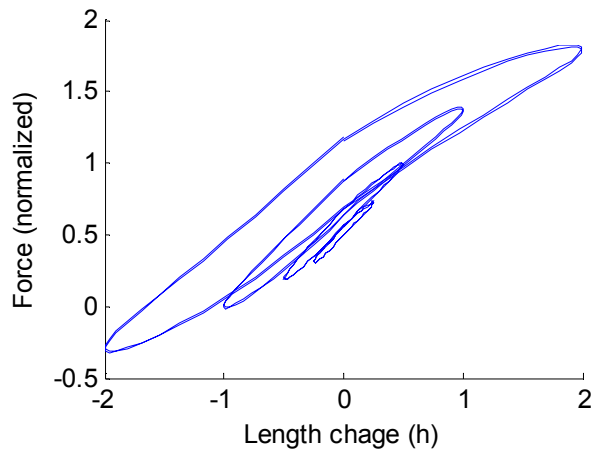


Figure 4.17: Sinusoidal oscillations of varying amplitude in the SDR model. Force is normalised to the peak contractile force.

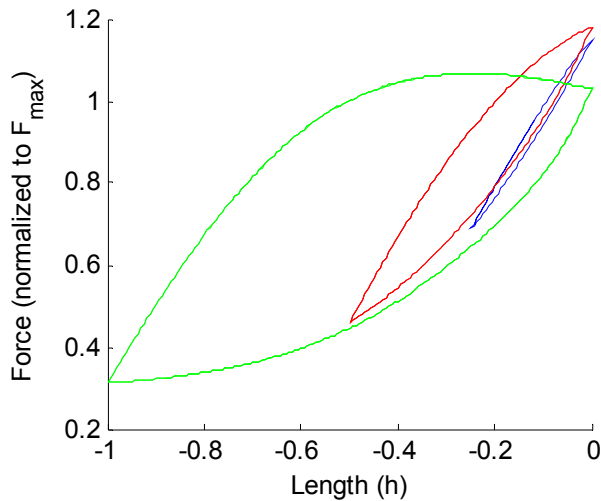


Figure 4.18: Constant velocity oscillations of varying amplitude in SDR model.

4.4.3 Discussion

The number of independent parameters in the SDR model is reduced compared to the HHM model from 6 rate constants to 4 rate constants. However this reduction results

in a less accurate modelling of shortening velocity and length oscillations, which could both be affected by either length adaptive processes or passive components.

A major disadvantage for the current research is the CPU intensive calculations required in both models. In a stochastic length adaptation model a large number of contractile elements needs to be simulated at the same time. The HHM and SDR models would require too much CPU time for such an approach.

4.5 Hill-Type model

A further simplified model of ASM contraction was developed based solely on the muscle's force-velocity relation. Commonly this force velocity relation is described by the Hill curve, which is measured by repeated shortening velocity experiments at different after loads. A single force-velocity element does not show gradual force development upon activation, but rather instantaneous full force development. More realistic is to couple the element with an elastic element in series. This elastic element represents the elasticity of the cytoskeletal network responsible for contractile element force transmission. When contraction is initiated the elastic element stretches while the contractile element shortens, until the force in the elastic element is equal to the contractile element force at $V=0$.

4.5.1 Methodology

The Hill model is based on the following force-velocity relation:

$$(V + b)(F + a) = (F_0 + a)b \quad (4.18)$$

With a and b constants and F_0 the force at which $V=0$. For length control simulation this relation is rewritten to:

$$V = \frac{F_0 + a}{F + a} b - b \quad (4.19)$$

Initially a and b are taken as constants, but they could be made time dependent to better describe the reduction in shortening velocity in time.

With a series elastic element of starting length L_{se} and stiffness k_{se} , and a contractile element of starting length L_{ce} , the force F can be written as:

$$F = (L_e + \Delta L_e)k = (L_{tot} - L_c - \Delta L_c)k \quad (4.20)$$

and

$$V = \frac{dL_c}{dt} \quad (4.21)$$

A 4/5 Runge-Kutta solver as described in Section 4.3.1 is used to solve for L_{ce} , and subsequently F . In isotonic situations the shortening velocity is calculated directly from the clamp force, with a constant length for the series elastic element.

Optimal length behaviour was implemented by introducing a two sided linear length dependence of F_0 , with a peak value at the optimal length.

Table 4-3: Parameter values of Hill type model.

Parameter	a	b	L_{se}	L_{ce}	F_0
Value	0.142	0.035	0.25	0.75	1

For Matlab implementation see Appendix A.3.

4.5.2 Results

For the model analysis the force velocity data for tracheal smooth muscle from [128] was used.

4.5.2.1 *Contraction*

Figure 4.19 shows the force development as a fraction of the maximum contractile force at 4 different values of K_{se} . The optimal length correction factor is not used for these simulations as the large length changes of the contractile element for low K_{se} values would result in very small forces. It is expected that the optimal length of the contractile element for force generation occurs at full contraction instead of at its starting length. The effect of this omission is a slightly faster force development.

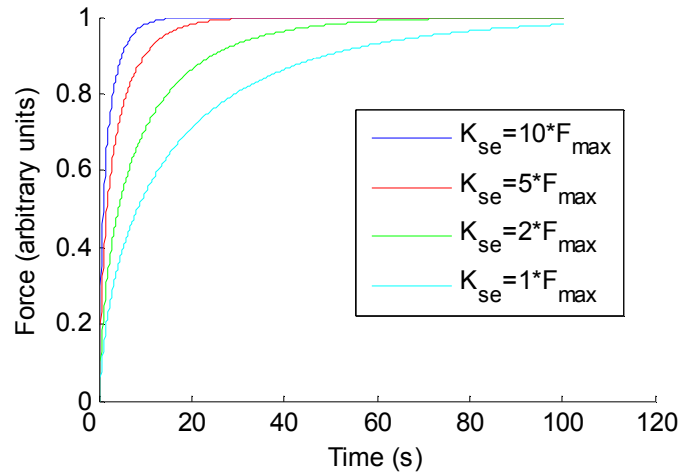


Figure 4.19: Force and contractile element length development at three series elastic element stiffness levels for Hill type model.

4.5.2.2 Shortening velocity

Based on the contraction simulations K_{se} was set to $5 \cdot F_{max}$ and the optimal length to $0.55 L_{tot}$, which is the length of the contractile element when fully contracted. With these values the set of shortening velocity manoeuvres used on the HHM and SDR models is repeated. The resulting force-velocity curves are shown in Figure 4.20. A slight reduction with time of the shortening velocity, particularly at small clamp forces, results. This is attributed to the contractile element not having reached its optimal length early in a contraction.

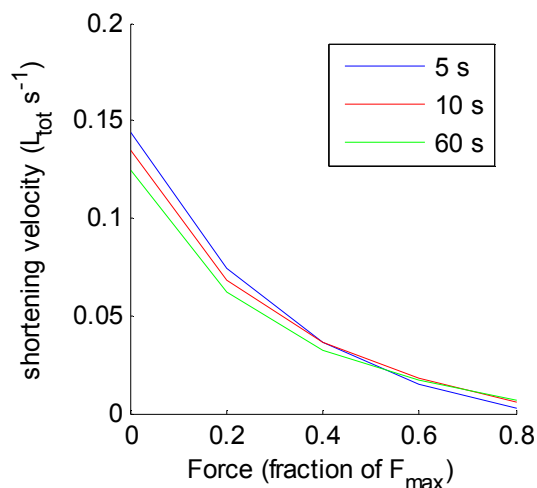


Figure 4.20: Shortening velocity at 3 time points for the Hill type model

4.5.2.3 Oscillations

Figure 4.21 shows the force-length plots in response to sinusoidal oscillations of varying amplitudes. The oscillations (0.2Hz) showed little hysteresis, but large peak forces. The force-length loops are almost symmetrical, with only small deviations because of the small deviations from optimal length. Oscillations with peak length equal to length prior to oscillation show an increased peak force for large amplitude oscillations, which disagrees with the experiments by Shen et al.

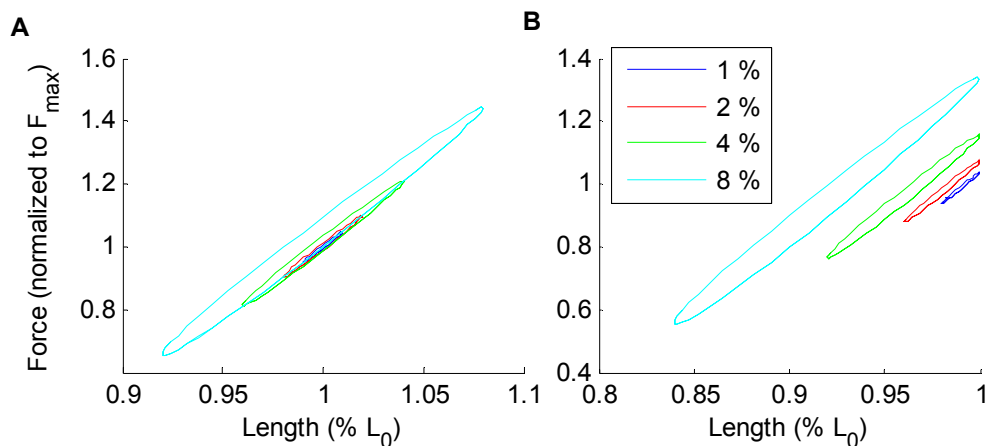


Figure 4.21: Sinusoidal oscillations simulated by the Hill-type model. Legend shows % length changes relative to L_0 .

4.6 Contractile model discussion

The relative quality of each of the models is discussed on their ability to fulfil the criteria described at the beginning of this chapter:

1. Contraction. Each of the presented models is able to simulate a simple contraction, with the accuracy strongly dependent on the parameter values.
2. Optimal length. The optimal length in each of the models is implemented through a force correction factor. This could be replaced by a length adaptation driven factor.
3. Shortening velocity. The HHM model describes the development of shortening velocity values in time most accurately; however the absolute values of shortening velocity in both the HHM and the SDR model are a factor

10 to 20 too low. Changing parameter values to fit the shortening velocity in both cases would require a greatly reduced phosphorylation rate to maintain an accurate speed of force development upon contractile stimulation. The Hill-type model is designed around the force velocity curve, and time dependent parameters would result in the right development of this curve in time as well.

4. Oscillations. The HHM model is the only model to show some accuracy with respect to simulating the results of Fredberg and Shen et al. The SDR and the Hill-type model both show high peak forces for sinusoidal oscillations. Some of the features of the oscillation response, as mentioned in Chapter 2, might be attributable to length adaptation and passive components.
5. The Hill type model is by far the least CPU intensive.
6. The HHM model parameters are hard to define uniquely for a specific tissue as most of the parameters can not be directly established. The SDR model parameters can be established more easily, yet not directly. The Hill type model parameters can be defined directly by fitting the Hill element to the force velocity curves and the elastic element using the force development during contraction.

For implementation into a length adaptation model the fifth criterion is important, while for the analysis of the individual contribution of contraction, length adaptation and passive components in ASM dynamics, the sixth criterion is of great importance. The difference in ability to describe experimental data is mainly expressed in the oscillation response. As this response might be due in part to passive dynamics, the contractile models can not be judged solely on this performance. Consequently in the following section the length adaptation model uses the Hill type model for its clearly defined parameters, ability to reasonably simulate contractile data and little CPU intensity.

4.7 Length adaptation

The net effects of length adaptation are primarily changes in shortening velocity and contractile force. These changes are believed to be caused by changes in contractile element organisation, filament overlap and filament length. The most successful

model in describing these changes is the stochastic network model by Silveria et al, see 2.4.4. This model showed the strength of the stochastic network approach. However, it is incapable of modelling contraction and relaxation of the muscle, instead calculating the force generating potential at any point in time. In this work a novel network model is proposed which uses Hill-type elements as described in the previous section. The model was specifically designed to extend the stochastic network force potential model to a dynamics force-length model.

For the length adaptation model to be successful, the main common features in the literature should be reproduced. These can be condensed into the following characteristics:

- Shortening velocity is proportional to length
 - Adaptation is instantaneous
- Contractile force is approximately constant independent of length
 - Contractile force reduces directly after a length change
 - Redevelopment of force occurs after several contraction relaxation cycles
- The features of the contractile model need to be preserved

There are indications that passive components are subject to length adaptation as well, but little data is available on the topic. As the passive component is addressed separately in Chapter 5, it is ignored in the current model.

4.7.1 Stochastic network model

The main assertion of the Silveira model, length adaptation based on contractile element reorganisation, is maintained in the current implementation of the model. However some major differences exist between the current implementation and the Silveira model:

- Hill Type elements. The contractile elements with potential contractile force are replaced by Hill type elements to simulate force development rather than force potential. This allows for the simulation of true dynamic conditions
- 1D network. The 2D random orientation filament network is simplified to a 1D axial orientation network. In the Silveira model the cause of near constant

contractile force at full adaptation is the length-width ratio of the network. In the current model an alternative approach to force development is used. The added complexity of the 2D network and the lack of visible [59] and mechanical [126] evidence for such a network structure in ASM cells make this feature unnecessary.

- Filament overlap. Where the Silveira model used an optimal length correction factor for element force development akin to the factors used in the previous sections, the proposed model addresses filament overlap directly, through the direct modelling of actin and myosin filament lengths and overlap.

The first and third changes are primarily incorporated to enable the simulation of true dynamic conditions, rather than force potential simulations. With those changes a more detailed analysis of the relative contribution of length adaptation and contraction in ASM dynamics can be conducted. The second change is included to achieve a simpler model, with less parameters to determine, without anticipated loss of quality.

4.7.2 Methodology

The model is centred on myosin filaments which can change in length but not in number. Each myosin filament can associate with actin filaments upon activation, and they can grow along the associated actin filaments. This affinity for myosin growth in the proximity of actin filaments was shown in [95]. Actin filaments are assumed to change with the length of the muscle and are abundant throughout the cells. Actin filaments have been shown to vary their length through polymerisation [60, 78, 81]. The abundance of actin relative to myosin filaments is suggested by several experiments [60].

4.7.2.1 *Filament overlap development*

The growth process of myosin is described below and shown in Figure 4.22:

1. First a myosin filament randomly associates with two actin filaments upon contractile activation. Each myosin filament is at least fully overlapped by the actin filaments, which is attributed to the abundance of actin. Myosin filaments activation is driven by a probability factor which is governed by the level of contractile activation of the model

2. In this model actin filaments do not change length while associated with myosin filaments, but the myosin filaments can grow along the actin filaments. This growth is limited by the extent of actin filament overlap.
3. Lowering/removing the level of contractile activation in the model will result in dissociation of myosin from actin. This allows the myosin filament to move freely within the cell upon length changes, which enables instantaneous shortening velocity adaption.
4. Upon increasing the activation level of the model the myosin filament reassociates with the actin filaments, again with a minimum of full overlap of the myosin. The now longer myosin filament and subsequent growth to full actin overlap results in an increased force generating potential. A sufficient number of contraction relaxation cycles results in optimal overlap of actin and myosin filaments.
5. Oscillations/large length changes cause inactive myosin filaments to depolymerise. Large forces in active contractile elements can cause dissociation from actin, which is equivalent to actin filaments dissociating from their focal adhesion points. The subsequently inactive myosin filament can depolymerise. Myosin filaments have been shown to be unstable when dephosphorylated [169].
6. The now smaller myosin filament will have to go through the activation relaxation process to increase in size.
7. The process starts anew.

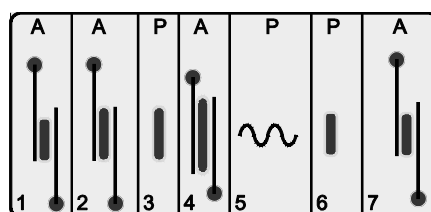


Figure 4.22: Evolution of an active element. A=in active state, P=in passive state. See text for explanation of figure.

When activated the contractile elements formed by the myosin filament and two associated actin filaments can contract as a single unit according to the Hill type

model (see Section 4.5). The filament overlap is implemented as a correction factor for maximum force development.

4.7.2.2 Network and network force

Initially the myosin filaments are equally spaced throughout the 1D network with a certain starting length below optimal length. Upon length changes the active elements deform proportional to their length through filament sliding governed by the Hill force-velocity relation. Inactive myosin filaments move with the network but do not deform.

The total force in the network is determined by the average cross-sectional force of the elements in the network. This is given by:

$$F = \sum_{i=1}^n \frac{L_{ce}}{L_{tot}} F_{ce} \quad (4.22)$$

With L_{ce} and F_{ce} the contractile element length and force respectively, L_{tot} the total network length and n the number of active contractile elements.

Actin lengths throughout the network are uniform, but vary with total network length. The relation between network length and actin length was chosen to assure a constant force for optimal filament overlap at all lengths. In case of optimal overlap:

$$F = \sum_{i=1}^n \frac{L_{actin}}{L_{tot}} F_{ce} \quad (4.23)$$

F_{ce} is proportional with the length of myosin, which is equal to the actin length at optimal overlap. With a constant number of elements the total force becomes:

$$F = C \frac{L_{actin}^2}{L_{tot}} \quad (4.24)$$

With C a constant. Consequently to keep F constant:

$$L_{actin} \sim \frac{1}{\sqrt{L_{tot}}} \quad (4.25)$$

4.7.2.3 Shortening velocity

The shortening velocity manoeuvres used for the contractile model analyses cannot be simulated by this model as force controlled simulations cannot be performed. However the instantaneous shortening velocity can be found from the organisation and length of contractile elements. As each contractile element is governed by the same force-velocity relationship, the unloaded shortening velocity in each element is the same. The total shortening velocity is then dependent only on the average number of active contractile elements in series. With significant overlap of elements, pure series configuration of contractile elements does not exist. However, the effective number of elements in series (CE_s) is related to the average number of elements in parallel (CE_p) and the total number of elements (CE_{tot}):

$$CE_s CE_p = CE_{tot} \quad (4.26)$$

CE_p follows from equation 4.15:

$$CE_p = \sum_{i=1}^n \frac{L_{ce}}{L_{tot}} \quad (4.27)$$

Which leads to an unloaded shortening velocity (V_s) of:

$$V_s = \frac{CE_{tot}}{\sum_{i=1}^n \frac{L_{ce}}{L_{tot}}} V_{ce} \quad (4.28)$$

With V_{ce} the shortening velocity of a contractile element.

For Matlab implementation see Appendix A.4.

4.7.3 Results

The model is analysed on its ability to simulate the features described in 4.7. The following simulations are performed:

- A repeated contraction-relaxation cycle is applied starting from suboptimal length myosin filaments.

- From optimal myosin filament length large length changes in both directions are applied and analysed for force and shortening velocity development in time.
- Oscillations are simulated to investigate whether the network context alters the Hill model response to oscillations.

4.7.3.1 Contractions

Figure 4.23 shows that several cycles of contraction-relaxation from a starting point of non-optimal myosin filament lengths result in a rapid increase in contractile force from the first to the second contraction and a gradually slowing increase in subsequent contractions.

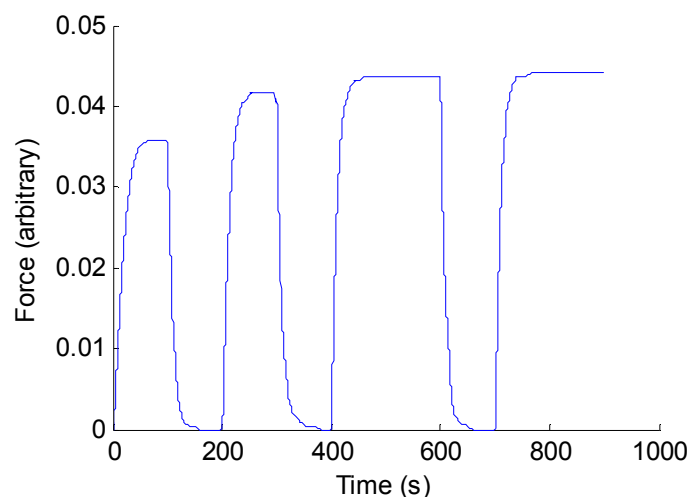


Figure 4.23: Gradual development peak contractile force in stochastic network model.

4.7.3.2 Length adaptation after length change

The force and shortening velocity development after a length change is shown in Figure 4.24. The force shows a distinct reduction after length changes in both directions, followed by an increase towards the optimal force. Shortening velocity adapts instantaneously. This is despite the fact that contractile elements with suboptimal filament overlap can be both longer and shorter than optimal overlap elements. The effects of both types of elements are cancelled out as the probability of each is the same.

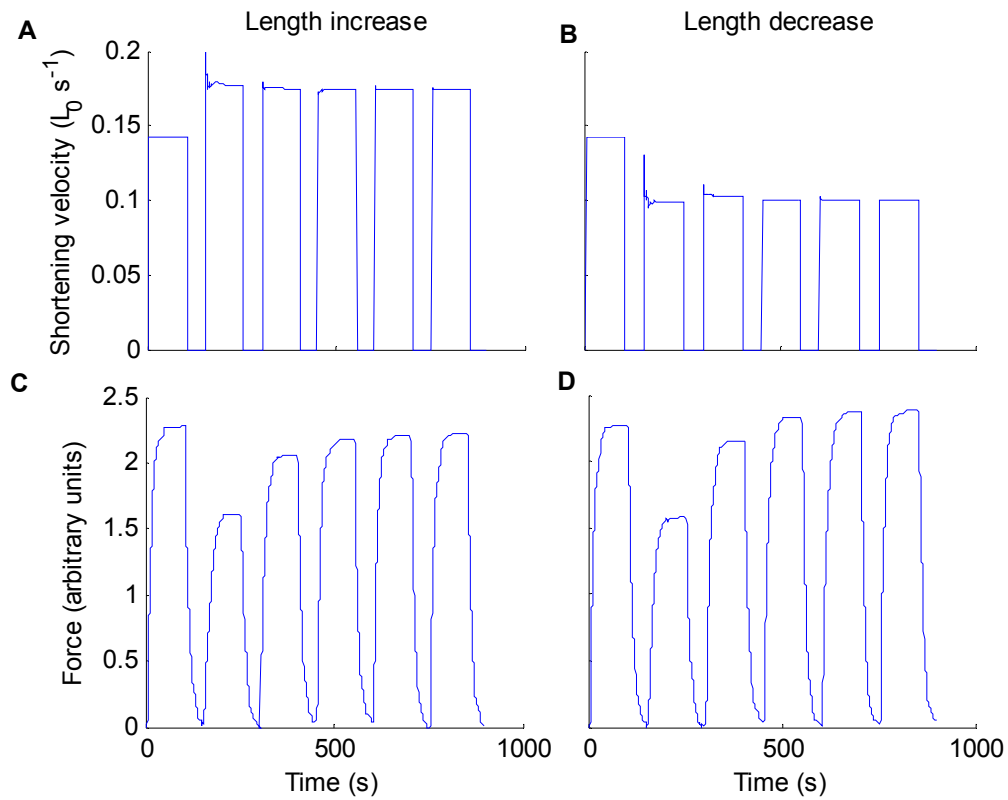


Figure 4.24: Shortening velocity in the length adaptation model.

4.7.3.3 Oscillations

As the model does not contain any elastic elements, the collective behaviour of all contractile elements is directly dependent on the force velocity relations of the elements. With the force dependent on the velocity, the force is 0.5π out of phase with the length oscillation. This results in a force-length loop as shown in Figure 4.25. In Figure 4.26, because of the disassociation of contractile elements at high force levels the maximum force during oscillation is limited. Myosin length reduction of the disassociated myosin filament can result in long term length reduction for large length oscillations.

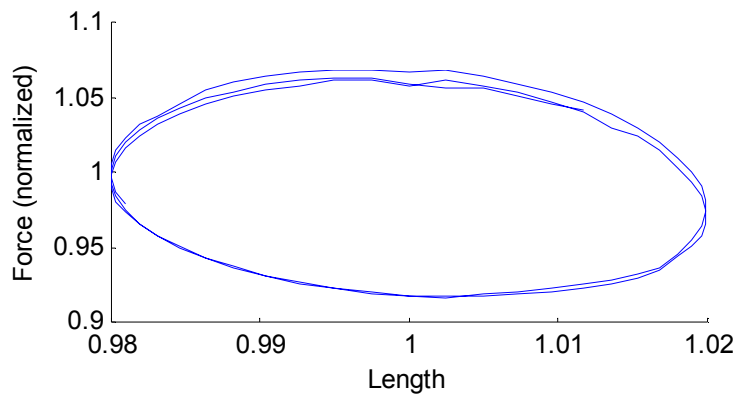


Figure 4.25: Force-length curve length oscillations.

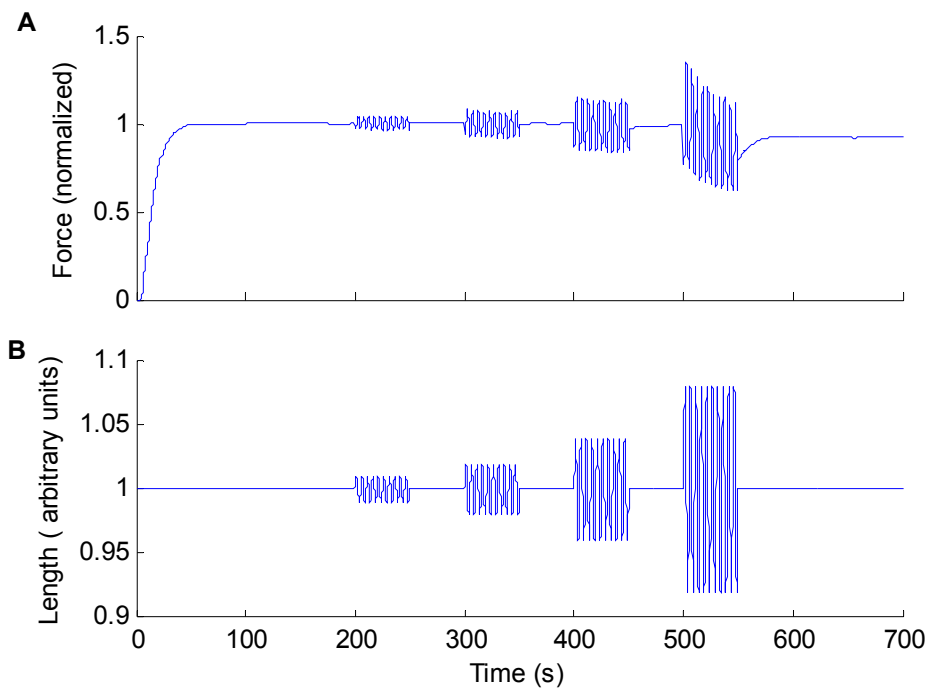


Figure 4.26: Length and Force traces during length oscillations

4.7.4 Discussion

The presented length adaptation model provides one of many possible explanations of the length adaptive process. While the features in Section 4.7 are described rather well by this model, the contractile element oscillation response is not modelled accurately. This is a direct result from the lack of elastic elements in the system. However, adding

elastic elements to the system requires a much more complicated model where the nodes form part of an elastic structure. With so many components in an interconnected network such a model can quickly become unstable. Without a good understanding of the nature of the passive dynamics this is not likely to be worth the effort.

One particular weakness of this model is the arbitrary reduction of myosin filament length in relaxed muscle during length changes. Myosin associates with different actin filaments upon each contraction, which means that myosin filament length needs to be reduced upon length changes to show an initial reduction in force as reported in experiments [96]. Arguably stretching the contractile element is more likely to cause this reduction than reducing its length, yet experimental results show a larger force decrease for length reductions [96]. The most likely cause for this force reduction is a reduction in force transmission through non-contractile components in the muscle. After a length reduction, the cytoskeleton, which likely exists of string like elements, has a lot of slack in internal connections. This slack greatly reduces the force transmission of contractile elements assuming they are suspended by the cytoskeleton. Large length increases might cause some cytoskeletal structures to break, also causing some reduction of force transmission. It is likely however that a larger proportion of taut elements will remain following length increases. The constant formation and dissolution of non-contractile structural elements [60] can gradually replace slack or broken links.

4.8 Closure

In this chapter the development of a contractile model and its inclusion in a developed length adaptation model was discussed. The following chapter looks at the passive dynamics of ASM.

CHAPTER 5

Passive Dynamics Models

5.1 Introduction

The experimental work in Chapter 3 and the literature study in Chapter 2 indicates that the passive dynamics of ASM are not fully understood. The research implies that the passive component of ASM dynamics may play a considerable role in the overall dynamic behaviour. Hence an understanding of the passive component is essential to understand ASM dynamics. In this chapter a modelling study into passive ASM dynamics is described. First the criteria on which the models are judged are described in Section 2. Next, in Section 3, the soft glasses theory [61, 155, 156, 170] is implemented as a stochastic element model as a starting point for the investigation of the passive dynamics. Subsequently a model consisting of an infinite series of springs and dampers is proposed and analysed in Section 4. Lastly two empirical models are described based on linear superposition through fractional calculus and logarithmic linear superposition (Section 5 and 6). The models are discussed in Section 7 on their ability to fulfil the criteria set in the second section.

5.2 Modelling criteria

The experimental investigation of Chapter 3 as well as cell level experiments by other groups [117, 171] has shown a variety of characteristics of ASM's passive behaviour. Many of these experiments have shown a form of power-law behaviour, which has thus far eluded successful modelling attempts. In this research 4 models are analysed for their ability to describe at least the following characteristics as found in Chapter 3:

1. Power law relaxation and force adaptation after step changes in length in both directions.
2. Amplitude dependency of power law relaxation
3. Asymptotic relation to zero (no negative forces)

Each of the models is first analysed on their ability to show power law behaviour after a step change in length. If the model is able to do so, further analysis into the response is instigated.

5.3 Soft glasses Rheology (SGR) Model

Although the soft glasses theory is mostly an observation, Sollich et al [155, 170] have modelled the response based on the assumptions central to the soft glasses theory. In the present research the central assumptions of the approach by Sollich et al. are implemented into a stochastic element model. This approach provides a more direct way of determining the predictions of the soft glasses theory, as well as a means for improvement of the model assumptions to better reflect experimental data.

5.3.1 Methodology

The original SGR model is derived as an analogue to the thermodynamics model by Bouchaud [172]. The model considers an infinite number of elements, each susceptible to externally applied strain. Each element finds itself trapped in place by surrounding elements. Such a trap is presented as an energy well of magnitude E , which determines the probability of yielding of the element after it is stretched. The differential equation for the probability $P(E,t)$ of finding an element in an energy well of depth E at time t is given by:

$$\frac{\partial}{\partial t} P(E,t) = -\Gamma_0 e^{-E/x} P(E,t) + \Gamma(t) \rho(E) \quad (5.1)$$

In which x is the noise temperature, which is a measure of the internal jostling of the elements. $\Gamma(t)$ is the rate and Γ_0 is the attempt frequency of hopping out of energy wells. The first term on the right hand side of equation 5.1 represents the probability of an element with energy well depth E to hop out of the energy well. After a hop out of a particular energy well the new energy well depth is randomly chosen according to the energy well distribution $\rho(E)$. The glass transition temperature x_g corresponds to a constant $P(E)$ in equilibrium, which is equivalent to setting $e^{\frac{E}{x}} \rho(E)$ as a constant. Hence, with x_g taken as 1, $\rho(E)$ is chosen as:

$$\rho(E) = e^{(-E)} \quad (5.2)$$

In the current implementation a certain number (N) of elements of equal initial length have an initial energy well distribution $\rho(E) = e^{(-E)}$. Such a distribution can be generated by using $E = -\ln(\text{rand})$ with rand a random number between 0 and 1. Each

of the elements deforms proportional to the total model deformation, which results in a stored elastic energy of:

$$E = \frac{1}{2} k l_y^2 \quad (5.3)$$

With k the stiffness and l_y the length change of an element. This results in an element yielding rate, according to equation 5.1, with Γ_0 , x_g taken as l :

$$R_y = e^{\frac{E-0.5kl^2}{x}} \quad (5.4)$$

For Matlab implementation see Appendix A.5.

5.3.2 Results

Power law relaxation. The model is run to simulate a single instantaneous length change. Figure 5.1 shows the force response on logarithmic axes. The force response is shown for four values of the noise temperature, each resulting in a convergence to a power law response with a power law exponent equal to the noise temperature. The result shows little dependency on the number of elements for $N > 10000$ or the time step resolution for $dt < 0.05$ s. The lack of an accurate simulation of power law relaxations directly after application of a length change makes the model unsuitable for investigation of superposition principles in ASM.

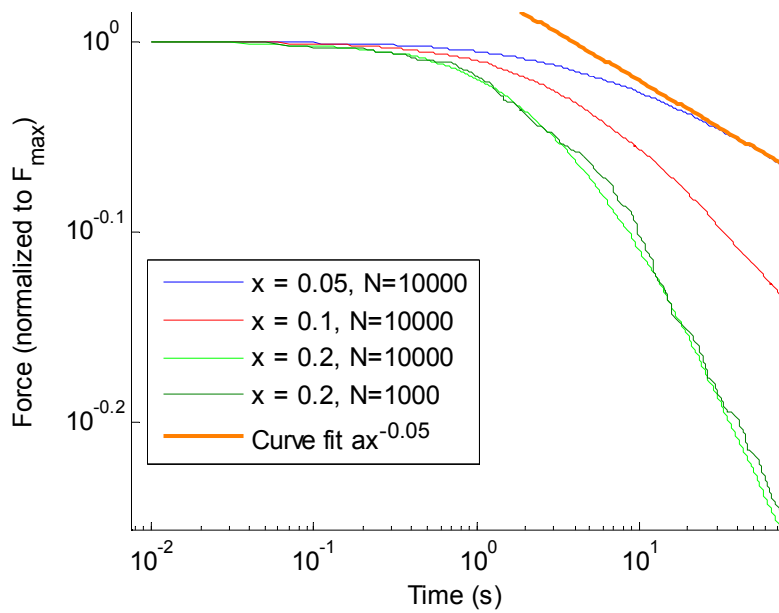


Figure 5.1: Step response SGR model. Different values of the noise temperature x lead to different power law exponents (orange line is a sample fit). The dark green line shows that a reduced number of elements results in noisier force response, but the initial slow force relaxation remains.

Amplitude dependent power law exponent. The power law exponent dependency on length change amplitude could be attributed to a change in noise temperature with length change amplitude. Consequently large amplitude oscillations raise the noise temperature and subsequent step length changes have higher power law exponents. This is contradicted by the experiments from Section 3.4.

Zero force asymptote. The elements in this model have both compressive and tensile strength to enable power law relaxation and force adaptation in both directions. However, the compressive strength of the elements can cause negative forces when negative length changes are applied.

An investigation into variable element sizes and gradual strain release of elements showed that power law relaxation instantaneously after a length change is possible, but this ability is dependent on the length change amplitude. Hence a model of this type is not able to show power law relaxation over a range of length changes.

5.4 Spring damper model

Here a model is presented which investigates if it is possible to create power law behaviour from a theoretically infinite combination of exponential responses. Such an

exponential response can be generated using a Maxwell body, which consists of a spring and damper in series. To create a large range of exponential responses a model is proposed which consist of large number of spring elements in series, with damper elements placed parallel to each spring element with one end connected to a fixed reference. The resulting model is displayed in Figure 5.2. The dampers represent the frictional energy losses inside the cell, which are modelled to be dependent on the absolute velocity of the nodes.

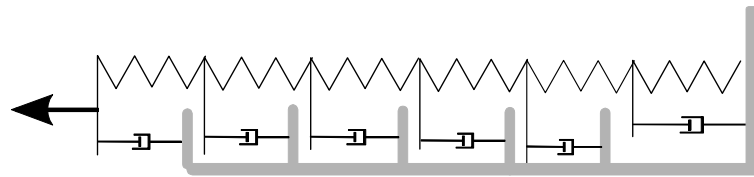


Figure 5.2: Representation of spring damper model

5.4.1 Methodology

With x_i the position of each node, L_i the unstrained length of an element and k_i and D_i the stiffness and damping coefficient of each element, the force balance on each node can be written as:

$$k_1(x_1 - L_1) + D_1\dot{x}_1 = k_2(x_2 - x_1 - L_2) \quad (5.5)$$

$$k_i(x_i - x_{i-1} - L_i) + D_i\dot{x}_i = k_{i+1}(x_{i+1} - x_i - L_{i+1}) \quad \text{for } 2 \leq i \leq n-2 \quad (5.6)$$

$$k_{n-1}(x_{n-1} - x_{n-2} - L_{n-1}) + D_{n-1}\dot{x}_{n-1} = k_n(L_{tissue} - x_{n-1} - L_n) \quad (5.7)$$

These equations are solved using a Runge-Kutta 4/5 procedure as described in 4.3.1.

For Matlab implementation see Appendix A.6.

5.4.2 Results

Power law relaxation. The response to a rapid length change in Figure 5.3 shows convergence to a power law relaxation with an exponent of -0.5. For larger values of D_i the convergence is slower, resulting in larger absolute forces, but the exponent of the power function convergence remains the same. For less elements, the curve shows not only a slower convergence, but an eventual deviation away from the power function as the model reaches steady-state.

Power law dependence on amplitude. Changing spring constants or damping coefficients does not alter the converging power law exponent. An analytical investigation of a similar model was conducted by Bates et al (2007) [173] to describe lung tissue, which included non-linear springs and dampers. Assuming spring stiffness of the form k^α and damping of the form D^β , it was found that the power law exponent is determined by $\alpha\beta/(\alpha + \beta)$, which in the special case of $\alpha=\beta=1$ leads to an exponent of 0.5.

Zero force asymptote. As the springs and dampers need to have both compressive and tensile strength to allow for power law behaviour in two directions of length changes, negative forces do occur.

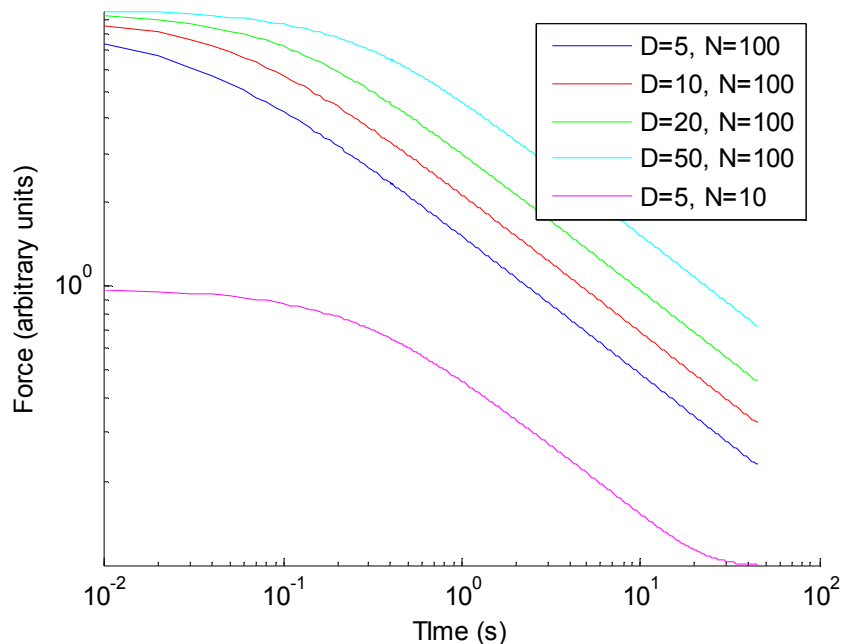


Figure 5.3: Force relaxation in response to length change in the spring damper model. The purple line shows that power law relaxation only occurs for a sufficient number of elements (N).

5.5 Fractional differentials

Most materials can be described in at least part of the operating range by behaviour equivalent to springs or spring damper combinations (viscoelastic elements). Force in springs is proportional to the strain while force in dampers is proportional to the first

derivative of the strain, i.e. the velocity of deformation. It has been proposed that some materials might behave with force dependent on length as a fractional power of the differential operator $D(=d/dt)$. In the following this will be referred to as the fractional derivative, in contrast to the integral derivative. This puts the material somewhere between springs and dashpots, hence it is often referred to as a springpot [174].

Introducing fractional derivatives does have its complications. Integer differentials depend on the local properties of a function only, but fractional differentials are affected by values further away from the local value of x as well. Calculating fractional differentials requires integration over the length of the function up to x . Surprisingly, this dependence on previous function values reduces in time according to a power law.

5.5.1 Methodology

If the fractional differential is given as the D operator with the fraction α as the power of D : D^α . Then the following must be true:

$$D^{\frac{1}{2}}(D^{\frac{1}{2}}(f(x))) = Df(x) \quad (5.8)$$

Or more general:

$$D^\alpha(D^{1-\alpha}(f(x))) = Df(x) \quad (5.9)$$

For fractional integrals this can be used to generate a general formula. For $\alpha=-1$ the first integral of a function $f(x)$ from 0 to x is:

$$D^{-1}f(x) = \int_0^x f(x)dx \quad (5.10)$$

Repeating the process gives:

$$D^{-2}f(x) = \int_0^x \int_0^s f(x)dsdx \quad (5.11)$$

Which for the n^{th} power of the D operator and using the Cauchy formula for repeated integration becomes:

$$D^{-n} f(x) = \frac{1}{(n-1)!} \int_0^x (x-y)^{n-1} f(y) dy \quad (5.12)$$

This can be extended to real values of n if instead of the factorial $\frac{1}{(n-1)!}$ the gamma function is used. The gamma function is an interpolation of the factorials for non-natural values of n with $\Gamma(n+1)=n!$.

$$D^{-\alpha} f(x) = \frac{1}{\Gamma(\alpha)} \int_0^x (x-\xi)^{\alpha-1} f(\xi) d\xi \quad (5.13)$$

This general formula can only be applied to fractional integrals, not to fractional differentials. Fractional differentials of order smaller than 1 can be calculated as:

$$D^{\alpha} f = D^1 D^{-(1-\alpha)} f \quad 0 < \alpha < 1 \quad (5.14)$$

For a single fractional derivative element a step increase in length would lead to a power law function, as can be seen from the fractional derivative of the function $f(t)=c$:

$$\begin{aligned} D^1 D^{-(1-\alpha)} c &= D \left(\frac{1}{\Gamma(1-\alpha)} \int_0^x (x-\xi)^{-\alpha} c d\xi \right) \\ &= D \left(-\frac{1}{\Gamma(1-\alpha)} \frac{1}{-\alpha+1} (x-x)^{-\alpha+1} c + \right. \\ &\quad \left. \frac{1}{\Gamma(1-\alpha)} \frac{1}{-\alpha+1} (x-0)^{-\alpha+1} c \right) \\ &= D \left(\frac{1}{\Gamma(1-\alpha)} \frac{1}{-\alpha+1} x^{-\alpha+1} c \right) \\ &= \frac{c}{\Gamma(1-\alpha)} x^{-\alpha} \end{aligned} \quad (5.15)$$

In most cases the fractional derivative can not be found analytically. The numerical approximation of the fractional derivative was calculated as follows:

In general the first order derivative of function of a function f in point x is defined as:

$$\frac{df(x)}{dt} = \lim_{h \rightarrow 0} \frac{f(x+h) - f(x)}{h} \quad (5.16)$$

The first order derivative of a fractional integral is then:

$$D^1 D^{-(1-\alpha)} f(x) = \lim_{h \rightarrow 0} \frac{\frac{1}{\Gamma(1-\alpha)} \left(\int_0^{x+h} (x+h-\xi)^{-\alpha} f(\xi) d\xi - \int_0^x (x-\xi)^{-\alpha} f(\xi) d\xi \right)}{h} \quad (5.17)$$

Substituting $\xi = \xi+h$ in the first integral gives:

$$\begin{aligned} D^1 D^{-(1-\alpha)} f(x) &= \lim_{h \rightarrow 0} \frac{\frac{1}{\Gamma(1-\alpha)} \left(\int_{-h}^x (x-\xi)^{-\alpha} f(\xi+h) d\xi - \int_0^x (x-\xi)^{-\alpha} f(\xi) d\xi \right)}{h} \\ D^1 D^{-(1-\alpha)} f(x) &= \lim_{h \rightarrow 0} \frac{\frac{1}{\Gamma(1-\alpha)} \left(\int_0^x (x-\xi)^{-\alpha} (f(\xi+h) - f(\xi)) d\xi \right)}{h} + \\ &\quad \lim_{h \rightarrow 0} \frac{\frac{1}{\Gamma(1-\alpha)} \left(\int_0^h (x+h-\xi)^{-\alpha} f(\xi) d\xi \right)}{h} \end{aligned} \quad (5.18)$$

Using the trapezium rule for approximating the integral with constant step size dt , using $t_n - t_i = t_{n-i}$ and $f(t_{i+1}) - f(t_i) = \Delta f_{i+1}$ gives:

$$D^1 D^{-(1-\alpha)} f(x) \approx \frac{1}{\Gamma(1-\alpha)} \frac{\sum_{i=0}^{\frac{t}{dt}-1} \left(t_{n-i}^{-\alpha} \Delta f_{i+1} + t_{n-(i+1)}^{-\alpha} \Delta f_{i+2} \right) + t_{n+1}^{-\alpha} f(0) + t_n^{-\alpha} f(t_1)}{2}$$

The first term in the sum for $i+1$ equals the second term for i . Consequently:

$$D^1 D^{-(1-\alpha)} f(t) \approx \frac{1}{\Gamma(1-\alpha)} \left(\left(\sum_{i=1}^{n-2} t_{n-i}^{-\alpha} \Delta f_{i+1} \right) + \frac{1}{2} \left(t_n^{-\alpha} \Delta f_1 + t_{n+1}^{-\alpha} f(0) + t_n^{-\alpha} f(t_1) \right) \right) \quad (5.19)$$

The fractional differential model was analysed in its simplest form:

$$F(t) = D^\alpha L(t) \quad (5.20)$$

For Matlab implementation see Appendix A.7.

5.5.2 Results

Power law relaxation. The response to a single length step is given in Figure 5.4, which confirms the analytical result from equation 5.13.

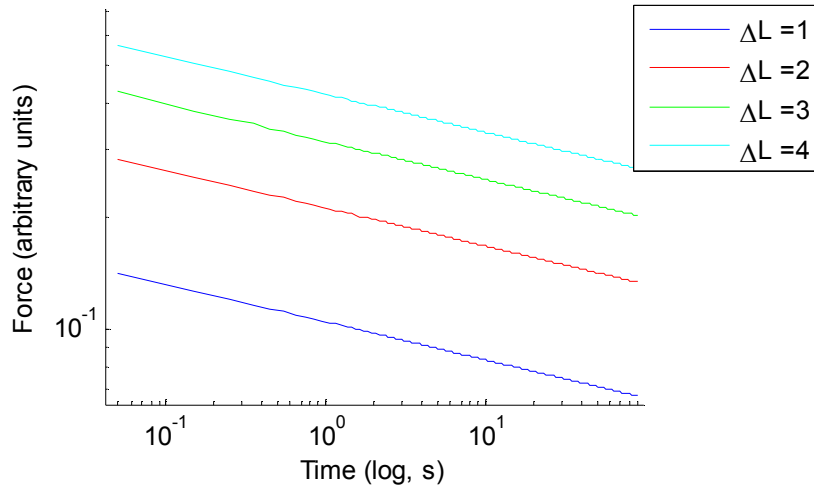


Figure 5.4: Double logarithmic plot of force response to step length change in fractional derivative model. Different amplitudes of length change ΔL do not change the power law exponent.

Power law exponent dependence on amplitude. The exponent of the power law of any step length change is dependent only on the fractional derivative operator α . The integral formulation means that linear superposition applies to the fractional differentials, which was confirmed in the model implementation. Consequently a prestress F_s can be added to the models: $F(t) = D^\alpha L(t) + F_s$. Similarly variation of α dependent on amplitude of stretch could be implemented through sequential integration in parts.

Zero force asymptote. In the current implementation of the fractional derivative model instantaneous stiffness is linear, based on linear superposition, which means that forces can become negative for sufficiently large shortening of the muscle. A different implementation of the fractional differential force-length relation might allow for zero force asymptotic behaviour.

The fractional differential model shows power law relaxation of the force relative to the force prior to the length change, unlike the previously discussed models. In

Chapter 3.4 it is shown that despite the relative origin of the power law, the force response could still resemble a power law function for small power law exponents. The perceived power law exponent in such cases will vary. To test if the relative force response to length changes shows a constant power law exponent the experiments from protocol 2 in Chapter 3 are plotted as relative force response in Figure 5.5. For positive length changes the power law exponent does seem to be near constant, while for negative length changes large differences are found.

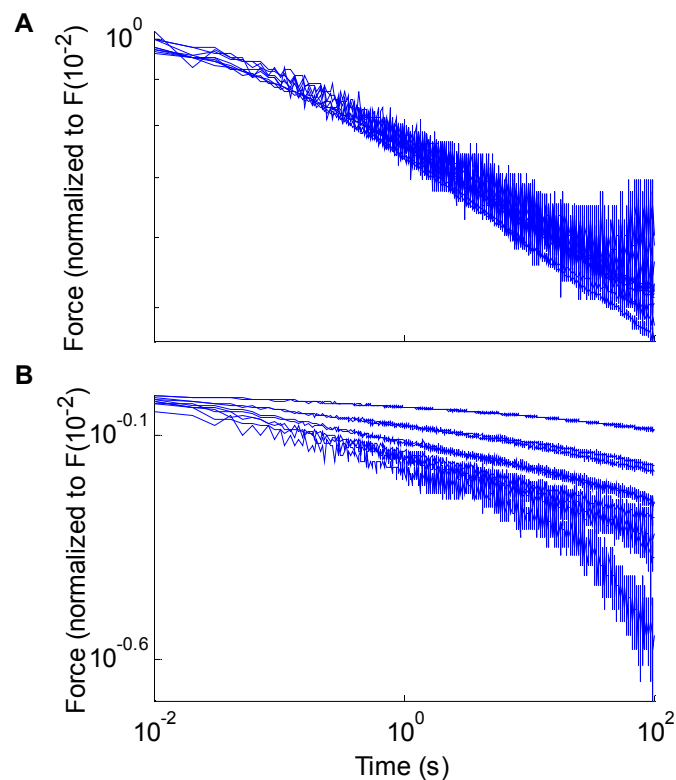


Figure 5.5: Relative force response to step length changes. Panel A shows positive length changes, panel B shows negative length changes.

5.6 Sequential multiplication: logarithmic superposition

The fractional derivative model shows in essence a power law relaxation with linear superposition, which leads to a constant relative power law exponent. However when subsequent power functions are multiplied, the exponents add up. This multiplication is equivalent to summation on a logarithmic scale:

$$at^b = e^{b \log(t) + \log a} \quad (5.21)$$

$$\begin{aligned} at^b ct^d &= e^{b \log(t) + \log(a)} e^{d \log(t) + \log(c)} \\ &= e^{b \log(t) + \log(a) + d \log(t) + \log(c)} = e^{(b+d) \log(t) + \log(ac)} = act^{b+d} \end{aligned} \quad (5.22)$$

Here an empirical model is proposed based on the novel idea of sequential multiplication.

5.6.1 Methodology

In sequential multiplication the force response to a single length change takes the form of a power law:

$$F(t) = F_0 a_i t^{\alpha_i} \quad (5.23)$$

In which both the multiplier a and the exponent α are dependent on the amplitude of the length change and F_0 is the force prior to the length change. The power law exponent and the multiplier are plotted against each other in Figure 5.6. Apparently the multipliers are related to power law exponents in a large range of length steps as:

$$\alpha \sim \log(a) \quad (5.24)$$

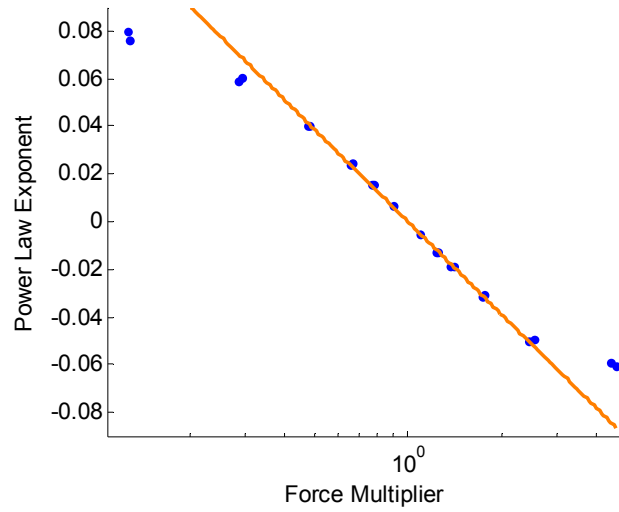


Figure 5.6: Force multiplier versus power law exponent for step length changes. Force multiplier represents the ratio of the power law fit multiplier over the force prior to a length change. The line represents a fit of the data of the form $a \cdot \log(x)$, fitted by ignoring the four absolute largest exponent data points.

All of the experiments in Chapter 3 showed no net force difference between the start and end of each experiment; hence for $t \rightarrow \infty$ and a net length change of 0 , the net force change should be zero as well. This condition is satisfied for two consecutive length changes of equal but opposite amplitude as follows.

The force response to two consecutive length changes is given by:

$$F(t) = F_0 a_2 (t - \Delta t)^{\alpha_2} a_1 t^{\alpha_1} \quad (5.25)$$

With Δt the time between the length changes. For length changes of equal but opposite amplitude, $a_1 a_2 = 1$ and $\alpha_1 + \alpha_2 = 0$ have to apply. With $\alpha = \log(a)$ and $\alpha_1 = -\alpha_2$:

$$a_1 a_2 = e^{\alpha_1} e^{-\alpha_1} = 1 \quad (5.26)$$

Which satisfies the conditions for zero net force difference.

For Matlab implementation see Appendix A.8.

5.6.2 Results

Power law relaxation. The sequential multiplication model is defined by its power law relaxation response to length changes

Exponent dependence on amplitude. The step amplitude dependence of the power law exponent and the multipliers is shown in Figure 5.7. the logarithmic superposition ensures a linear relationship between step amplitude and exponent.

Zero force asymptote. The sequential multiplication model shows zero force asymptotic behaviour as the multiplier and power function can not become negative. This is a direct consequence of the logarithmic relation between force multipliers and power law exponents, which by way of the direct dependence of the power law exponent on the length change results in:

$$a \sim e^{\Delta L} \quad (5.27)$$

In which $e^{\Delta L}$ is strictly positive.

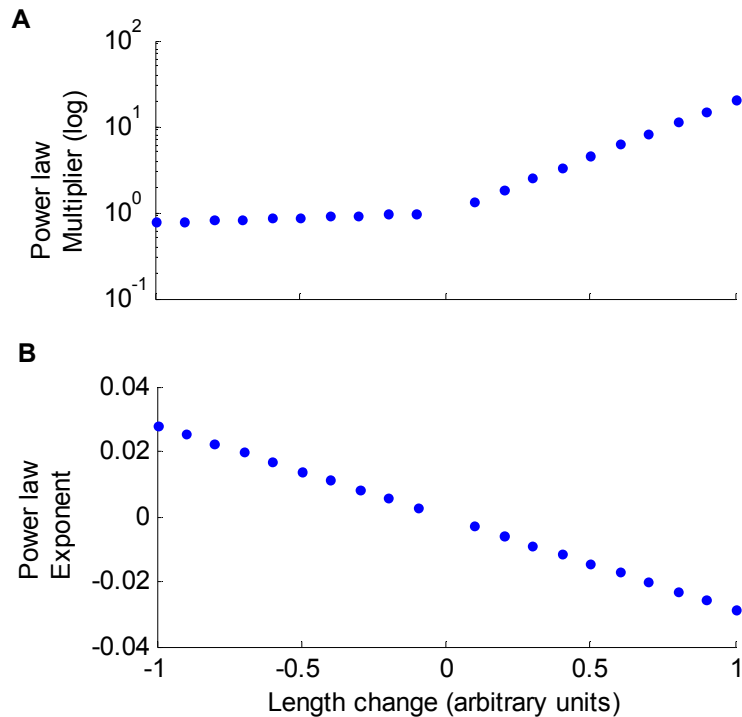


Figure 5.7: Step response power law parameters in the sequential multiplication model. Panel A shows the multipliers and panel B the power law exponents.

As the sequential multiplication model fulfils all three the criteria set in Section 5.2, the model is further investigated using sinusoidal length oscillations. Figure 5.8 shows that the banana shaped force-length loops found by Fredberg et al. [123] in contracted muscle appear naturally in relaxed muscle with the sequential model. The average loop force is quite different. When compared with the sinusoidal oscillations in relaxed muscle described in Section 3.4, a better similarity is found. Figure 5.9 shows the force-length loops of these oscillations, which show less hysteresivity but a similar banana shape and peak force progression. The irregularities for small forces in the force-length loop of the experiments are the result of control system resonance of the set-up at very small forces.

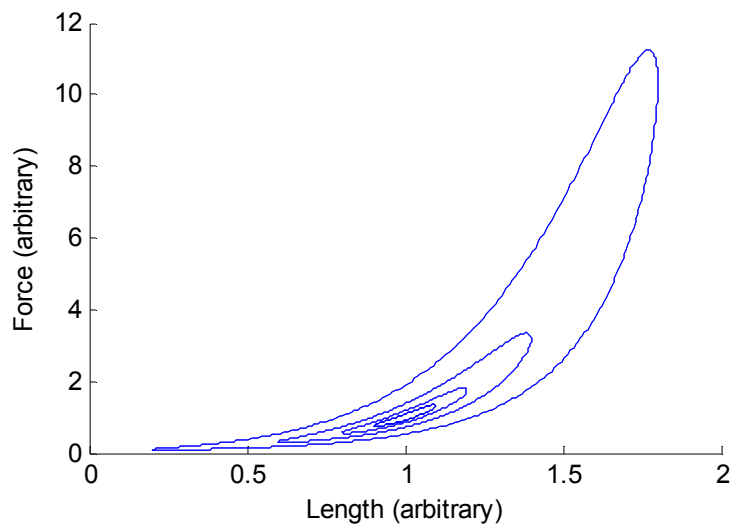


Figure 5.8: Force-length loops of sinusoidal oscillations in sequential multiplication model.

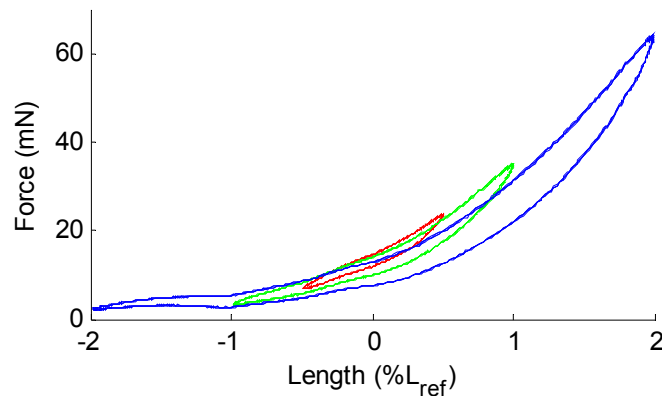


Figure 5.9: Force-length loops of oscillations in relaxed muscle.

5.7 Model comparison

The models based on the soft glasses theory and the spring damper model are not able to fulfil the three criteria described in Section 2. The current understanding of the dynamic response of the processes responsible for ASM passive dynamics seems insufficient for the development of a successful model based on these processes. The fractional differential model might be adaptable to satisfy the criteria better, either by including series and/or parallel elastic elements, or by changing the nature of the fractional differential relationship between force and length. In the literature springpot elements are usually modelled in a configuration with springs in conventional spring-dashpot arrangements such as Voigt or Maxwell elements [174]. The effect of these configurations varies. Any parallel elastic element results in a linear increase of the force with length, which does not affect the intrinsic power law behaviour. Any series elastic element alters the power law behaviour, but no testing of this effect has been performed. The sequential multiplication model showed the greatest agreement with the data from Chapter 4.

5.8 Closure

In this chapter the development of several models of the passive dynamics of ASM was discussed. The ability of the sequential multiplication model to satisfy all the set criteria with only 2 interrelated and length change dependent variables is promising for future study. In Chapter 6 a series of experiments is described to determine the

relations of the multiplier and exponents in the sequential multiplication model with length and/or force. Oscillation and consecutive length step data are presented for validation of the model. Chapter 7 describes an adjustment to the model to better represent the experimental data.

CHAPTER 6

Validation and Parameter Generation

6.1 Introduction

In this chapter a series of experiments is described to:

1. Determine whether experimental data on dynamics in relaxed, unstimulated ASM can be used to describe passive dynamics.

The observed level of tone (contractile force in the muscle) in relaxed muscle might affect the dynamics of the ASM passive component. Hence its role needs to be assessed.

2. Determine whether passive dynamics play a role in the dynamic response of contracted ASM.

These experiments enable insight into the individual contributions to ASM dynamics of the passive, contractile and length adaptive components.

3. Determine whether power law relaxation of force and power law force adaptation exists for single length changes in ASM tissues.

While the experiments in Chapter 3 suggest the existence of power law relaxation, an enhanced set of repeat experiments was conducted for statistical significance.

4. Provide quantitative data for further development and analysis of the sequential multiplicative model

The sequential multiplication model shows good agreement with qualitative observations in ASM passive dynamics, but quantitative data for multiplier and exponent relations with length and/or force are needed for further analysis

5. Validate the sequential multiplication model

Continuous length changes such as sinusoidal oscillations are used to validate the sequential multiplication model .

These experiments were performed at the Mayo Clinic College of Medicine in Rochester, Minnesota, USA. In this chapter, first a short description of tissue acquisition and reference length procedures followed by equipment, programs and materials is given in Section 2. The third section covers the experimental protocols and their rationale and purpose within the project. The fourth section covers the results of the experiments followed by the final section which contains the discussion and conclusions.

6.2 Protocols, Equipment and Programs

6.2.1 Tissue acquisition

A Yorkshire (age 9 months) pig lung with trachea, or a pig trachea only, was acquired from a local butcher and transported in Hank's Balanced Salt Solution (HBSS, composition in mM: 5.3 KCl, 0.44 KH₂PO₄, 137.9 NaCl, 0.336 Na₂PO₄, 2.33 CaCl₂ 0.79 MgSO₄, 10 Dextrose and 10 HEPES buffer) on ice. Upon arrival at the laboratory (within 1hr of acquiring the tissue) the trachea was dissected from the lung immediately and connective tissue and bloody tissues were removed to minimise contamination of the storage medium. The ends of the trachea were removed to avoid damaged tissues and the trachea was transferred to fresh HBSS solution at 4 °C. Part of the trachea was used directly and part stored for a maximum of 48 h before use.

Dissection procedures were similar to Section 3.2.4, except for the dissection solution which was HBSS.

6.2.2 Equilibration and reference length protocol

The ASM strip was equilibrated in PSS for 20 min. To determine the reference length the tissue was subjected to a repeating cycle of potassium depolarisation (PSS recipe with equimolar replacement of NaCl with KCl), PSS wash out and stretch. This cycle continued until the active force (difference between maximal contracted force and prior relaxed force) reached a plateau or peaked. This length will be referred to as the reference length. As the first few contractures with ACh 10⁻⁶M showed a gradual increase in force, the tissue was contracted at least two times prior to starting the

experiments. To ensure full recovery from prior length changes, all experiments were separated by a recovery period consisting of a contracture and subsequent relaxation in PSS for 9 minutes which was sufficient for the force to stabilise. Tissues were rejected as being nonviable if the contractile force was less than 80% of the initial contractile force in fresh tissue.

6.2.3 Equipment

The set-up used for this series of experiments is similar to that described in Chapter 3 with some minor differences (see Figure 6.1).

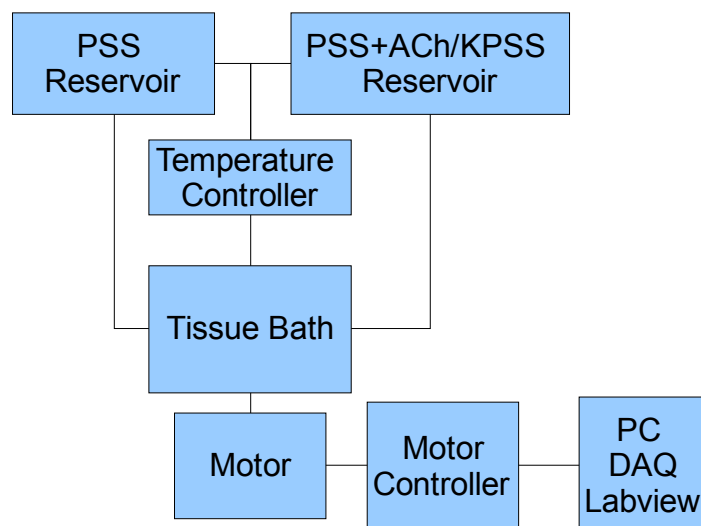


Figure 6.1: System Diagram of muscle test system hardware

Each of the components is described below:

- Tissue bath. This consists of a water jacketed reservoir with a 10 ml internal volume. Fluid removal and supply occurs through a single three way valve at the bottom of the water bath. The valve's two other ports connect to a vacuum pressurised waste bottle and a tube which leads to a switching valve for the two fluid reservoirs.

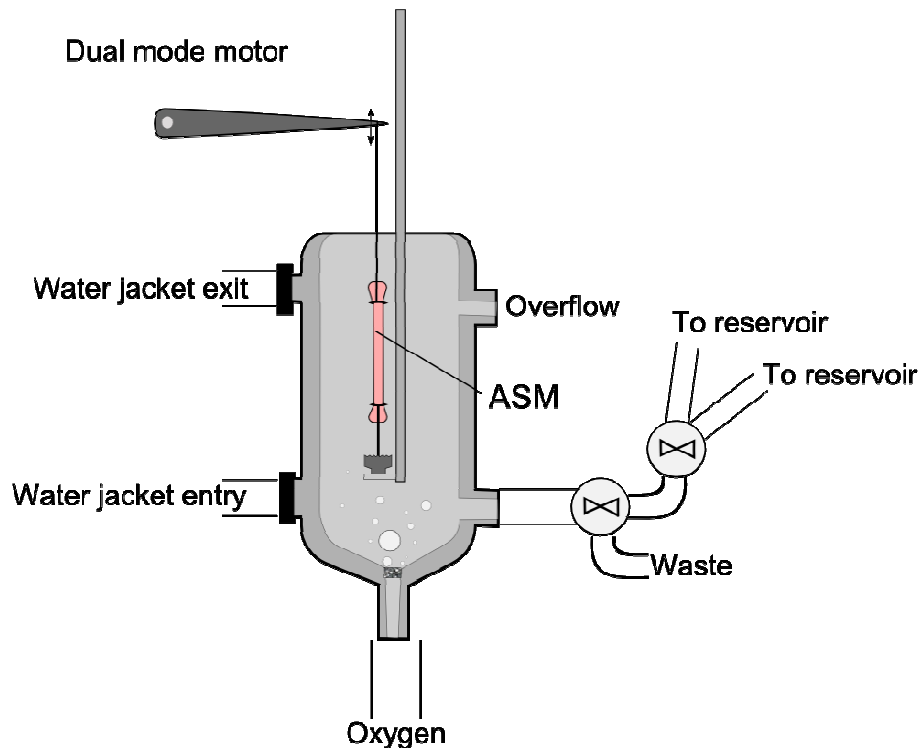


Figure 6.2: Tissue bath.

- Temperature controller. The water jackets for both reservoir and tissue bath are connected to a circulating water bath with temperature regulator.
- Motor and controller. The tissue is connected to a 300B dual mode Cambridge motor lever arm which is hooked up to a 300B controller. The controller has analogue in and output connections for force and length signals and dials to set the level of force and length at zero input voltage.
- DAQ system. A PC with a National instruments PCI-6281 DAQ card and a National instruments BNC-2090A analogue connector board is connected to the motor controller and signals are sent from and to the card by customised National Instruments Labview programs. Signal resolution is 20 times greater than the set-up described in Chapter 3.

6.2.4 Labview interface

The Labview interface consists of two programs, one for creating the length and force control signals files and one for reading these files and communicating them to the motor controller.

- Data_Generation.vi

A Labview program was developed to generate the length step and oscillation sequences. The sequences are created by adding the individual length signal sections one by one, which are written to a Labview native file format to conserve data and allow faster reading. To view the data a separate small program was written which converts the Labview native format to a TAB-delimited spreadsheet file. For detailed description of the program and its block diagram see Appendix A.1

- Data_Acquisition.VI

The data acquisition program reads the files created by the data generation program and writes the length and/or force signals to the National instruments DAQ board. Simultaneously the force and length data are read out and stored in a TAB-delimited spreadsheet file. An alarm sounds when manual input is required, such as when a fluid change is needed and at the end of a file. For detailed description of the program and its block diagram see Appendix A.2

6.3 Experimental protocols and rationale

All experiments were conducted at 23 °C as preliminary experiments showed a greater stability of force and longer tissue viability compared to physiological temperatures. Moreover, force generation is slower at low temperatures, but shows higher absolute values which improves signal to noise ratios [175, 176]. One series of experiments was conducted to assess power law relaxation in ASM at 37 °C using continuous square waves (0.5 Hz, 0.2 % L_{ref}).

6.3.1 Comparison of Contracted and Relaxed ASM.

The ASM underwent a series of experiments to identify the similarities and differences between contracted and relaxed muscle in their dynamic response. The purpose of this investigation was twofold. First, as subsequent experiments were designed for relaxed muscles which have considerable tone, the influence of cross-bridge cycling on the response of the relaxed muscle has to be assessed. Second, the influence of passive dynamics on dynamics response in contracted muscle needs to be investigated. The following experiments were conducted:

Sinusoidal oscillations. The first set of experiments was designed to assess the cross-bridge cycling activity in the muscle. Contracted ASM differs from relaxed muscle in the number of active cross-bridges. Evidently the influence of cross-bridge cycling on the dynamic response is much larger in contracted than relaxed muscle. To assess this difference, sinusoidal oscillations were applied to both contracted and relaxed muscle. The main reason for applying oscillations is that previous studies [123] showed that the hysteresivity, a measure of hysteresis of the force-length loop during oscillations, is indicative of cross-bridge cycling activity. A direct comparison between contracted and relaxed muscle on hysteresivity is predicted to reveal the differences in cross-bridge activity.

The peak length during these oscillations was set to the length immediately prior to oscillations, which minimises the potential influence of length adaptive or contractile element disruptive effects.

Sinusoidal oscillations of 0.5, 1, 2, 4, 8, and again 0.5 % of L_{ref} (peak to peak amplitudes) were applied in both relaxed and contracted ASM (contracted for 900 s before oscillation). Each oscillation had a duration of 100 s and a recovery period of 100 s. A separate second series of sinusoidal oscillations at 2 % L_{ref} with frequencies 0.2, 1, 5, and 10 Hz were also applied to both contracted and relaxed ASM.

Triangular wave oscillations. A second set of experiments was performed to investigate to what extent the force response data by Shen et al. [134] on triangular wave length oscillations in contracted muscle can be described by passive dynamics. Triangular waves of 2 % L_{ref} amplitude and frequencies of 0.2, 1 and 10 Hz were applied in contracted and relaxed muscle. These oscillations were preceded by step length changes of 0.5 % L_{ref} to investigate the relation between power law relaxation parameters and constant velocity length changes. In relaxed muscle this process was repeated at a length of 102 % L_{ref} to investigate the effect of this length change on the force response.

Shortening velocity after oscillations. To assess whether stretch activated increases in cross-bridge cycling occur, shortening velocity was measured directly after oscillations in contracted muscle. Some studies have shown or suggested that length changes in ASM result in either stretch activated signalling pathways, causing cross-

bridge activation [60], or increased cross-bridge cycling speeds as cross-bridges move from the latch state to a faster cycling state [115, 122, 131, 177]. As an indicator of these cross-bridge cycling speeds the shortening velocity after oscillations was compared with unperturbed muscle and early release measurements. The shortening velocity was examined by sudden release from length control to force control to 2.5 mN force (less than 10% of maximum contractile force). The shortening velocity was determined from the slope of the length signal 1-2 s after release. This process was repeated seven times under different conditions: Four variations in timing of the release (20, 40, 80, 700 s into a contracture) and three cases in which oscillations (0.2 Hz, 1 %, 2 % and 4 % of L_{ref}) were applied directly prior to release at 700 s into a contracture. The sequence of the variations was randomised.

Oscillations and square waves. To assess the relation between the shortening velocity data and the power law relaxation response, a continuous square wave was applied before and after oscillations in contracted and relaxed ASM. In relaxed muscle, oscillations of 0.5, 1 and 2 % L_{ref} amplitude at 0.2 Hz were applied, while in contracted muscle oscillations of 1, 2 and 4% L_{ref} amplitude at 0.2 Hz were applied. The two fold difference in amplitudes between contracted and relaxed muscle was used because preliminary experiments had shown very small effects of smaller oscillations in contracted compared to relaxed smooth muscle. The two fold difference was expected to provide sufficient overlap, yet still show the onset of oscillation effects for both contracted and relaxed muscles.

6.3.2 Step protocols

A series of step length change protocols were applied to the tissue to investigate the power law relaxation. Power law relaxation was defined as a force response to sudden length changes according to the formula $F(t)=at^{\alpha}$ with $t=0$ at the point in time just after the length change and a and α constants. The step length change protocols were divided into three types: simple length step (Figure 6.3A), two phase length step (Figure 6.3B) staircase (Figure 6.3C) and pulse staircase (Figure 6.3D). Each is described below.

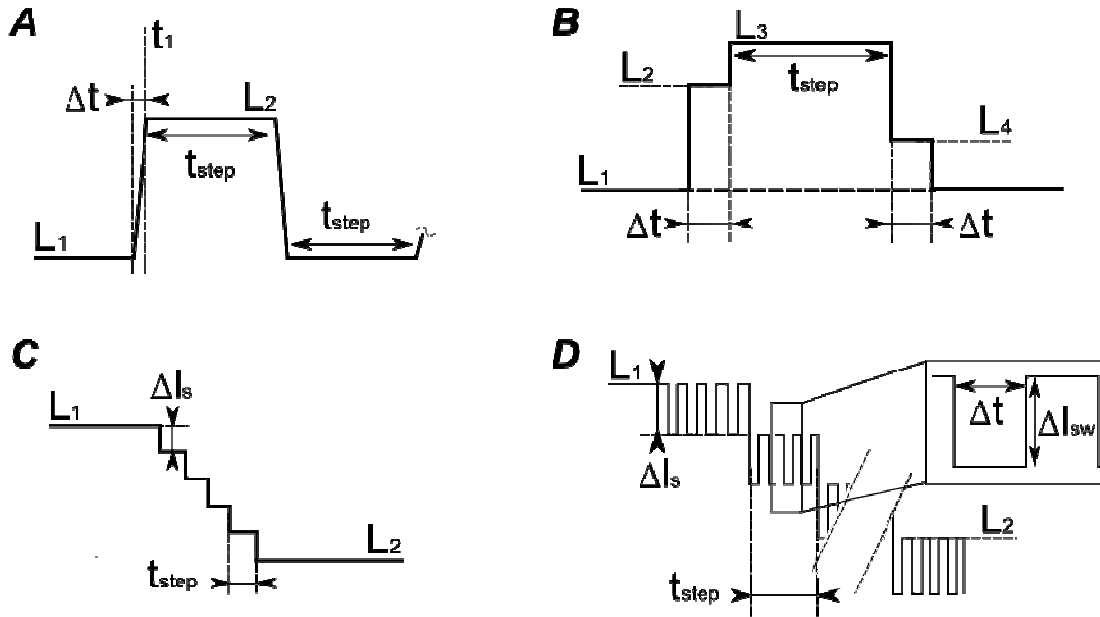


Figure 6.3: Representation of the various length step protocols used. A) Simple length steps are shown in A, with a ramp time given by Δt and a length increase L_2-L_1 equal to the subsequent length decrease after t_{step} seconds. In B the two-phase length step is shown, where the first phase consist of a length increase from L_1 to L_2 (all ramp times here equal to 0.001 s) and the second phase, consisting of a length increase to L_3 , which is maintained for t_{step} seconds. $L_4-L_3=L_2-L_1$. C shows the staircase function in which the length is changed from L_1 to L_2 in steps of magnitude ΔL_s and of duration t_{step} . In D a staircase function with superimposed square wave function is shown. Δt of the square wave is 1s and $\Delta L_{sw} = 0.25\% L_{ref}$.

Protocol 1: Single simple length step (Figure 6.3A). Simple length steps of varying amplitudes were applied to confirm the existence of power law relaxation and to assess the dependence of the power law relaxation on step length amplitude. Step amplitudes of 0.25, 0.5, 1, and 2% L_{ref} were applied in two directions. t_{step} was taken as 200 s and the ramp time Δt was taken as 0.001.

Protocol 2: Ramp time step (Figure 6.3A and B). Simple length steps with varying ramp times were applied to assess whether ramp times influence power law relaxation. Simple length steps with $\Delta L = -0.5\% L_{ref}$ were applied with ramp times (Δt) of 0.001, 0.01, 0.1, 1, and 10 s. All other length changes were applied with ramp time of 0.001 s. Subsequently two phase length steps of type B were applied, with $L_3-L_1 = -0.5\%$ and $L_3-L_2 = 0.25*(L_2-L_1)$ and a waiting time Δt of 0.1, 1, and 10 s.

Protocol 3: Two phase length step (Figure 6.3B). Two phase length steps of type B were applied to investigate sequential multiplication as found in Chapter 5. A series of two phase length steps were applied with variation in ratio of $(L_3-L_2)/(L_2-L_1)$ from 0.2 to 5 and -0.2 to -5 both for $L_3 > L_1$ and $L_3 < L_1$. $t_{step} = 200$ s, $\Delta t = 1$ s.

Protocol 4: *Staircase functions (Figure 6.3C).* To investigate the exponent and stiffness correlations with length or force, staircase functions of type C were applied to the tissue. Staircases of total amplitude $L_2-L_1=2\%$ and $-2\% L_{ref}$, $\Delta l_s=0.25$; 0.5 and $1\% L_{ref}$, and step duration $t_{step}=10$ s were applied. To assess the effect of the step duration a second set of experiments of total amplitude $L_2-L_1=2\%$ and $-2\% L_{ref}$, $\Delta l_s=0.25$ and $t_{step}=1, 10$ and 100 s was applied.

Protocol 5: *Superimposed square wave staircase (Figure 6.3D).* To assess whether the staircase function response is inherent to the muscle or a consequence of the applied protocol an alternative experiment was developed. Staircase functions with $\Delta l_s=0.5$ or $1\% L_{ref}$ and $L_2-L_1=-2$ or $2\% L_{ref}$ and $t_{step}=200$ s with a superimposed square wave of $0.25\% L_{ref}$ amplitude and a period of 2 s were applied.

A separate set of experiments was developed to assess power law relaxation in contracted muscle. The muscle was contracted with ACh. A continuous square wave of amplitude $0.25\% L_{ref}$ and period 2 s was applied while contracting (600 s) and relaxing (400 s) the muscle.

Statistical Analysis.

All data are given as mean values \pm SD where n equals the number of tissues. Significance was assessed using the student t-test (paired) and for multiple protocol comparison ANOVA. The level for acceptance was set at $P < 0.05$

6.4 Results

6.4.1 Dynamic response of contracted versus relaxed ASM

Sinusoidal oscillations. To test whether cross-bridge cycling contributes to the force response in relaxed ASM the effect of length oscillations is compared in both contracted and relaxed muscle. In Figure 6.4 two indicators of the response to these oscillations are compared: hysteresivity and asymmetry. The hysteresivity has previously been proposed as an indicator of cross-bridge cycling [123], while asymmetry results from the non-linearity of the force response. In Figure 6.4A hysteresivity is greater at oscillation amplitudes exceeding 2% of L_{ref} and in Figure 6.4B it is attenuated as the frequency increases above 1 Hz. Both trends exist in contracted and relaxed ASM. The absolute values of the hysteresivity and asymmetry

are significantly larger in relaxed muscle. Both relaxed and contracted ASM show an increased asymmetry with oscillation amplitude and frequency in Figure 6.4C and D. The increased asymmetry with oscillation amplitude is attributed to the larger force excursions, which results in more asymmetry when approaching zero force. Similarly the larger asymmetry values for relaxed muscle are attributed to the larger relative force excursions in relaxed muscle.

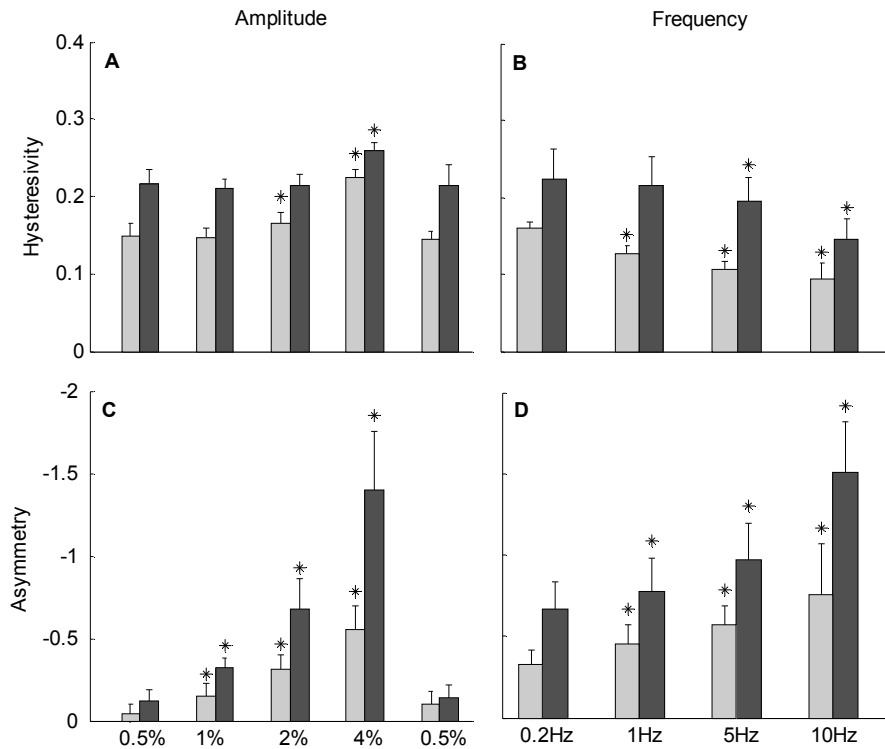


Figure 6.4: Hysteresivity dependence on amplitude (A) and frequency (B), and dependence of asymmetry on amplitude and frequency (C and D). Amplitude of oscillation is given in % L_{ref} . Shown are mean values \pm SD ($n=6$) *denote statistically different ($P<0.05$) from 0.5% oscillations (in A) and 0.2Hz oscillations (in B). All effects of length steps were fully reversible (A and C)

Triangular wave oscillations.

Figure 6.5 shows that triangular wave oscillations similar to the data by Shen et al. [134] follow similar trends in hysteresivity and asymmetry analogue to the sinusoidal length oscillations. The characteristic force-length loops of constant velocity oscillations show great similarity in Figure 6.6., which indicates that these loops are not caused by contractile dynamics. The hysteresivity in contracted muscle is relatively larger for constant velocity oscillations compared to sinusoidal oscillations.

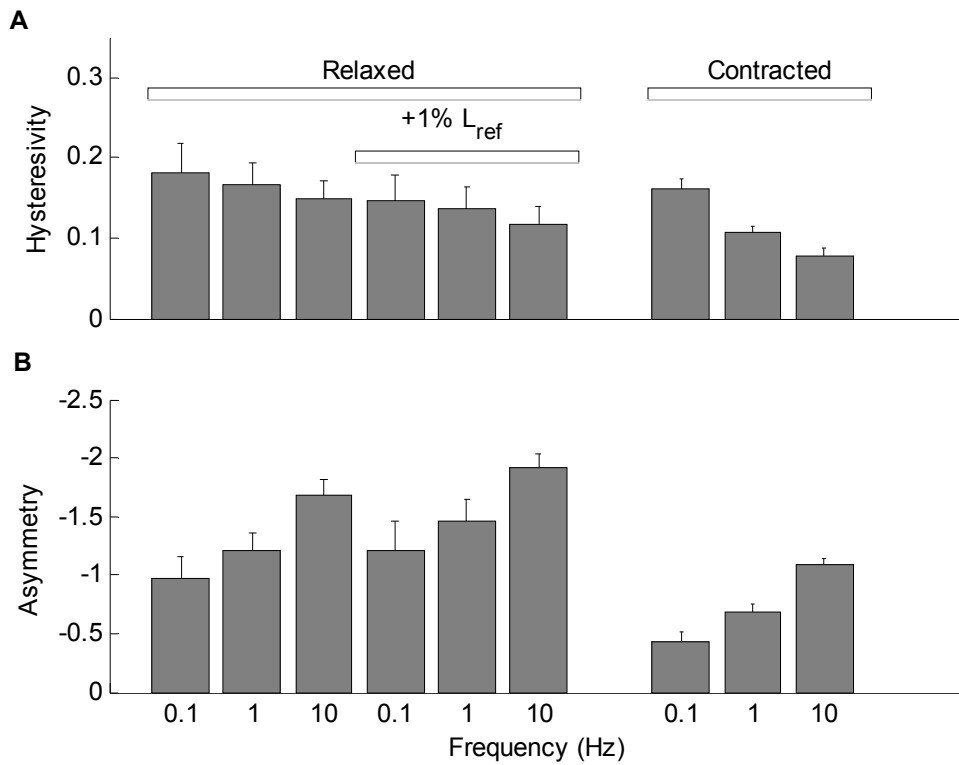


Figure 6.5: Hysteresivity and asymmetry versus frequency for triangular wave oscillations. Triangular wave oscillations of various frequencies were applied first at L_{ref} and subsequently at 101% L_{ref} in relaxed muscle. Next the oscillations were repeated in contracted muscle. Similar trends exist in relaxed and contracted muscle.

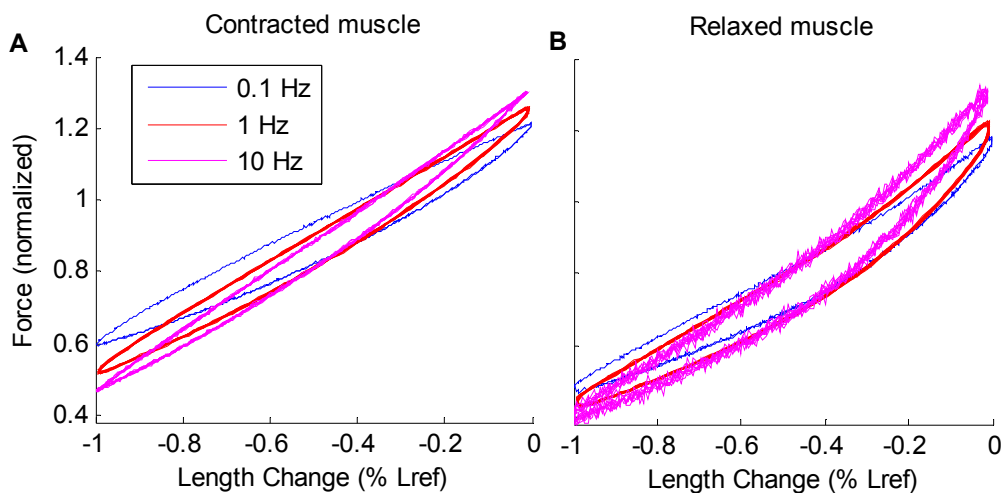


Figure 6.6: Sample of force-length loops of triangular wave oscillations at different frequencies. Relaxed muscles show a more asymmetrical loop compared to contracted muscle and a slightly large peak to peak force range.

Shortening velocity after oscillations. The shortening velocity is used as a measure of changes of cross-bridge cycling rates following oscillations in contracted muscle. Figure 6.7 shows that the shortening velocity is reduced in contracted ASM as compared to undisturbed muscle with a slight dependence of the reduction on the amplitude of oscillation. Shortening velocity at 20, 40, and 80 s after initiation of contracture increased compared to the reference shortening velocity at 700 s.

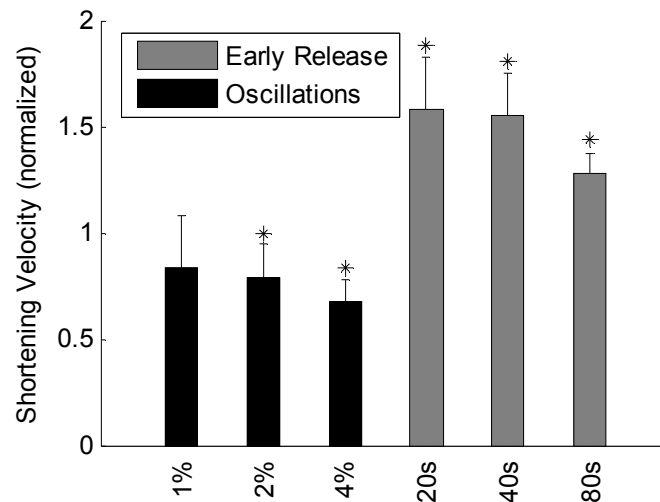


Figure 6.7: Normalised shortening velocity after oscillations or early release. Shortening velocity was normalised to values without oscillations after 700s of contracture (n=5) * denotes statistically different from unperturbed muscle.

Oscillations and square waves. To compare the shortening velocity after oscillations with power law relaxation data, oscillations in contracted and relaxed muscle are followed by square waves of small amplitude. Figure 6.8 shows a reduction in exponents for contracted muscle. As the oscillations are applied in sequence, the force in the contracted muscle increases slightly with each subsequent oscillation, while the largest amplitude oscillation permanently reduces the force in the tissue. These force developments mirror the exponent developments in contracted muscle. While force recovery from oscillations takes up to 50 s (hence a recovery period of 100 s was used) power law exponents settle on a stable value directly after oscillation, not to change until after the next oscillations. Relaxed muscles show a slight but not statistically significant decrease in exponents after oscillations, but with little consistency as can be seen from the much larger error bars.

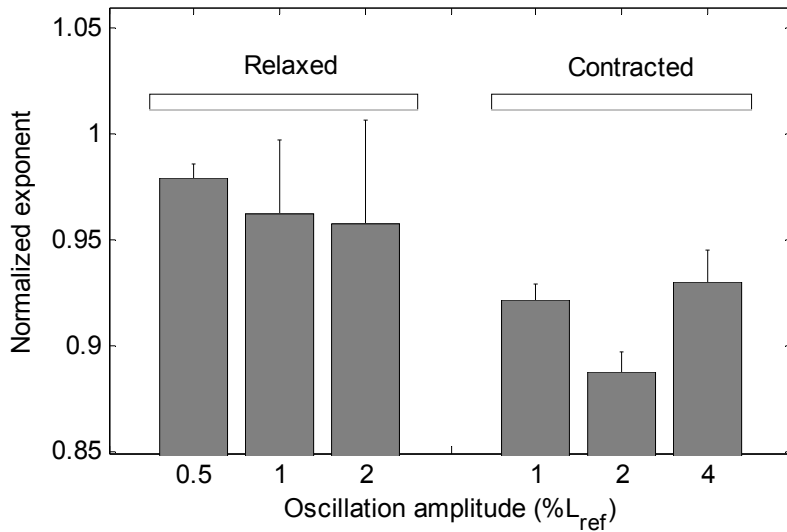


Figure 6.8: Exponent change after oscillations in contracted and relaxed muscle. Values are normalised to the exponent values prior to the first oscillation. Relaxed muscle oscillation amplitudes were smaller as higher amplitude oscillations resulted in too small signal to noise ratios for further analysis.

6.4.2 Power law confirmation and characterisation

To determine whether power law behaviour applies to ASM tissues, rapid length changes were applied and fitted with power functions. The force response to a single step length change (see Figure 6.3A) is fitted with a function of the form $F(t)=at^\alpha$ ($R^2_{\text{norm}}=0.996\pm 0.007$, $n=6$). The quality of this fit is better than fits of the force difference from the force prior to a length change. The power law behaviour is characterised with respect to the instantaneous stiffness and power law exponents. The instantaneous stiffness is analysed from staircase functions (see Figure 6.3C). The stiffness shows different correlations in different directions of length change: for positive length changes, the stiffness correlates linearly with F_{prior} ($R^2=0.96\pm 0.02$, $n=6$), while for negative length changes the stiffness correlates with F_{post} ($R^2=0.98\pm 0.01$, $n=6$). Similar correlations are found for staircase functions with superimposed square waves (Figure 6.3D) ($R^2=0.989\pm 0.006$ and $R^2=0.988\pm 0.005$, $n=6$).

Figure 6.9 shows that the power law exponents from curve fitting correlate with the ratio of F_{post} and F_{prior} according to $\alpha=a_2*\log(F_{\text{post}}/F_{\text{prior}})$. The average value for a_2 was -0.058 ± 0.0093 with $R^2=0.996\pm 0.003$ ($n=12$). Data from staircase functions do not conform to this correlation, with the first length step of a staircase section coinciding but subsequent steps progressively deviating.

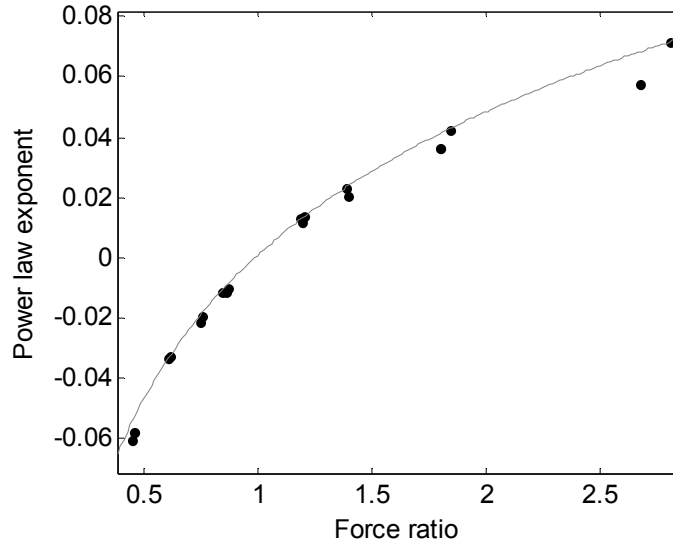


Figure 6.9: Sample of force ratio versus power law exponent correlation. Grey line represents curve fit $a_2 \cdot \ln(F_{\text{post}}/F_{\text{prior}})$. For all data a_2 was -0.058 ± 0.0093 with $R^2 = 0.996 \pm 0.003$ ($n=12$).

The effect of varying the ramp speeds Δt_r during one phase length steps (see Figure 6.3A) and two phase length steps of equal total amplitude (see Figure 6.3B) were investigated to determine the dependence of power law relaxation on the speed of length change. All of these relations converge to the same power law response. That is, they converged to a single power-law multiplier (one-way ANOVA $P = 0.29$ and $P = 0.20$ for positive and negative length changes ($n = 6$), respectively) and exponent (one-way ANOVA $P = 0.49$ and $P = 0.4$ for positive and negative length changes ($n = 6$), respectively).

6.4.3 Sequential multiplication

To examine whether sequential multiplication adequately describes the force response to consecutive length steps, two phase length steps with varying relative amplitudes were applied (see Figure 6.3B). The force response after each first length step is fitted with $F(t) = at^{\alpha_1}$ and after the second length step with $F(t) = bt^{\beta} (t + \Delta t)^{\alpha_2}$, where Δt is the time between the two length changes and a, b, α_1, α_2 and β are the fitting parameters determined by the least square fitting method. To assess the quality of fit difference between setting $\alpha_1 \neq \alpha_2$ (three parameter fit, sample in Figure 6.10A) and $\alpha_1 = \alpha_2$ (two parameter fit, sample in Figure 6.10B), the area between the fitting curve and the measured data on double logarithmic scale, as shown in Figure 6.11, is calculated. For positive ΔL_1 and negative ΔL_2 , sequential multiplication with full conservation of power law exponent applies, while in most other cases a three

parameter fit provides significantly better fits to the data. In all cases the three parameter fit provides a very high quality of fit, $R^2_{\text{norm}}=0.996\pm 0.01$, $n=6$.

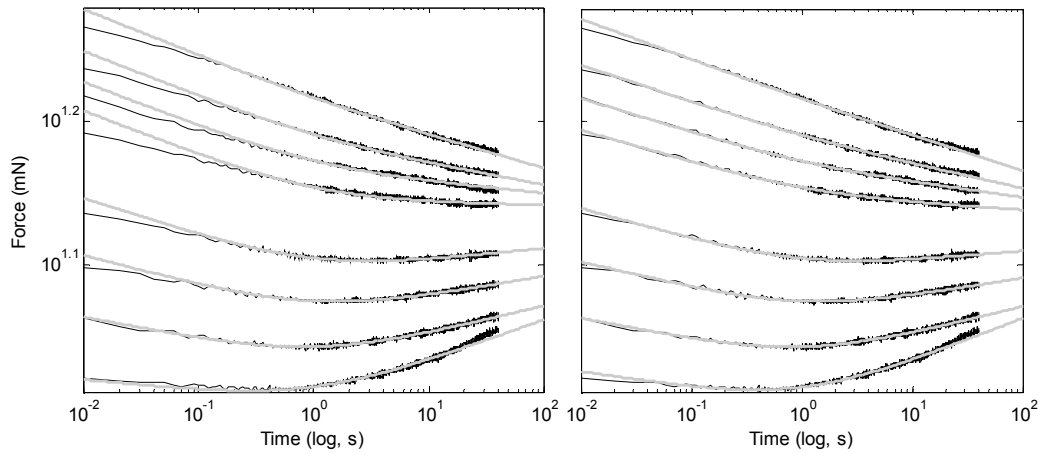


Figure 6.10: Sample of curve fits of negative length steps followed by positive length steps. Graphs show three parameter fit (left) and two parameter fit with predetermined c (right). Black lines are raw data, grey lines are fits.

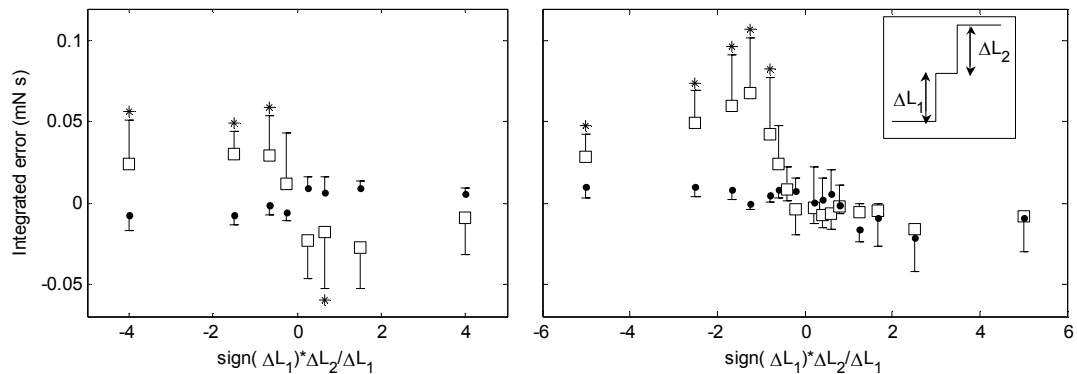


Figure 6.11: Quality of fit analysis using integrated error. Length changes of opposite direction are shown on the left, length change of equal direction are shown on the right. \square = two parameter fit with predetermined c (see text), \bullet = three parameter fit. Data marked with star show statistically significant difference of the absolute values of the integrated error.

6.4.4 Temperature effects

To test whether the findings at room temperature would apply at body temperature, the muscle was contracted at both 23°C and 37°C, while the length was perturbed by a continuous square wave. Force and stiffness increase slightly after the temperature change, but both return to the values prior to the temperature change after the

contracture at 37 °C (Figure 6.12). The power law exponent in both length change directions is not significantly affected by temperature changes.

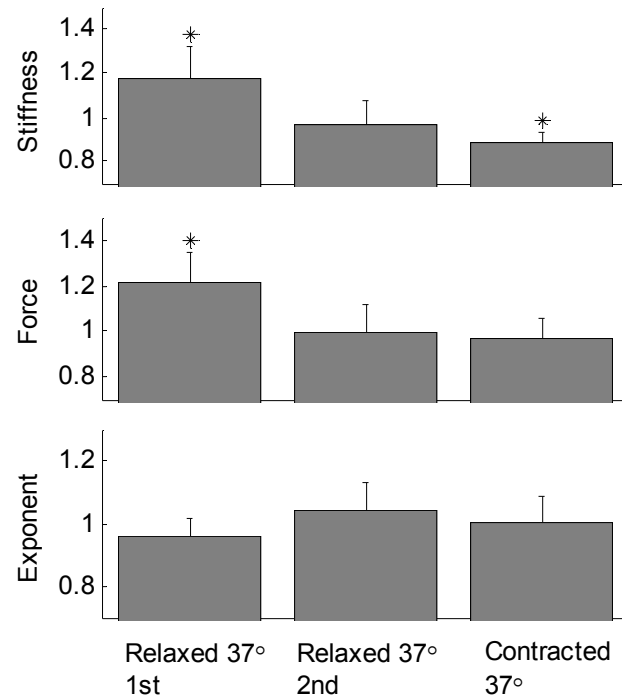


Figure 6.12: Temperature sensitivity of stiffness, force and power law exponent ($n=6$). The 1st bar shows the values in relaxed ASM 600 seconds after temperature change normalised to the values before the temperature change. The second bar shows the values for relaxed ASM after a contracture at 37 °C, also normalised to the values prior to temperature change. The third bar shows the 3 values for contracted ASM at 37 °C normalised to contracture at 23 °C. Stars denote statistically significant difference with 23 °C values.

6.5 Discussion and Analysis

The aims formulated in Section 6.1 are each addressed by the conducted experiments and discussed below. The first two aims on the importance of crossbridge dynamics in relaxed ASM and passive dynamics in contracted ASM are interrelated and are therefore discussed in a single subsection.

6.5.1 Comparing Contracted and Relaxed ASM

To assess the role of cross-bridge cycling in ASM dynamics, the oscillation response in contracted and relaxed muscle was investigated. While a certain level of tone exists in relaxed muscle [150], the reduced number of active cross-bridges compared with contracted muscle should reduce their effect on the dynamics of relaxed muscle.

However, the results have shown that there is little difference in the response of contracted and relaxed muscle. This indicates that the effect of cross-bridge cycling is minimal. Apparently the latch state [101] is not disturbed by oscillation, but rather provides a static stiffness when the muscle is fully contracted. An often used assessment of cross-bridge cycling activity is hysteresivity [123, 133]. This showed an increase for larger oscillations (Figure 6.4), but its value in describing cross-bridge activity is contradicted by the larger hysteresivity in relaxed muscle. Therefore, it seems likely that passive dynamics and not cross-bridge cycling determines both the hysteresivity and the asymmetry of force-length loops, while contractile elements raise the absolute force and stiffness values.

The observed slightly reduced shortening velocity after oscillation further supports this hypothesis. Shortening velocity in response to oscillations was previously investigated by Wang et al. [128], who showed a reduced shortening velocity in trachealis smooth muscle when oscillations were applied starting before the onset of a contracture. However, these experiments did not show whether the reduction could be attributed to the oscillations in relaxed muscle, at the onset of the contracture or in fully contracted muscle.

Although the term shortening velocity is used here, unlike in skeletal muscles the shortening velocity of the contractile elements can not be directly observed in ASM. Instead, in ASM it represents a point of balance of forces between the shortening contractile elements and the resistance to length changes of the non-contractile components. Assuming all other variables constant, an increase in contractile element shortening velocity should result in an increase of measured shortening velocity. The observation that the shortening velocity decreased rather than increased after oscillations confirms that cross-bridge cycling speed is either unaffected or reduced by oscillations. Their cycling speed may be too low to be affected by oscillations of 0.2Hz or more. If oscillations do not affect cross-bridge cycling speed in contracted muscle, there is little reason to expect a stretch activated increase in cross-bridge cycling speed in relaxed ASM. The tone in relaxed ASM probably provides a slightly increased absolute force level, but has no dynamic contribution. Consequently the hypothesis that cross-bridge cycling does not play a role in the response to length changes in relaxed ASM was confirmed.

All oscillations were applied with a peak oscillation length equal to the reference length. Large force reductions have been reported for oscillations with a mean length equal to the reference length [123], while no such reductions were found for peak oscillation length equal to reference length [134]. This difference in response in the literature indicates that the observed force reduction was likely the result of the larger peak length rather than the effect of oscillations on cross-bridge dynamics. Length changes above reference length have previously been shown to result in semi-permanent change of the force-length relation in both relaxed [159] and contracted smooth muscles [87]. Despite the difference in peak oscillation length, hysteresivity of oscillations in contracted ASM showed some similarity with the results presented by Fredberg et al [123].

6.5.2 Confirmation of Power law relaxation of force

The experiments provide direct evidence for the existence of absolute power law relaxation of force in response to sudden length changes in ASM tissues. These findings are consistent with the reported power law relaxation of stiffness in ASM cells after bead excitation [117]. This indicates that intercellular connections and differences between *in vivo* cells and cultured ASM cells do not affect the type of dynamic response. Furthermore, the force response to length change in the experiments could be accurately fitted with power laws from the first 0.01 s until several minutes after a length change. A single power function response over such a broad timescale indicates that relaxed ASM responds to length changes as a single mechanical entity. This also indicates that cross-bridge cycling does not affect the relaxed muscle response, as cross-bridge cycling can not be expected to influence the force response on very small timescales. The observation that length change velocity during a step length change did not affect the final force response challenges the concept of strain-induced fluidisation and subsequent solidification in the absence of strain as proposed in the soft glasses theory [61]. Conversely, when sequential multiplication is applied to continuous length changes, a ramped length change would result in convergence to the same power function independent of the speed of the length change because the total length change rather than the ramp speed would determine this power function.

6.5.3 Quantification of power law parameters

The linear relation between stiffness and force indicates that in terms of the power law behaviour the multiplier is dependent on force and the magnitude of length change. A direct correlation between stiffness and pre-stress has also been found in cultured ASM cells, which indicates that intercellular components and processes have little effect on the dynamic force response [112, 113, 169]. Further evidence of this is the finding that the power law relaxation exponent depends on the F_{post}/F_{prior} ratio (Figure 6.9). Through the stiffness correlation with F_{prior} , a correlation between F_{prior} and power law relaxation exponents results, which was also found in cells in [112, 113]. The finding that power law relaxation is independent of the speed of stretch also provides a novel explanation for the observed power law relation between cell stiffness and oscillation frequency [156]. After all, this finding implies that the effect of previous length changes decreases in time with a power function. Translated to length oscillations, the peak to peak force, and consequently the loop stiffness, will depend on the frequency of oscillation with a power function.

The experiments on length oscillations followed by square waves showed that while oscillations decrease the power law exponent, this exponent did not change in time after the oscillation. Apparently oscillations can cause a small length adaptive change which results in a change in exponent, but this change is permanent, at least as long as the relaxed or contracted state is maintained. Similar effects were observed in the simple length step experiments, where the first length change had a slightly higher power law exponent, while subsequent length changes did not show further change. Potentially after a contraction some weak cross links exist in the cells, which can be disrupted by length changes, changing the force response of the muscle.

6.5.4 Sequential multiplication

The finding that all two-phase step force responses were fitted accurately by a three parameter curve fit based on sequential multiplication (Figure 6.11) does not, by itself, confirm that sequential multiplication plays a role in ASM. However, the finding that a certain subset of two phase length step responses (i.e. where ΔL_1 is positive and ΔL_2 is negative, see Figure 6.3B) can be fitted with a two parameter curve fit with conservation of the power law exponent of the first length step, provides much stronger evidence that sequential multiplication is central to ASM

dynamics. For all other two phase length steps the power law exponent of the prior length step response was reduced in the three parameter curve fits. Sequential multiplication likely still applies in these cases, but interference between the two length changes resulted in a reduction of the effect of the first length change. The dependence of the power law response on amplitude of stretch rather than stretch velocity suggests that the interference is determined by the magnitude of the length changes and not the time between length steps.

6.5.5 Mechanical explanation

The experiments show that ASM dynamics conform to a single material response, with a long mechanical memory despite little being known about the molecular dynamics. This response is possibly the result of a large range of complex mechanisms inside the cells at different time scales. Perhaps the large protein molecules are subject to forced reptation [178] during stretch. With the many different protein sizes and entanglement in the cell this might smooth out to a single mechanical response.

While strain induced softening makes intuitive sense in cell mechanics, the results seem to contradict it. If the response to a length change would be to soften the cell, this is expected to be a uniform process throughout the cell. Yet sequential multiplication power law exponents to exist in parallel, which cannot be explained with a single softening parameter. Moreover it is also counterintuitive that strain softening in response to stretch is independent of the speed of application of the stretch as was found here.

6.6 Closure

A series of experiments to investigate power law relaxation and the role of cross-bridge cycling in relaxed and contracted ASM dynamics have been described in this chapter. In the following chapter the results from these experiments are used to validate the previously developed models, in particular the passive dynamics model.

CHAPTER 7

Model Validation and Adjustment

7.1 Introduction

The contractile/length adaptation model and the sequential multiplication model were investigated for their compliance with the experimental results of Chapter 6. The consequences of the experimental results on contracted ASM for the length adaptation model are discussed in Section 2. As the majority of experiments focused on relaxed ASM, a more in depth discussion of the consequences for the sequential multiplication model is given in Section 3. Also an improved version of this model is presented and validated in this section.

7.2 Length adaptation

While the experiments of Chapter 6 were primarily designed to investigate the passive dynamic behaviour of ASM, the experiments conducted to confirm the validity of pure passive response in relaxed ASM have several implications for length adaptation and contractile processes. Firstly the shortening velocity reduction after oscillation in contracted ASM is a strong indication that the biochemical explanation for force reduction from the 4 state model is inaccurate. During oscillations in contracted muscle, the 4 state model predicts a rapid increase in the number of phosphorylated cross-bridges, which have a higher cycling rate. Consequently the instantaneous shortening velocity is increased. Potentially, a very rapid return to slow cycling cross-bridges could occur after oscillations, yet this is not supported by model simulations. The shortening velocities of the Hill type model and the SDR model are not affected by oscillations. The actual reduction in shortening velocity can be attributed to slack in the cytoskeleton. A potentially reduced number of contractile elements and/or myosin heads does not reduce the shortening velocity of the cell at near zero loads, if the assumption of no internal resistance to shortening holds.

Oscillations in contracted and relaxed ASM show great similarity in force-length loops. In Section 7.3.3 of this chapter the ability of the sequential multiplication model to describe the force-length loops is investigated. It seems that cross-bridge

cycling is too slow to have much effect on the force response to oscillations of >0.2 Hz. The muscle is apparently unable to move from its latch state, but rather remains at very low cross-bridge cycling rates. Consequently the dynamics of the passive elements combined with the static stiffness of the contractile elements determines the force response of the tissue.

It has been shown previously that during ACh contractures the stiffness of the muscle keeps on increasing long after the force has plateaued [86]. During the onset of a contractile activation, when high levels of $[Ca^{2+}]_i$ exist, the contractile apparatus of the muscle responds rapidly, generating force at a high rate and allowing for high shortening velocities. Subsequently as $[Ca^{2+}]_i$ levels decrease, passive cross-linking might be locking up the contractile elements in an increasingly rigid cytoskeletal network. As a result the muscle can retain the force level without having to rely only on contractile action. Oscillations may cause some of these cross links to dissolve or plastically deform, which reduces the tension in the muscle and the transmission of contractile force. This might then be responsible for the reduced shortening velocity after oscillations. Such a sequence of events might provide an alternative explanation for the gradual force redevelopment after length changes and large oscillations in smooth muscle. The passive cross linking of contractile elements with the cytoskeleton may prevent further realignment of actin and myosin filaments as they are limited by the maximum force the cross-bridges can generate. Subsequent (partial) dissolution of these cross links when the contractile agonist is removed maintains the contractile elements in a slightly improved configuration, which upon contractile stimulation leads to an improved filament overlap.

7.3 Passive ASM

One of the key findings in Chapter 6 is that full multiplication of the force response in consecutive length steps applies in some but not all cases. While the force response to consecutive length changes can be described by a multiplication of the response to two individual length changes, the power law exponents are not necessarily maintained. An indication of the lack of full sequential multiplication is found when plotting length change amplitude versus power law exponent (Figure 7.1). Full sequential multiplication leads to a linear relationship between length change amplitude and power law exponent, as a length change of twice the magnitude would

result in twice the exponent. While this linearity seems to exist for small length changes, larger length changes show a smaller exponent than predicted by a linear relation.

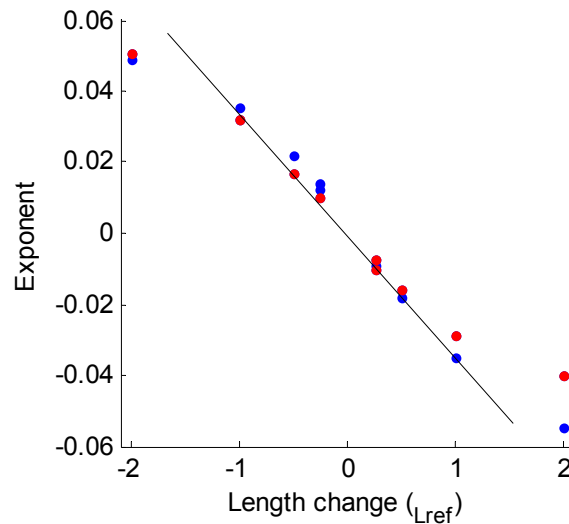


Figure 7.1: Sample of power law exponent versus length change amplitude. Red dots are length changes to L_{ref} , blue dots are length changes away from L_{ref} . Line represents linear correlation through zero.

The following findings have implications for the sequential multiplication model:

1. The power law response to length changes of equal amplitude but different speeds of length change converges to a single power function, with a unique multiplier and exponent
2. The power law multiplier is dependent on the force prior to a length change as well as the amplitude of the length change. A closer correlation exists for the force versus the relative force change upon a length change. However the first correlation is more applicable to the model.
3. The logarithmic relation between power law multiplier and power law exponent is confirmed.

Not all of the findings can be combined in a model on sequential multiplication. Some of the findings contradict each other in the context of pure sequential multiplication. For instance, force dependence of the power law multiplier suggests that in consecutive length changes, the product of the multipliers depends on the time between length changes. This is in contradiction with the first finding

of timing independent force response. Here adjustments to the model are proposed that combine the seemingly contradictory sequential multiplication principle with the non-linear relation between power law exponents and length change amplitude.

7.3.1 Methodology

The basis for the adjustment of the model is the assumption that the power law exponent and the power law multiplier relation with the length change amplitude is given, but not linear. Secondly the basis of superposition remains of the logarithmic variety, i.e. it is based on multiplication. The model has to be adjusted to allow for both these conditions to be satisfied. The following shows the derivation to incorporate both conditions and express the force as a function of the length history.

Given two consecutive length changes, the force response to the first length ΔL_1 is given by:

$$F(t) = F_0 a(\Delta L_1) t^{b(\Delta L_1)} \quad (7.1)$$

Where a and b are functions describing the multiplier and exponent dependency on ΔL . The force response to a second length change ΔL_2 at a time $t + \Delta t$ must then converge to:

$$F(t) = F_0 a(\Delta L_1 + \Delta L_2) (t - \Delta t)^{b(\Delta L_1 + \Delta L_2)} \quad (7.2)$$

However assuming logarithmic superposition, the actual response to the second length change equals:

$$F(t) = F_0 a(\Delta L_2) a(\Delta L_1) (t - \Delta t)^{b(\Delta L_2)} t^{b(\Delta L_1)} \quad (7.3)$$

To satisfy both conditions, the response to the second length change can be written as:

$$F(t) = F_0 a(\Delta L_2) (t - \Delta t)^{b(\Delta L_2)} \frac{a(\Delta L_1 + \Delta L_2)}{a(\Delta L_2)} (t)^{b(\Delta L_1 + \Delta L_2) - b(\Delta L_2)} \quad (7.4)$$

With $\Delta L_1 = L_2 - L_1$ and $\Delta L_2 = L_3 - L_2$ and generalised for n length steps from L_{n-1} to L_n this becomes:

$$F(t) = \prod_{i=1}^n \frac{a(L_n - L_{n-i})}{a(L_n - L_{n-i+1})} (t - t_i)^{b(L_n - L_{n-i}) - b(L_n - L_{n-i+1})} \quad (7.5)$$

In which the term $\prod_{i=1}^n \frac{a(L_n - L_{n-i})}{a(L_n - L_{n-i+1})}$ reduces to $a(L_n - L_0)$

This relation is equivalent to:

$$F(t) = a(L_n - L_0) e^{\sum_{i=1}^n (b(L_n - L_{n-i}) - b(L_n - L_{n-i+1})) \log(t - t_i)} \quad (7.6)$$

For $a(\Delta L)$ a function of the form $e^{a\Delta L}$ is chosen, while for $b(\Delta L)$ a two sided function of the form $b\Delta L + c\Delta L^2$ is chosen.

The model was implemented in Matlab (See Appendix A.9)

7.3.2 Results and discussion

The constants a, b and c were chosen based on curve fits to the step amplitude experiments in Chapter 6. Figure 7.2 shows a simulation of sinusoidal oscillation compared with the experimental results from Chapter 6. The reproduction of the total force excursion, the hysteresivity and the general force loop is quite accurate, though for large length excursions the peak force is depressed in the model, but not in the data. When simulating sinusoidal oscillation in contracted muscle the resulting force-length loops start out quite similar, but for larger oscillation amplitudes a much smaller force excursion is found. A change in the parameters of the passive dynamics is likely as a consequence of passive cross linking, yet for these simulations the parameters were assumed constant.

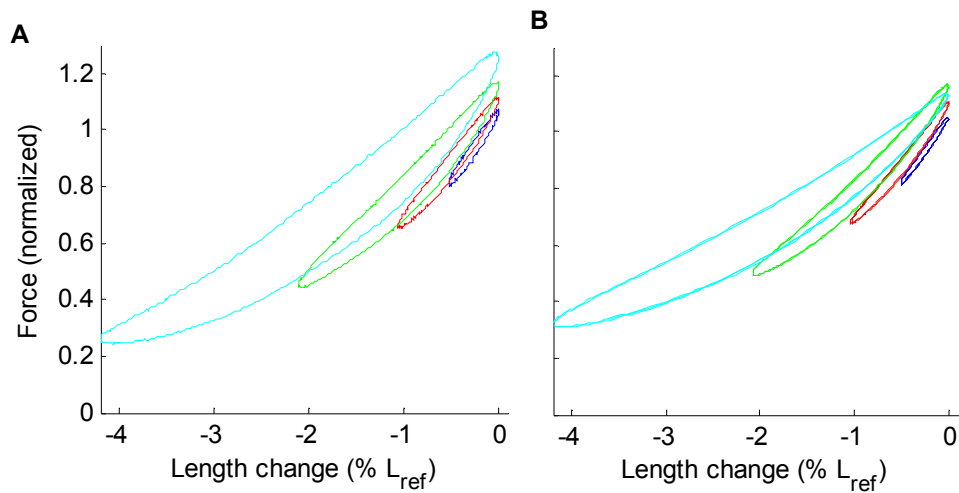


Figure 7.2: Force-length loops of sinusoidal oscillation. Experimental data on left, model data on right.

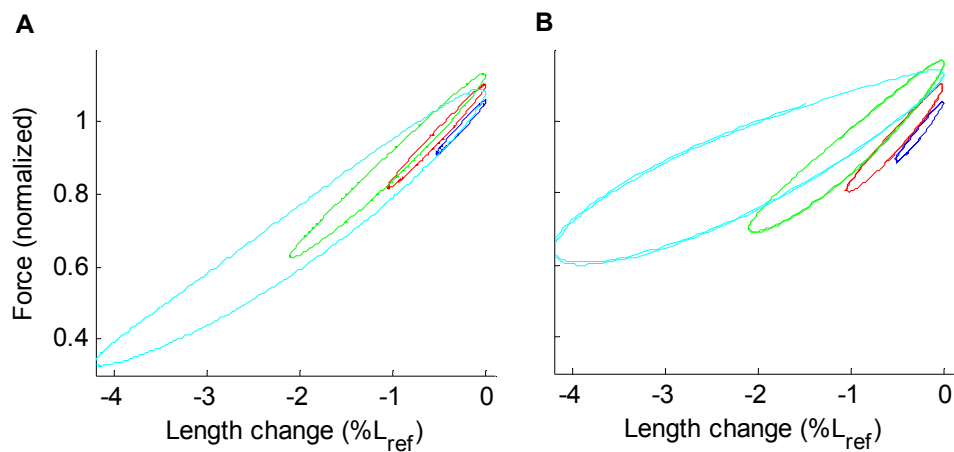


Figure 7.3: Force-length loops of sinusoidal oscillations in contracted ASM. Left panel shows experimental data, the right panel the simulation data.

For constant velocity oscillations a similar trend can be found. A good representation of force-length loops persist for oscillations in relaxed muscle, while contracted muscle shows less agreement for larger length excursions.

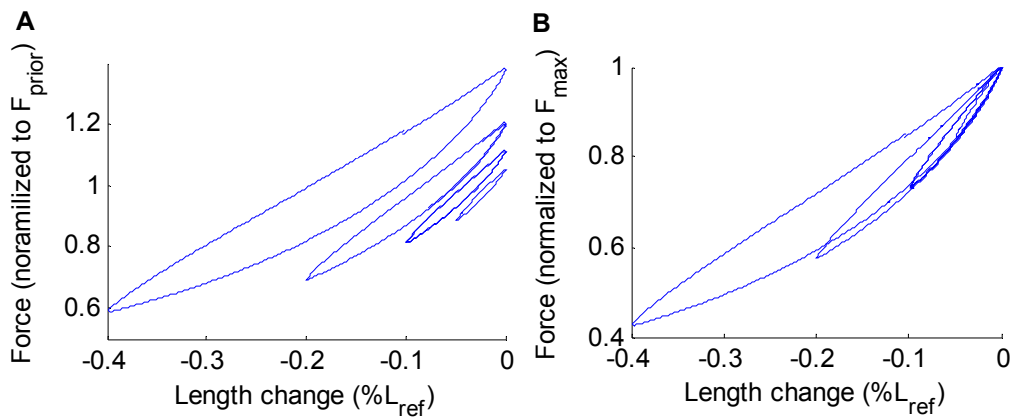


Figure 7.4: Simulation of triangular wave data.

Lastly the model is tested for successive rapid length changes. One difficulty in fitting the data is that the state of the tissue seems to have been changed from the step amplitude experiments to the consecutive length step experiments. To ensure a sufficiently high force for an acceptable signal to noise ratio and minimal background force fluctuations from the bubbling of the fluid, the consecutive length step experiments were performed at 102% of L_{ref} . Prior to the experiments a length step to the maximum length of the protocol was applied to minimise any length adaptive effects during the experiment itself. The prior step amplitude experiments however were all performed below L_{ref} as a smaller signal to noise ratio was sufficient for their analysis. Possibly the length change above L_{ref} changes the internal structure of the cells, causing the parameters of the adjusted sequential multiplication model to be changed. Figure 7.5A shows the fit using the unchanged parameters, and an attempt at improving the fit in panel B by adjusting the relation determining the multipliers. As the actual parameters are not known, this fitting process does not allow much insight into the ability of the model to replicate experimental data, however it does show that a single exponential relation for the multipliers generates a decent fit of the data. Exponents were not adjusted, as relaxation curves were simulated quite accurately with the original fitting. Future experimental investigation might shed more light on this issue. The observation that continuous length changes in relaxed ASM are modelled quite accurately is a better indication of the quality of the model.

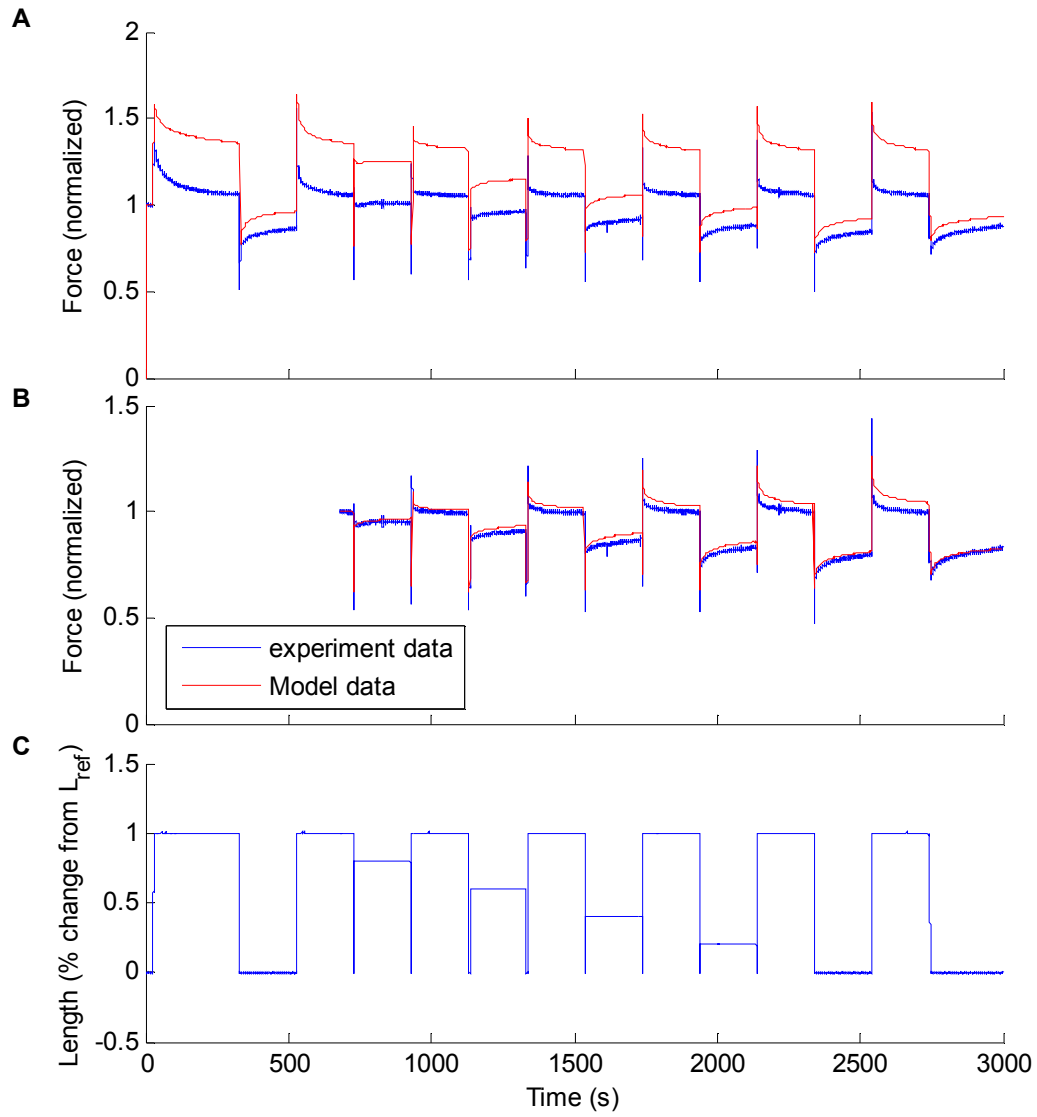


Figure 7.5: Force and length traces from model and experimental data. Top panel shows experimental data with the unadjusted model data, while the middle panel shows the adjusted model data. Forces are normalised to starting force.

CHAPTER 8

Conclusions and Future Work

8.1 Introduction

The main aim of this study was to investigate the relative contributions of the processes governing the mechanical behaviour of ASM. Three objectives were identified to address this aim. This thesis describes the results of the investigation for these objectives. In Chapter 1 and 2 the background of respiratory and airway physiology and the literature review of the existing knowledge and models of ASM were presented. A preliminary investigation in Chapter 3 provided the necessary experimental data for the development of passive dynamics models in Chapter 5. Chapter 4 used more widely available literature data on crossbridge dynamics to develop mathematical models, starting from the implementation of an existing cross-bridge model. In Chapter 6 an experimental study was presented which quantified ASM passive dynamics, validated the passive dynamics model and investigated the relative importance of passive and crossbridge dynamics in both relaxed and contracted muscle. Chapter 7 described how these results were used to adjust and validate the mathematical models.

8.2 Conclusions

In this section the conclusions of the investigation into each of the three objectives formulated in 2.6 are presented.

Quantify ASM passive dynamics.

An extensive literature review was presented which revealed that despite a century of research into ASM many aspects of its behaviour are not fully understood. The primary processes involved in ASM dynamics were identified: Cross-bridge dynamics, length adaptation and passive dynamics. The existing research on the passive component of ASM response was found to be insufficient for the purposes of quantitative modelling of tissue response. Consequently a preliminary experimental study was conducted to investigate

the passive behaviour further. Power law relaxation of force and sequential multiplication of force response to length changes was found in this study.

Develop an ASM dynamics model with a contractile, length adaptation and passive dynamics component.

After an initial separation of these three models a combined contractile-length adaptation model was developed as well as a separate passive dynamics model. The passive dynamics component showed to be a highly complex model to develop, partially because of the lack of quantitative data in the literature, and the lack of understanding of the dynamics of the internal processes in the tissue. The novel approach here was to use the step response of the muscle to develop a model with predictive capabilities for continuous length changes. This approach was chosen because of the relaxation behaviour of the muscle. This way individual length changes could be analysed according to their initial force response and subsequent relaxation, rather than trying to decipher the compound response occurring in oscillations. The lack of a known mechanical equivalent (springs and damper combinations) meant that close investigation of the frequency response of the muscle would not have revealed sufficient information to develop a model in the time domain nor the frequency domain.

The contractile model investigation started from the implementation of the HHM model, which has been used often in the literature and is generally perceived as the best attempt at modelling ASM cross-bridge cycling. The number of independent parameters of the model and the lack of physiological evidence of the central dephosphorylated latch bridge led to the development of two simplified models. The first followed the same implementation as the HHM model but was reduced from 4 to 2 effective states. The second model combined a contractile element based on the Hill force-velocity curve with a series elastic spring to represent the cytoskeletal context. This second model proved to be sufficiently accurate in modelling characteristics of ASM contractions, while being considerably less CPU intensive. This is necessary for implementation in the model of length adaptation.

A model of length adaptation using the Hill element contractile model was developed. Most of the features of length adaptation regarding shortening velocity and force development were described accurately by the model. It was suggested that incorporating the cytoskeletal context using moveable nodes rather than the currently implemented rigid nodes would improve the ability of the model to describe force depression after shortening and simulate force control.

Validate the developed models

Experiments were conducted to validate the passive component model. Close agreement between experiments and model predictions was found, although room for improvement remains. The principle of sequential multiplication proposed in this work was partially confirmed, and with some minor adjustments the model was capable of simulating both step length changes and continuous length changes in relaxed muscle quite accurately. In contracted muscle the model likely requires adjustment of governing parameters, but the experimental data strongly suggested that passive dynamics plays an important if not dominant role in contractile dynamics.

The length adaptation model provided an accurate representation of the trends in length-force and length-shortening velocity relations, however the shortcomings of published shortening velocity experiments and the lack of force controlled simulation capabilities limit more rigorous testing of the model. Comparison with literature data for the investigated contractile models showed that one of the predictions of the HHM cross-bridge model is contradicted by the conducted experiments on oscillations and shortening velocity.

The main aim of this work to understand the relative contributions of cross-bridge cycling, length adaptation and passive dynamics on ASM dynamics has been fulfilled to a great extent in this work. The experiments and modelling work have shown that passive dynamics play an important role even in contracted muscle, while cross-bridge dynamics seem to influence the contractile dynamics little. Cross-bridge cycling of course determines the force development upon contraction in ASM, but likely this cycling slows down to such a degree further along in the contraction that it

does not affect the dynamic response much. This slowing down can be attributed to a reduced $[Ca^{2+}]_i$ as well as increased non-contractile cross-linking in the cytoskeletal network.

The length adaptation investigation has shown a possible explanation for length adaptive effects reported in the literature. While the model still requires more development to include passive elements, it does represent the first mathematical model to explain force and shortening velocity in length adaptation through the dynamics of the actin and myosin filaments. Particularly it is the first mathematical model to explain why force adaptation is gradual with repeating contraction-relaxation cycles while shortening velocity adapts instantaneously.

The sequential multiplication model, while not perfect, has shown great promise in capturing the major phenomena observed in relaxed ASM. This understanding may provide the ground work in the search for a process based model.

8.3 Future work

The major weakness of the length adaptation – contraction model is the lack of a passive component context and the inability of force control simulation. Both deficiencies are strongly interrelated and could result in valuable future research. This requires the modelling of the cytoskeletal network with freely moveable nodes (dense bodies/dense plaques) and the inclusion of passive elements with power law behaviour. A first step could be the inclusion of string-like elastic elements, which model the development of slack after length reductions, and the constant breaking and replacing of passive and potentially active links. In a stochastic network setting such an approach would require a large number of elements and nodes to get representative repeatable results. Accordingly a major challenge will be to keep the required computation times down, because of the high degree of interrelated mechanics between nodes.

With respect to passive dynamics much more needs to be known about the processes that lead to power law relaxation behaviour. Both the experimental results and the presented model indicate that while the processes responsible for the power law relaxation behaviour are complex, the behaviour itself is not. Future work can lead to a more elegant formulation of the passive dynamics model, which may be applicable

to many different tissue types, and could potentially be applied to some inorganic material behaviour as well.

In its current form the models do not directly allow for simulation of the conditions in asthmatic muscle. Experiments on asthmatic muscle are problematic as the validity of animal models with respect to asthma is uncertain, and human tissue is usually derived from lobectomies, rather than tracheas. This requires testing of complete airways rather than ASM tissues as the muscle cannot be easily dissected from the airway wall. The modelling and experiments have shown that oscillations of breathing frequencies or higher do not have much effect on the contractile dynamics of the muscle. However the amplitude of those oscillations and general increases in length can greatly affect the contractibility of the muscle. Potentially asthmatic ASM is more rigid in its internal structure, resulting in less change of its contractile apparatus after stretch. Furthermore the increase in volume of both the muscle and other airway wall components could severely reduce the airway diameter fluctuations during breathing and deep inspiration in asthmatics, which would reduce any beneficial effects these fluctuations might have.

Bibliography

1. **Holt, S. and R. Beasley.** *The burden of asthma in New Zealand.* 2002, Wellington. 48. ISBN: 0-86471-095-X
2. **Rizzo, M.C.V. and D. Sole.** Inhaled corticosteroids in the treatment of respiratory allergy: safety vs. efficacy. *Jornal de Pediatria* 82(5): 198-205, 2006.
3. **Matsumoto, H., K. Ishihara, T. Hasegawa, B. Umeda, A. Niimi, and M. Hino.** Effects of Inhaled Corticosteroid and Short Courses of Oral Corticosteroids on Bone Mineral Density in Asthmatic Patients. *Chest* 120: 1468-1473, 2001.
4. **Boulet, L.P.,** Perception of the role and potential side effects of inhaled corticosteroids among asthma patients. *Chest* 113(3): 587, 1998.
5. **Shen, X., S.J. Gunst, and R. Tepper.** Effect of tidal volume and frequency on airway responsiveness in mechanically ventilated rabbits. *J Appl Physiol* 83(4): 1202-1208, 1997.
6. **Salerno, F.G., R. Pellegrino, G. Trocchio, A. Spanevello, V. Brusasco, and E. Crimi.** Attenuation of induced bronchoconstriction in healthy subjects: effects of breathing depth. *J Appl Physiol* 98: 817-821, 2005.
7. **Salerno, F.G., P. Guido, and A. Spanevello.** Tidal breathing affects airway responsiveness to methacholine. *Monaldi Arch Chest Dis* 56(6): 504-507, 2001.
8. **Singh, V., A. Wisniewski, J. Britton, and A. Tattersfield.** Effect of yoga breathing exercises (pranayama) on airway reactivity in subjects with asthma. *The Lancet* 335(8702): 1381-1383, 1990.
9. **Brown, R. and W. Mitzner.** Effects of tidal volume stretch on airway constriction in vivo. *J Appl Physiol* 91(5): 1995-1998, 2001.
10. **Stephens, N.L., W. Li, H. Jiang, H. Unruh, and X. Ma.** The biophysics of asthmatic airway smooth muscle. *Respir Physiol Neurobiol* 137(2-3): 125-140, 2003.
11. **Fredberg, J.J.,** Airway smooth muscle in Asthma. *Am J Respir Crit Care Med* 161: S158-S160, 2000.
12. **Romanet-Manent, S., D. Charpin, A. Magnan, A. Lanteaume, and D. Vervloet.** Allergic vs nonallergic asthma: what makes the difference? *Allergy* 57(7): 607-613, 2002.
13. **Stern, E.J., C.M. Graham, W.R. Webb, and G. Gamsu.** Normal trachea during forced expiration: dynamic CT measurements. *Radiology* 187(1): 27-31, 1993.
14. **Coburn, R.F., D. Thornton, and R. Arts.** Effect of trachealis muscle contraction on tracheal resistance to airflow. *J Appl Physiol* 32(3): 397-403, 1972.
15. **Marieb, E.N.,** *Human Anatomy & physiology.* 4th ed. 1998, Menlo Park, California: Addison Wesley Longman. ISBN: 978-0805341966
16. **Marklund, B., A. Tunsæter, and C. Bengtsson.** How often is the diagnosis bronchial asthma correct? *Family Practice* 16 (2): 112-116, 1999.
17. **Hickey, A.J.,** *Inhalation aerosols, physical and biological basis for therapy.* Vol. 94. 1996. ISBN: 0-8247-9702-7

18. **Salpeter, S.R., N.S. Buckley, T.M. Ormiston, and E.E. Salpeter.** Meta-Analysis: Effect of Long-Acting beta-Agonists on Severe Asthma Exacerbations and Asthma-Related Deaths. *Annals of Internal Medicine* 144(12): 904-914, 2006.
19. **Mchugh, P., F. Aitcheson, B. Duncan, and F. Houghton.** Buteyko breathing technique for asthma: an effective intervention. *Journal of the new zealand medical association* 116(1187), 2003.
20. **Bowler, S.D., A. Green, and C.A. Mitchell.** Buteyko breathing techniques in asthma: a blinded randomised controlled trial. *The medical journal of australia* 169: 575-578, 1998.
21. **Manocha, R., G.B. Marks, P. Kenchington, D. Peters, and C.M. Salome.** Sahaja yoga in the management of moderate to severe asthma: a randomised controlled trial. *Thorax* 57: 110-115, 2002.
22. **Mitzner, W.,** Bronchial Thermoplasty in asthma. *Allergology International* 55: 225-234, 2006.
23. **Yim, S., J.J. Fredberg, and A. Malhotra.** Continuous positive airway pressure for asthma: not a big stretch? *Eur Respir J* 29(2): 226-228, 2007.
24. **Kamm, R.D.,** Airway Wall Mechanics. *Annual review in Biomedical Engineering* 1: 47-72, 1999.
25. **Ramos-barbon, D., M.S. Ludwig, and J.G. Martin.** Airway remodeling. *Clinical Reviews in Allergy and Immunology* 27: 3-21, 2004.
26. **James, A.L., P.D. Pare, and J.C. Hogg.** The mechanics of airway narrowing in asthma. *Am J Respir Crit Care Med* 139: 246 - 246, 1989.
27. **An, S.S., T.R. Bai, J.H.T. Bates, J.L. Black, R.H. Brown, V. Brusasco, P. Chitano, L. Deng, M. Dowell, D.H. Eidelman, B. Fabry, N.J. Fairbank, L.E. Ford, J.J. Fredberg, W.T. Gerthoffer, S.H. Gilbert, R. Gosens, S.J. Gunst, A.J. Halayko, R.H. Ingram, C.G. Irvin, A.L. James, L.J. Janssen, G.G. King, D.A. Knight, A.M. Lauzon, O.J. Lakser, M.S. Ludwig, K.R. Lutchen, G.N. Maksym, J.G. Martin, T. Mauad, B.E. McParland, S.M. Mijailovich, H.W. Mitchell, R.W. Mitchell, W. Mitzner, T.M. Murphy, P.D. Pare, R. Pellegrino, M.J. Sanderson, R.R. Schellenberg, C.Y. Seow, P.S.P. Silveira, P.G. Smith, J. Solway, N.L. Stephens, P.J. Sterk, A.G. Stewart, D.D. Tang, R.S. Tepper, T. Tran, and L. Wang.** Airway smooth muscle dynamics: a common pathway of airway obstruction in asthma. *Eur Respir J* 29(5): 834-860, 2007.
28. **Haraguchi, M., S. Shimura, and K. Shirato.** Morphometric Analysis of Bronchial Cartilage in Chronic Obstructive Pulmonary Disease and Bronchial Asthma. *Am J Respir Crit Care Med* 159(3): 1005-1013, 1999.
29. **Moreno, R.H., C. Lisboa, J.C. Hogg, and P.D. Pare.** Limitation of airway smooth muscle shortening by cartilage stiffness and lung elastic recoil in rabbits. *J Appl Physiol* 75(2): 738-744, 1993.
30. **Hoppin, F.G., Jr.,** Parenchymal mechanics and asthma. *Chest* 107(3): 140S-144, 1995.
31. **Mauad, T., L.F.F. Silva, M.A. Santos, L. Grinberg, F.D.C. Bernardi, M.A. Martins, P.H.N. Saldiva, and M. Dolhnikoff.** Abnormal Alveolar Attachments with Decreased Elastic Fiber Content in Distal Lung in Fatal Asthma. *Am J Respir Crit Care Med* 170(8): 857-862, 2004.
32. **Gelb, A.F., J. Licuanan, C.M. Shinar, and N. Zamel.** Unsuspected Loss of Lung Elastic Recoil in Chronic Persistent Asthma. *Chest* 121(3): 715-721, 2002.

33. **Anafi, R.C. and T.A. Wilson.** Airway stability and heterogeneity in the constricted lung. *J Appl Physiol* 91(3): 1185-1192, 2001.
34. **Winkler, T. and J.G. Venegas.** Complex airway behavior and paradoxical responses to bronchoprovocation. *J Appl Physiol* 103(2): 655-663, 2007.
35. **Brown, R.H. and W. Mitzner.** The myth of maximal airway responsiveness in vivo. *J Appl Physiol* 85(6): 2012-2017, 1998.
36. **Martin, J.G., A. Duguet, and D.H. Eidelman.** The contribution of airway smooth muscle to airway narrowing and airway hyperresponsiveness in disease. *Eur Respir J* 16: 349-354, 2000.
37. **Hirst, S.J., T.R. Walker, and E.R. Chilvers.** Phenotypic diversity and molecular mechanisms of airway smooth muscle proliferation in asthma. *Eur Respir J* 16: 159-177, 2000.
38. **Seow, Chun Y., R.R. Schellenberg, and Peter D. Pare.** Structural and Functional Changes in the Airway Smooth Muscle of Asthmatic Subjects. *Am J Respir Crit Care Med* 158(5): 179S-186, 1998.
39. **Antonissen, L.A., R.W. Mitchell, E.A. Kroeger, W. Kepron, K.S. Tse, and N.L. Stephens.** Mechanical alterations of airway smooth muscle in a canine asthmatic model. *J Appl Physiol* 46(4): 681-687, 1979.
40. **Duguet, A., K. Biyah, E. Minshall, R. Gomes, C.-G. Wang, M. Taoudi-Benchekroun, J.H.T. Bates, and D.H. Eidelman.** Bronchial Responsiveness among Inbred Mouse Strains . Role of Airway Smooth-Muscle Shortening Velocity. *Am J Respir Crit Care Med* 161(3): 839-848, 2000.
41. **Turner, D.J., P.B. Noble, M.P. Lucas, and H.W. Mitchell.** Decreased airway narrowing and smooth muscle contraction in hyperresponsive pigs. *J Appl Physiol* 93(4): 1296-1300, 2002.
42. **Wang, L. and P.D. Pare.** Deep inspiration and airway smooth muscle adaptation to length change. *Respir Physiol Neurobiol* 137(2-3): 169-178, 2003.
43. **Noble, P.B., P.K. McFawn, and H.W. Mitchell.** Intraluminal pressure oscillation enhances subsequent airway contraction in isolated bronchial segments. *J Appl Physiol* 96: 1161-1165, 2004.
44. **Fredberg, J.J.,** Airway obstruction in asthma: does the response to a deep inspiration matter? *Respiratory Research* 2(5), 2001.
45. **Skloot, G., S. Permutt, and A. Togias.** Airway Hyperresponsiveness in Asthma: A Problem of Limited Smooth Muscle Relaxation with Inspiration. *Journal of Clinical investigation* 96: 2393-2403, 1995.
46. **Burns, G.P. and G.J. Gibson.** Airway Hyperresponsiveness in Asthma: Not Just a Problem of Smooth Muscle Relaxation with Inspiration. *Am J Respir Crit Care Med* 158: 203-206, 1998.
47. **Burns, G.P. and G.J. Gibson.** A novel hypothesis to explain the bronchconstrictor effect of deep inspiration in asthma. *Thorax* 57: 116-119, 2002.
48. **Wang , L., P.D. Pare, and C.Y. Seow.** Effect of length oscillation on the subsequent force development in swine tracheal smooth muscle. *J Appl Physiol* 88: 2246-2250, 2000.
49. **Jensen, A., H. Atileh, B. Suki, E.P. Ingenito, and K.R. Lutchen.** Signal transduction in smooth muscle: selected contribution: airway caliber in healthy and asthmatic subjects: effects of bronchial challenge and deep inspirations. *J Appl Physiol* 91(1): 506-515, 2001.

50. **King, G.G., B.J. Moore, C.Y. Seow, and P.D. Pare.** Time course of increased airway narrowing caused by inhibition of deep inspiration during methacholine challenge. *Am J Respir Crit Care Med* 160(2): 454-457, 1999.
51. **Nadel, J.A. and D.F. Tierney.** Effect of a previous deep inspiration on airway resistance in man. *J Appl Physiol* 16(4): 717-719, 1961.
52. **Gunst, S.J., X. Shen, R. Ramchandani, and R.S. Tepper.** Bronchoprotective and bronchodilatory effects of deep inspiration in rabbits subjected to bronchial challenge. *J Appl Physiol* 91(6): 2511-2516, 2001.
53. **Brusasco, V., E. Crimi, G. Barisione, A. Spanevello, J.R. Rodarte, and R. Pellegrino.** Airway responsiveness to methacholine: effects of deep inhalations and airway inflammation. *J Appl Physiol* 87(2): 567-573, 1999.
54. **Gunst, S.J., J.Q. Stropp, and J. Service.** Mechanical modulation of pressure-volume characteristics of contracted canine airways in vitro. *J Appl Physiol* 68: 2223-2229, 1990.
55. **Salerno, F.G., N. Shinozuka, J.J. Fredberg, and M.S. Ludwig.** Tidal volume amplitude affects the degree of induced bronchoconstriction in dogs. *J Appl Physiol* 87(5): 1674-1677, 1999.
56. **Salerno, F.G., N. Shinozuka, J.J. Fredberg, and M.S. Ludwig.** Tidal volume amplitude affects the degree of induced bronchoconstriction in dogs. *J Appl Physiol* 87(5): 1674-1677, 1999.
57. **Kleinsasser, A., I.M. Olfert, A. Loekinger, G.K. Prisk, S.R. Hopkins, and P.D. Wagner.** Tidal volume dependency of gas exchange in bronchoconstricted pig lungs. *J Appl Physiol* 103(1): 148-155, 2007.
58. **McClellan, M.A., M.J. Matheson, K. McKay, P.R.A. Johnson, A.C. Rynell, A.J. Ammit, J.L. Black, and N. Berend.** Low lung volume alters contractile properties of airway smooth muscle in sheep. *Eur Respir J* 22(1): 50-56, 2003.
59. **Kuo, K.-H., A.M. Herrera, and C.Y. Seow.** Ultrastructure of airway smooth muscle. *Respir Physiol Neurobiol* 137(2-3): 197-208, 2003.
60. **Gunst, S.J. and D.D. Tang.** The contractile apparatus and mechanical properties of airway smooth muscle. *Eur Respir J* 15(3): 600-616, 2000.
61. **Fabry, B. and J.J. Fredberg.** Remodeling of the airway smooth muscle cell: are we built of glass? *Respir Physiol Neurobiol* 137(2-3): 109-124, 2003.
62. **Huxley, A.F.,** Muscle Structure and Theories of Contraction. *Progress in Biophysics and Molecular Biology* 7: 255-318, 1957.
63. **Huxley, H.E.,** Review: Fifty Years of muscle and the sliding filament hypothesis. *European Journal of Biochemistry* 271: 1403-1415, 2004.
64. **Hai, C.M. and R.A. Murphy.** Cross-bridge phosphorylation and regulation of latch state in smooth muscle. *Am J Physiol Cell Physiol* 254(1): C99-106, 1988.
65. **Hai, C.M. and R.A. Murphy.** Regulation of shortening velocity by cross-bridge phosphorylation in smooth muscle. *Am J Physiol Cell Physiol* 255(1): C86-94, 1988.
66. **Xu, J.Q., B.A. Harder, P. Uman, and R. Craig.** Myosin filament structure in vertebrate smooth muscle. *J Cell Biol* 134(1): 53-66, 1996.
67. **Craig, R. and J. Megerman.** Assembly of smooth muscle myosin into side-polar filaments. *J Cell Biol* 75(3): 990-996, 1977.
68. **Butler, T.M. and M.J. Siegman.** Control of cross-bridge cycling by myosin light chain phosphorylation in mammalian smooth muscle. *Acta physiologica Scandinavica* 164: 389-400, 1998.

69. **Lecarpentier, Y., F.X. Blanc, S. Salmeron, J.C. Pourny, D. Chemla, and C. Coirault.** Myosin cross-bridge kinetics in airway smooth muscle: a comparative study of humans, rats, and rabbits. *Am J Physiol Lung Cell Mol Physiol* 282: L83-L90, 2002.
70. **Vibert, P. and W. Lehman.** Three-dimensional Reconstruction of Caldesmon-containing Smooth Muscle Thin Filaments. *The Journal of Cell Biology* 123: 313-321, 1993.
71. **Morgan, K.G. and S.S. Gangopaghyay.** Signal Transduction in Smooth Muscle Invited Review: Cross-bridge regulation by thin filament-associated proteins. *J Appl Physiol* 91: 953-962, 2001.
72. **Paul, R.J.,** Smooth muscle energetics and theories of cross-bridge regulation. *American Journal of Physiology - Cell Physiology* 258(27): C369-C375, 1990.
73. **Takahashi, K., R. Yoshimoto, K. Fuchibe, A. Fujishige, M. Mitsui-Saito, M. Hori, H. Ozaki, H. Yamamura, N. Awata, S. Taniguchi, M. Katsuki, T. Tsuchiya, and H. Karaki.** Regulation of Shortening Velocity by Calponin in Intact Contracting Smooth Muscles. *Biochemical and Biophysical Research Communications* 279: 150-157, 2000.
74. **Tseng, S., R. Kim, T. Kim, K.G. Morgan, and C.M. Hai.** F-actin disruption attenuates agonist-induced [Ca²⁺], myosin phosphorylation, and force in smooth muscle. *Am J Physiol Cell Physiol* 272(6): C1960-1967, 1997.
75. **Rembold, C.M., R.L. Wardle, C.J. Wingard, T.W. Batts, E.F. Etter, and R.A. Murphy.** Cooperative attachment of cross bridges predicts regulation of smooth muscle force by myosin phosphorylation. *American Journal of Physiology - Cell Physiology* 287: C594-C602, 2004.
76. **Gunst, S.J., D.D. Tang, and A. Opazo Saez.** Cytoskeletal remodeling of the airway smooth muscle cell: a mechanism for adaptation to mechanical forces in the lung. *Respir Physiol Neurobiol* 137(2-3): 151-168, 2003.
77. **Dowell, M.L., O.J. Lakser, W.T. Gerthoffer, J.J. Fredberg, G.L. Stelmack, A.J. Halayko, J. Solway, and R.W. Mitchell.** Latrunculin B increases force fluctuation-induced relengthening of ACh-contracted, isotonicly shortened canine tracheal smooth muscle. *J Appl Physiol* 98: 489-497, 2005.
78. **Mehta, D. and S.J. Gunst.** Actin polymerization stimulated by contractile activation regulates force development in canine tracheal smooth muscle. *J Physiol* 519.3: 829-840, 1999.
79. **An, S., R. Laudadio, J. Lai, R. Rogers, and J.J. Fredberg.** Stiffness changes in cultured airway smooth muscle cells. *J Physiol* 283: C792-C801, 2002.
80. **Laudadio, R., E. Millet, B. Fabry, S. An, J.P. Butler, and J.J. Fredberg.** Rat airway smooth muscle cell during actin modulation: rheology and glassy dynamics. *American Journal of Physiology* 289: 1388-1395, 2005.
81. **Herrera, A.M., E.C. Martinez, and C.Y. Seow.** Electron microscopic study of actin polymerization in airway smooth muscle. *American Journal of Physiology* 286: L1161-L1168, 2004.
82. **Kuo, K.-H., L. Wang, P.D. Pare, L.E. Ford, and C.Y. Seow.** Myosin thick filament lability induced by mechanical strain in airway smooth muscle. *J Appl Physiol* 90: 1811-1816, 2001.
83. **Halayko, A.J. and Y. Amrani.** Mechanisms of inflammation-mediated airway smooth muscle plasticity and airways remodeling in asthma. *Respir Physiol Neurobiol* 137(2-3): 209-222, 2003.

84. **Black, J.L., J.K. Burgess, and P.R.A. Johnson.** Airway smooth muscle--its relationship to the extracellular matrix. *Respir Physiol Neurobiol* 137(2-3): 339-346, 2003.
85. **Pratusevich, V.R., C.Y. Seow, and L.E. Ford.** Plasticity in canine airway smooth muscle. *J Gen Physiol* 105(1): 73-94, 1995.
86. **Gunst, S.J., R.A. Meiss, M.-F. Wu, and M. Rowe.** Mechanisms for the mechanical plasticity of tracheal smooth muscle. *Am J Physiol Cell Physiol* 268: C1267-C1276, 1995.
87. **Gunst, S.J. and M.F. Wu.** Plasticity in Skeletal, Cardiac, and Smooth Muscle Selected Contribution: Plasticity of airway smooth muscle stiffness and extensibility: role of length-adaptive mechanisms. *J Appl Physiol* 90: 741-749, 2000.
88. **Halayko, A.J. and J. Solway.** Plasticity in Skeletal, Cardiac, and Smooth Muscle Invited Review: Molecular mechanisms of phenotypic plasticity in smooth muscle cells. *J Appl Physiol* 90: 358-368, 2001.
89. **Lambert, R.K., P.D. Pare, and C.Y. Seow.** Mathematical description of geometric and kinematic aspects of smooth muscle plasticity and some related morphometrics. *J Appl Physiol* 96: 469-476, 2004.
90. **Seow, C.Y. and F. J.J.,** Signal Transduction in Smooth Muscle Historical perspective on airway smooth muscle: the saga of a frustrated cell. *J Appl Physiol* 91: 938-952, 2001.
91. **Stephens, N.L., A.J. Halayko, and X. Ma.** The new kid on the airway smooth muscle block: plasticity theory and series-to-parallel filament transition. *J Appl Physiol* 89: 867-868, 2000.
92. **Gunst, S.J. and J.J. Fredberg.** Airway Hyperresponsiveness: From Molecules to Bedside Invited Review: The first three minutes: smooth muscle contraction, cytoskeletal events, and soft glasses. *J Appl Physiol* 95: 413-425, 2003.
93. **Silveira, P., J.P. Butler, and J.J. Fredberg.** Length adaptation of airway smooth muscle: a stochastic model of cytoskeletal dynamics. *J Appl Physiol* 99: 2087-2098, 2005.
94. **Wang, L., P.D. Pare, and C.Y. Seow.** Plasticity in Skeletal, Cardiac, and Smooth Muscle Selected Contribution: Effect of chronic passive length change on airway smooth muscle length-tension relationship. *J Appl Physiol* 90: 734-740, 2000.
95. **Seow, C.Y.,** Myosin filament assembly in an ever-changing myofilament lattice of smooth muscle. *American Journal of Physiology - Cell Physiology* 289: C1363-C1368, 2005.
96. **Ali, F., L. Chin, P.D. Pare, and C.Y. Seow.** Mechanism of partial adaptation in airway smooth muscle after a step change in length. *J Appl Physiol* 103(2): 569-577, 2007.
97. **Smolensky, A.V., J. Ragozzino, S.H. Gilbert, C.Y. Seow, and L.E. Ford.** Length-dependent filament formation assessed from birefringence increases during activation of porcine tracheal muscle. *J Physiol* 563: 517-527, 2005.
98. **Jones, K.A., R.R. Lorenz, Y.S. Prakash, G.C. Sieck, and D.O. Warner.** ATP hydrolysis during contraction of permeabilized airway smooth muscle. *Am J Physiol Lung Cell Mol Physiol* 277(21): L334-L342, 1999.
99. **Hai, C.M. and R.A. Murphy.** Sr²⁺ activates cross-bridge phosphorylation and latch state in smooth muscle. *American Journal of Physiology* 255 (Cell Physiology 24): C401-C407, 1988.

100. **Hai, C.M. and R.A. Murphy.** Cross-bridge dephosphorylation and relaxation of vascular smooth muscle. *Am J Physiol Cell Physiol* 256: c282-c287, 1989.
101. **Dillon, P.F. and R.A. Murphy.** Tonic force maintenance with reduced shortening velocity in arterial smooth muscle. *Am J Physiol Cell Physiol* 242(11): C102-C108, 1982.
102. **Mitchell, R.W., C.Y. Seow, T. Burdyga, R. Maass-Moreno, V. Pratusевич, J. Ragozzino, and L.E. Ford.** Relationship between myosin phosphorylation and contractile capability of canine airway smooth muscle. *J Appl Physiol* 90: 2460-2465, 2001.
103. **Cremonese, C.R. and M.A. Geeves.** Interaction of Actin and ADP with the Head Domain of Smooth Muscle Myosin: Implications for Strain-Dependent ADP Release in Smooth Muscle. *Biochemistry* 37(7): 1969-1978, 1998.
104. **Dantzig, J.A., R.J. Barsotti, S. Manz, H.L. Sweeney, and Y.E. Goldman.** The ADP Release Step of the Smooth Muscle Cross-Bridge Cycle Is Not Directly Associated with Force Generation. *Biophys J* 77(1): 386-397, 1999.
105. **Sweeney, H.L.,** Regulation and Tuning of Smooth Muscle Myosin. *Am J Respir Crit Care Med* 158(5): 95S-99, 1998.
106. **Bai, T.R., J.H.T. Bates, V. Brusasco, B. Camoretti-Mercado, P. Chitano, L.H. Deng, M. Dowell, B. Fabry, L.E. Ford, J.J. Fredberg, W.T. Gerthoffer, S.H. Gilbert, S.J. Gunst, C.M. Hai, A.J. Halayko, S.J. Hirst, A. James, L.J. Janssen, K.A. Jones, G.G. King, O.J. Lakser, R.K. Lambert, A.-M. Lauzon, K.L. Lutchen, G.N. Maksym, R.A. Meiss, S.M. Mijailovich, H.W. Mitchell, H.W. Mitchell, W. Mitzner, T.M. Murphy, P.D. Pare, R.R. Schellenberg, C.Y. Seow, G.C. Sieck, P.G. Smith, A.V. Smolensky, J. Solway, N.L. Stephens, A.G. Stewart, D.D. Tang, and J. Wang.** On the terminology for describing the length-force relationship and its changes in airway smooth muscle. *J Appl Physiol* 97: 2029-2034, 2004.
107. **Small, E.V. and M. Gimona.** The cytoskeleton of the vertebrate smooth muscle cell. *Acta Physiologica Scandinavica* 164(4): 341-348, 1998.
108. **Kim, H.R. and C.M. Hai.** Mechanisms of mechanical strain memory in airway smooth muscle. *Canadian Journal of Physiology and Pharmacology* 83: 811-815, 2005.
109. **Ford, L.E. and S.H. Gilbert.** The significance of variable passive compliance in smooth muscle. *J Appl Physiol* 102(5): 1735-1736, 2007.
110. **Smolensky, A.V. and L.E. Ford.** The extensive length-force relationship of porcine airway smooth muscle. *J Appl Physiol* 102(5): 1906-1911, 2007.
111. **Mehta, D., M.F. Wu, and S.J. Gunst.** Role of contractile protein activation in the length-dependent modulation of tracheal smooth muscle force. *Am J Physiol Cell Physiol* 270(1): C243-252, 1996.
112. **Stamenovic, D., B. Suki, B. Fabry, N. Wang, and J.J. Fredberg.** Rheology of airway smooth muscle cells is associated with cytoskeletal contractile stress. *J Appl Physiol* 96: 1600-1605, 2003.
113. **Wang, N., I.M. Tolic-Norrelykke, J. Chen, S.M. Mijailovich, J.P. Butler, J.J. Fredberg, and D. Stamenovic.** Cell prestress. I. Stiffness and prestress are closely associated in adherent contractile cells. *Am J Physiol Cell Physiol* 282(3): C606-616, 2002.
114. **Smith, P.G., L. Deng, J.J. Fredberg, and G.N. Maksym.** Mechanical strain increases cell stiffness through cytoskeletal filament reorganization. *Am J Physiol Lung Cell Mol Physiol* 285(2): L456-463, 2003.

115. **Mijailovich, S.M., J.P. Butler, and J.J. Fredberg.** Perturbed Equilibria of Myosin Binding in Airway Smooth Muscle: Bond-Length Distributions, Mechanics, and ATP Metabolism. *Biophys J* 79(5): 2667-2681, 2000.
116. **Blanc, F.-X., C. Coirault, S. Salmeron, D. Chemla, and Y. Lecarpentier.** Mechanics and crossbridge kinetics of tracheal smooth muscle in two inbred rat strains. *Eur Respir J* 22: 227-234, 2003.
117. **Trepat, X., L. Deng, S.S. An, D. Navajas, D.J. Tschumperlin, W.T. Gerthoffer, J.P. Butler, and J.J. Fredberg.** Universal physical responses to stretch in the living cell. *Nature* 447(7144): 592-595, 2007.
118. **Opazo Saez, A., R.R. Schellenberg, M.S. Ludwig, R.A. Meiss, and P.D. Pare.** Tissue elastance influences airway smooth muscle shortening: Comparison of mechanical properties among different species. *Canadian Journal of Physiology and Pharmacology* 80: 865-871, 2002.
119. **Ramchandani, R., X. Shen, C.L. Elmsley, W.T. Ambrosius, S.J. Gunst, and R.S. Tepper.** Differences in airway structure in immature and mature rabbits. *J Appl Physiol* 89(4): 1310-1316, 2000.
120. **Wang, L., P. Chitano, and T.M. Murphy.** A maturational model for the study of airway smooth muscle adaptation to mechanical oscillation. *Canadian Journal of Physiology and Pharmacology* 83: 817-824, 2005.
121. **Lambert, R.K., T.A. Wilson, R.E. Hyatt, and J.R. Rodarte.** A computational model for expiratory flow. *J Appl Physiol* 52(1): 44-56, 1982.
122. **Fredberg, J.J., D.S. Inouye, S.M. Mijailovich, and J.P. Butler.** Perturbed equilibrium of myosin binding in airway smooth muscle and its implications in bronchospasm. *Am J Respir Crit Care Med* 159: 959-967, 1999.
123. **Fredberg, J.J., D. Inouye, B. Miller, M. Nathan, S. Jafari, S.H. Raboudi, J.P. Butler, Shore, and U. Sanocka.** Airway smooth muscle, tidal stretches, and dynamically determined contractile states. *Am J Respir Crit Care Med* 156: 1752-1759, 1997.
124. **Raboudi, D.H., B. Miller, J.P. Butler, S.A. Shore, and F. J.J.,** Dynamically Determined Contractile States of Airway Smooth Muscle. *Am J Respir Crit Care Med* 158: S176-S178, 1998.
125. **Maksym, G.N., L. Deng, N.J. Fairbank, C.A. Lall, and S.C. Connolly.** Beneficial and harmful effects of oscillatory mechanical strain on airway smooth muscle. *Canadian Journal of Physiology and Pharmacology* 83: 913-922, 2005.
126. **Meiss, R.A. and R.M. Pidaparti.** Mechanical state of airway smooth muscle at very short lengths. *J Appl Physiol* 96(2): 655-667, 2004.
127. **Shen, X., R.S. Tepper, and S.J. Gunst.** Pharmacological modulation of the mechanical response of airway smooth muscle to length oscillation. *J Appl Physiol* 83(3): 739-745, 1997.
128. **Wang, L., P.D. Pare, and C.Y. Seow.** Changes in force-velocity properties of trachealis due to oscillatory strains. *J Appl Physiol* 92: 1865-1872, 2002.
129. **Gunst, S.J.,** Contractile force of canine airway smooth muscle during cyclical length changes. *J Appl Physiol* 55(3): 759-769, 1983.
130. **Du, Y., A.M. Al-Jumaily, and H. Shukla.** Smooth muscle stiffness variation due to external longitudinal oscillations. *Journal of Biomechanics* 40(14): 3207-3214, 2007.
131. **Latourelle, J., B. Fabry, and J.J. Fredberg.** Dynamic equilibration of airway smooth muscle contraction during physiological loading. *J Appl Physiol* 92: 771-779, 2002.

132. **Fredberg, J.J.**, Airway narrowing in asthma: dose speed kill? *Am J Physiol Lung Cell Mol Physiol* 283: L1179-L1180, 2002.
133. **Fredberg, J.J., K.A. Jones, M. Nathan, S. Raboudi, Y.S. Prakash, S.A. Shore, J.P. Butler, and G.C. Sieck.** Friction in airway smooth muscle: mechanism, latch, and implications in asthma. *J Appl Physiol* 81(6): 2703-2712, 1996.
134. **Shen, X., M.F. Wu, R.S. Tepper, and S.J. Gunst.** Mechanisms for the mechanical response of airway smooth muscle to length oscillation. *J Appl Physiol* 83(3): 731-738, 1997.
135. **Anafi, R.C. and T.A. Wilson.** Empirical model for dynamic force-length behavior of airway smooth muscle. *J Appl Physiol* 92: 455-460, 2002.
136. **Bates, J.H.T. and A.M. Lauzon.** Modeling the oscillation dynamics of activated airway smooth muscle strips. *Am J Physiol Lung Cell Mol Physiol* 289: L849-L855, 2005.
137. **Fredberg, J.J.**, Frozen objects: Small airways, big breaths, and asthma. *Journal of allergy and clinical immunology* 106: 615-624, 2000.
138. **Bursac, P., G. Lenormand, M. Oliver, D.A. Weitz, V. Viasnoff, J.P. Butler, and J.J. fredberg.** Cytoskeletal remodelling and slow dynamics in the living cell. *Nat Mater* 5: 557-561, 2005.
139. **Huxley, H.E.**, A PERSONAL VIEW OF MUSCLE AND MOTILITY MECHANISMS. *Annual Review in Physiology* 58: 1-19, 1996.
140. **Zahalak, G.I.**, A Distribution-Moment Approximation for Kinetic Theories of Muscular Contraction. *Mathematical biosciences* 55: 89-114, 1981.
141. **Finer, J.T., R.M. Simmons, and J.A. spudich.** Single myosin molecule mechanics: piconewton forces and nanometre steps. *Nature* 368: 113-119, 1994.
142. **Kamm, K.E. and J.T. Stull.** Myosin phosphorylation, force, and maximal shortening velocity in neurally stimulated tracheal smooth muscle. *Am J Physiol Cell Physiol* 249(18): C238-C247, 1985.
143. **Murphy, R.A. and C.M. Rembold.** The Latchbridge hypothesis of smooth muscle contraction. *Canadian Journal of Physiology and Pharmacology* 83: 857-864, 2005.
144. **Murphy, R.A.**, What is special about smooth muscle? The significance of covalent crossbridge regulation. *The FASEB Journal* 8(3): 311-318, 1994.
145. **Metzger, J.M.**, Myosin binding-induced cooperative activation of the thin filament in cardiac myocytes and skeletal muscle fibers *Biophys J* 68(4): 1430-1442, 1995.
146. **Hai, C.M. and H.R. Kim.** An expanded latch-bridge model of protein kinase C-mediated smooth muscle contraction. *J Appl Physiol* 98(4): 1356-1365, 2005.
147. **Somlyo, A.P. and A.V. Somlyo.** Ca²⁺ Sensitivity of Smooth Muscle and Nonmuscle Myosin II: Modulated by G Proteins, Kinases, and Myosin Phosphatase. *Physiol Rev* 83(4): 1325-1358, 2003.
148. **Deng, L., N.J. Fairbank, B. Fabry, P.G. Smith, and G.N. Maksym.** Localized mechanical stress induces time-dependent actin cytoskeletal remodeling and stiffening in cultured airway smooth muscle cells. *Am J Physiol Cell Physiol* 287: C440-C448, 2004.
149. **Silberstein, J. and C.M. Hai.** Dynamics of length-force relations in airway smooth muscle. *Respiratory Physiology & Neurobiology* 132: 205-221, 2002.

150. **Deng, L., N.J. Fairbank, D.J. Cole, J.J. Fredberg, and G.N. Maksym.** Airway smooth muscle tone modulates mechanically induced cytoskeletal stiffening and remodeling. *J Appl Physiol* 99: 634-641, 2005.
151. **Seow, C.Y., V. Pratusевич, and L.E. Ford.** Series-to-parallel transition in the filament lattice of airway smooth muscle. *J Appl Physiol* 89: 869-876, 2000.
152. **Herrera, A.M., B.E. McPharland, A. Bienskowska, R. Tait, and P.D. Pare.** Sarcomers of smooth muscle: functional characteristics and ultrastructural evidence. *Journal of cell science* 118: 2381-2392, 2005.
153. **Kuo, K.-H., A.M. Herrera, L. Wang, P.D. Pare, L.E. Ford, N.L. Stephens, and C.Y. Seow.** Structure-function correlation in airway smooth muscle adapted to different lengths. *American Journal of Physiology - Cell Physiology* 285: C384-C390, 2003.
154. **Silveira, P. and J.J. Fredberg.** Smooth muscle length adaptation and actin filament length: a network model of the cytoskeletal dysregulation. *Canadian Journal of Physiology and Pharmacology* 83: 923-931, 2005.
155. **Sollich, P.,** Rheological constitutive equation for a model of soft glassy materials. *Phys Rev E* 58: 738-759, 1998.
156. **Fabry, B., G.N. Maksym, J.P. Butler, M. Glogauer, D. Navajas, and J.J. Fredberg.** Scaling the microrheology of living cells. *Phys Rev Lett* 87: -, 2001.
157. **Lenormand, G. and J.J. Fredberg.** Deformability, dynamics, and remodelling of cytoskeleton of the adherent living cell. *Biorheology* 43: 1-30, 2006.
158. **Gunst, S.J.,** Effect of length history on contractile behavior of canine tracheal smooth muscle. *Am J Physiol Cell Physiol* 250(1): C146-154, 1986.
159. **Speich, J.E., C. Dosier, L. Borgsmiller, K. Quintero, H.P. Koo, and P.H. Ratz.** Adjustable passive length-tension curve in rabbit detrusor smooth muscle. *J Appl Physiol* 102(5): 1746-1755, 2007.
160. **Chan, W.-L., J. Silberstein, and C.M. Hai.** Mechanical strain memory in airway smooth muscle. *Am J Physiol Cell Physiol* 278(5): C895-904, 2000.
161. **Speich, J.E., K. Quintero, C. Dosier, L. Borgsmiller, H.P. Koo, and P.H. Ratz.** A mechanical model for adjustable passive stiffness in rabbit detrusor. *J Appl Physiol* 101(4): 1189-1198, 2006.
162. **Qi, D., R.W. Mitchell, T. Burdyga, L.E. Ford, K.-H. Kuo, and C.Y. Seow.** Myosin light chain phosphorylation facilitates in vivo myosin filament reassembly after mechanical perturbation. *American Journal of Physiology - Cell Physiology* 282: C1298-C1305, 2002.
163. **Seow, C.Y. and N.L. Stephens.** Force-velocity curves for smooth muscle: analysis of internal factors reducing velocity. *Am J Physiol Cell Physiol* 251(3): C362-368, 1986.
164. **Avanzolini, G. and A. Cappello.** The characteristics method applied to the study of muscle dynamics. *Bulletin of Mathematical Biology* 46(5-6): 827-844, 1984.
165. **Seow, C.Y. and N.L. Stephens.** Changes of tracheal smooth muscle stiffness during an isotonic contraction. *American Journal of Physiology - Cell Physiology* 256(2): C341-350, 1989.
166. **Seow, C.Y. and N.L. Stephens.** Time dependence of series elasticity in tracheal smooth muscle. *J Appl Physiol* 62(4): 1556-1561, 1987.

167. **Mijailovich, S.M., J.J. Fredberg, and J.P. Butler.** On the Theory of Muscle Contraction: Filament Extensibility and the Development of Isometric Force and Stiffness. *Biophys J* 71: 1475-1484, 1996.
168. **Wang, J., H. Jiang, and N.L. Stephens.** A modified force-velocity equation for smooth muscle contraction. *J Appl Physiol* 76(1): 253-258, 1994.
169. **Bosse, Y., A. Sobieszek, P.D. Pare, and C.Y. Seow.** Length Adaptation of Airway Smooth Muscle. *Proc Am Thorac Soc* 5(1): 62-67, 2008.
170. **Sollich, P., F. Lequeux, P. Hébraud, and M.E. Cates.** Rheology of Soft Glassy Materials. *Phys Rev Lett* 78(10): 2020, 1997.
171. **Trepat, X., M. Grabulosa, F. Puig, G.N. Maksym, D. Navajas, and R. Farre.** Viscoelasticity of human alveolar epithelial cells subjected to stretch. *Am J Physiol Lung Cell Mol Physiol* 287(5): L1025-1034, 2004.
172. **Monthus, C. and J.-P. Bouchaud.** Models of traps and glass phenomenology. *Journal of Physics A: Mathematical and General* (14): 3847, 1996.
173. **Bates, J.,** A Recruitment Model of Quasi-Linear Power-Law Stress Adaptation in Lung Tissue. *Ann Biomed Eng* 35(7): 1165-1174, 2007.
174. **Schmidt, A. and L. Gaul.** On the numerical evaluation of fractional derivatives in multi-degree-of-freedom systems. *Signal Processing* 86(10): 2592-2601, 2006.
175. **Bratton, D.L., D.T. Tanaka, and M.M. Grunstein.** Effects of temperature on cholinergic contractility of rabbit airway muscle. *J Appl Physiol* 63(5): 1933-1941, 1987.
176. **Meiss, R.A. and R.M. Pidaparti.** Active and passive components in the length-dependent stiffness of tracheal smooth muscle during isotonic shortening. *J Appl Physiol* 98(1): 234-241, 2005.
177. **Fredberg, J.J.,** Airway smooth muscle in asthma -- perturbed equilibria of myosin binding. *Am J Respir Crit Care Med* 161(3): S158-S160, 2000.
178. **Gennes, P.G.d.,** Reptation of a polymer chain in the presence of fixed obstacles. *J Chem Phys* 55: 572-579, 1971.

Appendix A : Matlab Modelling Code

A.1 Latch bridge

This code describes the implementation of the Latch bridge model. After the initial declaration of the variables, initialization of the constants and setting the length history, the main calculation loop is entered. First the variation of the phosphorylation rates in time is defined. Subsequently a While loop is entered with three possible scenarios: contractile element only; contractile element + series elastic element; contractile element + parallel elastic element. Iteration schemes are described in the methodology section and applied here. For each scenario a common calculation block for state transitions and grid shifting is applied, as well as a common calculation of overall attachment, detachment and phosphorylation. State transitions are calculated in a Runge Kutta 4/5 scheme using myosin head location dependent rate constants defined in sub-function f. Depending on the analysis mode (force versus length control) and the while loop scenarios the While loop condition is calculated based on the current error, or the loop is exited on the first run if iterations are unnecessary.

```
clear all;
clc;
%Definition of all rate constants
Const.h=1;
Const.fp=0.88;
Const.gp1=0.22;
Const.g1=0.01;
Const.gp2=4.4;
Const.g2=0.2;
Const.gp3=0.66;
Const.g3=0.03;
Const.K1=0.35;
Const.K2=0.1;
Const.K6=0.35;
Const.K5=0.1;
% Definition of grid size(N), number of grids (grids), simulation
% duration (Tend) length range for optimal length determination
% (Lrange), timestepsize(dt)
Tend=670;
grids=5;
N=40;
Lrange = 4;
dt=0.1;
% intialisation of variables
t=0;
j=1;
% intialisation of variable size (no growing variables in a loop)
xbasedt=zeros(Tend/dt,2);      %[Myosin position; time step size]
Forcemode=zeros(Tend/dt,1);    %Force or length control mode
```

```

Fpattern=zeros(Tend/dt,1);      %Force in case of Force control
L=zeros(Tend/dt,1);             %Total length
F=zeros(Tend/dt,1);            %Total Force
Fstore=zeros(Tend/dt,1);       %Temporary force, force control
ATPdetach=zeros(Tend/dt,1);    %ATPase activity for detachment
attach=zeros(Tend/dt,1);       %number of attached species
ATPphos=zeros(Tend/dt,1);      %number of phosphorylated species
K=zeros(Tend/dt,1);            %stiffness
errits=zeros(Tend/dt,1);       %number of iterations
timer=[0:0.1:Tend];            %number of time steps past

%initial conditions for different species: w(1,:)=detach,dephos;
w(2,:)=detach,phos; w(3,:)=attach, phos; w(4,:)=attach, dephos
w(1:4,1:N*grids)=0;
w(1,0.5*(grids-1)*N+1:0.5*(grids+1)*N) =1;

% Length/force history definition
% varies per simulation, this one provides constant velocity
% oscillation data at 4 amplitudes
for i=1:800
    xtemp1(i)=abs(10-mod(i,20))/40-0.25;
    xtemp2(i)=abs(20-mod(i,40))/40-0.5;
    xtemp3(i)=abs(40-mod(i,80))/40-1;
    xtemp4(i)=abs(80-mod(i,160))/40-2;
end
xtemp(1:500)=0;
xtempall=[xtemp xtemp xtemp xtemp1 xtemp xtemp2 xtemp xtemp3 ...
    xtemp xtemp4 xtemp]';
Forcemode(length(xtempall))=false;
xbasedt(:,1)=xtemp;
xbasedt(:,2)=dt;

% main time loop
while t < Tend
    t=t+dt;
    dt=xbasedt(j,2);
    %all heads start as unphosphorylated detached. at t=5
    %contractile activation is initiated by setting
    % Const.K1=Const.K6=0.35 after 5 seconds this is reduced to
    % const.K1=Const.K6=0.06 to reflect the reduced Ca2+
    % concentrations.
    if t <5
        Const.K1=0;
    elseif t >=5 && t <10
        Const.K1=0.35;
        Const.K6=0.35
    else
        Const.K1=0.06;
        Const.K6=0.06;
    end
    %starting iteration loop for force control. in case of length
    %control (Forcemode(j)=false this loop only runs once
    err = true;
    it = 1;
    while err == true

```

At this point three different versions diverge, to describe:

1. No series or elastic element
2. A series elastic element
3. A parallel elastic element

Each is shown separately:

```

1   if Forcemode(j) == false
       %x contains the x-positions of all myosin heads on
       %grid
       x=xbasedt(j,1)-0.5*(grids-1)+[1/N:1/N:grids];
       dx=xbasedt(j+1,1)-xbasedt(j,1);
       L(j)=xbasedt(j,1);
       err = false;
     else
       %Force control: first iteration uses previous length
       x=L(j-1)-0.5*(grids-1)+[1/N:1/N:grids];
       if it < 2
           dx=0;
           L(j)=L(j-1);
       elseif it == 2
           %second iteration estimates dx based on control
           %force, calculated force in 1st iteration, and
           %stiffness.
           dxstore(1)=dx;
           dx=dx+(Fpattern(j)-F(j))/K(j);
           L(j)=L(j-1)+dx;
           Fstore(j)=F(j);
       else
           %later iterations check if error is less than
           %10^-9, if so, loop quits. otherwise another
           %estimate of dx is made based on the previous two
           %findings for dx.(see text Thesis)
           if abs(Fpattern(j)-F(j)) < 1e-9
               err=false;
               clear errF
           else
               dxstore(2)=dx;
               dxtemp=(F(j)-Fpattern(j))*(dxstore(2)-...
                   dxstore(1))/(Fstore(j)-F(j));
               L(j)=L(j-1)+dx+dxtemp;
               dxstore(1)=dxstore(2);
               dxstore(2)=dx+dxtemp;
               dx=dx+dxtemp;
               Fstore(j)=F(j);
           end
       end
     end
end

```

```

2   if Forcemode(j) == false
       x=Lce(j-1)-0.5*(grids-1)+[1/N:1/N:grids];
       if it < 2
           dx=0;
           Lce(j)=Lce(j-1);
       elseif it == 2
           dxstore(1)=dx;

```

```

        if K(j)==0;
            dx=0;
        else
            dx=dx+(xbasedt(j,1)-L(j))*(K(j)+Kse)/(K(j)*Kse);
        end
        Lce(j)=Lce(j-1)+dx;
        Lstore=L(j);
    else
        if abs(xbasedt(j,1)-L(j)) < 1e-9
            err=false;
            clear errF
        else
            dxstore(2)=dx;
            dxtemp=(L(j)-xbasedt(j,1))*(dxstore(2)-...
                dxstore(1))/(Lstore-L(j));
            dxstore(1)=dxstore(2);
            dxstore(2)=dx+dxtemp;
            dx=dx+dxtemp;
            Lstore=L(j);
            Lce(j)=Lce(j-1)+dx;
        end
    end
end
else
x=L(j-1)-0.5*(grids-1)+[1/N:1/N:grids];
if it < 2
    dx=0;
    Lce(j)=Lce(j-1);
elseif it == 2
    dxstore(1)=dx;
    dx=dx+(Fpattern(j)-F(j))/(K(j));
    Lce(j)=Lce(j-1)+dx;
    Fstore(j)=F(j);
else
    if abs(Fpattern(j)-F(j)) < 1e-9
        err=false;
        clear errF
    else
        dxstore(2)=dx;
        dxtemp=(F(j)-Fpattern(j))*(dxstore(2)-...
            dxstore(1))/(Fstore(j)-F(j));
        Lce(j)=Lce(j-1)+dx+dxtemp;
        dxstore(1)=dxstore(2);
        dxstore(2)=dx+dxtemp;
        dx=dx+dxtemp;
        Fstore(j)=F(j);
    end
end
end
end

```

3

```

if Forcemode(j) == false
    x=xbasedt(j,1)-0.5*(grids-1)+[1/N:1/N:grids];
    dx=xbasedt(j+1,1)-xbasedt(j,1);
    L(j)=xbasedt(j,1);
    err = false;
else
x=L(j-1)-0.5*(grids-1)+[1/N:1/N:grids];
if it < 2
    dx=0;
    L(j)=L(j-1);
elseif it == 2
    dxstore(1)=dx;
    dx=dx+(Fpattern(j)-F(j))/(K(j)+Kpe);

```

```

        L(j)=L(j-1)+dx;
        Fstore(j)=F(j);
    else
        if abs(Fpattern(j)-F(j)) < 1e-9
            err=false;
            clear errF
        else
            dxstore(2)=dx;
            dxtemp=(F(j)-Fpattern(j))*(dxstore(2)-...
                dxstore(1))/(Fstore(j)-F(j));
            L(j)=L(j-1)+dx+dxtemp;
            dxstore(1)=dxstore(2);
            dxstore(2)=dx+dxtemp;
            dx=dx+dxtemp;
            Fstore(j)=F(j);
        end
    end
end

```

```

% Calculating ATP rates, phosphorylation and detachment rates

```

```

ATPdetach(j)=sum(w(3,1:find(x>0,1)-1)*Const.gp2)+...
    sum(w(3,find(x>0,1):find(x>1,1)-1)*(Const.gp1).*...
    x(find(x>0,1):find(x>1,1)-1))+sum(w(3,find(x>1,1):...
    length(x))*(Const.gp1+Const.gp3))+sum(w(4,1:...
    find(x>0,1)-1)*Const.g2)+sum(w(4,find(x>0,1):...
    find(x>1,1)-1)*(Const.g1).*x(find(x>0,1):...
    find(x>1,1)-1))+sum(w(4,find(x>1,1):length(x))...
    *(Const.g1+Const.g3));
attach(j)=sum(w(2,find(x>0,1):find(x>1,1)-1)*(Const.fp).*...
    x(find(x>0,1):find(x>1,1)-1));
ATPphos(j)=sum(w(1,:)*Const.K1)+sum(w(4,:)*Const.K6);

```

```

% main calculation for state transitions, calls function
% f(w,x,dt,Const)

```

```

for i=1:grids*N
    k1 = dt*f(w(:,i),x(i),dt,Const);
    k2 = dt*f(w(:,i)+0.5*k1,x(i)+0.5*dx,dt,Const);
    k3 = dt*f(w(:,i)+0.5*k2,x(i)+0.5*dx,dt,Const);
    k4 = dt*f(w(:,i)+k3,x(i)+dx,dt,Const);
    wnew(:,i) = w(:,i) + (k1 + 2*k2 + 2*k3 + k4)/6;
end

```

```

% grid shifting of unbound myosin

```

```

shift = -round(xbasedt(j,1)*N);
for i=1:N
    vect=[i:N:grids*N];
    inA=vect(find(shift+0.5*(grids-1)*N < vect & vect < ...
        shift+0.5*(grids+1)*N));
    for p=0:grids-1
        if p*N+i ~= inA
            wnew(1:2,inA)=wnew(1:2,inA)+wnew(1:2,p*N+i);
            wnew(1:2,p*N+i)=0;
        end
    end
end
end

```

```

% calculation of Force and stiffness. Alpha is the correction
% factor for filament overlap (optimal length)
alpha=-(abs(L(j))/Lrange)+1;
K(j)=alpha*(sum(sum(wnew(3:4,:)))));

```

Three variations based on series and parallel elastic elements :

1	$F(j)=\alpha*(\sum(wnew(3,:).*(x+dx))+wnew(4,:).*(x+dx))$;
2	$F(j)=\alpha*(\sum(wnew(3,:).*(x+dx))+wnew(4,:).*(x+dx))$; $L(j)=Lce(j)+F(j)/Kse$;
3	$F(j)=\alpha*(\sum(wnew(3,:).*(x+dx))+wnew(4,:).*(x+dx)) \dots$ $+Kpe*L(j)$;

```

errF(it,1:2)=[F(j) dx];
errits(j)=it;
it=it+1;
end %end of iteration loop

```

```
w=wnew;
```

```

% display elaped time
if mod(t,100*dt) <1*dt
disp(t)
end

```

```
j=j+1;
```

```
end
```

With as a subfunction **f(w,x,Const):**

```
function dn = f(n,x,dt,Const)
```

```
[K3,K4,K7]=Kcalc(x, Const);
```

```

dn = [-Const.K1*n(1)+Const.K2*n(2)+K7*n(4); ...
Const.K1*n(1)-(Const.K2+K3)*n(2)+K4*n(3); ...
-(K4+Const.K5)*n(3)+K3*n(2)+Const.K6*n(4); ...
-(K7+Const.K6)*n(4)+Const.K5*n(3)];

```

```
function [K3,K4,K7] = Kcalc(x,Const)
```

```

if x <0
K3=0;
K4=Const.gp2;
K7=Const.g2;
elseif x > 1
K3=0;
K4=(Const.gp1+Const.gp3)*x;
K7=(Const.g1+Const.g3)*x;
else
K3=Const.fp*x;
K4=Const.gp1*x;

```

```
        K7=Const.g1*x;  
    end  
end  
end
```

A.2 Strain Dependent Release

The model is the same as the Latch bridge model, however with the following constants:

```
%Definition of all constants
Const.h=1;
Const.fp=0.88;
Const.gp1=0.01;
Const.g1=0;
Const.gp2=0.2;
Const.g2=0;
Const.gp3=0;
Const.g3=0;
Const.K1=1;
Const.K2=0;
Const.K6=0;
Const.K5=0;
Lrange = 10;
```

And a changed subfunction f2:

```
function dn = f2(n,x,dt,Const)

[K3,K4,K7]=Kcalc(x, Const);

dn = [-Const.K1*n(1)+Const.K2*n(2)+K7*n(4); ...
      Const.K1*n(1) - (Const.K2+K3) *n(2) +K4*n(3); ...
      -(K4+Const.K5) *n(3) +K3*n(2) +Const.K6*n(4); ...
      -(K7+Const.K6) *n(4) +Const.K5*n(3) ];

function [K3,K4,K7] = Kcalc(x,Const)

if x <0
    K3=0;
    K4=Const.gp2;
    K7=Const.g2;
elseif x > 1
    K3=0;
    K4=(Const.gp1+Const.gp3) *x;
    K7=(Const.g1+Const.g3) *x;
else
    K3=-(Const.fp) * (x-0.5*Const.h) ^2+0.25*Const.fp;
    K4=Const.gp1;
    K7=Const.g1;
end

end
end
```

A.3 Hill-type

The Hill type model implementation uses the same Runge Kutta 4/5 procedure defined in the previous two models. However in this model the F_0 value of the force-velocity curve has to be calculated prior to each step in the Runge Kutta process as it is dependent on the length of the element.

```
clear all
close all

% variable initiation
j=1;
L1(1)=0.75;
t=0;
a=0.142;
dt=0.1;
Tend=300;
b=0.035216;
P0=1;
k=10;
L0=0.25;
% definition of length excitation pattern
for i=1:800
    xtemp1(i)=1+0.04*sin((2*pi/50)*i);
    xtemp2(i)=1+0.08*sin((2*pi/50)*i);
    xtemp3(i)=1+0.12*sin((2*pi/50)*i);
end
xtemp(1:500)=1;
xtempall=[xtemp xtemp xtemp xtemp1 xtemp xtemp2 xtemp xtemp3...
    xtemp]';
L2=xtempall;
Lrange=1;
% Force control mode switch
Forcemode(1:length(xtempall))=false;
while t < Tend
    j=j+1;
    t=t+dt;
    % optimal length correction factor (P0 is the force at which
    % V=0
    P0=-(abs(L1(j-1)-0.75)/Lrange)+1;
    % in case of length control Runge Kutta 4/5 is used to
    % calculate the new length of the contractile element and
    % subsequently the length of the series elastic element from the
    if Forcemode(j)==false
        F1=(L2(j-1)-L1(j-1)-L0)*k;
        P0=-(abs(L1(j-1)-0.75)/Lrange)+1;
        k1 = dt*((P0+a)*b/(F1+a)-b);
        F1=((L2(j-1)+L2(j))/2-(L1(j-1)-0.5*k1)-L0)*k;
        P0=-(abs(L1(j-1)-0.75)/Lrange)+1;
        k2 = dt*((P0+a)*b/(F1+a)-b);
        F1=((L2(j-1)+L2(j))/2-(L1(j-1)-0.5*k2)-L0)*k;
        P0=-(abs(L1(j-1)-0.75)/Lrange)+1;
        k3 = dt*((P0+a)*b/(F1+a)-b);
        F1=(L2(j)-(L1(j-1)-k3)-L0)*k;
        P0=-(abs(L1(j-1)-0.75)/Lrange)+1;
```

```
k4 = dt*((P0+a)*b/(F1+a)-b);  
L1(j) = L1(j-1) - (k1 + 2*k2 + 2*k3 + k4)/6;  
F(j)=(L2(j)-L1(j)-L0)*k;  
else  
L1(j)=L1(j-1)-dt*((P0+a)*b/(Fcont(j)+a)-b);  
L2(j)=L1(j)+L0+Fcont(j)/k;  
F(j)=Fcont(j);  
end  
end
```

A.4 Length Adaptation

The following model diagram describes the model flow:

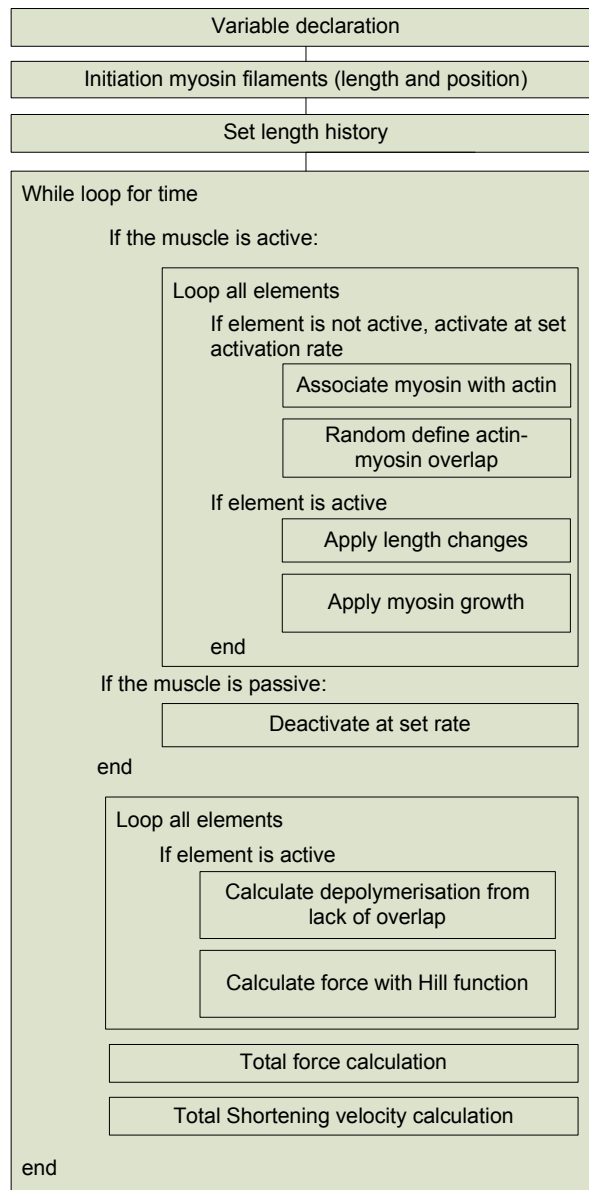


Figure A.1: Mode diagram of length adaptation model.

```

clear;
% initialisation of variables
dt=0.1;
t=0;
j=1;
tend=700;
forcelength=0.05;
ratelength=1;
ratedetach=0.5;
actinlength=0.1;

Mgrow=0.0035;
breaking=0.4;
binding=0.1;
  
```

```

grid=400;
rateK=.8;
K0=0.0001;
depol=0.1;
F=zeros(tend/dt,1);
lossfactor=40;
% Hill type element constants
a=0.1*0.142;
b=0.035216;

%initialisation of Myosin head array
for i = 1:grid
    m0=actinlength + ((i-1)/grid)*(1-2*actinlength);
    m1=20/grid;
    M(i,:)= [0 0 0 0 0 m0+m1 m0 0 0 0];
    %M(,1:2) represent the unstrained x positions of the
    %contractile element. M(,3:4) represent the strained
    %end positions of these elements. M(,5:6) represent
    %the start and end positions of the myosin filament
    %[xup xdown dxup dxdown mup mdown K flength active]
    Moverlap(i)=m1;
end

% definition of contractile pattern and length pattern
active(1:round(tend/dt)+5)=1;
active(1:round(5/dt))=0;
L(1:round(tend/dt)+5)=1;
for i=1:500
    xtemp1(i)=1+0.01*sin((2*pi/50)*i);
    xtemp2(i)=1+0.02*sin((2*pi/50)*i);
    xtemp3(i)=1+0.04*sin((2*pi/50)*i);
    xtemp4(i)=1+0.08*sin((2*pi/50)*i);
end
L(2001:2500)=xtemp1;
L(3001:3500)=xtemp2;
L(4001:4500)=xtemp3;
L(5001:5500)=xtemp4;
%start of the main loop
while t < tend
    t=t+ dt;
    j=j+1;
    timer(j)=t;
    actinlength=sqrt(L(j))/10;
    if active(j) == 1
        for i= 1:grid

            % procedure to calculate the length changes of the myosin
            % filaments as well as the binding of bare myosin with
            % new actin filaments.
            if rand < binding*dt & M(i,9)==0
                M(i,9)=1;
                % length of Myosin is defined
                lengthM=M(i,5)-M(i,6);
                % if the length of Myosin is larger than the
                % available active actin length, the Myosin length
                % instantly reduces to the available actin length
                % Aup and Adown are the length of actin stretching
                % below and above the myosin attached zone, which
                % together with myosin length sum to the total

```

```

% length of the contractile element
if lengthM > (actinlength)
    M(i,5)=M(i,5)-0.5*(lengthM-(actinlength));
    M(i,6)=M(i,6)+0.5*(lengthM-(actinlength));
    Aup=0;
    Adown=0;
else
    %Aup and Adown are randomly determined to
    %gradually move to optimal length
    Aup=(actinlength-lengthM)*rand;
    Adown=(actinlength-lengthM)*rand;
end
M(i,1)=M(i,5)+Aup;
M(i,2)=M(i,6)-Adown;
% M(,8) equals the total length of the unstrained
% contractile element
M(i,8)= M(i,1)-M(i,2);
% the starting length of the contractile element is
% unstrained, hence equal to M(,8)
M(i,3:4)=M(i,1:2);

elseif M(i,9) == 1
    % calculating the strained length of the contractile
    % element, proportional to the original element
length

    % to tissue length ratio
    lengthchange=(L(j)-L(j-1))*(M(i,1)-M(i,2));
    % calculating actual start and end positions of the
    % contractile element
    M(i,3)=M(i,1)+lengthchange*0.5;
    M(i,4)=M(i,2)-lengthchange*0.5;
    % Defines the growth of the myosin filament. If the
    % growth rate would cause it to grow beyond the
    % bonding length of the actin filament, it is not
    % allowed to grow
    if M(i,5)+ Mgrow*dt < min(M(i,3),M(i,4)...
        +actinlength)
        M(i,5)=M(i,5)+Mgrow*dt;
    end
    if M(i,6)-Mgrow*dt > max(M(i,3)-actinlength,M(i,4))
        M(i,6)=M(i,6)-Mgrow*dt;
    end
    %calculates the breaking of the myosin filament as
    %a result of the force put on the contractile
    %element. Minimum force is arbitrary
    if (Flocal(i)-0.113)*(1/rand)*dt>breaking
        M(i,9)=0;
    end
end
end

else
    % calculates dissociation of myosin as background rate
    for i =1:grid
        chance=rand;
        if chance < 0.1*dt & M(i,9)==1
            M(i,9)=0;
            M(i,3:4)=0;
            M(i,1:2)=0;
            M(i,8)=0;
        end
    end
end

```

```

    end
end
for i = 1:grid
    if M(i,9)==1
        %calculates depolymerisation of myosin based on the
        %amount of not fully overlapped myosin
        if M(i,5) > min(M(i,3), M(i,4)+actinlength)

            M(i,5)=M(i,5)-(M(i,5)-min(M(i,3), M(i,4)+...
            +actinlength))*depol*dt;

        end
        if M(i,6) < max(M(i,3)-actinlength, M(i,4))
            M(i,6)=M(i,6)+(max(M(i,3)-actinlength, M(i,4)+...
            -M(i,6))*depol*dt;

        end
        Moverlap(i)=min([M(i,3); M(i,5); M(i,4)+...
            actinlength])-max([M(i,4); M(i,6);...
            M(i,3)-actinlength]);
        Alength=(M(i,3)-M(i,4));
        stiffchange=(Moverlap(i)-M(i,7))*rateK*dt;
        M(i,7)=M(i,7) + stiffchange;

        %calculates force based on Hill element
        P0=Moverlap(i);
        V=((L(j)-L(j-1))/dt)*(M(i,3)-M(i,4));
        Flocal(i)=((P0+a)*b)/(V+b);

        ending=round((M(i,1))*100);
        start=round((M(i,2))*100);
    else
        % if element is not active, it does not bear force
        Flocal(i)=0;
        % myosin filament disintegrates from length changes
        loss=rand*abs(L(j)-L(j-1))*dt*lossfactor*(M(i,5)-M(i,6));
        M(i,5)=M(i,5)-0.5*loss;
        M(i,6)=M(i,6)+0.5*loss;
    end
end
Alloverlap(j)=sum(Moverlap);
F(j)=sum((M(:,3)-M(:,4))/L(j)).*Flocal');
% shortening velocity calculation
alllength(j)=sum((M(:,3)-M(:,4)));
if sum((M(:,3)-M(:,4))) > 0 & active(j)==1;
    Vs(j)=sum(M(:,9))*L(j)/sum(abs(M(:,3)-M(:,4)).*M(:,9))*a;
else
    Vs(j)=0;
end

if mod(t,20) < 0.2
    clc
    t
end
end
end

```

A.5 Soft Glasses Rheology

```
clear all
close all
t=0; %time
tstep=0.01; %simulation time step
gridsize=20000; %number of elements
L0(1:gridsize)=1; %element length
Ltissue(1)=1; %tissue length
j=1;
k=1; %element stiffness
strain=zeros(gridsize,1); %element strains
x=0.2; %noise temperature

% Energy well distribution: rho(E)=exp(-E)
Ewell=zeros(gridsize,1);
for i=1:gridsize
    Ewell(i)=-log(1-rand);
    strain(i)=0;
end

% main loop
while t<100
    t=t+tstep;
    j=j+1;
    % Length history
    if t >5
        Ltissue(j)=1.1;
    else
        Ltissue(j)=1;
    end
    % calculation of strain in each element, followed by a
    % conditional yield based on elastic energy stored in the element
    for i=1:gridsize
        strain(i)=strain(i)+Ltissue(j)-Ltissue(j-1);
        if (exp(-(Ewell(i)-0.5*strain(i)^2)/x))*tstep > rand
            Ewell(i)=-log(1-rand);
            strain(i)=0;
        end
        Flink(i)=((strain(i)))*k;
    end
    % as element length and tissue length are taken as equal
    % (without loss of generality) the total force is the sum of
    % the force in the elements.
    Ftot(j)=sum(Flink);

    % progress display
    if mod (t,10)< tstep
        t
    end
end
end
```

A.6 Spring Damper Model

This implementation allows for the definition of variable length of the elastic elements, but this is not used in this work. Calculation of node forces inside the time loop is analogue to the description in the methodology.

```
clear all;
j=1;
elements=10;
tstep=0.01;
tend=100;
t=0;

% element length definition. allows for variable lengths, as long
% as the sum of the elements is 1.
L(1:elements)=0.1;
L=L/sum(L);

%definition of stiffness,dampers and the location of the nodes
for i=1:elements
    k(i)=1/L(i);
    damp(i)=5;
    x(i) = sum(L(1:i));
end
x(elements)=[];
damp(elements)=[];
% builds a sparse matrix m with the multipliers of the location
% vector x.
m0=zeros(elements-1,elements-1);
m1=sparse([1:elements-1],[1:elements-1],[k(1:elements-1)+k(2:elements)]);
m2=sparse([1:elements-2],[2:elements-1],[-k(2:elements-1)]);
m3=sparse([2:elements-1],[1:elements-2],[-k(2:elements-1)]);
m2(elements-1,elements-1)=0;
m3(elements-1,elements-1)=0;
m=m0+m1+m2+m3;
m(elements-1,elements-2:elements-1)=[-k(elements-1),...
    k(elements-1)+k(elements)];

% length data
Ltot(1:5/tstep)=1;
Ltot(5/tstep:tend/tstep+10)=1.1;

% main loop
while t<tend
    j=j+1;
    timer(j)=t;
    h=tstep; %the step size
    % built length dependent vector
    mc(elements-1)=-L(elements-1)*k(elements-1)+L(elements)*...
        k(elements)-Ltot(j)*k(elements);
    % Runge kutta process to determine x+dx/dt
    k1 = h * (m*x'+mc')./damp';
    k2= h * (m*(x+0.5*k1')'+mc')./damp';
    k3 = h * (m*(x+0.5*k2')'+mc')./damp';
    k4 = h * (m*(x+0.5*k3')'+mc')./damp';
```

```

x(1:elements-1) = x(1:elements-1) - 1/6*(k1' + k2' + k3' + k4');
% Force calculation based on force in the last node
F(j)=(Ltot(j)-x(elements-1)-L(elements))*k(elements);

t=t+tstep;
if mod(t,tend/100) < tstep
    round(t*100/tend)
    for i=1:elements-2
        x2(round(t*100/tend),:)=x';
    end
end
end
hold on
loglog([0:0.01:45],F(500:5000))

```

A.7 Fractional Differentials

See methodology for description of the calculation of de force.

```
clear all
close all

alpha=0.05;           % fractional differential order
deltat=0.1;          % timestepsize
tend = 200;          % simulation duration
t=0;                 % start time
j=1;                 % loop iteration start
F=zeros(tend/deltat,1); % Force initiation

% length history definition
x(1:100)=0;
x(101:1000)=0.2;
x(1001:10000)=0;

% timer initiation
timer(1)=0;

% main loop
while t < tend-deltat
    t=t+deltat;
    j=j+1;
    timer(j)=t;

    % Force calculation. uses the assumption that L(0) and L(1)=0.
    % 0.5*deltat is added to the time values to avoid infinitely
    % large force values (from 0^-n). this is equivalent to assuming
    % that each length change is applied a half timestep out of sync
    % with the timer.
    F(j)=(sum((t+0.5*deltat-timer(2:j)).^(-alpha).*...
        (x(2:j)-x(1:j-1))))+0.5*(timer(j)+0.5*deltat)^...
        (-alpha)*x(1))/gamma(1-alpha);

    if mod(t,tend/20) < deltat
        t
    end
end
plot(F)
```

A.8 Sequential multiplication (as in Chapter 5)

This is the original version of the sequential multiplication model. the next section describes the upgraded version of Chapter 7. In this model the force is calculated directly within the time loop from the piecewise product of a multiplier array (factor) and the piecewise power of a time array with an exponent array.

```
close all

% custom function which deletes all variabels except specified
% ones. A and B variables are kept as this model simulates
% experimental results directly from the length data of the
% experiments (A). this is afterwards compared with the force data
% from the experiments (B). the experimental data is sampled at 100
% Hz.
keep A B E ;

deltat=0.3; % timestep
tend =1000; % simulation duration

% initiation of vector variables
exponent=zeros(1,tend/deltat); % exponent
F=zeros(1,tend/deltat); % force
t=zeros(1,tend/deltat); % time

astart=10; % starting point used from exp. data
j=1; % iteration start
F(1)=(B(5)); % starting force=exp. starting force
factor(1)=B(5);

a=-0.25; % constant for exponent
b=-13; % constant for multiplier

A(1:3)=A(5:7); % removes artificial start of file
% length glitches

% length history based on experiment length history, vecor
% corrected for length step size.
L=1*(A(astart+1:100*deltat:end)-mean(A(1:100)));
L0=L(1);

% main loop
while t(j) < tend-deltat
    t(j+1)=t(j)+deltat;
    j=j+1;

    % symmetrical dL based multipliers and exponents
    dl=(L(j)-L(j-1));
    exponent(j)=-0.25*dl;
    factor(j)=exp(-13*exponent(j));

    % force calculation
    F(j)=prod(factor(1:j)).*(t(j)+0.5*deltat-t(1:j)).^exponent(1:j);
```

```
    if mod(t(j),tend/20) < deltat
        t(j)
    end
end
plot([0.01:0.01:tend],B(1:tend/0.01))
hold on
plot([0:deltat:tend],F,'r')
```

A.9 Sequential Multiplication (as in Chapter 7)

This program is similar to the previous implementation, however the multiplier (factor) and exponent are now defined based on the current and historic length.

```
close all

% custom function which deletes all variables except specified
% ones. A and B variables are kept as this model simulates
% experimental results directly from the length data of the
% experiments (A). this is afterwards compared with the force data
% from the experiments (B). the experimental data is sampled at 100
% Hz.
keep A B E ;

deltat=0.3; % timestep
tend =500; % simulation duration

% initiation of vector variables
exponent=zeros(1,tend/deltat); % exponent
F=zeros(1,tend/deltat); % force
t=zeros(1,tend/deltat); % time

astart=10; % starting point used from exp. data
j=1; % iteration start
F0=(B(astart)); % starting force=exp. starting force
F(1)=F0;

% constants for multiplier and exponent fits with length change
c=4;
a=-0.37271;
amin=-0.39;
b=0.96518;
bmin=-0.73002;

A(1:3)=A(5:7); % removes artificial start of file
% length glitches

% length history based on experiment length history, vector
% corrected for length step size.
L=1*(A(astart+1:100*deltat:end)-mean(A(1:100)));
L0=L(1);

while t(j) < tend-deltat
    t(j+1)=t(j)+deltat;
    j=j+1;

    % determines the exponent fitting function values for given
    deltaL
    for i=0:j-1
        if L(j)-L(j-i)>0
            b1=a*(L(j)-L(j-i))+b*(L(j)-L(j-i))^2;
        else
            b1=amin*(L(j)-L(j-i))+bmin*(L(j)-L(j-i))^2;
        end
    end
end
```

```

end
if L(j)-L(j-i+1) >0
    b2=a*(L(j)-L(j-i+1))+b*(L(j)-L(j-i+1))^2;
else
    b2=amin*(L(j)-L(j-i+1))+bmin*(L(j)-L(j-i+1))^2;
end
exponent(i+1)=b1-b2;
end

% total factor at time t only depends on length difference
% with starting length
factor=exp(c*(L(j)-L0));

% Force calculation
F(j)=F0*factor*prod((t(j)+0.5*deltat-t(1:j)).^exponent(j:-1:1));

% progress indicator
if mod(t(j),tend/20) < deltat
    t(j)
end
end
plot([0.01:0.01:tend],B(astart+1:astart+tend/0.01))
hold on
plot([deltat:deltat:length(F)*deltat],F,'r')

```

Appendix B : Matlab Experiment Analysis Code

All of the experiments were analysed using matlab code applied directly to the raw data from the Labview Data Acquisition programs. This was necessary to exclude bias from manual analysis.

For each experiment series individual analysis matlab m-files were created. For each type of experiment the common elements are shown here.

B.1 Simple length step, staircase and two phase length step protocols

B.1.1 File Selection Loop

```
clear all
% Defines which files should be read. Array l() always contains only
% the experiments from a single protocol, to allow protocol
% specific analysis
l(1).path='G:\H\Ijpma\9_16_2009\amplitude_step_3000_2\';
l(2).path='G:\H\Ijpma\9_16_2009\amplitude_step_3000_3\';
l(3).path='G:\H\Ijpma\9_17_2009\amplitude_step_3000_4\';
l(4).path='G:\H\Ijpma\9_17_2009\amplitude_step_3000_5\';
l(5).path='G:\H\Ijpma\9_18_2009\amplitude_step_3000_6\';
l(6).path='G:\H\Ijpma\9_18_2009\amplitude_step_3000_7\';

% Main loop for cycling through the files for analysis
for i=1:6
    close all
    % Keeps only variables i and l, clears all others
    keep i l
    % Loads 100Hz file data
    pathname=l(i).path;
    load([pathname 'Filesmall'])
    % Assigns length data to A and force data to B
    B=Filesmall(:,3);
    A=Filesmall(:,2);
    % While analysis is only performed on raw data, a filtered
    % set is also generated for visualisation
    a=[1/4 1/4 1/4 1/4];
    b=1;
    D=filter(a,b,A);
    D=D(3:end);
```

B.1.2 Finding Step Response Length Change Points

```
% Determines the position of length changes avor 20 sample
% blocks
Lfind=zeros(round((length(A)-20)/20-5),1);
for i=2:(length(A)-20)/20-5
    Lfind(i)=range(A((i-1)*20:(i)*20));
end
% Clears noise less than 10% of maximum length change
Lfind(find(Lfind<max(Lfind)/10))=0;
```

```

% Extracts length change points and converts to real sample
% points
dummy1=find(Lfind==0);
Lfindpoint=dummy1(find(diff(dummy1)>1)+1)*20;
% Around Lfindpoint the extreme force point is sought, with
% orientation of extremity based on direction of length change.
for i=1:length(Lfindpoint)
    if A(Lfindpoint(i)-10)>A(Lfindpoint(i)-50)
        PeakF(i)=find(B(Lfindpoint(i)-50:Lfindpoint(i)-10) ...
            ==max(B(Lfindpoint(i)-50:Lfindpoint(i)-10),1) ...
            +Lfindpoint(i)-50;
    else
        PeakF(i)=find(B(Lfindpoint(i)-50:Lfindpoint(i)-10)==...
            min(B(Lfindpoint(i)-50:Lfindpoint(i)-10),1) ...
            +Lfindpoint(i)-50;
    end
end
% Removes length changes within 0.2 second of eachother, which
% is technically possible if the location of Lfindpoint is
% exactly halfway a length change.
PeakF=PeakF([ find(diff(PeakF)>20) end ]);
% Adds end of file point as the end of the last length change
PeakF(end+1)=length(A);

```

B.1.3 Power Law Fitting Procedures

The following code is common for simple step and staircase protocols, but a different fitting function is used for two phase length steps (code shown under a).

```

% Main analysis loop
for i=1:length(PeakF)-1
    % Array E contains all analysis data
    E(i,1)=PeakF(i);
    % Analysis of force response to length change. Ezfit
    % determines the fit according to specified fitting
    % function using least square fitting procedure.
    if PeakF(i+1)-PeakF(i) <500
        dummy=ezfit([0.01:0.01:(PeakF(i+1)-PeakF(i) ...
            -14)/100],B(PeakF(i):PeakF(i+1)-15),'power');
    else
        dummy=ezfit([0.01:0.01:5],B(PeakF(i):...
            PeakF(i)+499),'power');
    end
    % Multiplier of power function fit
    E(i,2)=dummy.m(1);
    % Exponent of power function fit
    E(i,3)=dummy.m(2);
    % Regression coefficient
    E(i,4)=dummy.r;
    % Magnitude of length change
    E(i,5)=A(PeakF(i)+10)-A(PeakF(i)-100);
    % Length after length change
    E(i,6)=A(PeakF(i)+10);
    % Force before length change
    E(i,7)=mean(B(PeakF(i)-30:PeakF(i)-15));
    % Force at two fixed points after length change
    E(i,8)=mean(B(PeakF(i)+100:PeakF(i)+110));
    E(i,9)=mean(B(PeakF(i)+900:PeakF(i)+920));
end
End

```

A Code for two phase length steps

```
for i=1:length(PeakF)-1
    % Array E contains all analysis data
    E(i,1)=PeakF(i);
    % Analysis of force response to length change. Ezfit
    % determines the fit according to specified fitting
    % function using least square fitting procedure.
    if PeakF(i+1)-PeakF(i) < 500
        dummy=eZfit([0.01:0.01:(PeakF(i+1)-PeakF(i)...
            -14)/100],B(PeakF(i):PeakF(i+1)-15),'power');
    else
        if i>1 & E(i,1)-E(i-1,1) < 500
            dummy=eZfit([0.01:0.01:20.01],B(E(i,1):E(i,1)+2000),...
                ['a*x^b*(x+' num2str((E(i,1)-E(i-1,1))/100)...
                '^c;log']);
            dummy2=eZfit([0.01:0.01:20.01],B(E(i,1):E(i,1)+2000),...
                ['a*x^b*(x+' num2str((E(i,1)-E(i-1,1))/100)...
                '^' num2str(E(i-1,3)) ';log']);
        else
            dummy=eZfit([0.01:0.01:(PeakF(i+1)-PeakF(i)...
                -14)/100],B(PeakF(i):PeakF(i+1)-15),'power');
        end
    end

    end
    if length(dummy.m)==2
        % Multiplier of power function fit
        E(i,2)=dummy.m(1);
        % Exponent of power function fit
        E(i,3)=dummy.m(2);
        % Regression coefficient
        E(i,5)=dummy.r;
    else
        % Multiplier of power function fit
        E(i,2)=dummy.m(1);
        % Exponent of power function fit 1
        E(i,3)=dummy.m(2);
        % Exponent 2nd power function
        E(i,4)=dummy.m(3);
        % integrated error value
        E(i,5)=dummy.r2;
        % Exponent 1st power function under full sequential
        % multiplication assumption.
        E(i,6)=dummy2.m(2);
        % integrated error value
        E(i,7)=dummy2.r2;
    end

    % Magnitude of length change
    E(i,8)=A(PeakF(i)+10)-A(PeakF(i)-100);
    % Length after length change
    E(i,9)=A(PeakF(i)+10);
    % Force before length change
    E(i,10)=mean(B(PeakF(i)-30:PeakF(i)-15));
    % Force at two fixed points after length change
    E(i,11)=mean(B(PeakF(i)+100:PeakF(i)+110));
    E(i,12)=mean(B(PeakF(i)+900:PeakF(i)+920));
end
```

B.1.4 Plotting and Data Storage

```
figure
% The force response of all length steps is plotted on double
% logarithmic paper, and normalized to the starting force.
for i=1:length(E(:,1));
    h=loglog([0.01:0.01:10],B(E(i,1):E(i,1)+999)/B(E(i,1)));
    hold on
end
% The figure is stored both as a .png and a .fig file, with the
% file name determined by the experiment path
dummy2=find(pathname=='\');
saveas(h,['G:\H\Ijpm\amplitude_step_analysis\' ...
    pathname(dummy2(end-1)+1:dummy2(end)-1) '_Force_norm.png'])
saveas(h,['G:\H\Ijpm\amplitude_step_analysis\' ...
    pathname(dummy2(end-1)+1:dummy2(end)-1) '_Force_norm.fig'])
keep A B E D D2 filename pathname h Files small dummy2
% A cleaned up set of analysis arrays and the original data are
% saved in the directory of the experiments and the analysis
% directory.
save([pathname 'analysis.mat'])
save(['G:\H\Ijpm\amplitude_step_analysis\' ...
    pathname(dummy2(end-1)+1:dummy2(end)-1) '_analysis.mat'])

end
```

B.2 Continuous square waves

The continuous square waves applied to both isometric contractions and staircase functions require a higher sampling rate for accurate analysis. Hence the 3kHz data files are used for analysis. the full analysis file is shown here

```
clear all
% Defines which files should be read. Array l() always contains only
% the experiments from a single protocol, to allow protocol
% specific analysis
l(1).path='B:\experiments_mayo\10_14_2009\multistep_steps_3000_1\';
l(2).path='B:\experiments_mayo\10_15_2009\multistep_steps_b_3000_2\';
l(3).path='B:\experiments_mayo\10_16_2009\multistep_steps_b_3000_3\';
l(4).path='B:\experiments_mayo\10_16_2009\multistep_steps_b_3000_4\';
l(5).path='B:\experiments_mayo\10_16_2009\multistep_steps_b_3000_5\';
l(6).path='B:\experiments_mayo\10_20_2009\multistep_steps_b_3000_6\';
l(7).path='B:\experiments_mayo\10_20_2009\multistep_steps_b_3000_7\';

% Main loop for cycling through directories
for q=1:6
    close all
    % Keeps only variables q and l, clears all others
    keep q l
    % Defines path of files
    pathstart=l(q).path;
    % initialize subfile array
    n=[];
    % A bug in Labview causes some experiments to have a first file
    % called File, while other have a first file called File_1. This
    % is tested here.
    if exist([pathstart 'File'])==2;
        n(1).path=[pathstart 'File'];
    end
end
```

```

end
% The array with the subfile names is filled, until File_#n
% does not exists.
i=1;
while exist([pathstart 'File_' int2str(i)])==2;
n(length(n)+1).path=[pathstart 'File_' int2str(i)];
i=i+1;
end
% All analysis results are written to Ekeep, for all files.
Ekeep=[];
% Main loop for cycling through subfiles
for j=1:length(n)-1
    keep 1 Ekeep j pathstart n q
    % load subfile
    filename=n(j).path
    load([filename]);

    % Assigns length data to A and force data to B
    B=filename(:,3);
    A=filename(:,2);
    keep A B
    % Determines the position of length changes avor 20 sample
    % blocks
    Lfind=zeros(round((length(A)-40)/40-5),1);
    for i=2:(length(A)-40)/40-5
        Lfind(i)=range(A((i-1)*40:(i)*40));
    end
    % Clears noise less than 10% of maximum length change
    Lfind(find(Lfind<max(Lfind)/10))=0;
    % Extracts length change points and converts to real sample
    % points
    dummy1=find(Lfind==0);
    Lfindpoint=dummy1(find(diff(dummy1)>1)+1)*40;
    % Around Lfindpoint the extreme force point is sought, with
    % orientation of extremity based on direction of length
change.
    for i=1:length(Lfindpoint)
        if A(Lfindpoint(i)-10)>A(Lfindpoint(i)-50)
            PeakF(i)=find(B(Lfindpoint(i)-50:Lfindpoint(i)-10)...
                ==max(B(Lfindpoint(i)-50:Lfindpoint(i)-10)),1)...
                +Lfindpoint(i)-50;
        else
            PeakF(i)=find(B(Lfindpoint(i)-50:Lfindpoint(i)-
10))==...
                min(B(Lfindpoint(i)-50:Lfindpoint(i)-10),1)...
                +Lfindpoint(i)-50;
        end
    end
    % Removes length changes within 0.2 second of eachother,
which
    % is technically possible if the location of Lfindpoint is
    % exactly halfway a length change.
    PeakF=PeakF([ find(diff(PeakF)>40) end ]);
    % Adds end of file point as the end of the last length change
    PeakF(end+1)=length(A);
    % to correct for the force changes occuring during
    % contraction or during length chnages beyond the square
    % wave, the power law curve fitting is conducted on a
    % corrected force, with the correction factor determined by
    % the average force over 2 step length changes (6000
    % samples).

```

```

% First the mean values are determined
meanB=zeros(1,length(B)-6500);
for j=1:100:length(B)-6000
    meanB(j+3000)=mean(B(j:j+6000));
end
% Then the vector of mean values is expanded to assure a
% starting value and an end value exist at meanB(1) and
% meanB(length(A))
x=find(meanB);
meanB=[meanB(x(1)) meanB];
meanB(length(A))=meanB(x(end)+1);
x=find(meanB);
% The meanB vector is interpolated to form a vector corfac
% which has the same length as vectors A and B.
x2=1:length(A);
corfac=interp1(x,meanB(find(abs(meanB)>0)),x2);
% Main analysis loop
for i=1:length(PeakF)-1
    % Array E contains all analysis data
    E(i,1)=PeakF(i);

    % Analysis of force response to length change. Ezfit
    % determines the fit according to specified fitting
    % function using least square fitting procedure.
    if PeakF(i)+1999<length(A)
        dummy=eZfit([1/3000:1/3000:2/3],B(PeakF(i):...
PeakF(i)+1999)./corfac(PeakF(i):PeakF(i)+1999)'...
        , 'power');
    else
        dummy=eZfit([1/3000:1/3000:(length(A)-PeakF(i))/...
3000],B(PeakF(i):length(A)-1)./corfac(...
PeakF(i):length(A)-1)', 'power');
    end
    % Multiplier of power function fit
    E(i,2)=dummy.m(1);
    % Exponent of power function fit
    E(i,3)=dummy.m(2);
    % Regression coefficient
    E(i,4)=dummy.r;
    % Magnitude of length change
    E(i,5)=A(PeakF(i)+10)-A(PeakF(i)-100);
    % Length after length change
    E(i,6)=A(PeakF(i)+10);
    % Force before length change
    E(i,7)=mean(B(PeakF(i)-30:PeakF(i)-15));
    % Force at two fixed points after length change
    E(i,8)=corfac(PeakF(i));
end

% Analysis results written to E are moved to Ekeep
if exist('Ekeep') && exist('E')
    Ekeep(end+1:end + length(E(:,1)),:)=E;
elseif exist('E')
    Ekeep=E;
end
end

% Figures with exponents and multipliers are plotted and stored,
% and all data is saved in .mat files.
dummy2=find(pathstart=='\');

```

```

h=plot(Ekeep(:,2).*Ekeep(:,8),Ekeep(:,2).*Ekeep(:,8)-
Ekeep(:,7),'.b')
saveas(h,['B:\experiments_mayo\multistep_steps_b\' ...
pathstart(dummy2(end-1)+1:dummy2(end)-1) '_stiff.png'])
saveas(h,['B:\experiments_mayo\multistep_steps_b\' ...
pathstart(dummy2(end-1)+1:dummy2(end)-1) '_stiff.fig'])
figure
h2=plot(Ekeep(find(Ekeep(:,3)<0),3))
saveas(h2,['B:\experiments_mayo\multistep_steps_b\' ...
pathstart(dummy2(end-1)+1:dummy2(end)-1) '_exponent.png'])
saveas(h2,['B:\experiments_mayo\multistep_steps_b\' ...
pathstart(dummy2(end-1)+1:dummy2(end)-1) '_exponent.fig'])
keep Ekeep pathstart dummy2 n q
save([pathstart 'analysis.mat'])
save(['B:\experiments_mayo\multistep_steps_b\' ...
pathstart(dummy2(end-1)+1:dummy2(end)-1) '_analysis.mat'])
close all
end

```

B.3 Sinusoid identification and analysis

All sinusoidal protocols were analysed similarly, although for the high frequency oscillations the high sample rate data was used, which was not necessary for the oscillation amplitude experiments

```

clear all
close all
l(1).path='B:\experiments_mayo\8_28_2009\oscillate_frequency_pass_2\'
;
l(2).path='B:\experiments_mayo\9_3_2009\oscillate_frequency_pass_3\'
l(3).path='B:\experiments_mayo\9_3_2009\oscillate_frequency_pass_4\'
l(4).path='B:\experiments_mayo\9_4_2009\oscillate_frequency_pass_5\'
l(5).path='B:\experiments_mayo\9_6_2009\oscillate_frequency_pass_6\'
l(6).path='B:\experiments_mayo\9_9_2009\oscillate_frequency_pass_7\'
for j=1%:6
pathstart=l(j).path;
close all
load([pathstart 'Filesmall'])
A=Filesmall(:,1);
B=Filesmall(:,3);
% Finds the begin (p) and end (p2) positions of the
% oscillations
a=[1 find(abs(diff(A(1:10:end)))>0.0004)' length(A)/10];
p=a(find(diff(a)>100)+1);
p2=a(find(diff(a)>100));
% Initialize the hysteresivity and asymmetry parameters
hyst=zeros(length(A),1);
asym=zeros(length(A),1);
% Loop for analysis
for i=1:3
% Defines the loop length, being the number of samples per
% oscillation
rangeloop=[p(i)*10:p2(i+1)*10];
points=diff(find(A(rangeloop+50)<(min(A)-
max(A))*0.5+max(A)));
looplength=floor(mean(points(find(points(1:900)>5)))+...
mean(diff(find(points(1:900)>5))))-1;

```

```

% Procedure for finding the hysteresivity of the
% force-length loops and the asymmetry
for j=rangeloop(1):rangeloop(end)-looplefth-1
    % First the extreme length points are identified
    a1=find(A(j:j+looplefth)==max(A(j:j+looplefth)),1)-1;
    a2=find(A(j:j+looplefth)==min(A(j:j+looplefth)),1)-1;
    % The relative position of the points a1 and a2
    % determines what defines the upper half and what the
    % lower half of a force-length loop
    if a1>a2
        F1=[B(j+a1:(j+looplefth))' B(j:j+a2)'];
        L1=[A(j+a1:(j+looplefth))' A(j:j+a2)'];
        F2=[B(j+a2:j+a1)'];
        L2=[A(j+a2:j+a1)'];
    else
        F2=[B(j+a2:(j+looplefth))' B(j:j+a1)'];
        F1=[B(j+a1:j+a2)'];
        L2=[A(j+a2:(j+looplefth))' A(j:j+a1)'];
        L1=[A(j+a1:j+a2)'];
    end
    % The upper and lower areas are cacluated, and
    % subsequently the asymmetry factor is calculated
    symarea1=abs(sum(diff(L2).*(F2(1:length(F2)-1)+...
        F2(2:length(F2)))/2)-(A(j+a1)-A(j+a2))*...
        (B(j+a1)+B(j+a2))/2);
    symarea2=abs(sum(diff(L1).*(F1(1:length(F1)-1)+...
        F1(2:length(F1)))/2)-(A(j+a1)-A(j+a2))*...
        (B(j+a1)+B(j+a2))/2);
    asym(j)=(symarea1+symarea2)/(symarea1-symarea2);
    % The hysteresivity as defined by Fredberg et al. is
    % calculated from the force-length loop as well
    F=[B(j+a2:(j+looplefth))' B(j:j+a2)'];
    L=[A(j+a2:(j+looplefth))' A(j:j+a2)'];
    Area=0.5.*sum(F(1:length(F)-1).*diff(L)-...
        L(1:length(F)-1).*diff(F));
    hyst(j)=tan(asin(4*abs(Area)/(3.1415962*...
        range((B(j:j+looplefth))) *...
        range((A(j:j+looplefth))))));
end
end
end

```

This section is omitted for amplitude variation only protocols

```

% The higher frequency oscillations require analysis of the
% 3kHz sample rate files. First the directory is read for the
% existing files starting with Fi*
t=dir([pathstart 'Fi*']);
dum1=[];
% A number of operations are performed to clean and analyse this
% file list. First the Files file is removed from the list
for i=1:length(t)
    if length(t(i).name) > 4
        if t(i).name(1:5)=='Files'
            dum1(end+1)=i;
        end
    end
end
end
t(dum1)=[];
% Next the files are sorted by date to assure the right

```

```

% sequence for analysis
for i=1:length(t)
    dummy(i)=datenum(t(i).date);
end
[dummy1,dummy2]=sort(dummy);
t=t(dummy2);
% The file required for analysis of the force-length loops is
% selected, and the smaple number within that file is found
sizeall=sum([t.bytes]);
filespot=p2(5)*10*sizeall/length(A);
i=1;
tot=0;
while tot<filespot
    tot=tot+t(i).bytes;
    i=i+1;
end
% The file is loaded and the spot to start analysis is defined
D=load([pathstart t(i-1).name]);
A1=D(:,1);
B1=D(:,3);
spot=round((1-(tot-filespot)/t(i-1).bytes)*length(D));
% The loop length is defined and the hysteresivity and
% asymmetry arrays are initiated
points=diff(find(A1(1:spot)<(min(A)-max(A))*0.5+max(A)));
looplefth=floor(mean(points(find(points(1:900)>5))+...
    mean(diff(find(points(1:900)>5))))-1;
hysth=zeros(spot,1);
asymh=zeros(spot,1);
% Procedure for finding the hysteresivity of the
% force-length loops and the asymmetry
for q=1:spot-looplefth*2
    % First the extreme length points are identified
    a1=find(A1(q:q+looplefth)==max(A1(q:q+looplefth)),1);
    a2=find(A1(q:q+looplefth)==min(A1(q:q+looplefth)),1);
    % The relative position of the points a1 and a2
    % determines what defines the upper half and what the
    % lower half of a force-length loop

    if a1>a2
        F1=[B1(q+a1:(q+looplefth))' B1(q:q+a2)'];
        L1=[A1(q+a1:(q+looplefth))' A1(q:q+a2)'];
        F2=[B1(q+a2:q+a1)'];
        L2=[A1(q+a2:q+a1)'];
    else
        F2=[B1(q+a2:(q+looplefth))' B1(q:q+a1)'];
        F1=[B1(q+a1:q+a2)'];
        L2=[A1(q+a2:(q+looplefth))' A1(q:q+a1)'];
        L1=[A1(q+a1:q+a2)'];
    end
    % The upper and lower areas are cacluated, and
    % subsequently the asymmetry factor is calculated
    symareal=abs(sum(diff(L2).* (F2(1:length(F2)-1)+...
        F2(2:length(F2)))/2))-abs((A1(q+a1)-A1(q+a2))*...
        (B1(q+a1)+B1(q+a2))/2);
    symarea2=abs(sum(diff(L1).* (F1(1:length(F1)-1)+...
        F1(2:length(F1)))/2))-abs((A1(q+a1)-A1(q+a2))*...
        (B1(q+a1)+B1(q+a2))/2);
    asymh(q)=(symareal+symarea2)/(symareal-symarea2);
    % The hysteresivity as defined by Fredberg et al. is
    % calculated from the force-length loop as well
    F=[B1(q+a2:(q+looplefth))' B1(q:q+a2)'];

```

```

L=[A1(q+a2:(q+looplevelength))' A1(q:q+a2)'];
Area=0.5.*sum(F(1:length(F)-1).*diff(L)-...
L(1:length(F)-1).*diff(F));
hysth(q)=tan(asin(4*abs(Area)/(3.1415962*...
range((B1(q:q+looplevelength))*...
range((A1(q:q+looplevelength))))));
end


---


% plots and saves the analysed data
h=plot(abs(hyst))
hold on
h=plot(abs(hysth),'r')
dummy2=find(pathstart=='\');
xlabel('Length change (% L_{ref})');
ylabel('Force(normalized)')
saveas(h,['B:\experiments_mayo\oscillate_frequency_pass\' ...
pathstart(dummy2(end-1)+1:dummy2(end)-1)
'_hysteresivity.png'])
saveas(h,['B:\experiments_mayo\oscillate_frequency_pass\' ...
pathstart(dummy2(end-1)+1:dummy2(end)-1)
'_hysteresivity.fig'])
figure
h2=plot(asym)
hold on
h2=plot(asymh)
saveas(h2,['B:\experiments_mayo\oscillate_frequency_pass\' ...
pathstart(dummy2(end-1)+1:dummy2(end)-1) '_asymmetry.png'])
saveas(h2,['B:\experiments_mayo\oscillate_frequency_pass\' ...
pathstart(dummy2(end-1)+1:dummy2(end)-1) '_asymmetry.fig'])
keep A B j dummy2 l p p2 pathstart hyst hysth r2 r2h
save([pathstart 'analysis.mat'])
save(['B:\experiments_mayo\oscillate_frequency_act\' ...
pathstart(dummy2(end-1)+1:dummy2(end)-1) '_analysis.mat'])
close all
keep l j
end

```

Appendix C : Labview Programs

For both the experiments in Chapter 3 and in Chapter 6 Labview control programs have been written. Great similarity exists between the programs for the two experiment sessions. Therefore rather than describing each individually the more advanced programs used for the experiments in Chapter 6 are shown here. In the explanations VI stands for Virtual Instrument, the name National Instruments Labview uses for generated programs and subprograms. Labview version 8.5 was used.

C.1 Data_Generation.vi

C.1.1 Front panel

This program generates the force and/or length change data for the data acquisition program. Each panel generates a signal type according to the values of the parameters. Pressing the Add buttons results in one signal concatenated to the existing signal. The green sound button when activated writes a code line to the file to indicate if a fluid change has to occur, or if a length mode to force mode change occurs.

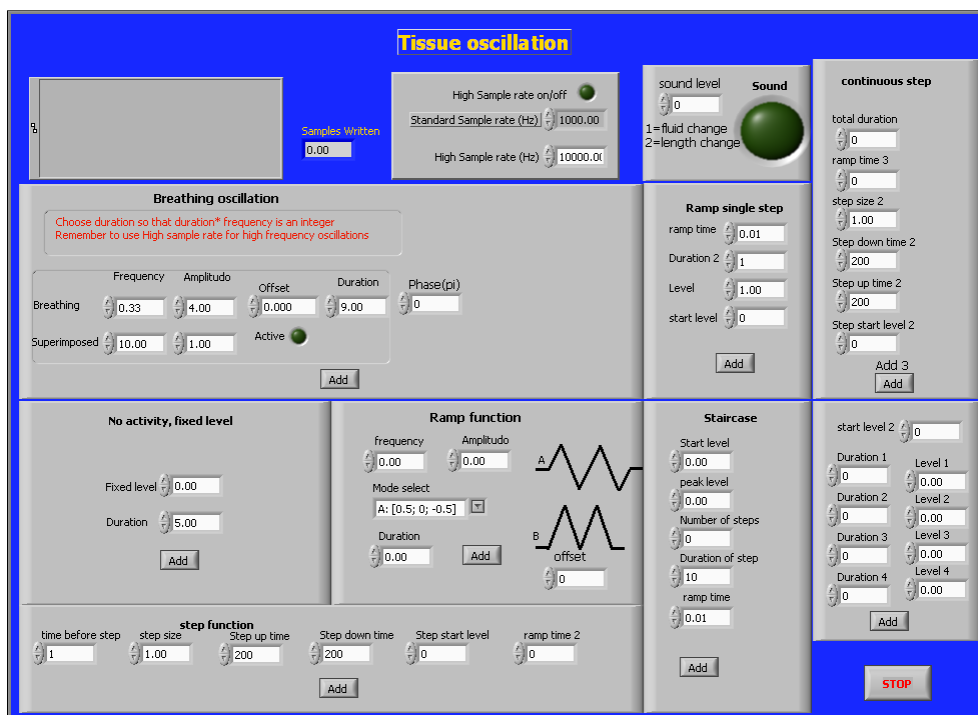


Figure C.2: Front panel Data_generation.vi

C.1.2 Block diagram

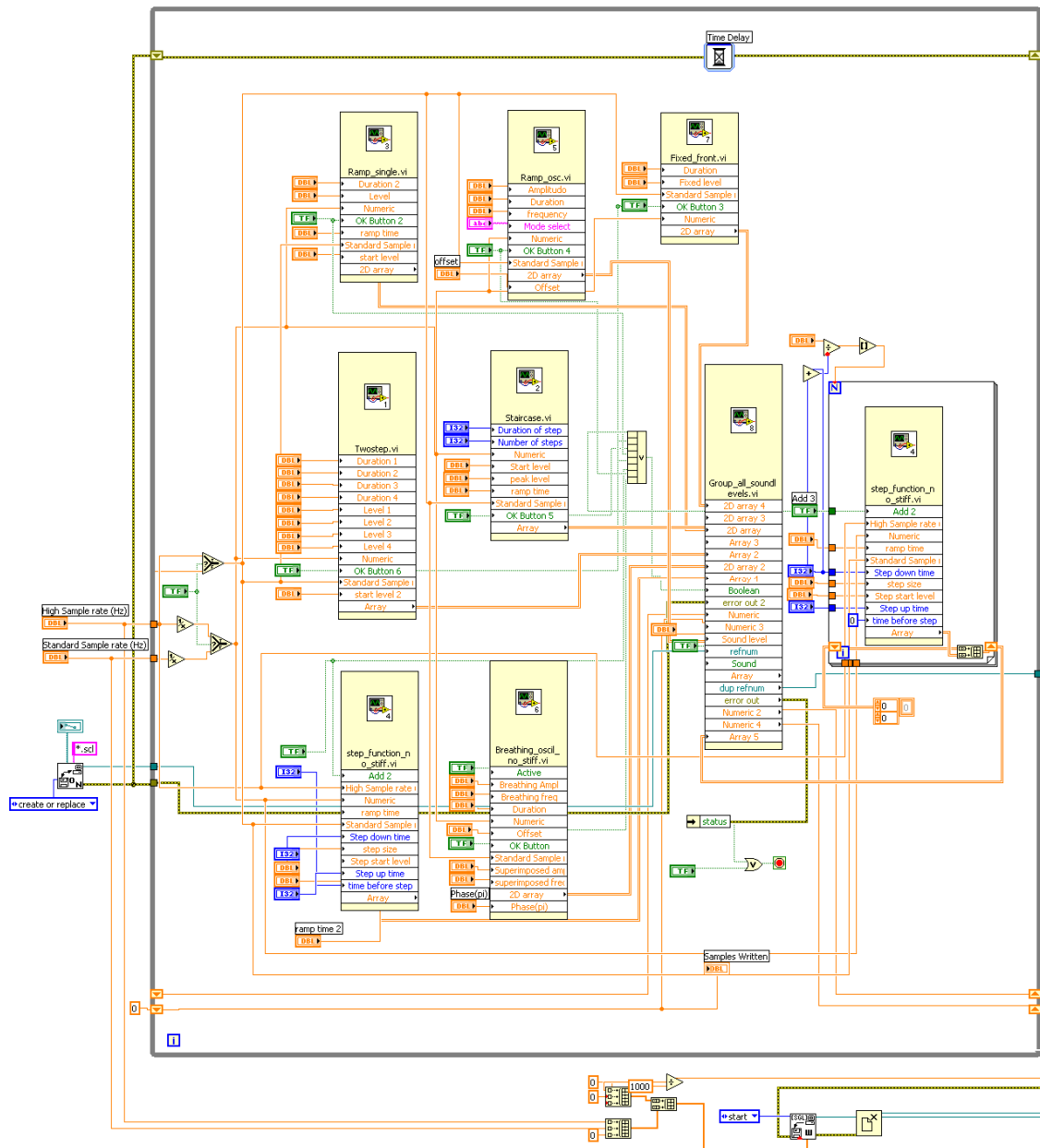


Figure C.3: Block diagram *Data_generation.vi*

The main block diagram is subdivided in sub VIs for each signal type displayed on the front panel and a sub VI for the grouping, processing and writing of the file data. Each signal type sub VI has 2 common inputs, and one common output. The inputs are the sample rate and the reciprocal of the sampling rate, and the output contains the data array. Each block is activated by the add buttons on the front panel. The bottom right corner writes the sampling rate information to the start of the file after the stop button on the front panel has been pressed.

C.1.3 Sub-VI *Ramp_single.vi*

This sub-VI calls the sub-VI fixedlevelramp.vi once.

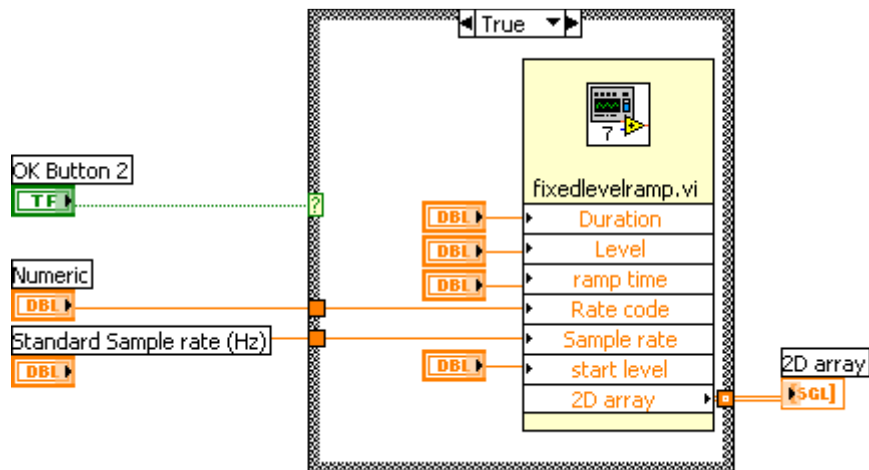


Figure C.4: Block diagram `Ramp_single.vi`

C.1.4 Sub-VI `fixedlevelramp.vi`

A ramp from a certain *start level* to end *Level* with a set *ramp time* is generated. In all signal sub-Vis *total duration* and *sample rate* are used to generated the right signal, while *rate code* is the code from the sound button on the front panel.

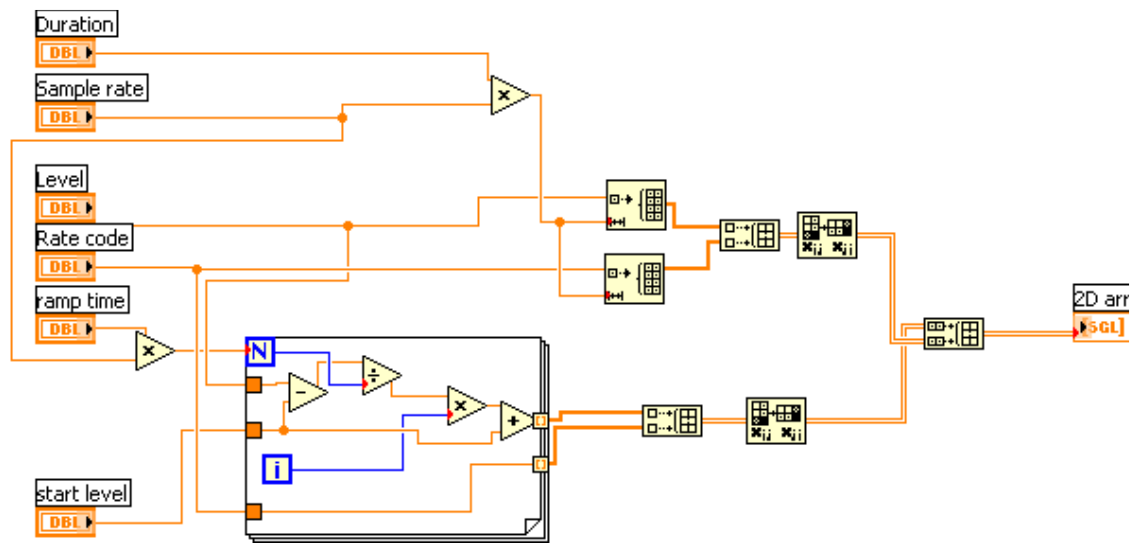


Figure C.5: Block diagram `fixedlevelramp.vi`

C.1.5 Sub-VI `Ramp_osc.vi`

The `Ramp_osc.vi` is a front for generating triangular wave oscillations. The sub-VI for generating such waves is called `sheneq.vi` after the triangular wave experiments by Shen et al. [134].

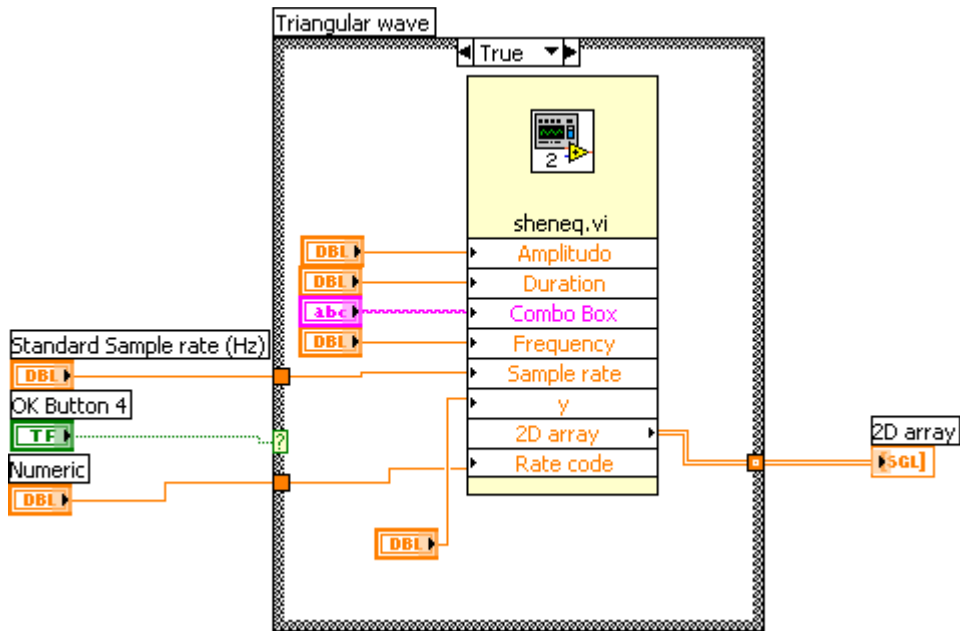


Figure C.6: Block diagram Ramp_osc.vi

C.1.6 Sub-VI Sheneq.vi

While the triangular wave generator is used to generate the wave signal, some preconditioning of the input parameters is performed.

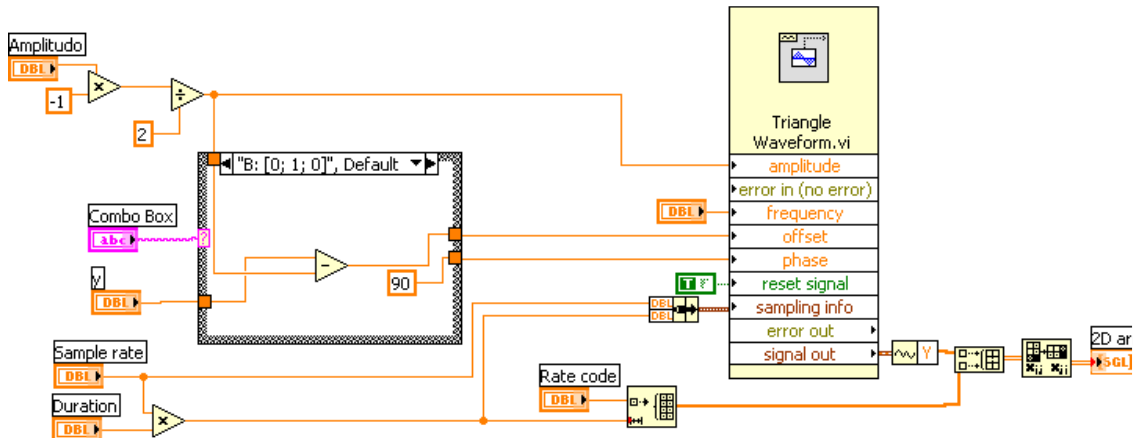


Figure C.7: Block diagram Sheneq.vi

C.1.7 Sub-VI fixed_front.vi

This sub-VI generates a constant length/force for a specific duration using the fixedlevel vi.

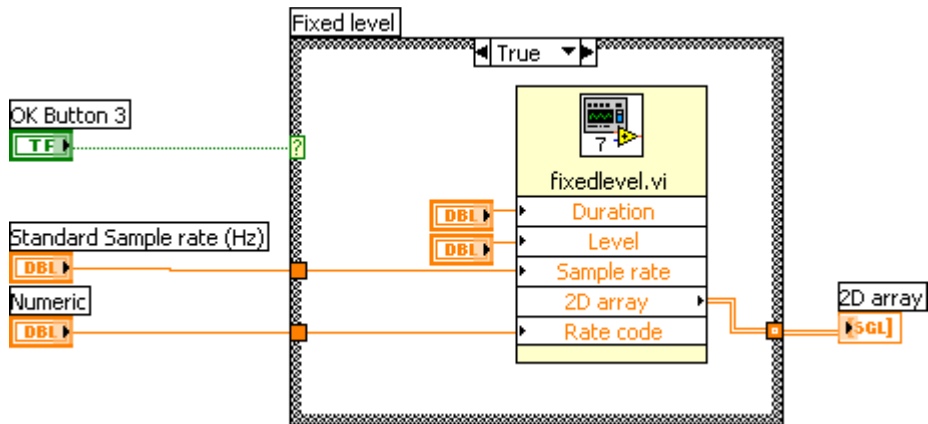


Figure C.8: Block diagram *fixed_front.vi*

C.1.8 Sub-VI *fixedlevel.vi*

A constant output signal at *level* for a specific *Duration* and *Sample rate* is generated.

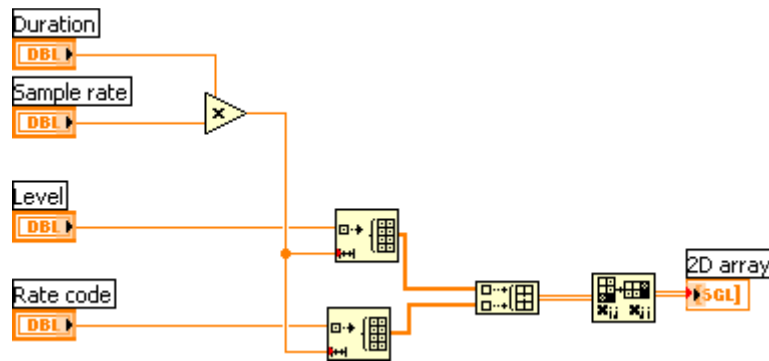


Figure C.9: *Fixedlevel.vi*

C.1.9 Sub-VI *Two_step.vi*

Two-step.vi is a sub-VI which generates a two phase length step. Each length change is ramped and a specific duration until the next length change is applied.

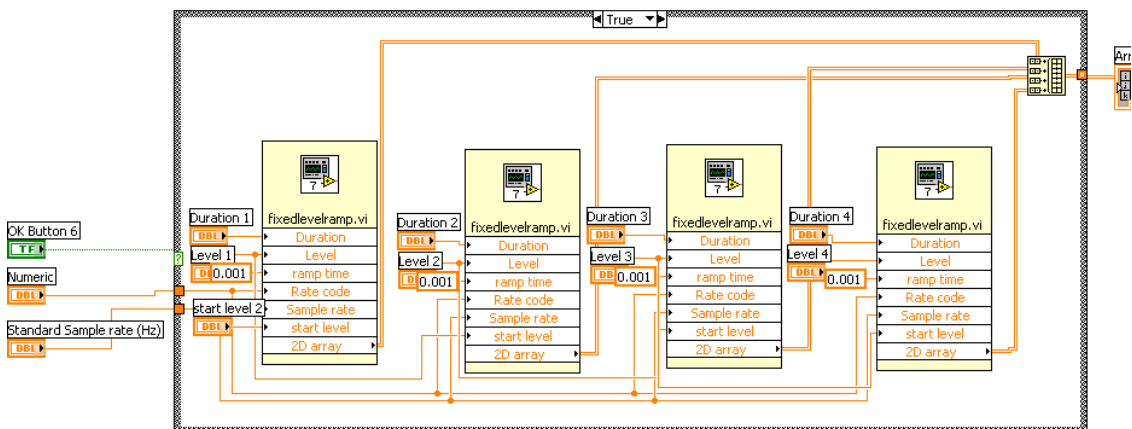


Figure C.10: Block diagram *Two_step.vi*

C.1.10

C.1.11 Sub-VI Staircase.vi

A staircase function consisting of ramped length changes with a fixed start level and peak level is generated. Step size is calculated from the total level difference and the number of steps.

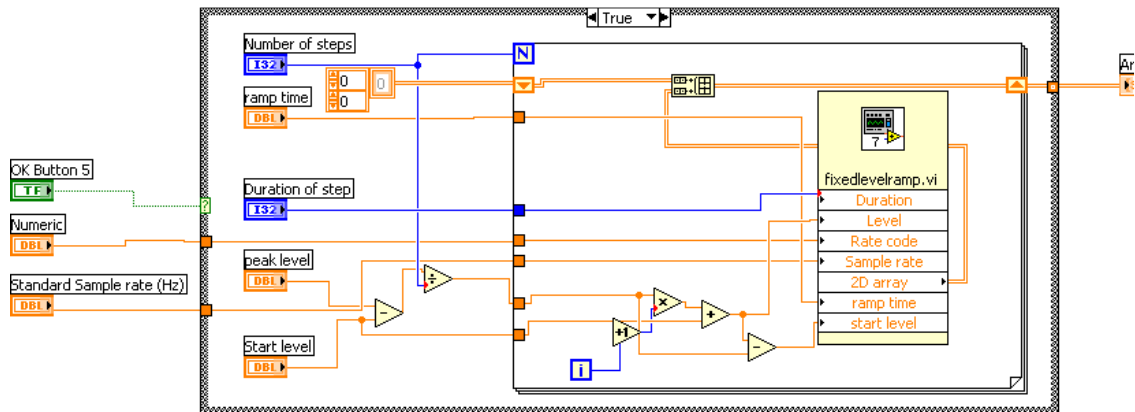


Figure C.11: Block diagram staircase.vi

C.1.12 Sub-VI Step_function.vi

This vi is similar to Two_step.vi, but with only two length changes, always returning to the starting length.

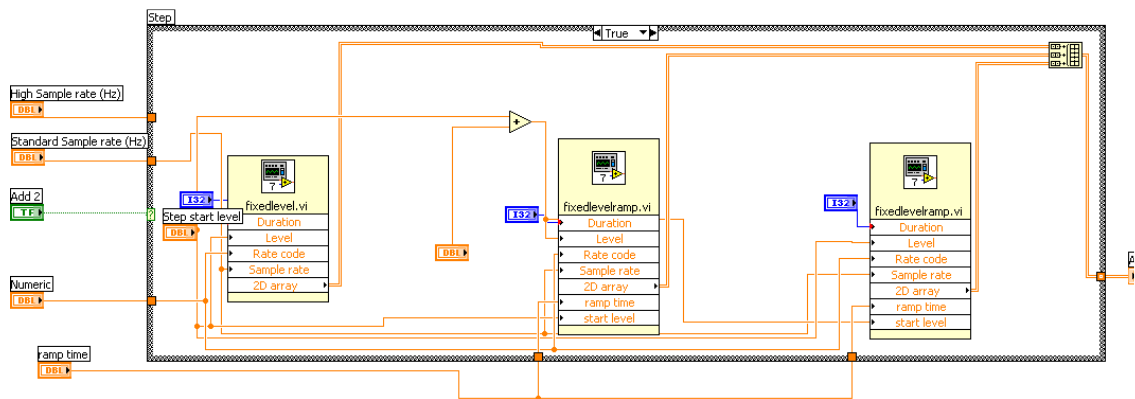


Figure C.12: Block diagram Step_function.vi

C.1.13 Sub-VI Breathing_oscil.vi

This VI can generate both simple sinusoidal oscillations of specific frequency and amplitude, as well as sinusoidal oscillations with superimposed small amplitude sinusoidal oscillations, each with individually determined frequency and amplitude and duration.

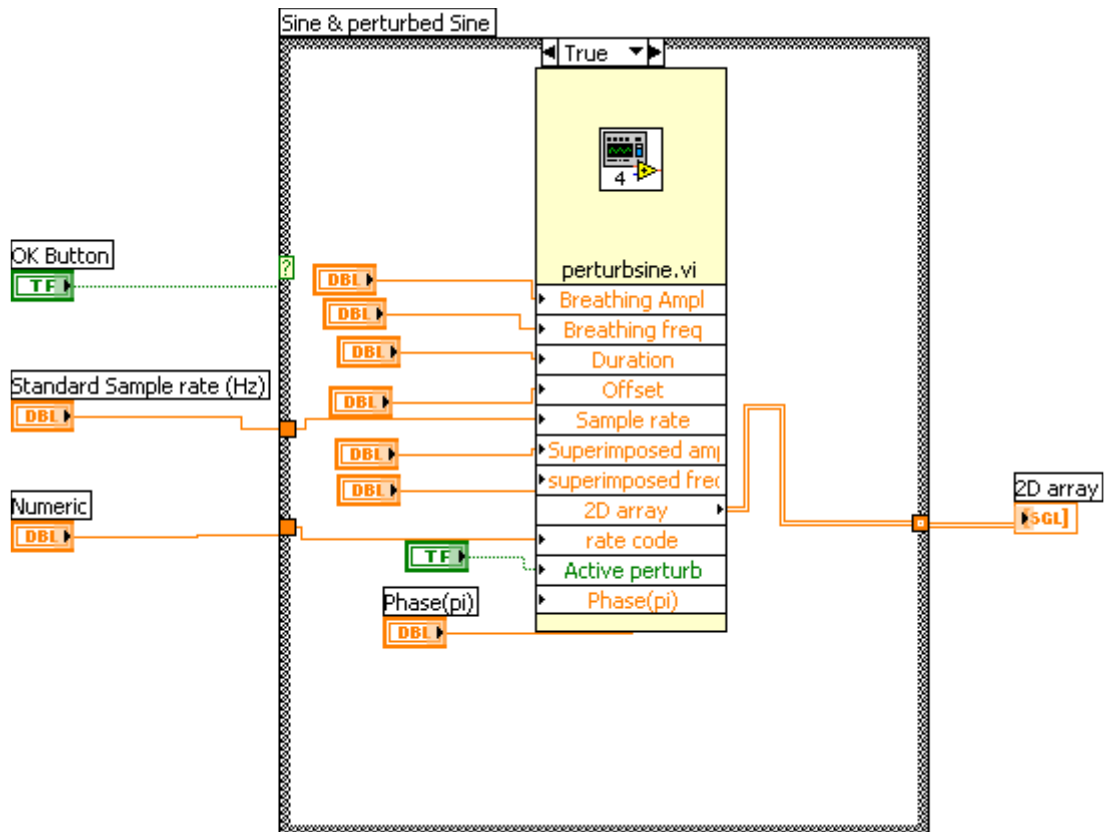


Figure C.13: Block diagram *Breathing_oscil.vi*

C.1.14 Sub-VI *Perturbsin.vi*

Two separate sinusoidal wave generators are combined, of which the superimposed oscillation can be stopped by switching *Active perturb* on the front panel.

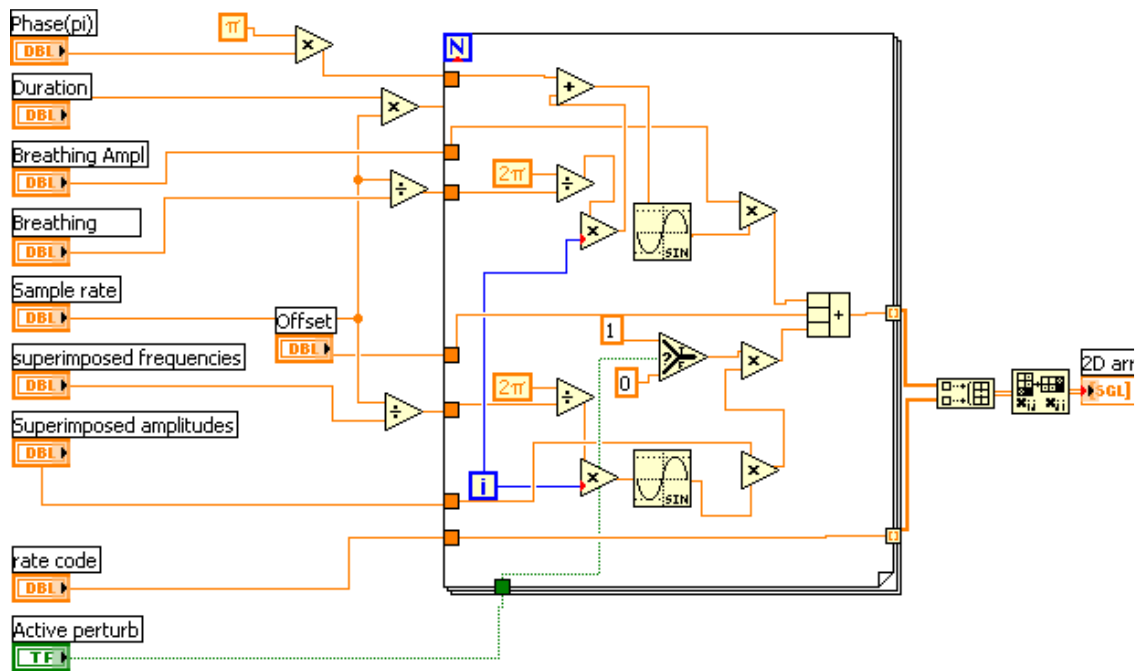


Figure C.14: Block diagram perturb sine.vi

C.1.15 Sub-VI Group_all.vi

All the array outputs of the individual sub VIs are bundled in this VI by concatenating. Only when the Add button of the respective signal is activated will the signal be added. Subsequently the signal is written in Labview binary file format at 3000 Hz.

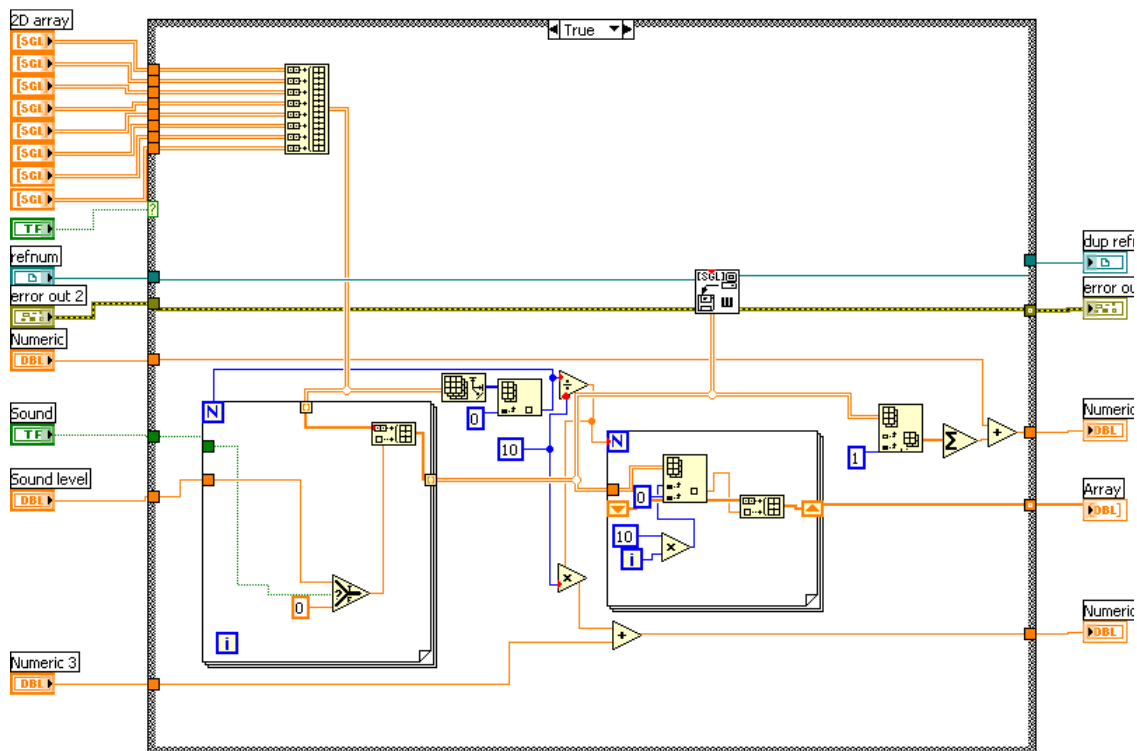


Figure C.15: Block diagram Group_all.vi

C.2 Data_Acquisition.vi

C.2.1 Front panel

A large array of file names generated by the Generate_data.vi exists on the front panel. The actual number of files to be read can be set. The scaling factor sets how many volts of length signal is required for a 1% L_{ref} length change. the Offset provides the ability to increase the base level length. The two bottom right boxes provide information on the current simulation, and the 3 charts plot continuously the length and force in and out traces as well as the original file data.

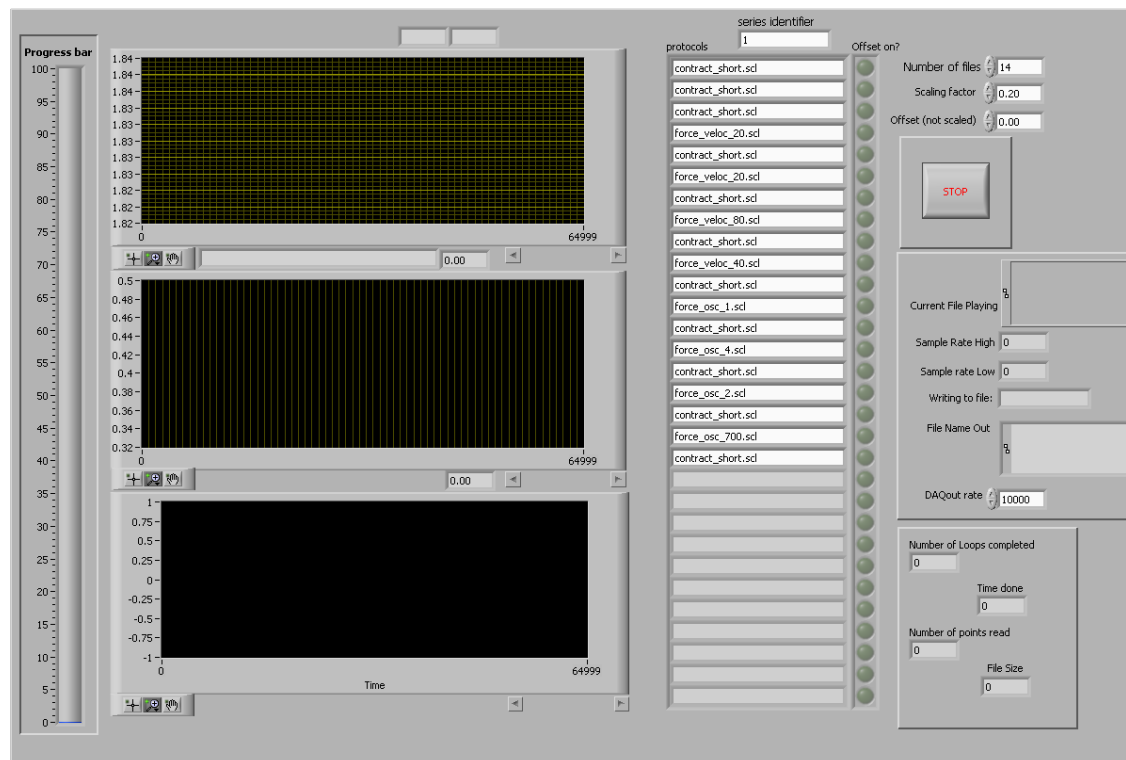


Figure C.16: Front panel Data_Acquisition.vi

C.2.2 Block diagram data_acquisition.vi

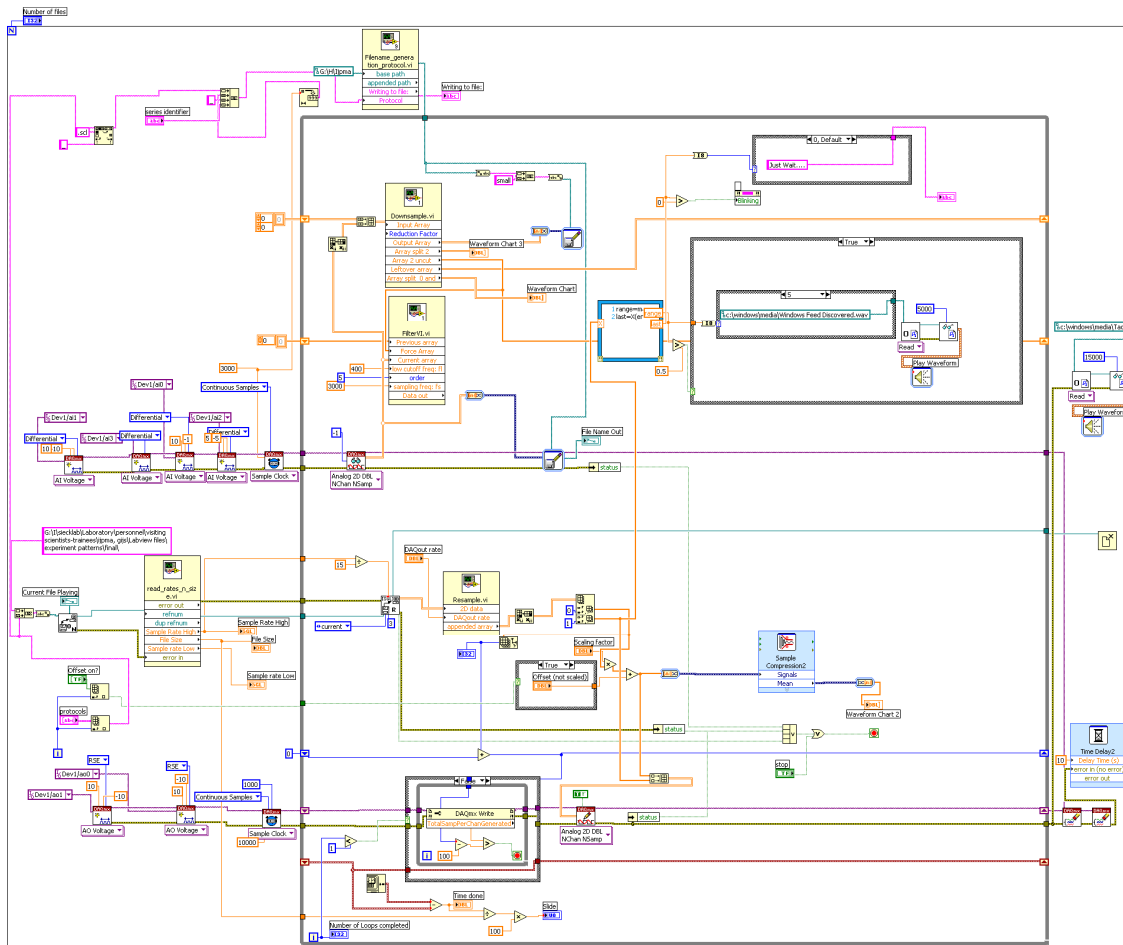


Figure C.17: Data_Acquisition.vi

Data_Acquisition.VI is wrapped in two loops, a For Loop that determines the *number of files* to be played, while the While loop is responsible for the cyclical reading and writing of data.

Within the for loop both the reading and writing is initialized. 3 Channels are continuously read: Force, Length feedback, Length signal. Meanwhile the length or force is written to the DAQ card.

In the while loop the read and write procedures are separated, with the reading procedure made timing dependent on the writing procedures. The data acquisition takes place at 3000 Hz, which is both written directly to the acquisition file and filtered in Filter.vi and subsequently written to the same acquisition file. Additionally the data is down sampled by a factor 30 to result in a 100Hz data stream for quick analysis and for graphing in the front panel charts. This data is written to a separate file.

For writing the data firstly the lengthfile generated in Data_generation.vi is read and resampled in resample.vi to 10kHz. Subsequently the length data is scaled to compensate for differences in muscle reference length. The offset procedure allows for a series of experiments to be performed at a different base length. The length data is joined into one array and written to the DAQ board. The length data is compressed to allow graphing on the front panel.

The DAQmx Write Case loop runs only in the first cycle of the While loop to reset the DAQmxwrite procedure. The constant restarting of the DAQmx out procedures at the start of each file can cause errors otherwise.

Before the next file is initiated a time delay is inserted to allow finalizing of the read and write procedures.

C.2.3 Sub VI Read_rates_n_sizes.vi

This sub-VI reads the first line of a file for information on sample rates, file size and file reading issues.

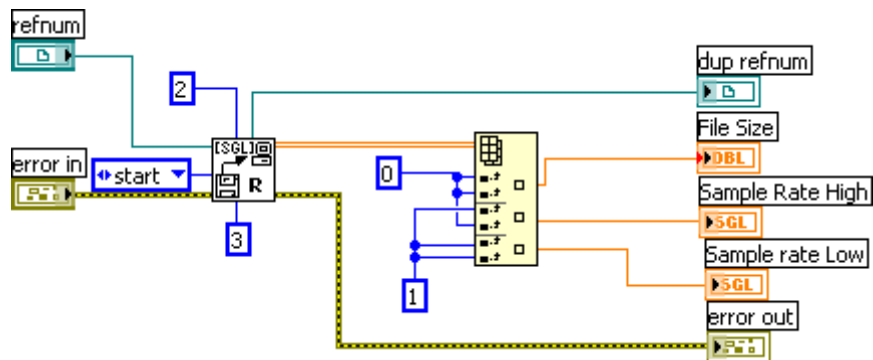


Figure C.18: read-rates_n_sizes.vi

C.2.4 Sub VI Filename_generation.vi

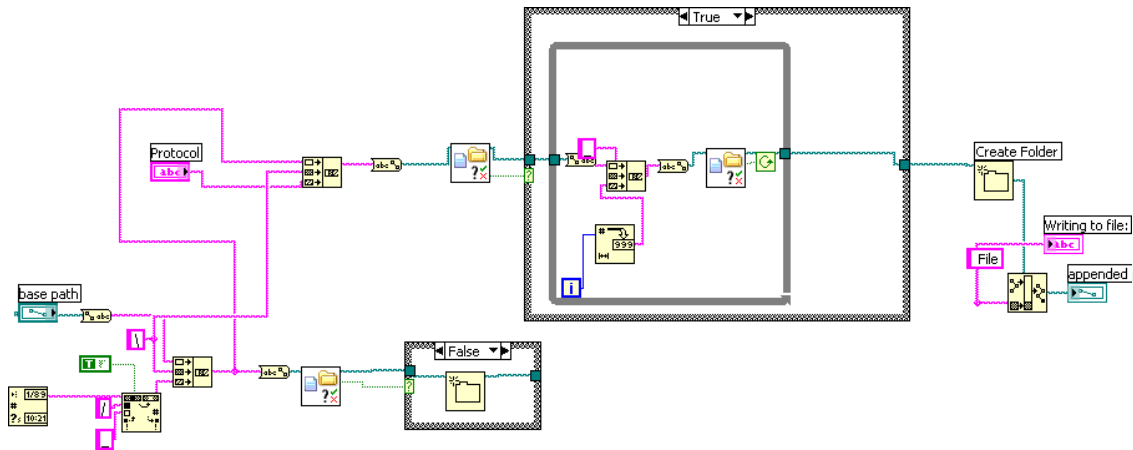


Figure C.19: *Filename_generation.vi*

This VI generates a unique directory based on the current date with a sub directory based on the current file being played. The files are written both at 3000 Hz in files of 10Mb and a single 100Hz sample rate file

C.2.5 Sub VI Downsample.vi

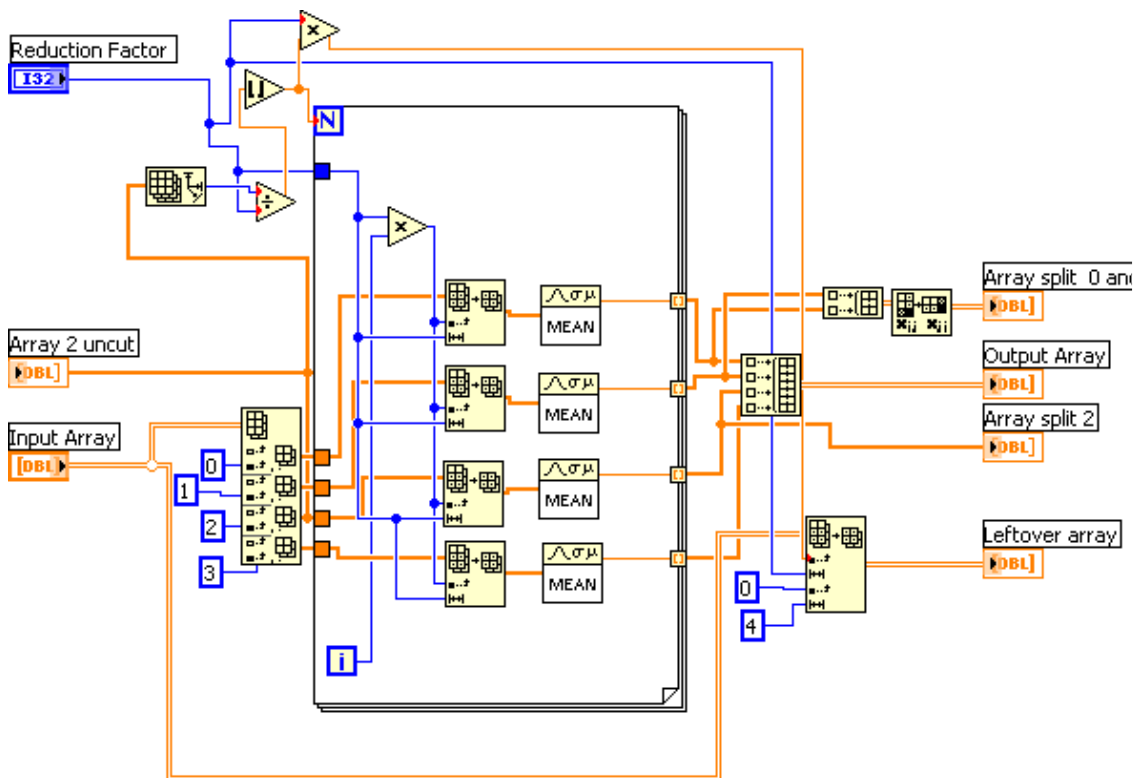


Figure C.20: *Downsample.vi*

Downsample.vi reduces the sample rate to 100 Hz for writing to “Filesmall “. Instead of taking every 30th sample (the value of *Reduction factor*) the mean of the 30 samples is used, which greatly reduces the noise level. The split array outputs are for the different graphs on the front panel.

C.2.6 Sub VI FilterVI.VI

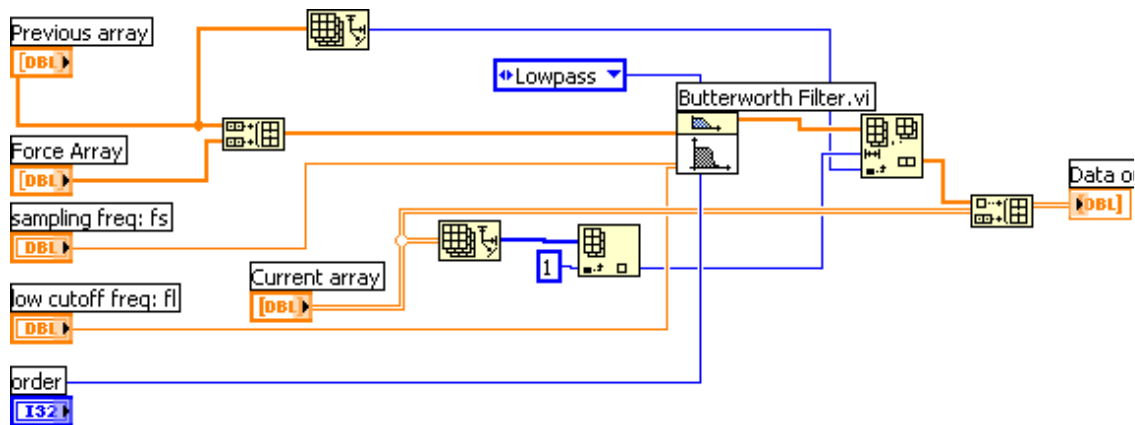


Figure C.21: FilterVI.vi

This filter provides a reduced noise signal based on the Labview built in butterworth filter. The filtered result was not used for final analysis as the rapid length change response was affected by the filter.

C.2.7 Sub VI Resample.vi

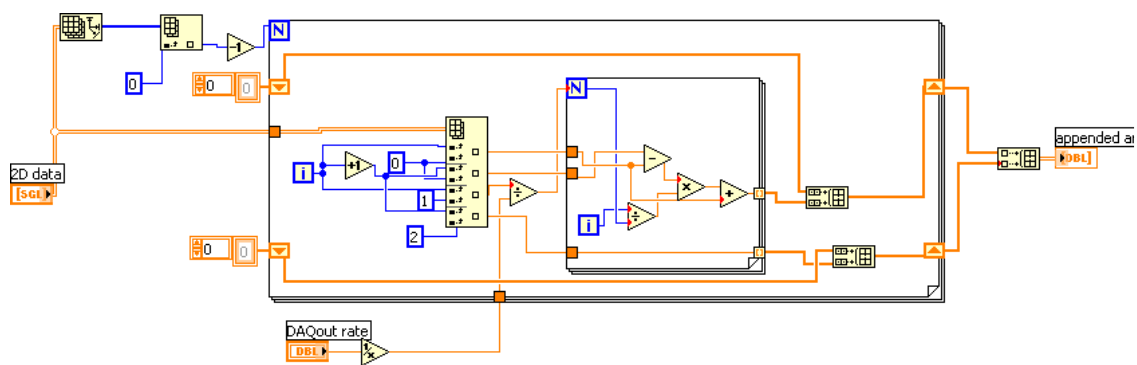


Figure C.22: Resample.vi

The resample VI up samples the data from the Generate_data.vi from the original sampling rate (default 1kHz) to the *DAQout rate* (default 10 kHz) to minimize the

required file size for the source data, while reducing 1kHz resonance issues in the set-up.